This electronic thesis or dissertation has been downloaded from the King's Research Portal at https://kclpure.kcl.ac.uk/portal/

Using hypobaric pressure to control percutaneous drug penetration

Masoomi, Parastoo

Awarding institution:
King's College London

The copyright of this thesis rests with the author and no quotation from it or information derived from it may be published without proper acknowledgement.

END USER LICENCE AGREEMENT

Unless another licence is stated on the immediately following page this work is licensed

under a Creative Commons Attribution-NonCommercial-NoDerivatives 4.0 International

licence. https://creativecommons.org/licenses/by-nc-nd/4.0/

You are free to copy, distribute and transmit the work

Under the following conditions:

- Attribution: You must attribute the work in the manner specified by the author (but not in any way that suggests that they endorse you or your use of the work).
- Non Commercial: You may not use this work for commercial purposes.
- No Derivative Works - You may not alter, transform, or build upon this work.

Any of these conditions can be waived if you receive permission from the author. Your fair dealings and other rights are in no way affected by the above.

Take down policy

If you believe that this document breaches copyright please contact librarypure@kcl.ac.uk providing details, and we will remove access to the work immediately and investigate your claim.

Download date: 09. Nov. 2023

Using Hypobaric Pressure to Control Percutaneous Drug Penetration

Parastoo Masoomi

King's College London

A thesis submitted for the degree of

Doctor of Philosophy

April, 2019

DEDICATION

To my father,

For your advice, patience, and unwavering confidence in me.
And because you always understood.
For your diligence, dexterity and years of toil.
And laughing and causing considerable mirth along the way.
For your familiar exuberance, devotion and dedication to family.
And building our home and filling it with love.
For being my rock, my confidant, my superstar.
I dedicate this thesis to you and your memory.

(1955-2018)

تقدیم به پدرم ...

Acknowledgements

The work presented in this thesis would not have been possible without my close association with many people who were always there when I needed them the most. I take this opportunity to acknowledge them and extend my sincere gratitude for helping me make this Ph.D. thesis a possibility.

I would like to thank my supervisor, Dr Stuart Jones, for the patient guidance, encouragement and advice he has provided throughout my time as his student. I have been extremely lucky to have a supervisor who cared so much about my work, and who responded to my questions and queries so promptly whilst I came to terms with particularly difficult personal circumstances. I am also extremely obliged to Dr Andrew Chan for his ongoing help and valuable input throughout the PhD process.

I would like to thank my fellow PhD students for their company over the last four years and for creating such a friendly and enjoyable atmosphere in which to work. In particular, Laura, Jesmine, Dona, Ayasha, Makiko and Osama. I wish also to acknowledge all the members of staff at King's College University who helped me in my supervisor's absence. In particular, I would like to thank Dr Arcadia Woods.

I would like to express my deepest gratitude to my family for their continuous and unparalleled love, help and support. To Shakiba for her unconditional support during the last 10 years. I am grateful to my sister Baraneh, for always being there for me as a friend. To my loving mother Mojgan, for her patience, support and motivation. I am forever indebted to my late father Rahmat, for giving me the opportunities and experiences that have made me who I am. He selflessly encouraged me to explore new directions in life and seek my own destiny.

Finally, I would like to thank Dr Pranay Seshadri, for his love, patience, support and for instilling in me confidence and a drive for pursuing strength to conclude this step of our journey.

Abstract

Drug delivery via the skin is attractive, but it is challenging and thus it is an area of continual research. Challenges arise in this field because only a narrow range of drugs naturally diffuse into the cutaneous tissue. This natural passive skin diffusion process is largely dictated by the drugs physicochemical characteristics. Only moderately lipophilic, low molecular weight agents accumulate in sufficient concentrations in the systemic circulation after topical delivery to elicit a clinical effect. The inability of drugs to pass into the skin has been addressed in previous work through chemical and physical methods of penetration enhancement, but using the currently available technologies it remains problematic to force compounds through the skin without damaging the tissue. The aim of this project was to investigate if the application of topical hypobaric pressure, a new physical technique to enhance topical drug delivery, could be used to facilitate drug delivery into the skin without skin damage.

To study the effect of local hypobaric pressure changes upon drug penetration into the skin three model systems were selected based on their different physicochemical properties; minoxidil (a small drug that passes into the skin via the hair follicles), dextran (a model macromolecule), and nanosized carriers (to simulate a drug delivery system). Application of the device (built-in-house) gave a stable pressure reading for 60 min. Histology, showed hypobaric pressure up to 400 $\pm$ 50 mBar did not damage the skin. The application of hypobaric pressure (400 $\pm$ 50 mbar) was shown to be significantly ($P < 0.05$) enhance drug deposition in the skin for the majority of test systems. For example, an enhancement ratio of 16.5, 5.3 and 5.2 was observed for minoxidil in *stratum corneum*, epidermis and dermis respectively. For solid lipid nanoparticles an enhancement ratio of 1.2, 8.8 and 7.8 was recorded for *stratum corneum*, epidermis and dermis respectively. For the dextran (FD-4) the enhancement ratios were 2.9, 2.0 and 1.2 for *stratum corneum*, epidermis and dermis respectively. The hypobaric enhanced skin permeation was dependent on the test systems size, surface charge, and hydrophobicity. Confocal microscope images showed the solid lipid nanoparticle enhancement was through the intercellular and follicular pathways, whereas the dextran enhancement was through the intercellular pathway when hypobaric pressure was applied.

In conclusion the results obtained from this project suggested that the application of hypobaric pressure was an effective, safe and promising method to enhance the delivery of drugs into the skin and it warrants further assessment *in vivo* to enable its clinical use.

Contents

List of Figures **ix**

List of Tables **xiv**

List of Abbreviations **xvi**

1 Introduction **1**

1.1 General introduction 1
1.2 Drug delivery to skin 2
1.3 Skin structure 5
1.3.1 *Stratum corneum* 6
1.3.2 Epidermis 7
1.3.3 Dermis 9
1.3.4 Hypodermis 10
1.3.5 Skin appendages 10
1.4 Routes of drug penetration into the skin 11
1.4.1 Permeation via the *stratum corneum* 11
1.4.2 Permeation via Appendages 12
1.5 Factors affecting drug permeation 13
1.5.1 Physiological factors 13
1.5.2 Properties of the drug 14
1.5.3 Properties of the vehicle 15
1.6 The prediction of percutaneous drug delivery 15
1.6.1 Mathematical models 15
1.6.2 *In vitro* methodology 18
1.6.3 *In vivo* methodology 19
1.7 Strategies to enhance percutaneuos drug delivery 20
1.7.1 Passive methods 20
1.7.2 Active methods 26
1.8 Limitations of current enhancement methods 33
1.9 Aim and scope of this thesis 34

2 Analytical method development **35**
2.1 Introduction . . . 35
2.2 Materials . . . 41
2.3 Methods . . . 41
2.3.1 High performance liquid chromatography (HPLC) . . . 41
2.3.2 Chemical stability assessment of minoxidil . . . 43
2.3.3 Fluorescence Spectroscopy . . . 43
2.3.4 Fluorescence chemical stability . . . 46
2.3.5 Data analysis . . . 46
2.4 Results . . . 47
2.4.1 High performance liquid chromatography (HPLC) . . . 47
2.4.2 Minoxidil chemical stability . . . 48
2.4.3 Fluorescence Spectroscopy . . . 50
2.4.4 Fluorescence stability . . . 55
2.5 Discussion . . . 58
2.6 Conclusion . . . 61

3 Modifying the *in vitro* permeation of minoxidil using hypobaric pressure **62**
3.1 Introduction . . . 62
3.2 Materials . . . 65
3.3 Methods . . . 65
3.3.1 Minoxidil vehicle optimisation . . . 65
3.3.2 Minoxidil vehicle-skin interactions . . . 66
3.3.3 Orange G quantification . . . 69
3.3.4 Hypobaric device verification . . . 69
3.3.5 *In vitro* minoxidil permeation . . . 71
3.3.6 Skin histology studies . . . 72
3.3.7 *Ex vivo* deposition study . . . 72
3.3.8 Statistical analysis . . . 74
3.4 Results and Discussion . . . 75
3.4.1 Minoxidil vehicle optimization . . . 75
3.4.2 Effect of minoxidil vehicle on skin integrity . . . 78
3.4.3 Hypobaric method verification . . . 79
3.4.4 *In vitro* minoxidil permeation . . . 80
3.4.5 Skin integrity after application of hypobaric pressure . . . 85
3.4.6 *Ex vivo* porcine skin minoxidil deposition study . . . 86
3.5 Conclusion . . . 89

4 Investigation of the effect of hypobaric pressure on macromolecules 90
4.1 Introduction . . . 90
4.2 Materials . . . 92
4.3 Methods . . . 93
4.3.1 Dextran extraction recovery . . . 93
4.3.2 Dextran permeation study . . . 93
4.3.3 Confocal Microscopy . . . 94
4.3.4 Statistical analysis . . . 95
4.4 Results and Discussion . . . 96
4.4.1 Dextran extraction recovery . . . 96
4.4.2 Dextran permeation studies . . . 96
4.4.3 Dextran skin distribution . . . 101
4.5 Conclusion . . . 105

5 Investigation of hypobaric pressure on nanoparticle penetration into the skin 106
5.1 Introduction . . . 106
5.2 Materials . . . 109
5.3 Methods . . . 109
5.3.1 Solid lipid nanoparticle fabrication . . . 109
5.3.2 SLN size analysis . . . 110
5.3.3 SLN Zeta potential determination . . . 111
5.3.4 Dye loading and purification of SLN . . . 111
5.3.5 *In vitro* permeation of solid lipid nanoparticles using hypobaric pressure . . . 112
5.3.6 α-TP liposome fabrication . . . 113
5.3.7 α-TP liposome size analysis . . . 113
5.3.8 α-TP liposome zeta potential determination . . . 114
5.3.9 Dye loading and purification of α-TP liposome . . . 114
5.3.10 *In vitro* permeation of α-TP liposome using hypobaric pressure 114
5.3.11 FluoSphere^{TM} . . . 115
5.3.12 FluoSpheres^{TM} characterisation . . . 115
5.3.13 *In vitro* permeation of FluoSpheres^{TM} using hypobaric pressure 115
5.3.14 Confocal microscopy . . . 116
5.3.15 Data analysis . . . 117
5.4 Results and Discussion . . . 118
5.4.1 Solid lipid nanoparticle characterisation . . . 118
5.4.2 SLN loading determination . . . 120
5.4.3 *In vitro* permeation of SLN using hypobaric pressure . . . 121

5.4.4 α-TP Liposome characterisation 123
5.4.5 α-TP Liposome loading determination 127
5.4.6 *In vitro* permeation of α-TP Liposome using hypobaric pressure 129
5.4.7 FluoSpheres^{TM} characterisation 132
5.4.8 *In vitro* permeation of FluoSpheres particles using hypobaric pressure 134
5.4.9 Nanoparticle skin distribution 137
5.5 Conclusion 141

6 General discussion **142**
6.1 Future work 150

References **152**

List of Figures

1.1 Schematic representation of the skin layers and appendage, taken from (Alexander et al., 2012) 5
1.2 Schematic representation of the "bricks and mortar" model for human *stratum corneum*, with the corneocyte "bricks", the intercellular lipid "mortar", and the corneodesmosomes connecting the corneocytes, taken from (Wickett and Visscher, 2006). 6
1.3 Schematic representation of the epidermis showing the main layers, taken from (Wickett and Visscher, 2006) 7
1.4 The routes of drug penetration across the skin. (1) through continuous *stratum corneum*; (2) via the sweat ducts or (3) through the hair follicles, taken from (Daniels, 2004). 11
1.5 Schematic representation of the *stratum corneum* and the intercellular and transcellular routes of penetration, taken from (Hadgraft and Lane, 2016). 12
1.6 Graph representing how to determine steady state flux (used to calculate the permeability coefficient) and lag-time. The steady-state flux (J_{ss}) is the slope of the linear part of the graph of the cumulative amount penetrated as a function of time. The lag time is the time intercept of the linear portion of the graph (Holmgaard and Nielsen, 2009). 17
1.7 Mechanisms of action of chemical penetration enhancer with the intercellular lipids (A), desmosomes and protein structures (B), and with corneocytes (C), taken from (Barry, 2004). 22
1.8 Graph representing transdermal drug delivery by iontophoresis (Daniels, 2004). 27
1.9 The mechanism of electroporation enhancing transdermal delivery of sinomenine hydrochloride; A) control and B) The intercellular intervals and epidermal cracks of skin were increased after the electroporation stimulation (Feng et al., 2017). 28
1.10 Schematic expression of drug delivery facilitated by sonophoresis (Daniels, 2004). 28

1.11 Techniques of drug delivery to the skin using microneedles (MN). A) first administrated to the skin B) then used for drug delivery (Kim et al., 2012). 29
1.12 A schematic representation of hydrogel-forming microneedles (Larraneta et al., 2016). 30
1.13 The transdermal delivery of insulin after injection with a needle, and a contemporary jet injector. Insujet^{TM} (Courtesy of the European Pharma Group). 30
1.14 A schematic representation of the microdermabrasion procedure (Gill, 2017). 31
1.15 Schematic drawing of the tape-strip technique (Van der Molen et al., 1997). 32

2.1 Summary of five HPLC minoxidil calibration curves. Each point represents the concentration of minoxidil vs. peak area ± S.D. (the error bars of the standard deviation is too small to be seen (n=3). . 47
2.2 Representative calibration curve for a) FD-4, b) FD-10, c) FD-70 and d) FD-150 dextran in PBS using intraday data mean ± SD (n=3, error bars too small to be seen). 51
2.3 A summary of the three data sets generates for the intraday precision for nile red in ethanol: PBS (pH 7.4). Data is the mean ± SD(n=3, error bars too small to be seen). 53
2.4 Representative calibration curve for red dye fluorescence in (methyl pyrrolidone: PBS) using intraday data mean ± SD (n=3, error bars too small to be seen). 54
2.5 Fluorescence stability of a) FD-4, b) FD-10, c) FD-70 and d) FD-150 in different concentrations over 156 h, mean ± SD (n=3, error bars too small to be seen). samples were stored at room temperature. . . 56
2.6 Fluorescence stability of nile red in different concentrations over 24 h, mean ± SD (n=3, error bars too small to be seen). 57
2.7 Fluorescence stability of red dye in different concentrations over 24 h, mean ± SD (n=3, error bars too small to be seen). 57

3.1 Chemical structure of minoxidil. 63
3.2 Chemical structure of Orange G. 64
3.3 Design of a traditional Franz cell (PermeGear, 2018). 68
3.4 Pressure diffusion Franz cell 3 D drawings generated in AutoCad LT software (Autodesk, Farnborough, UK), a) front view, b) hypobaric chamber (Inacio, 2015). 70

3.5 In-house developed pressure cell set up. Hypobaric pressure was generated by extracting air using syringes and changes in hypobaric pressure were recorded with a manometer (Inacio, 2015). 70
3.6 skin layers were spiked with a known amount of drug in each layer . 74
3.7 The solubility and ionisation percentage of minoxidil in PBS at different pH from 3.0 to 7.4. Data shown is the mean ± standard deviation . Error bars are too small to be seen (n=3). 75
3.8 The solubility of minoxidil in (PBS: ethanol: propylene glycole) at different pH from 3.0 to 7.4. Data shown is the mean ± standard deviation. Error bars are too small to be seen (n=3). 76
3.9 Permeation profile of orange G in two conditions, damaged and intact skin membrane. Data shown is the mean ± standard deviation (n=5). 78
3.10 Pressure profile of pressure device without adjustment (n=1). . . . 79
3.11 Pressure profile of barometric device with adjustment. Data point represents ± standard deviation (n=4). 79
3.12 Permeation profile of minoxidil across silicone membrane at different concentrations. Data points represent the mean cumulative minoxidil amount over 120 h (n=5). 81
3.13 Minoxidil permeation profile under atmospheric (1010 mBar) and hypobaric (450 ± 50 mBar) pressure through silicone membrane over 24 h. Each point represents mean ± standard deviation (n=5). . . . 82
3.14 Permeation profile of minoxidil across porcine skin. Data points represent the mean cumulative minoxidil amount over 24 h. Data represents ± standard deviation (n=5). Error bar are too small to be seen on some points. 84
3.15 Vertical displacement of porcine ear samples after removal from Franz diffusion cell. a) porcine skin at atmospheric pressure (control). b) porcine skin after application of hypobaric pressure for 1 h. 85
3.16 Porcine skin histology a) atmospheric pressure (control), and b) after application of hypobaric pressure for 1 h. 86
3.17 *Ex vivo* deposition of minoxidil in porcine skin under atmospheric (1010 mBar) and hypobaric (450 ± 50 mBar) pressure conditions. Data point represent ± standard deviation (n=5) 3h. 87

4.1 *In vitro* permeation of FDs at atmospheric pressure. The data represents the percentage of dextran transfered into the receiver fluid after 2 h transport study. Each point represents mean ± standard deviation (n=3). 97

4.2 Dextran in porcine skin layers after delivery at atmospheric (1010 mBar) and hypobaric (450 ± 50 mBar) pressures. Bars represent mean ± standard deviation (n=3) for both conditions. ER (enhancement ratio) represents the ratio between the % amount of dextran found under hypobaric and atmospheric conditions. a) 4 kDa, b) 10 kDa, c) 70 kDa and d) 150 kDa. 100
4.3 Diagram showing the difference between tight junctions and gap junctions (Biology Arizona, 2002). 103
4.4 Confocal microscopic examination after topical administration of FD-4 and FD-70 dextran under atmospheric conditions (1010 mBar) and hypobaric conditions (450 ± 50 mBar): control samples at atmospheric (a) and (b); topical FD-4 delivery under atmospheric conditions (c) and upon hypobaric pressure (d); topical FD-70 delivery under atmospheric conditions (e) and upon hypobaric pressure (f). Magnification × 10. The arrows indicate the hair follicles. . . . 104

5.1 : lipid nanocapsule preparation using phase inversion method Heurtault et al. (2002). 110
5.2 Size distribution by intensity of: a) lipid nanoparticle suspension and b) nile-red loaded lipid nanoparticle suspension, measured using zeta nanosizer. 118
5.3 Changes in size for solid lipid nanoparticles over 24 h. Each data point represents mean ± standard deviation (n=3). 119
5.4 Percentage of nile red remaining in solid lipid capsules after incubation at 32°C over 6 h. Each data point represents mean ± standard deviation (n=3). 120
5.5 *In vitro* profile of SLN deposition in porcine skin layers under atmospheric (1010 mBar) and hypobaric (450 ± 50 mBar) pressure conditions. Each point represents mean ± standard deviation (n=5). * Statistically significant ($P < 0.05$). 122
5.6 Zeta potential of liposomes with increasing mol % ratio of α-TP. Each data point represents mean ± standard deviation (n=3). . . 124
5.7 Changes in size of pure DPPC and pure α-TP over 4 weeks. Each data point represents mean ± standard deviation (n=3). 126
5.8 Changes in size of DPPC and α-TP mixtures over 4 weeks. Each data point represents mean ± standard deviation (n=3). 126
5.9 Percentage of nile red remaining in liposomes after incubation at 32°C for 1, 2, 24 and 48 h. Data represents mean ± standard deviation for α-TP:DPPC 1:1 and 3:7 liposomes (n=3) and percentage from n=1 for α-TP:DPPC 7:3, pure DPPC and α-TP liposomes. 128

5.10 Permeation of liposomes with α-TP:DPPC mol ratio of 3:7 into individual skin layer under atmospheric (1010 mBar) and hypobaric pressure (450 ± 50 mBar). Data represents mean ± standard deviation (n=5). 130
5.11 Permeation of liposomes with α-TP:DPPC mol ratio of 1:1 into individual skin layer under atmospheric (1010 mBar) and hypobaric pressure (450 ± 50 mBar). Data represents mean ± standard deviation (n=5). 130
5.12 Changes in size for polystyrene nanoparticles over 3 h. Each data point represents mean ± standard deviation (n=3). 133
5.13 Percentage of dye remaining in polystyrene particles after incubation at 32°C over 3 h. a) 100 nm, b) 500 nm and c) 1000 nm. Each data point represents mean ± standard deviation (n=3) 133
5.14 Percentage of polystyrene nanoparticles in different size. Data represents mean ± standard deviation (n=5). 134
5.15 Permeation of polystyrene particles into individual skin layer under atmospheric (1010 mBar) and hypobaric pressure (450 ± 50 mBar). a) 100 nm, b) 500 nm and c) 1000 nm. Data represents mean ± standard deviation (n=5). 136
5.16 Confocal microscopic examination after topical administration of polystyrene and solid lipid nanopartciles under atmospheric (1010 mBar) and hypobaric (450 ± 50) pressure conditions: a) & d) control, b) polystyrene at atmospheric pressure, c) polystyrene at hypobaric pressure, e) solid lipid at atmospheric pressure and f) solid lipid at hypobaric pressure. 139

6.1 Diagram representing the effect of topical hypobaric pressure upon minoxidil skin delivery. 145
6.2 Diagram representing the influence of hypobaric pressure in permeation of different size dextran through the skin. 1) Epidermis and 2) dermis. 147
6.3 Diagram representing the influence of hypobaric pressure in permeation of different size nano-size compounds through the skin. 149

List of Tables

1.1 Summary of benefits and limitations of delivering therapeutic agents via the skin. 4

2.1 Physicochemical properties of the model penetrators. 39
2.2 Summary of model drug/probes properties. 40
2.3 Appropriate solvent mixture for probes. 44
2.4 Volume of standard solution required for (FITC)-dextran calibration curve. 44
2.5 Volume of standard solution required for nile red fluorescence calibration curve. 45
2.6 Volume of standard solution required for red dye fluorescence calibration curve. 45
2.7 Minoxidil assay variance; Summary of intra-day and inter-day variability. Data represent mean standard deviation, n=18 for intra-day, n=18 for inter-day. CV represents coefficient of variation. 48
2.8 Day 30-calibration curve data represent mean ± SD; n=6; CV represents coefficient of variation between day 1 and day 30 (n=6) . 49
2.9 Stability of minoxidil standards, assessed by the comparison of peak area at day 1 and day 30; temperature below 8°C (n=6) 49
2.10 Wavelength of maximal excitation λ_{maxex} (nm) and λ_{maxem} (nm) for nile red, polystyrene microspheres and FITC-dextran. 50
2.11 Intra and inter day variation FD-4 as a function of concentration in PBS. Intraday results calculated from measurements made in triplicate at each concentration (n=9). Inter day variation results measured over 3 days (n=9). 51
2.12 Intra and inter day variation FD-10 as a function of concentration in PBS. Intraday results calculated from measurements made in triplicate at each concentration (n=9). Inter day variation results measured over 3 days (n=9). 52
2.13 Intra and inter day variation FD-70 as a function of concentration in PBS. Intraday results calculated from measurements made in triplicate at each concentration (n=9). Inter day variation results measured over 3 days (n=9). 52

2.14 Intra and inter day variation FD-150 as a function of concentration in PBS. Intraday results calculated from measurements made in triplicate at each concentration (n=9). Inter day variation results measured over 3 days (n=9). 52
2.15 LOD and LOQ of various dextran molecular weights. 52
2.16 Intra and inter day variation in nile red fluorescence as a function of concentration in a mixture of ethanol and PBS. Intraday results calculated from measurements made in triplicate at each concentration (n=9). Inter day variation results measured over 3 days (n=9). . . . 53
2.17 Intra and inter day variation in polystyrene red dye fluorescence as a function of concentration when dissolved mixture of methyl pyrrolidone: PBS. Intraday results calculated from measurements made in triplicate at each concentration (n=9). Inter day variation results measured over 3 days (n=9). 55
2.18 Summary of all analytes used. 60

3.1 Permeation of minoxidil through artificial membranes using different dose and pressure. (Mean of n=5 ± SD). 81

4.1 Physicochemical properties of FITC-Dextrans (FDs) (Sigma-Aldrich). 92
4.2 Dextran extraction recovery. Data represents the mean ± standard deviation (n=3). 96
4.3 Dextran mass that has penetrated the *stratum corneum* employing hypobaric pressure. ∗ represents no enhancement in hypobaric pressure in contrast with atmospheric pressure. Data represents the mean ± standard deviation (n=3). 101

5.1 size and zeta potential for unloaded LNP and nile red-loaded lipid nanocapsule. Data represent mean ± SD (n=3). 119
5.2 SLN mass per area deposition in porcine skin layers under atmospheric (1010 mBar) and hypobaric (450 ± 50 mBar) pressure conditions, and their recovery %. Each point represents mean ± standard deviation (n=5). 122
5.3 Size and zeta potential for unloaded LNP and nile red-loaded lipid nanocapsule. Data represent mean ± SD (n=3). 125
5.4 Size, zeta potential and dye loading efficiency for nile red incorporated liposomes. Data represent mean ± standard deviation (n=3). 127
5.5 Size and zeta potential for FluoSpheres polystyrene particles. Data represent mean ± SD (n=3). 132
5.6 Summary of nanoparticles permeation enhancement. sc: stratum corneum, epi: epidermis and der: dermis 140

List of Abbreviations

A	Skin area
AUC	Area under the curve
A_s	Peak symmetry
C_v	Initial concentration
Da	Dalton
Der	Dermis
Epi	Epidermis
ER	Enhancement ratio
FTIR	Fourier Transform Infrared spectroscopy
HPLC	High Performance Liquid chromatography
h	Path length/barrier thickness
ICH	International Conference on Harmonisation
J_{ss}	Steady-state flux
K_p	Permeability coefficient
LOD	Limit of detection
LP	Liposome
Log P	Partition coefficient
LOQ	Limit of quantification
mBar	millibar
MeOH	Methanol
mg	milligram

MW	Molecular weight
nm	nanometre
O/W	Oil in water
PBS	Phosphate buffer saline
PDI	Polydispersity index
PG	Propylene glycol
PS	Polystyrene nanoparticles
Q	Cumulative amount
SC	Stratum corneum
SD	Standard deviation
SLN	Solid lipid nanoparticles
UV	Ultraviolet

1 Introduction

1.1 General introduction

Drug delivery to the skin is an important route of therapeutic compound administration (Cross and Roberts, 2004). This route of delivery offers some advantages including the potential to form a drug reservoir that can be detached from the body and the option of a convenient and painless means to deliver a therapeutic compound over a period of day from a single application (Guy and Hadgraft, 2003; Williams, 2003; Bronaugh and Maibach, 2005; Prausnitz et al., 2004; Joshi and Raje, 2002).

The key functions of the skin are to limit chemical entry into the body and control transcutaneous water loss (Potts and Francoeur, 1991; Prausnitz and Langer, 2008). The outermost layer of the skin, the *stratum corneum*, is the most challenging barrier to overcome. The unique structure of this layer only allows the permeation of molecules with a relatively small molecular weight (< 500 Da) and adequate lipophilicity ($1 < \text{Log P} < 3$) (Naik et al., 2000; Barry, 1983). Therefore, strategies need to be developed to allow drugs which have properties out side these limits to be delivered via the skin.

The currently available skin penetration techniques can be classified as those employing chemical or those applying physical enhancement methods. However, clinically, drug delivery via the skin is still limited to a defined set of molecular

charactrestics as many of the developed skin penetration enhancement methods can only be employed with a restricted number of chemicals.

Recently, hypobaric pressure, which is a physical enhancement method, has been used to enhance chemical penetration into the skin. Inacio (2015) reported that hypobaric pressure alters the mechanical and morphological properties of the skin, which resulted in an enhancement in drug deposition within the epidermal layer. The enhancement of chemicals permeation in the skin was explained by the reduction in the corneocyte size, expansion of the follicular infundibula and reduction in skin thickness. However, further investigation on a wider range of molecules is required to show the potential of this technique to enhance skin drug delivery. **The aim of this project was to investigate if the application of topical hypobaric pressure, a new skin physical penetration enhancement technique, could be used to improve drug delivery of 'problematic molecules' (e.g., very large molecules or those that require carriers) into the skin without skin damage**. To develop a new skin delivery method, it is important to have a good background knowledge of skin. Thus, first Chapter of this thesis will describe the skin structure and the various methods that have been employed to enhance skin drug delivery. The application of hypobaric pressure has previously shown to enhance compounds skin permeation; this data will be revisited and the need for additional work in this area will be outlined.

1.2 Drug delivery to skin

The most conventional routes of drug delivery are the oral and parenteral routes. The majority of small molecule compounds are delivered orally (Anselmo and Mitragotri, 2014; Han and Das, 2015). The oral route is the most convenient and patient-friendly way of drug delivery (Brambilla et al., 2014; Ita, 2014). However, oral delivery is extremely challenging for larger molecules such as therapeutic proteins and peptides, due to their fast degradation in the stomach and low permeability across the epithelium of the gastrointestinal tract (Schoellhammer et al., 2014). The parenteral route is the primary mode of administration for these larger compounds

(Anselmo and Mitragotri, 2014; Schoellhammer et al., 2014; McCrudden et al., 2013), but this invasive mode of administration is often distressing to patients and requires a trained administrator (Schoellhammer et al., 2014; McCrudden et al., 2013; Kermode, 2004). As a result of the inherent limitations of these oral and parenteral routes of drug delivery, percutaneous drug delivery has been proposed as an alternative delivery route.

Drug delivery into the skin can be classified into two groups: transdermal and dermal, according to the drug's target site. Transdermal delivery aims to administer the drug into systemic circulation, while dermal delivery attempts to target the drug at the pathological site within the skin. Transdermal systems are designed to increase the flux across the skin, but dermal systems aim to increase retention within the layers (Hsieh, 1994). For both transdermal and dermal methods of delivery the drug molecules have to diffuse across the outermost layer of the skin (*stratum corneum*), which is the main barrier for skin administration. The transdermal drug delivery advantages and disadvantages are summarised in (see Table 1.1).

Table 1.1: Summary of benefits and limitations of delivering therapeutic agents via the skin.

Benefits	Limitations
• Avoidance of hepatic first-pass metabolism and the GI tract (Barry, 1983).	• Small molecular weight drugs with a MW $<$ 500 Da easily diffuse across the SC barrier, but aother molecules may be problematic (Barry, 1983).
• Reduction in side-effects linked to systemic toxicity (Kornick et al., 2003).	• Only drugs with a logP between 1-3 could pass into the skin (Williams, 2003).
• Large surface area available for administration (Cevc, 1997).	• Skin allergic reaction or irritation with some active drugs, formulations and devices (Hogan and Maibach, 1990).
• Direct access to target or diseased site. Topical treatment of skin disorders such as psoriasis (Pavliv et al., 1994).	• Drug metabolism by the enzymes in the skin may lessen its efficacy (Steinsträsser and Merkle, 1995).
• Sustained or controlled delivery over a prolonged period of time (Škalko et al., 1992; Schreier and Bouwstra, 1994; Souto et al., 2004).	

1.3 Skin structure

To understand drug delivery using the skin, it is important to have knowledge of the fundamental characteristics of the skin anatomy and physiology. Hence, this will be the first topic of discussion in this Chapter.

The skin is the largest organ in the human body, accounting for greater than 10% of body weight with surface area of around 1.7 m^2 (Brown et al., 2006; Benson, 2012). The most important role of the skin is to provide a physical barrier against the external environment. It also regulates the body's homeostasis by limiting water loss, electrolyte balance and internal temperature. Furthermore, it protects the body against microorganisms, toxins and ultraviolet radiation damage (Barry, 1983).

The skin consists of four main layers: *stratum corneum* (nonviable epidermis), the remaining layers of the epidermis (viable epidermis), dermis and subcutaneous layer (hypodermis). Skin appendages include hair follicles, nails and sweat glands (Figure 1.1) (Walters and Roberts, 2002).

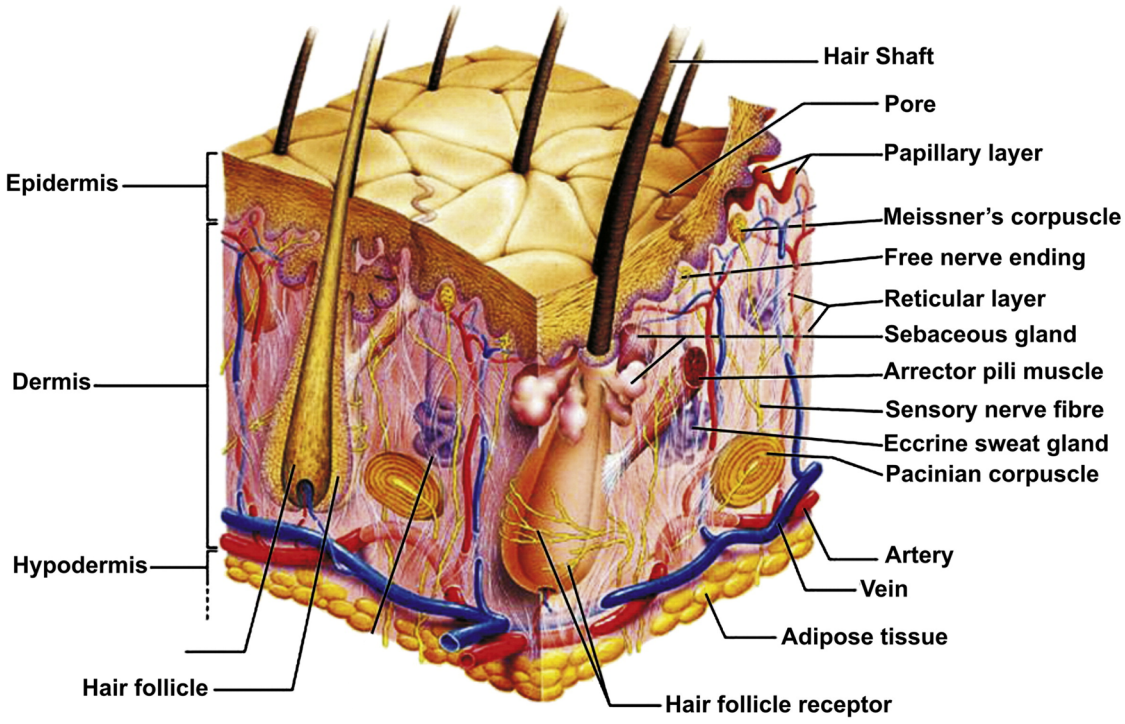

Figure 1.1: Schematic representation of the skin layers and appendage, taken from (Alexander et al., 2012)

1.3.1 *Stratum corneum*

The *stratum corneum*, or horny layer, is the outermost layer of the skin. The *SC* is the most restrictive barrier for percutaneous drug delivery. The *SC* thickness is between 10 to 20 μm (Bouwstra et al., 2003; Huang et al., 2005). It is known as "brick and mortar" structure model (Figure 1.2) that is composed of 10 to 25 layers of dead keratinocytes (corneocytes) embedded in a "mortar" of the intercellular lipid matrix (Bouwstra et al., 1997; Norlen, 2008). The corneocytes represent the "bricks", that are flat and elongated cells (up to 1.5 μm thick and 50 μm in diameter) with no nucleus and cell organelles (Benson, 2012). The cells are interlinked by desmosomes that give the supporting structure to this layer (Menon, 2002). The *stratum corneum* layer is composed of about 75-80% proteins and 5-15% lipids (Williams, 2003). The unique arrangement and structure of the intercellular lipids in multiple lamellar layers within a continuous lipid domain is essential for *stratum corneum* barrier function. The main components of the lipid domains are ceramides, cholesterol, and free fatty acids, which varies among different individuals and body sites (Lampe et al., 1983). The *stratum corneum* lipids are packed in multiple bilayers, but unlike other lipid bilayers in the body they lack phospholipids (Augustijns and Brewster, 2007). This "brick and mortar" structure is the main barrier for the permeability of compounds in and out of the skin (Elias, 2005).

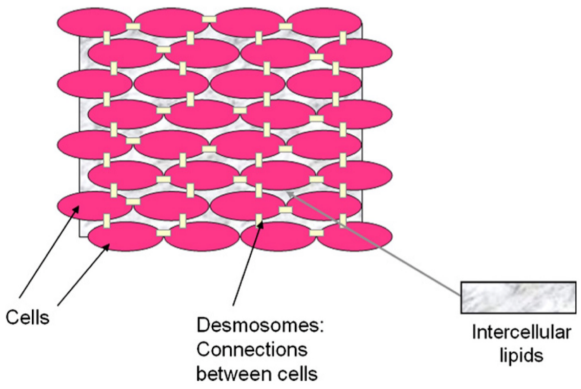

Figure 1.2: Schematic representation of the "bricks and mortar" model for human *stratum corneum*, with the corneocyte "bricks", the intercellular lipid "mortar", and the corneodesmosomes connecting the corneocytes, taken from (Wickett and Visscher, 2006).

1.3.2 Epidermis

The epidermis is a complex multilayer tissue with a thickness of 50-100 μm (Bolognia et al., 2012). It is an avascular membrane, which contains keratinocytes as the predominant cells. The keratinocytes are in a continuous state of renewal through differentiation, proliferation and keratinisation; here each layer has a different degree of differentiation (Brown et al., 2006). Therefore, the keratinocytes structure and composition changes during their transport from the *stratum basale* to the *stratum corneum*. By the time these cells have reached the *stratum corneum* they turn into corneocytes, which is known to be a nonviable epidermis. The viable epidermis is known as the epidermal layers below the *stratum corneum* (Benson and Watkinson, 2012; Madison, 2003). To summarise, the layers from bottom to the top are the: *stratum basale*, *stratum spinosum*, *stratum granulosum*, and *stratum corneum* (Figure 1.3) (Montagna, 2012). These are described in detail below.

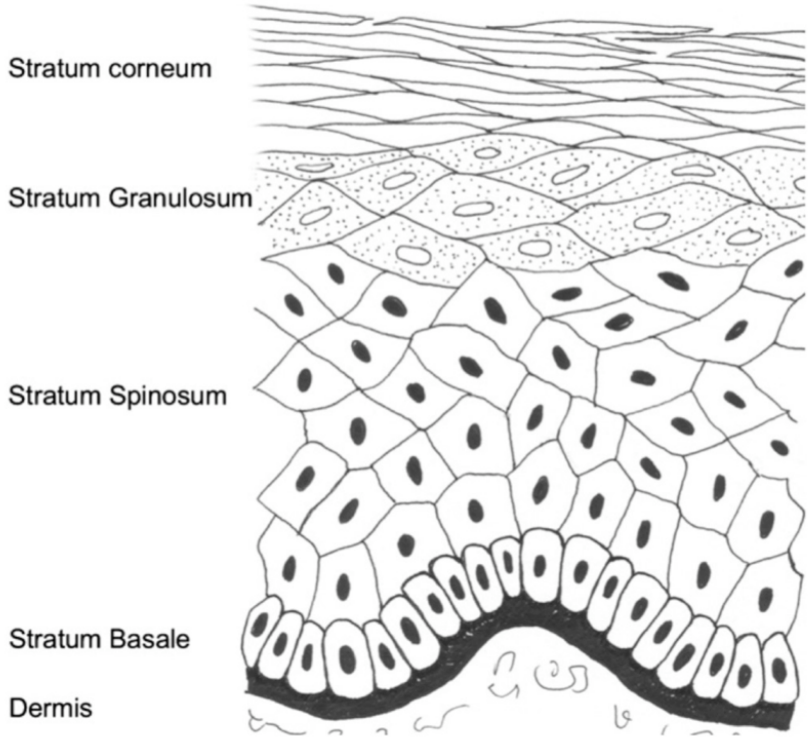

Figure 1.3: Schematic representation of the epidermis showing the main layers, taken from (Wickett and Visscher, 2006)

The *stratum basale* is the deepest layer of the epidermis, and the closest layer to the dermis. It contains a single layer of columnar keratinocytes that are attached to the basement membrane via hemidesmosomes. These cells reproduce constantly through mitosis to keep the epidermis replenished. In human skin, the replacement of these cells takes about 30 days depending on different factors such as the region of the body, age and disease conditions (Monteiro-Riviere, 2010). This is the only layer in the epidermis in which keratinocytes are able to undergo cell division (Menon, 2002).

The *stratum spinosum* layer is located above the stratum basale. It is composed of two to six layers of keratinocytes. Their morphology transforms from columnar to polygonal, and they have an enlarged cytoplasm containing keratin filaments and organelles in contrast with other layers (Benson and Watkinson, 2012).

The next layer is *stratum granulosum*, which is composed of several layers of flattened cells arranged in parallel sacks to the epidermal-dermal junction. The noticeable feature of this layer is the presence of small lamellar granules, which are also known as lamellated bodies and membrane coated granules (Monteiro-Riviere, 2010).

Lipophilic drugs can be trapped in the *stratum corneum* without further diffusion into the viable epidermis. This could be due to the higher water content of this layer in contrast with the *stratum corneum* (Scheuplein and Blank, 1971). Another factor, that can influence the drug penetration and retention within the layers, is the agent binding to the cellular components (Liu et al., 1991; Hikima et al., 2002). The latter factor has been previously studied by Bhatt et al. (2008), who reported a higher amount of tecnazene in the epidermal layers than those estimated from the permeation model, because of tissue binding.

In single layer epithelia, such as the small intestine, intercellular junctions have shown to be the main barrier in restricting paracellular diffusion. One example of this is the penetration of water and solutes through intercellular spaces (Madara, 1998). On the other hand, in multilayer epithelia, such as the epidermis, the role of intercellular junctions is not fully understood. That said, it has been suggested that

tight junctions in the *stratum granulosum* play an important role in the permeability barrier function of the epidermis (Furuse et al., 2002; Yuki et al., 2007).

1.3.3 Dermis

The dermis (1-2 mm thick) is located underneath the epidermis, it begins below basement membrane, and it provides the skin with mechanical support (Bouwstra et al., 2003). This layer is composed of dense uneven connective tissue that contains collagen fibres and elastin fibrosis. The collagen supports the skin structure, while elastic tissue provides flexibility. The predominant components of the dermis are fibroblasts, which could perform cell renewal, mast cells and macrophages, which are responsible for immune and inflammatory response. It should be noted that the dermis layer has low resistance to drug permeation.

The highly vascularised network in the dermis regulates the elimination of the permeants from the dermo-epidermal junction into the bloodstream. This results in a concentration gradient between the applied drug on the skin surface and the dermis layer. Here, lymph vessels play an important role in removal of the permeants, especially for larger permeants such as interferons (Cross and Roberts, 1993).

Despite having a low resistance to drug permeation, the permeation of highly lipophilic agents to the deeper tissues of the dermis may be compromised as a result of its higher hydration level (Benson, 2012; Riviere and Monteiro-Riviere, 2005). In addition, the spread of blood vessels network within this layer has an influence upon the agent's permeation and localisation. For example, the co-administration of vasoactive drugs, have been shown to enhance drug absorption into systemic circulation as a result of local vasculator dilation (Riviere et al., 1991; Singh and Roberts, 1994). Typically, vasodilation enhances the drug absorption into the systemic circulation; this has been reported previously by Riviere et al. (1991) for lidocaine when co-administrated with a vasoactive agent.

1.3.4 Hypodermis

Beneath the dermis is a structured fatty layer known as the hypodermis or subcutaneous layer. It acts as a protection barrier against physical shock, thermal insulation, energy provider for the upper layers and facilitates the skin binding to the fascia and skeletal muscle (Walters and Roberts, 2002).

1.3.5 Skin appendages

The three main skin appendages are hair follicles, sebaceous glands and sweet glands, all of which are located in the dermis. With regards to drug permeation, it should be noted that these routes are not mutually exclusive, as the drugs may take more than one permeation pathway, depending on their physiological characteristics.

Hair follicles are spread all over the body with a few exceptions such as palms, soles and lips. Although the opening of hair follicles represent a fractional area of about 0.1% of the total skin surface (Higuchi, 1962; Scheuplein, 1967), they extend into the deep layers of the tissue hence they have a greater area for drug delivery into the skin (Otberg, Richter, Schaefer, Blume-Peytavi, Sterry and Lademann, 2004).

The sebaceous glands associated with each hair follicle produce oily sebum, which is composed of free fatty acids, cholesterol, cholesterol esters, squalene, waxes and triglycerides (Valiveti et al., 2008; Wells and Lubowe, 1964; Greene et al., 1970; Nordstrom et al., 1986). The function of the sebum major is to lubricate the skin surface, and maintain a skin surface pH of about 5 (Williams, 2003; Benson and Watkinson, 2012).

There are approximately 2.5 million sweat glands on the entire human body surface (Beatty, 1995). There are two types of sweat glands: apocrine and eccrine, which are divided according to their function and shape. The apocrine sweat glands are larger and have ducts that empty into the hair follicles. They are found in specific areas in human body such as axillae, nipples and eyelids. The eccrine are about ten times smaller than the apocrine glands, and are distributed in the rest of the human body (Montagna, 2012). The eccrine sweat glands open directly onto the skin surface and are able to excrete fluids for electrolytes homeostasis,

and secrete sweat in response to heat, exercise and emotional stress (Bensouilah and Buck, 2006; Monteiro-Riviere, 2010).

1.4 Routes of drug penetration into the skin

To design a new percutaneous delivery system, it is necessary to understand all potential chemical penetration routes into the skin. There are three main routes across the skin for the penetration of chemicals: directly through the continuous *stratum corneum* (transcellular), intercellular routes, and appendageal route (Figure 1.4).

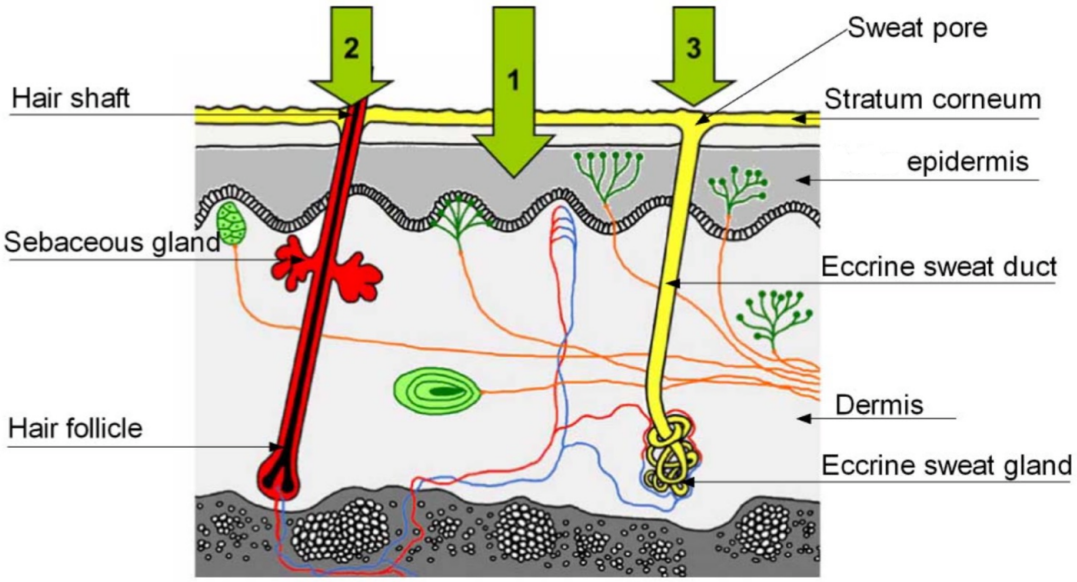

Figure 1.4: The routes of drug penetration across the skin. (1) through continuous *stratum corneum*; (2) via the sweat ducts or (3) through the hair follicles, taken from (Daniels, 2004).

1.4.1 Permeation via the *stratum corneum*

Permeation via the *stratum conreum* is achieved through transcellular and intercellular routes (Figure 1.5). The transcellular pathways are considered a route for relatively polar molecules through the *stratum corneum* (Scheuplein, 1965). The corneocytes have an intracellular matrix that can be hydrated and hence more

polar in nature compared to the lipids, thus diffusion involves frequent partitioning between this polar environment and the lipophilic domains around the corneocytes (Benson and Watkinson, 2012). Intercellular diffusion is achieved through lipids.

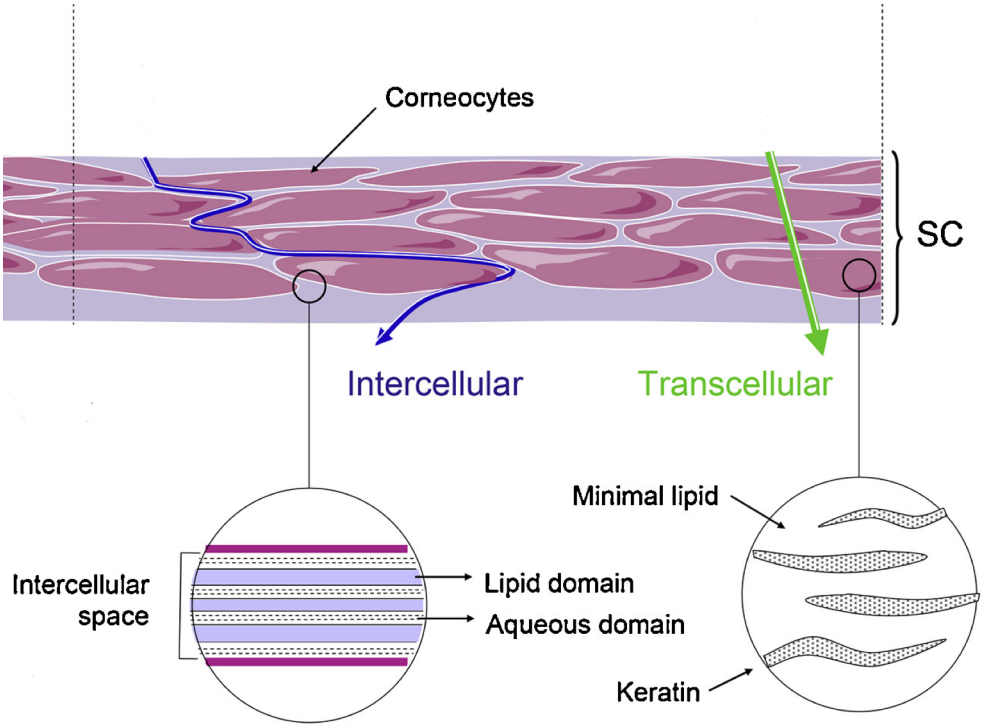

Figure 1.5: Schematic representation of the *stratum corneum* and the intercellular and transcellular routes of penetration, taken from (Hadgraft and Lane, 2016).

1.4.2 Permeation via Appendages

The importance of appendageal route versus the *stratum corneum* pathways was questioned for many years (Sloan, 1992; Bronaugh and Maibach, 2005) due to the comparatively smaller area of the skin that the appendages occupy. For instance, it was shown that the appendageal routes had a small contribution (5-10%) in the steady flux of steroids through excised human skin (Siddiqui et al., 1989). However, this pathway seems to be the portal for the permeation of ionic molecules (Grimnes, 1984) and larger polar molecules such as DNA (Li et al., 1993), which have difficulty penetrating through the intact *stratum corneum*. Moreover, Scheuplein (1965) reported that within the lag phase of diffusion, the influence of the appendageal route

is very important. In addition, a few studies reported the accumulation of certain compounds in the follicular region (Kao et al., 1988; Schaefer et al., 1990), which are important for the treatment of follicular related skin disorders such as alopecia.

Previous investigations have focused on the hair follicles as a possible route for both systemic and localised drug delivery. Preliminary studies on this theory were reviewed by (Barry, 2002), and more advanced methods such as fluorescence microscopy and confocal laser scanning microscopy were used to obtain a better understanding of drug delivery through this route (Schaefer and Lademann, 2001). In a recent study on the transdermal permeation of caffeine through follicular route, Kattou et al. (2017) reported that the follicular route provides not only short time fast diffusion, but it improves the overall systemic bioavailability. This newly developed 2D model have measured the caffeine disposition and localised distribution in lipid, corneocytes, viable dermis, dermis and the hair follicles, which is normally challenging to measure experimentally. Permeation through the appendageal route is either through the eccrine sweat glands duct or the follicular duct. The component of eccrine sweat glands is largely hydrophilic, while the follicular ducts is lipophilic, as a result of oily sebum excretions (Williams and Barry, 1992; Bronaugh and Maibach, 2005; Barry, 1987). Toll et al. (2004) proposed that larger particles (i.e. 750, 1500 nm) tend to deposit high concentrations of compounds in the follicular duct, while smaller particles (40 nm) particularly in barrier disrupted skin, tend to release active moieties to certain cell types, for example stem cells and multiple precursor cells.

1.5 Factors affecting drug permeation

1.5.1 Physiological factors

Drug permeation through the skin can be affected by several physiological factors such as age, anatomical skin, gender, ethnicity and some skin conditions. Over years the skin epidermis become thinner and corneocytes lose their adherent property; although the *stratum corneum* thickness remains untouched (Batisse et al., 2002). Aging also affects the lipid composition, which may cause a reduction in the major lipid level, especially for ceramides. Moreover, the dermis becomes atrophic

and comparatively acellular and avascular. This lipid reduction can cause skin dehydration, which results in the skin permeability of hydrophilic compounds (Walters, 2002*a*; Roskos et al., 1989). In contrast, the skin barrier function in younger skin is considerably lower, which may be responsible for an improved permeability (Giusti et al., 2001). Anatomical site plays an important role in the skin permeability, owing to differences in morphologic and functional characteristics, and the skin barrier function. The gender factor has shown a relatively small difference in the epidermal barrier, which is related to the basal transepidermal water loss (TEWL) differences between male and female skin types (Benson, 2012; Cua et al., 1990; Tupker et al., 1989). It has been reported that ethnicity can influence the skin permeability, however, it is far less profound than inter-individual differences within ethnic units (Darlenski and Fluhr, 2012). Finally, the skin condition (i.e. healthy, abraded, or diseased) can affect the skin permeation. For example, skin conditions such as psoriasis, eczema and acne can reduce the barrier function (Benson, 2012; Alexander et al., 2012).

1.5.2 Properties of the drug

The steady-state permeation, flux (J), of a drug penetrating the *stratum corneum* can be described by Fick's first law of diffusion:

$$J = \frac{dQ}{dT} = \frac{DPC_v}{h} \tag{1.1}$$

where Q is the amount permeating a unit area of skin per time T, D is the diffusion coefficient of the permeant in the skin, P is the partition coefficient between the *stratum corneum* and the vehicle, C_v is the applied concentration of permeant, and h is the diffusional path length.

According to Equation (1.1), a suitable candidate for transdermal delivery requires certain physicochemical characteristics, including a high, but balanced partition coefficient. Therefore, a log P(ow) between 1 and 3 is ideal, as too hydrophilic molecules are incapable of partitioning from the vehicle into the *stratum corneum*. However, highly lipophilic molecules will get stuck in the intercellular

stratum corneum lipids without penetrating into the relatively aqueous viable epidermis. Moreover, ionised molecules have a lower permeability coefficient in contrast with their respective unionised form, due to their lower value of log P in the ionised form (Barry, 2001; Hadgraft, 2004; Lane et al., 2012). Another important factor is a low molecular weight, as the size of the molecule will affect the diffusivity (D) through the *stratum corneum*. As a rule of thumb, candidate molecules for transdermal delivery need to be < 500 Da in size, however, they need an adequate aqueous solubility (> 1 mg.mL^{-1}) (high donor concentration, C_v to maintain a high concentration gradient, which is the driving force for the permeability) to increase the flux. Lastly, a melting point of < 200°C is a desirable physicochemical property, as it correlates with good solubility of the molecule in the intercellular *stratum corneum* lipid layer. Furthermore, transdermal drug candidates require a high therapeutic potency (deliverable dose preferably < 20 mg per day), low oral bioavailability, short biological half-live, and they should not irritate the skin (Naik et al., 2000; Finnin et al., 2011).

1.5.3 Properties of the vehicle

To develop an effective transdermal delivery method, it is important to pay attention to the design of a suitable vehicle. As the vehicle can influence the drug release from the formulation, i.e. controlling the vehicle/*stratum corneum* partition coefficient, it can modify the skin barrier properties and increase drug solubility in the uppermost layer. The *stratum corneum* can be influenced through interactions with its lipids and proteins, or through enhanced skin hydration via occlusion (Walters, 2002*b*; Vitorino et al., 2013).

1.6 The prediction of percutaneous drug delivery

1.6.1 Mathematical models

The passive transport rate of a therapeutic agent through skin barrier can be calculated and/or predicted using mathematical models. The therapeutic agents have to diffuse the avascular and lipophilic structure of the *stratum corneum* and

then enter the more aqueous lower layers (epidermis and dermis) and eventually through the blood circulation. The permeability coefficient of a compound and its lipophilicity show a positive correlation, i.e., if one increases the other one increases too (Roy and Flynn, 1989). Lipophilic agents more easily diffuse through the *stratum corneum* compared to hydrophilic agents, however, the penetration rate reduces when they enter the hydrophilic epidermis, which results in reduction in the penetration rate. Small uncharged molecular weight compounds have a better chance to penetrate the skin barrier (Guy et al., 1987), unlike the charged that have difficulty to penetrate when they are applied in aqueous solutions, due to the ions which generates a field of stable hydration that expands the size of penetrating component (Grandjean, 1990).

The permeation of agents through the multiple barriers of the skin structure is a multifactorial procedure. There are different approaches to understand a chemical's skin penetration, such as suggesting that the *stratum corneum* is the main barrier for the skin delivery. As chemicals diffuse through this barrier mainly via passive diffusion (Scheuplein and Blank, 1971) thenceforth solutes mass transfer via the skin can be described by Fick's first law. According to the Fick's first law of diffusion, the flux (J_{ss}) can be calculated by Equation (1.2), which gives a suitable estimation of flux rates related to skin penetration (Fick, 1855).

$$J_{ss} = K_P * \Delta C \tag{1.2}$$

where J_{ss} represents the flux of penetrant at steady-state conditions, also known as absorption rate, K_P is the permeability coefficient of the penetrant through the membrane barrier and ΔC is the concentration gradient across the membrane. *In vitro* studies are performed to measure J_{ss} as represented in (Figure 1.6). The lag time can also be calculated using this figure, which is important for duration of transport studies.

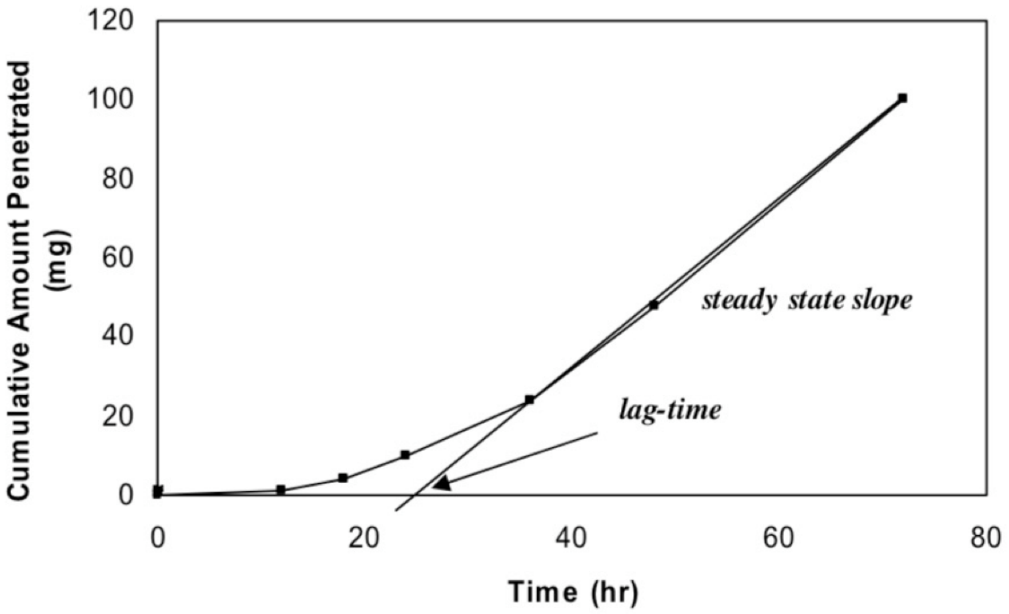

Figure 1.6: Graph representing how to determine steady state flux (used to calculate the permeability coefficient) and lag-time. The steady-state flux (J_{ss}) is the slope of the linear part of the graph of the cumulative amount penetrated as a function of time. The lag time is the time intercept of the linear portion of the graph (Holmgaard and Nielsen, 2009).

An adoptation of Fick's first law by Higuchi (1960), emphasised the importance of the thermodynamic activity. In this mathematical model, it was assumed that the maximum rate of diffusion per unit time, (J_{max}), was proportional to the thermodynamic activity of the penetrate agent and not its concentration as shown by Equation (1.3).

$$J_{max} = DS_S/h \tag{1.3}$$

where D represents the diffusion coefficient of the penetrate agent , S_s shows the maximum solubility of the penetrate agent in the *stratum corneum* and h represents the thickness of the barrier (Higuchi, 1961).

According to Equation (1.3), the flux of an agent from saturated solutions is constant, irrespective of the saturated concentration of their vehicle, since all saturated solutions have a thermodynamic activity of 1 (Bronaugh and Maibach, 1989). Although, it should be noted there are some conditions that apply to this model, such

as sink condition, membrane rate controlled movement, no influence of the vehicle on the barrier, thermodynamic activity is uniform throughout the formulation and only one agent is penetrating through the membrane (Higuchi, 1960).

However, it is essential to take into account the heterogeneity of the skin structure that facilitates at least two potential pathways (e.g, polar and non-polar). Many scientists have designed mathematical models on the basis of two penetration layers; (i) non-viable lipophilic *stratum corneum* and (ii) viable hydrophilic layer that allows the consideration of non-polar and polar pathways (Anissimov and Roberts, 2009; Chien et al., 1989).

1.6.2 *In vitro* methodology

Several *in vitro* techniques have been used to study drug skin delivery and localisation within different skin layers. These models are used to measure the penetration of agents through the skin membrane into a fluid reservoir. They also help to cost-effectively screen several of formulations in a short period of time (Bronaugh and Maibach, 1989). By employing *in vitro* studies, where appropriate conditions are used, it is expected to achieve a decent correlation between *in vitro* and *in vivo* studies (Hadgraft et al., 1993). Normally the test compounds in an *in vitro* study are applied to the surface of the skin which is sandwiched between donor and receiver compartments. The amount of compound that penetrates the membrane is measured in the receiver fluid as a function of time. An infinite or finite dose of the test compound is applied depending on the experimental requirements (OECD, 2004). All these models are designed at a constant pressure (e.g., atmospheric).

The use of Franz diffusion cell (Figure 3.3) to measure skin permeability is one of the most frequently used *in vitro* systems, which provides key information about the skin-drug interactions and formulation (Franz, 1975, 1978). It is normally used with human or animal skin. Although, synthetic membranes can be used when the biological membranes are not accessible. However, sometimes in preliminary experiments synthetic membrane are used to mimic the biological skin and for formulation quality control (Twist and Zatz, 1988, 1986; Corbo, 1993). Biological

and synthetic membrane can be mounted on the Franz cell and separate the donor from the receiver compartment. While using biological membrane, it is important to place the *stratum corneum* in contact with the donor compartment. Moreover, the receiver compartment temperature has to keep at 37°C to provide the temperature of 32°C on the skin surface to mimic the biological skin condition. Additionally, the receiver fluid must be kept homogenous using a stirring bar. The fluid in the receiver compartment is taken at predefined time intervals and replaced with the same volume of a fresh fluid (Franz, 1975).

The solubility of the test compounds is an important factor, since it can affect the sink capacity sampling frequency as well as the receiver compartment size. The receiver compartment size controls interference when receiver fluid reaches a specific degree of saturation (Brain et al., 1998).

The barrier integrity of the membrane can be assessed through capacitance measurement. This value specifies the capability of the membrane to separate electrical charge (Holmgaard and Nielsen, 2009).

1.6.3 *In vivo* methodology

In vivo models provide a useful information regarding the influence of the cutaneous blood flow when agents penetrate into the skin (Godin and Touitou, 2007). In this method, the formulation is applied at a predetermined time intervals into the same skin area and the cutaneous absorption is estimated through measuring the amount of drug within the skin layers and/or in the urine or blood. These data can help to estimate the systemic bioavailability of the drug and/or its metabolites in the blood or urine (Akrill et al., 2002; Roberts and Cross, 1999; Brooke et al., 1998).

One of the commonly used *in vivo* methods to determine the pharmacokinetics of cutaneous absorption is microdialysis. This method employs a semi-permeable dialysis membrane in a microdialysis probe, implanted into the dermis of the desired skin area to determine absorption. The probe is gradually perfused with physiological solution, which imitates the blood circulation (Kreilgaard, 2002; Schnetz and Fartasch, 2001; Morgan et al., 2003). The microdialysis avoids reference exposure,

facilitates the investigation of skin metabolism and allows different sampling areas to be examined simultaneously. However, this method is not practical for the investigation of larger compounds or those with several protein-bound compounds, due to the low recovery percentage. Moreover, the insertion of the probe may cause skin sensitivity that can affect the skin absorption process (Kezic, 2008).

In this PhD the *in vivo* studies were not performed due to the time frame of the project. However, this could be investigated in a future project using hypobaric pressure.

1.7 Strategies to enhance percutaneuos drug delivery

In this PhD thesis, hypobaric pressure as a new skin delivery enhancement method will be investigated. In order to investigate this newly developed method, it is important to review the available percutaneous drug delivery strategies. Often the challenging area in the skin delivery is to overcome the *stratum corneum* barrier and accomplishing a suitable balance between an effective drug delivery strategy and its safety issues. Normally, this involves targeted localisation of the compounds, which is not easy to achieve utilising a delivery strategy that is cost-effective and easy to administrate for the patients (Prausnitz and Langer, 2008). Several common enhancement methods have been described in the following sections to contemplate the place of hypobaric pressure method within the other strategies. These methods can be divided into two categories: passive and active methods (Alexander et al., 2012).

1.7.1 Passive methods

Supersaturated systems

A supersaturated solution is achieved when the amount of drug dissolved in an environment surpasses its equilibrium solubility. These solutions permit an escalation in the driving force by increasing the concentration of the compound in the vehicle solution. To produce a supersaturated solution and overcome its

long-term stability problem, various techniques have been used including (i) mixed co-solvents (i.e. propylene glycol and water) with antinucleant polymers to prevent or delay crystallisation and (ii) controlled modifications in drug concentrations as a result of solvent evaporation (Pellett et al., 1997; Morgan et al., 1998; Lane et al., 2012; Naik et al., 2000; Jones et al., 2009; Benaouda et al., 2012).

Chemical penetration enhancers

Chemical penetration enhancers are pharmacologically inactive agents that can temporarily reduce the barrier properties of the *stratum corneum*. They work by modifying the drug partition and diffusion into the *stratum corneum* (Suhonen et al., 1999).

These enhancers are reported to increase permeation through intracellular (protein modification) and intercellular (lipid bilayer interaction) permeation routes (Barry, 1991, 2001). They can interact with the lipid polar headgroups through forming H-bonding and/or ionic forces, which results in the hydration spheres of the lipid bilayers, or diffusion between the hydrophobic lipid tails (such as terpenes). These mechanisms can manipulate the lipid packing, which increases the lipid fluidity and promotes drug-skin permeability. Moreover, disturbance in the lipid structure can occur when the chemical enhancer forms pools in the skin, due to their structure (polar head and long saturated alkyl chain i.e., oleic acid), promoting the drug to permeate quicker either via them or the defects between the pools and the lipids order (Figure 1.7A). Other chemical enhancers increase the skin permeability through extracting the skin lipids (i.e., ethanol) (Lane et al., 2012; Ongpipattanakul et al., 1991).

Chemical enhancers can also affect the proteins in the *stratum corneum*. For example, intracellular keratin modification can cause swelling that enhances skin hydration (Figure 1.7C). They can also influence the desmosome in corneocytes (Figure 1.7B).

Another mechanism in which chemical enhancers modify drug permeation, is by changing the drug or co-solvent partitioning into the *stratum corneum*, for example, propyleneglycol and ethanol (Hadgraft, 1999).

Finally, chemical enhancers improve the thermodynamic activity of the vehicle or encourage the solubilisation of the drug in the vehicle (Williams and Barry, 2012).

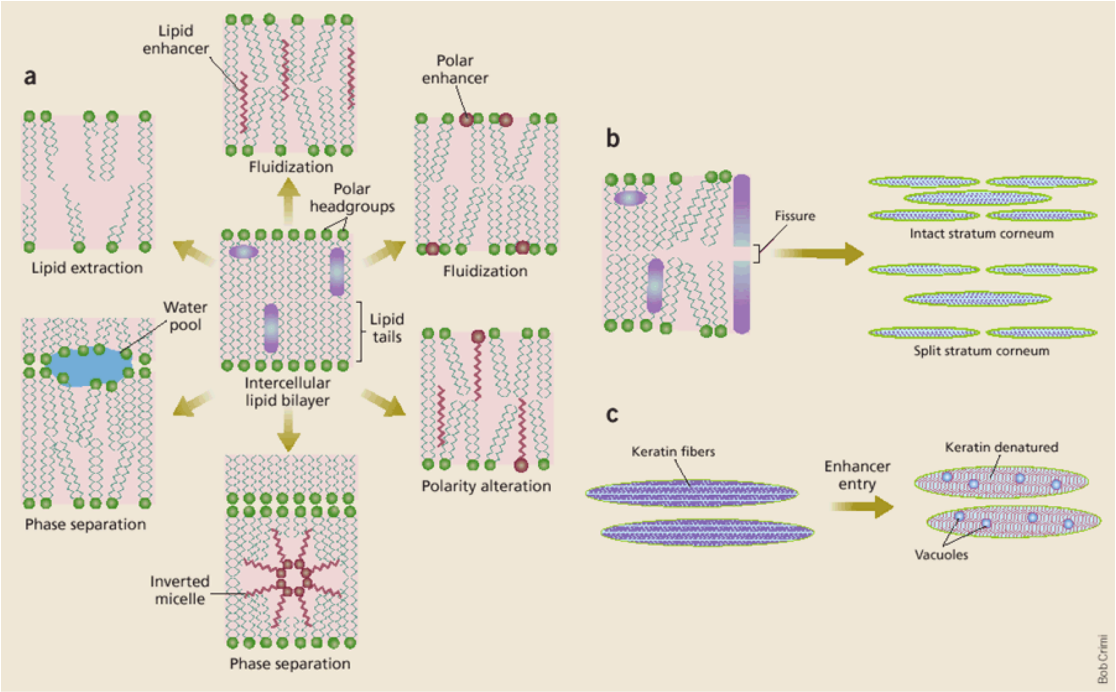

Figure 1.7: Mechanisms of action of chemical penetration enhancer with the intercellular lipids (A), desmosomes and protein structures (B), and with corneocytes (C), taken from (Barry, 2004).

Nanocarrier systems

Nanotechnology provides a new opportunity in drug delivery. Nanotechnology in skin delivery can be defined as the method that allows the delivery of a encapsulated active within a range of nanometre sizes. Nanoparticles mainly rely on their submicron size and large surface-to-volume ratio to offer advantages (Singh and Lillard Jr, 2009). In this PhD, different types of nanocarriers were employed to testify the influence of hypobaric pressure; solid lipid nanoparticles, liposomes and polymer nanoparticles.

Solid lipid nanoparticles

Solid lipid nanoparticles are smaller than μm in size (Schwarz et al., 1994; Müller et al., 2000). The lipid phase normally consists of fatty acids, partial glycerides steroids and wax. However, an emulsifier, such as Polysorbate 80, Poloxamer 188, polyglycerol methylglucose distearate, saccharose fatty acid esters and lecithin (Schäfer-Korting et al., 2007) is required to stabilize these particles. Solid lipid nanoparticles are commonly manufactured through high pressure homogenisation or precipitation of a microemulsion formation. The homogenisation method utilises hot and cold techniques (Müller et al., 2000, 2002; Bunjes and Koch, 2005; Mehnert and Mäder, 2012; Santos Maia et al., 2002). In the hot homogenisation technique, the lipid melt is dispersed over a hot surfactant solution using high-speed stirring. The obtained pre-emulsion is passed through a high pressure homogeniser to generate a hot oil-in-water nanoemolsion. The lipid recrystallizes to form solid lipid nanoparticles as the hot nanoemulsion temperature is dropped down to room temperature. It is important for lipids (i.e., glycerides) with a low melting point (close to room temperature) that the nanoemulsion must be cooled to lower temperatures to begin recrystallization. The hot homogenisation technique is an appropriate option for temperature sensitive compounds, when the hot temperature exposure time is comparatively short (Müller et al., 2000).

The cold homogenisation technique is a suitable option for manufacturing solid lipid particles with extremely temperature-sensitive and/or hydrophilic compounds, which could partition from the melted lipid phase to water through a hot homogenisation method (Müller et al., 2002). In the cold method, the melted lipid (including the drug) is cooled, and then crushed to microparticles that are then dissolved in a cold surfactant solution to produce a pre-emulsion. At this point, the pre-emulsion is homogenised into solid lipid nanoparticles at a temperature close to room temperature. As homogenisation results in an increase in the temperature, the difference between the lipid melting point and the homogenisation temperature must be significant enough to evade melting of lipid in the homogeniser.

In the micro-emulsion method for producing solid lipid nanoparticles, the melted lipids and the surfactant solution aqueous phase requires to be at the same temperature. Commonly used surfactant and co-surfactant are bile salts, lecithin and alcohol (i.e., butanol). The oily phase and the aqueous phases are mixed at an appropriate ratio to produce a micro-emulsion, then cool down in a cold aqueous medium (approx. 2-3 °C) using constant mechanical starring, to make sure that nanoparticles are shaped by precipitation (Gasco, 1997). Another method for producing solid lipid nanoparticles is precipitation method (Sjöström et al., 1993). In this method, lipids are dissolved in an organic solvent then the aqueous phase is added to provoke emulsification (Siekmann and Westesen, 1996). Finally, the organic solvent evaporates and lipid precipitates produce the solid lipid nanoparticles. The disadvantage of employing this technique is using organic solvents.

Application of solid lipid nanoparticles have shown to improve the transdermal delivery of some drugs. For instance, particles containing, soybean lecithin, tristearin glyceride and polyethylene glycol 400 stearate enhanced the permeation of triptolide by 3-fold in contrast with the simple application of triptolide (Mei et al., 2003).

Solid lipid nanoparticles have been manufactured in a broad range of application, they showed to be beneficial for transdermal delivery, due to their unique characterisations for maintaining the drugs on the *stratum corneum* layer. Moreover, their ability to form an occlusive adhesive film on the skin upper layers help to maintain the stability of the drug (Müller and Dingler, 1998; Wissing and Müller, 2001; De Vringer and De Ronde, 1995; Zhai and Maibach, 2001; Wissing and Müller, 2003*b*).

Liposomes

Liposomes are formed of surfactant, phospholipids and block copolymers; the application of these carriers have been shown to be a useful technique for enhancing drug delivery through the skin (Kawasaki and Player, 2005). The capability of liposomes to attract both lipophilic and hydrophilic compounds facilitates a broad range of drugs to be encapsulated by these carriers (e.g., DNA, imaging agents and proteins (Allen and Cullis, 2004; Lasic, 1995). The application of liposome

nanoparticles in transdermal drug delivery offers many advantages linked to their capacity for a flexible self-assembly, administered by a number of soft interactions that control colloidal stability of actives in bioenvironments, therefore avoiding undesirable tissue and cellular uptake (Sackmann, 1995; Gutberlet and Katsaras, 2001; Israelachvili, 1985; Romero and Morilla, 2013; Moghimi et al., 2001). Liposome properties can be readily manipulated, for example, their size, charge, morphology, interaction of the surface with polymers and ligands and lipid composition. These properties have the capability to control their colloidal stability and biological fate (Lombardo et al., 2016).

Phospholipids are normally contain of one hydrophilic head and two hydrophobic tails. According to the configuration of the phospholipids, liposomes can be positive, negative or neutral. Once phospholipids are dispersed in water, they aggregate impulsively into bilayers, which look like the structures they produce in biological membranes. The ultimate structure, morphology, and physicochemical properties of lipid-based liposomes are varied based on the nature, geometry and size of their lipid components, concentration, surface charge and temperature (Romero and Morilla, 2013; Moghimi et al., 2001; Aharon et al., 2011; Obata et al., 2010; Lombardo et al., 2015).

The size of liposomes used in therapeutic applications is between 50 to 500 nm (Moghimi et al., 2001). The release rate of drug from these carriers is highly dependent on the phospholipid bilayers that the drug has to diffuse through during release. In general, the larger multilamellar lipid particles are easier to make and have a better entrapped volume compared to this better drug loading unilamellar lipid carriers. Unilamellar liposomes demonstrate a quicker drug release rate than multilamellar liposomes (Lombardo et al., 2016).

Polymer nanoparticles

Polymeric nanoparticles are defined as sub-micron (approx. 1 to1000 nm) colloidal particles comprising agents encapsulated within or adsorbed to macromolecular compounds (polymer) (Kreuter, 2014). They can be classified into natural and

synthetic polymers based on their source (Rytting et al., 2008). Polymeric nanoparticles can be synthesised through dispersion of preformed polymer or monomer polymerisation (Rao and Geckeler, 2011). polymeric nanoparticles have a greater encapsulation efficiency and a better storage stability in contrast with lipidic nanocarriers (Andrade et al., 2011).

Polymer nanoparticles that encapsulate fluorescent dye with size range between 50 to 300 nm have attracted attention in recent years. Due to their unique properties and nanoscale size distribution. Different technique has been developed to synthesis polystyrene nanoparticles for example, emulsion polymerisation, emulsifier free polymerisation, precipitation polymerisation and dispersion polymerisation (Lu et al., 2010; Lin et al., 1999; Eshuis et al., 1991; Waich et al., 2010).

Dye-loaded polystyrene nanoparticles are commonly used in various fields of technology such as ceramics manufacturing, paint coating and recently in biomedical procedures. For example, diagnostics, controlled drug release, bioaffinity chromatography biomolecule adsorption, and phagocytosis investigation (Reese and Asher, 2002; Radomska-Galant and Basinska, 2003; Gonzalez et al., 2008; Pirogov et al., 2003; Kakabakos et al., 1990; Tuncel and Piskln, 1991).

1.7.2 Active methods

In the active methods of transdermal drug delivery, external energy is used as driving force to decrease the barrier function of the *stratum corneum*. These manipulations involve the application of several forms of energy (i.e., heat and electrical), or breaking, reducing, or weakening the *stratum corneum* barrier by mechanical forces (Brown et al., 2006).

Electrical assisted methods

Electrical assisted methods include iontophoresis, electroporation and sonophoresis. Iontophoresis (Figure 1.8) is a noninvasive technique that uses a small electric current to assist the diffusion of ionic molecules through the skin. It is mainly applicable for ionic and polar compounds for example, peptides that are problematic to across the

skin under normal conditions (Grice et al., 2012). This method uses two electrodes submerged in a solution containing the drug. By applying voltage through the electrodes, drug molecules (charged ions) start to move from the electrodes into the skin (Guy et al., 2000). Iontophoresis enhances the delivery of drug through the skin via three mechanisms: electrorepulsion of charged solutes by the electrode, electroosmotic effects on unionised, polar molecules and permeabilisation of the skin by the electric current (Naik et al., 2000; Grice et al., 2012).

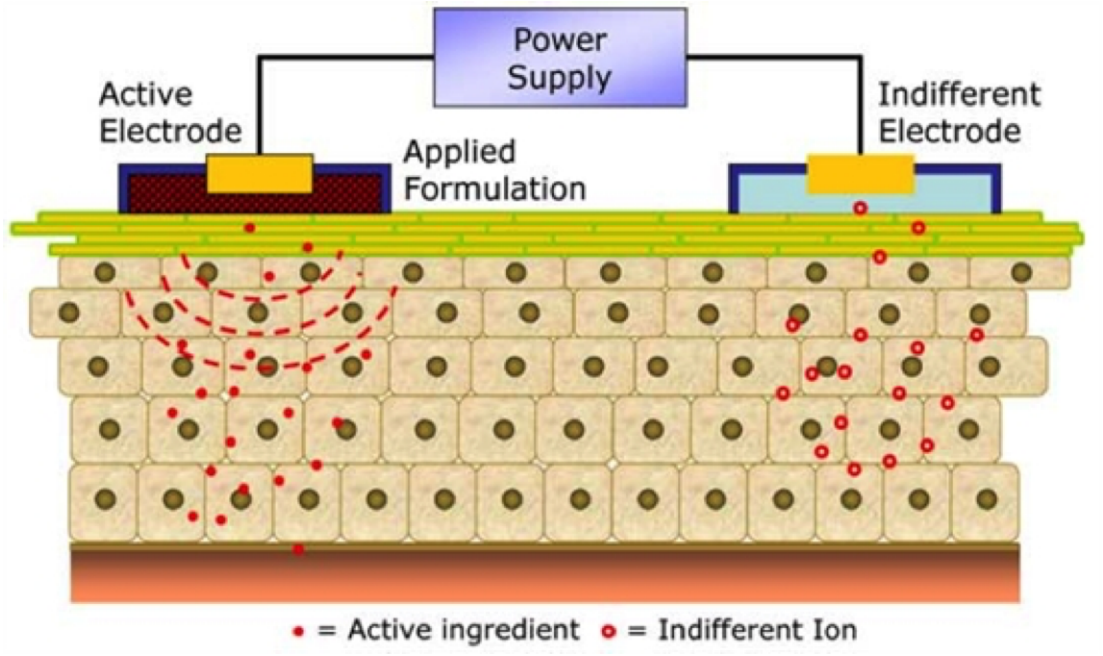

Figure 1.8: Graph representing transdermal drug delivery by iontophoresis (Daniels, 2004).

In the electroporation (Figure 1.9) technique, a high electrical voltage (> 50V) is applied to the skin for a very short period of time, which results in a formation of aqueous pores (less than 10 nm) on the *stratum corneum*. The advantage of this technique for transdermal delivery is, it can be applied to different range of compounds, due to a lack of restrictions on the molecule size, lipophilicity and charge (Grice et al., 2012; Denet et al., 2004).

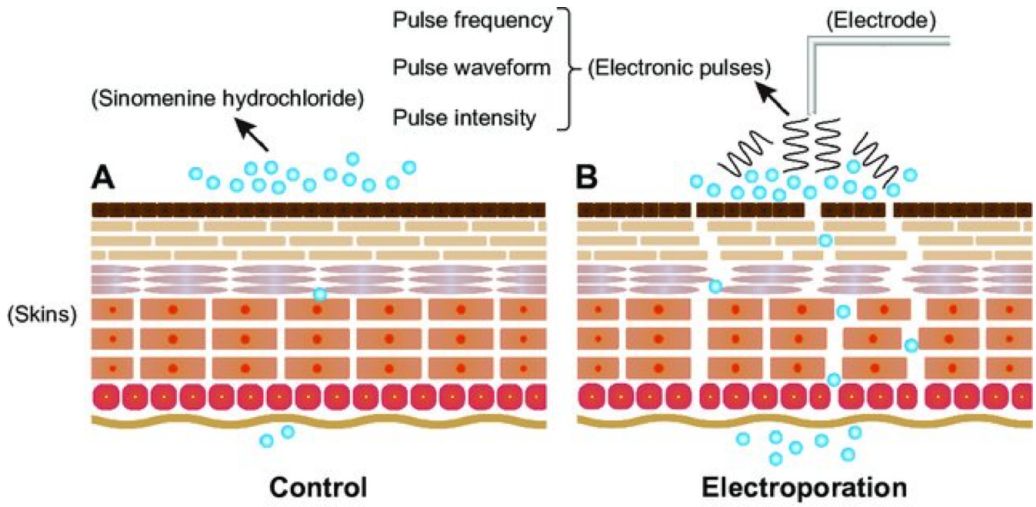

Figure 1.9: The mechanism of electroporation enhancing transdermal delivery of sinomenine hydrochloride; A) control and B) The intercellular intervals and epidermal cracks of skin were increased after the electroporation stimulation (Feng et al., 2017).

Sonophoresis (Figure 1.10) uses ultrasound energy to enhance the permeation of drug through the skin. A low-frequency of ultrasound (less than 100 kHz) can manipulate the lipid bilayer of *stratum corneum* via several mechanisms. For example, cavitation, which cause formation of gas bubbles through small hydrophilic channels in the *stratum corneum*, increase the temperature and pressure vibration (Joshi and Raje, 2002). This method has been used for enhancing the transport of drugs, macromolecules, oligonucleotides, DNA and vaccines (Smith, 2007)

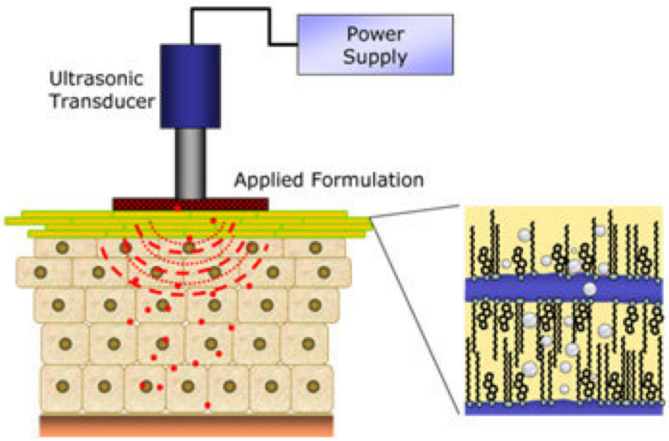

Figure 1.10: Schematic expression of drug delivery facilitated by sonophoresis (Daniels, 2004).

Mechanical methods

Microneedle arrays are minimally-invasive devices that are used to penetrate the skin (Donnelly, Singh, Morrow and Woolfson, 2012; Larraneta et al., 2016; Prausnitz, 2004). This system uses small micron-sized needles as a mechanical approach to by-pass the *stratum corneum*, generating micro-channels in the skin, to facilitate drug delivery at a desired depth (Tanner and Marks, 2008). Microfabrication methods have been designed for metal, silicon, polymers, and sugar-based microneedle, containing solid and hollow bores with various geometries and dimensions. There are four main techniques for skin drug delivery using microneedles (Figure 1.11): 1) hollow microneedles, in which drug in form of solution is active and passively administrated via the bore of microneedles (poke and flow technique), 2) solid microneedles, which pierce the skin, prior to the application of a patch (poke and patch technique), 3) polymeric microneedles, in which the drug encapsulated (dissolving or porous microneedles), for a controlled drug release (poke and release technique), and 4) drug coated microneedles, that insert them into the skin for drug release via hydration of the coating (coat and poke technique) (Bouwstra and Ponec, 2006; van der Maaden et al., 2012). Microneedles have been used to facilitate the transdermal delivery of drugs, proteins, and particles in an easy and pain-free way, as they do not enter the papillary dermis where the nerve endings are placed (Tanner and Marks, 2008). Although the safety issues regarding to the self-administration may be a disadvantage of this method of drug delivery (Liu et al., 2012).

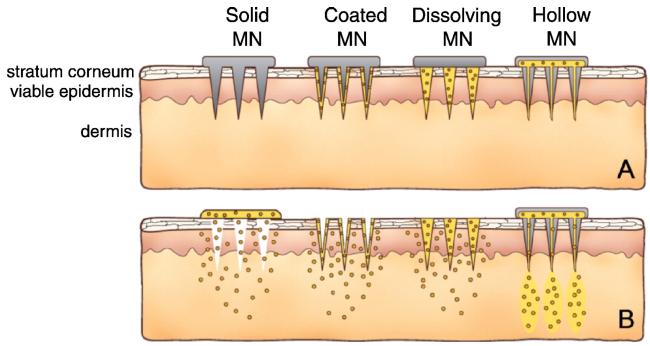

Figure 1.11: Techniques of drug delivery to the skin using microneedles (MN). A) first administrated to the skin B) then used for drug delivery (Kim et al., 2012).

Moreover, a relatively new type of microneedle is made of hydrogel-forming materials(Figure 1.12). This type of microneedle arrays was first introduced by (Donnelly, Singh, Garland, Migalska, Majithiya, McCrudden, Kole, Mahmood, McCarthy and Woolfson, 2012; Woolfson et al., 2009). This technique the skin drug delivery is controlled by the crosslink density of the hydrogel system instead of the *stratum corneum*. One of the most important advantage of using this novel technique in contrast with the traditional microneedle, is to avoid the need for patient hospitalization, which is essential in infusion dosing (Donnelly, Singh, Garland, Migalska, Majithiya, McCrudden, Kole, Mahmood, McCarthy and Woolfson, 2012).

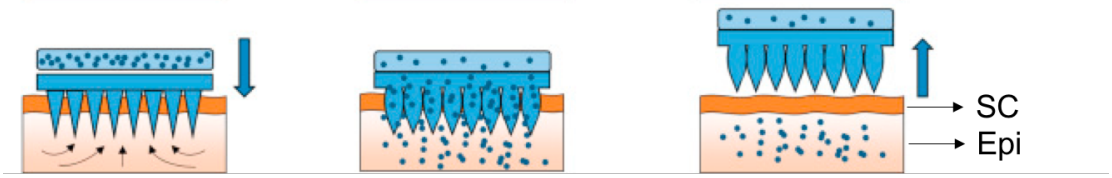

Figure 1.12: A schematic representation of hydrogel-forming microneedles (Larraneta et al., 2016).

Needleless jet injectors (Figure 1.13) are a painless method to substitute traditional needle injection. They overcome the resistance of the *stratum corneum* through propel powders or liquids at high velocity into skin. It has been mainly used in the transdermal delivery of larger compunds (e.g., proteins and peptides) (Benson and Namjoshi, 2008).

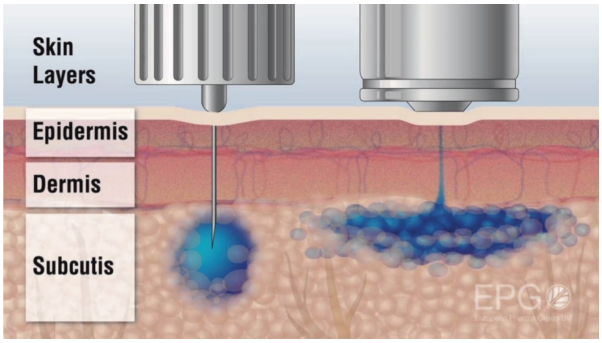

Figure 1.13: The transdermal delivery of insulin after injection with a needle, and a contemporary jet injector. Insujet^{TM} (Courtesy of the European Pharma Group).

Microdermabrasion (Figure 1.14) is a skin resurfacing technique (Koch and Hanasono, 2001). It was first introduced in 1985 in Italy. In this technique, the main intention is to scrape the skin mechanically. The microdermabrasion device works by dragging the skin into a handpiece with a suction tube. Simultaneously, a second tube deposits aluminum oxide crystals into the skin, to cause a mild mechanical abrasion. Then, the crystals and skin debris are extracted from the skin via suction tube into the waste container (Spencer, 2005). Following the microdermabrasion impact on the skin, it may increases the substances penetration through the skin by reducing the *stratum corneum* thickness (Grice et al., 2012; Prausnitz and Langer, 2008).

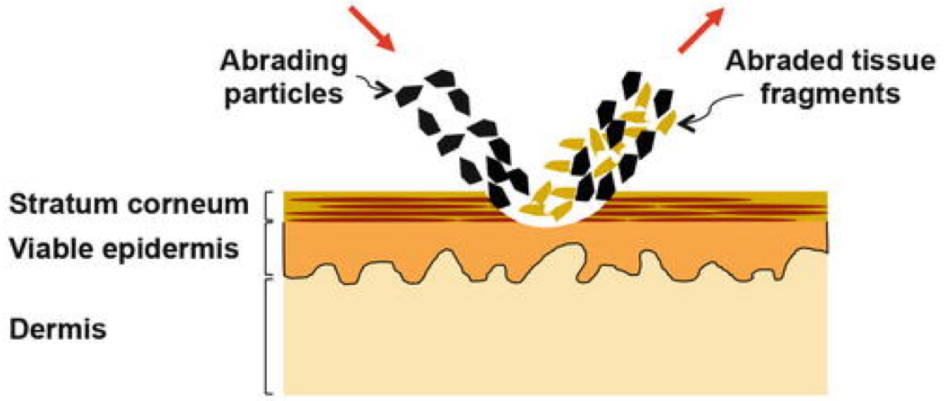

Figure 1.14: A schematic representation of the microdermabrasion procedure (Gill, 2017).

Tape stripping (Figure 1.15) is a method for topical delivery studies. In this method *stratum corneum*, which is the skin main barrier is removed. Tape stripping is useful in both *in vitro* and *in vivo* studies. The amount of *stratum corneum* removed by a tape strip depends on several factors. Such as anatomical site, age and race. It can influence the size of the corneocytes, the number of cell layers in *stratum corneum*, the thickness of *stratum corneum* and the arrangement and amount of lipids in this layer. Other factors that can affect *stratum corneum* removal include the type of adhesive tape, the application pressure onto the skin, the duration of the pressure, the removal force and the vehicles used (Zhao et al., 2010).

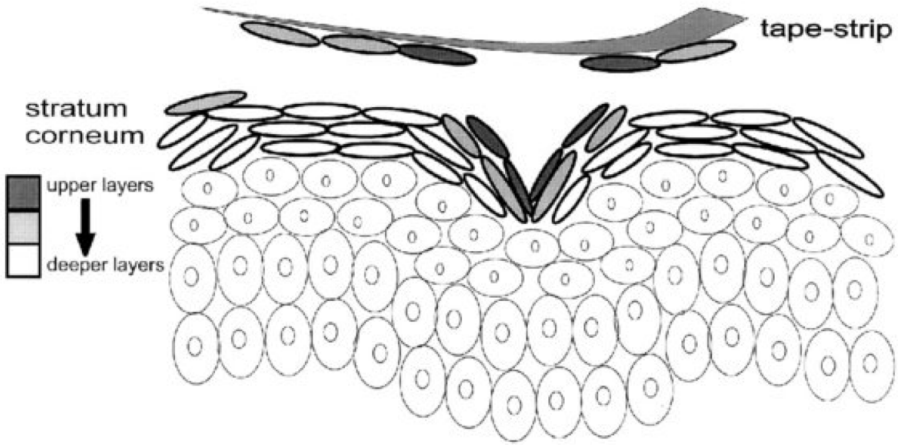

Figure 1.15: Schematic drawing of the tape-strip technique (Van der Molen et al., 1997).

Hypobaric pressure

The application of pressure has been shown to offer a potentially non-invasive and simple technique of enhancing percutaneous delivery (Brown et al., 2006). It is believed that the enhancement is linked to the increase in transcutaneous flux to either an enhanced the permeation thorough the transappendageal pathway or an improved in the partition of the compound within the *stratum corneum* under the influence of pressure fluctuation (Treffel et al., 1993).

Moreover, the application of local hypobaric pressure can modify the mechanical and physiological structure of the skin. For example, enlargement of the follicular infundibula, reduced corneocyte size and skin thinning. Moreover, the application of hypobaric pressure can increase the haemodynamic response (i.e., blood circulation) (Inacio, 2015). The use of hypobaric pressure to deliver compounds percutaneously is a promising approach. However, further investigation is required, which will be covered in the subsequent chapters.

The few studies that have investigated how the application of pressure (either hypobaric or hyperbaric) can influence the skin properties suggesting that it may be useful to enhance drug permeation into the skin. For example, the application of hypobaric pressure (0.25 bar) has been shown to increase the permeation of caffeine

by 1.8-fold (Treffel et al., 1993). Another study reported that the application of hypobaric pressure (500 mBar) caused a reduction in epidermis thickness and caused blood vessels enlargement in the dermal layer (Childers et al., 2007). Furthermore, suction cups, which generate 400-600 mBar hypobaric pressure, were reported to significantly increase transepidermal water loss (Pedersen and Jemec, 2006). Finally, in a more recent study on tetracaine, diclofenac diethylamine and aciclovir, hypobaric pressure was shown to modify the percutaneous penetration of these agents through enlargement of the follicular infundibula, reduction in corneocyte size and reduction in skin thickness (Inacio, 2015). Although, further investigations were required to assess the influence of hypobaric pressure on a wider range of compounds.

1.8 Limitations of current enhancement methods

Due to the selective characteristic of the skin barrier, only a small number of compounds can be delivered into the skin effectively (Paudel et al., 2010). Expanding the availability of novel percutaneous delivery methods that include a wider range of compounds is desirable. Currently, several approaches provide considerable enhancement in the rate of delivery of therapeutic compounds through the skin. However, the improvement, in skin delivery to-date can still be further expanded. Therefore, novel percutaneous delivery methods should be further examined in this field.

1.9 Aim and scope of this thesis

The whole human body can be exposed to hypobaric pressure fluctuations both totally (i.e., the entire body) and locally (i.e., use of suction in a small area). For instance, pressure fluctuation on commercial flights (hypobaric pressure of approx. 850 mBar vs. atmospheric pressure of 1010 mBar) (Muhm et al., 2007) are well tolerated. Physiological alterations in blood flow and respiration during hypobaric pressure fluctuation has been studied, but the consequences of these alterations at a local level has had little investigation. Therefore, in this thesis various compounds with different size and physicochemical properties have been investigated to understand how different compounds can be influenced in terms of the permeation using hypobaric pressure.

The aim of this project was to investigate if the application of topical hypobaric pressure, a new physical technique to enhance topical drug delivery, could be used to enhance drug delivery of various range of compounds into the skin without skin damage.

In order to fulfil the aim of this thesis; in the first experimental Chapter three analytical methods for the determination of minoxidil, (FITC)-dextran and the probes encapsulated in the nanocarriers were verified. In the second experimental Chapter, the influence of hypobaric pressure upon the delivery of minoxidil was investigated. In the third experimental Chapter, the influence of hypobaric pressure on the permeation of macromolecules (4 - 150 kDa) was assessed. In the final experimental Chapter, the influence of hypobaric pressure on the percutaneous delivery of nanomaterials into the skin was investigated.

2

Analytical method development

2.1 Introduction

To study the effect of local hypobaric pressure changes upon drug penetration, three model systems were selected: a small molecular weight drug, a series of marcomolecules and a range of nanoparticles. Minoxidil (an anti-alopecia drug) was used as a model small molecular weight compound that diffuses through the skin via the follicular route (Grice et al., 2010). A series of (FITC)-dextrans of increasing molecular weight (4, 10, 70 and 150 kDa) were used as model macromolecules because these fluorescent permeants allow both the quantification of skin deposition and visualisation of localisation in the skin using fluorescence spectroscopy. The third model system was nanocarriers (solid lipid nanoparticles, liposomes and polystyrene microspheres), which can be made of different materials. These nanoparticles can be fabricated to display different surfaces properties. The strategy of using a diverse series of model penetrants to investigate the ability of a methodology to enhance membrane penetration has been reported in previous studies (Guy and Hadgraft, 1988; Aungst et al., 1990). For instance, to investigate the skin permeation enhancement of a high velocity injection, a group of peptides, proteins and oligonucleotides were studied (Burkoth et al., 1999). In other work to study the influence of a erbium:YAG laser in transdermal drug delivery, indomethacin and

nalbuphine were utilised due to their differences in lipophilicity (Lee et al., 2008). Comparing different model penetrates widens the scope of knowledge on how novel methods enhance skin delivery, by revealing links between the physicochemical properties of the penetrants and their delivery enhancement.

Minoxidil (see Table 2.1 & 2.2) is the only available drug approved by the FDA for the treatment of male and female hair loss. Various studies have confirmed its success in reversing the progressive miniaturization of hair follicles linked to alopecia (Messenger and Rundegren, 2004). However, minoxidil shows limited skin penetration. Consequently, patients must apply this pharmaceutical formulation at least twice a day to achieve a pharmacological effect (Gelfuso et al., 2011). Hence, there is room for the development of novel delivery strategy for the topical treatment of hair loss using minoxidil.

Dextrans (see Table 2.1) are highly hydrophilic polysaccharides that are commercially available in different sizes (from 3 to 2000 kDa). The dextran molecule is often used as a model for proteins as it is chemically very stable. Furthermore, it can be linked to fluorescein isothiocyanate (FITC) (see Table 2.2). Dextrans typically show poor skin penetration owing to their high molecular weight and hydrophilicity, but it is commonly used to understand new strategies to enhance skin delivery because its entry into the skin indicates penetration enhancement strategy success (Yan et al., 2010).

The use of nanocarriers in consumer products have increased in the recent years (Kessler, 2011). In addition to their increased use, they have increased in complexity (Buzea et al., 2007). For example, in the 1990's nanosized zinc oxide and titanium were employed in sun protection and cosmetic products to shield human skin against UV radiation (Suzuki, 1987). More recently, silica and fullerenes have been introduced into cosmetic products for the same purpose (Contado, 2015; Xiao et al., 2006). Inorganic nanomaterials find it difficult to penetrate intact skin (Watkinson et al., 2013), but several studies suggest that the newer nanocarriers are able to penetrate through the skin, depending on their size, material, and charge (Fernandes et al., 2015).

2. Analytical method development

Nanocarriers could penetrate the skin, depending on their size and chemical properties via one of three routes: intracellularly via corneocytes, intercellularly around corneocytes, or through hair follicles (Baroli et al., 2007). Methods for tracking nanocarriers in biological environments such as skin include, X-ray diffraction, radioactivity, fluorescence spectroscopy (Cartier et al., 2007) and scanning electron microscopes (SEM). Fluorescence spectroscopy is preferred in terms of its cost, simplicity and sensitivity (Gul et al., 2009). A fluorescence marker can be encapsulated in a nanoparticle matrix or it can be chemically linked to the particle to track the nanoparticles in the skin (Gul et al., 2009). Chemical linkage is preferred as it generates a more robust method. However, the linkage may affect the physicochemical properties of the nanocarrier. Encapsulation of the fluorescence marker is feasible, but the markers should have a high affinity for the particle matrix and be resilient to leakage.

To study the effect of hypobaric pressure on these three model agents, analytical methods were required to track their entry into the skin. The literature documents several methods for the quantitative assay of minoxidil, i.e., UV spectrophotometry (Zaheer et al., 2012), RP-HPLC (Siddiraju and Sahithi, 2015), stability indicating HPLC (Vairale et al., 2012), electrochemical determination (Pfaffen and Ortiz, 2006) and a voltammetric method (Ahmadi et al., 2012). More specifically, minoxidil has been previously detected using HPLC and UV with a limit of detection (LOD) and limit of quantification (LOQ) of 0.05 μg.mL^{-1}, 0.18 μg.mL^{-1} and 0.19 μg.mL^{-1}, 0.63 μg.mL^{-1} respectively (Zhao et al., 2010). Elsewhere, minoxidil determination in human plasma was successful using HPLC with electrochemical detection. The method was specific and sensitive with a LOD of 500 pg.mL^{-1}, however, the method failed to differentiate between minoxidil and minoxidil sulphate due to rapid autohydrolysis of minoxidil sulphate to minoxidil (Carrum et al., 1986). Another study, for determination of minoxidil in human serum used an ion-pair revered-phase HPLC method. The ion-pair method reported a LOD of 50 pg, which was 3-5 times more sensitive than the data obtained with UV-spectrophotometry (Golden and Zoutendam, 1987). Although, several methods have higher sensitivity, HPLC-UV

detection of minoxidil was considered the most appropriate technique for skin penetration studies because it was considered relatively inexpensive, rapid and more practical compared to the other aforementioned methods.

(FITC)-dextran quantification has previously been reported using fluorescence spectroscopy (Lee et al., 2008; Fujiwara et al., 2005; Ohkuma et al., 1982). According to Inacio et al. (2016) the fluorescence LOD and LOQ of 4 kDa and 10 kDa were 0.027 μg.mL^{-1}, 0.089 μg.mL^{-1}, 0.77 μg.mL^{-1} and 0.258 μg.mL^{-1} respectively. Fluorescence spectroscopy is inexpensive and the most commonly used analytical method for detection of dextran.

The quantification of nanocarriers is normally achieved via a probe encapsulated in the nanocarriers core. Nile red (see Table 2.2) was chosen, as a particle probe for solid lipid nanoparticles and vitmine E liposomes, because it has a hydrophobic character with a high affinity for the nanoparticle lipid matrix (Chana et al., 2015; Greenspan and Fowler, 1985; Jose and Burgess, 2006). This was important for future permeation studies in Chapter 5. In addition, FluoSpheres commercially manufactured polystyrene particles, loaded with a proprietary probe (see Table 2.2), which used polymer particles typically show little or no photobleaching (ThermoFisher, 2018). To quantify the amount of probe it was necessary to measure their chemical stability during the course of experiment. Detection and quantification of nile red can be achieved using fluorescence spectroscopy. Therefore, it was important to develop a fit for purpose assay. In a previous study, LOD and LOQ of nile red were reported to be 0.002 μg.mL^{-1} and 0.006 μg.mL^{-1} respectively (Chana et al., 2015). Fluorescence spectroscopy data based on the literature indicated that the sensitivity of the assay would be insufficient for suspension loading determination and for subsequent experiments.

The aim of this Chapter was to demonstrate that three analytical methods for the determination of minoxidil, (FITC)-dextran and the probes encapsulated in the nanocarriers were 'fit for the purpose' in terms of their intended use in the experimental work described in subsequent chapters of this thesis.

Table 2.1: Physicochemical properties of the model penetrators.

Penetrate	Size (nm)	Structure	Charge
Minoxidil	1.18	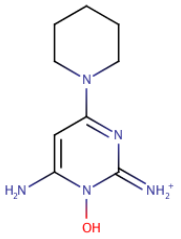	+ve
Dextran 4,000 - 150,000 Da	$\sim$ 1.4 - 8.5	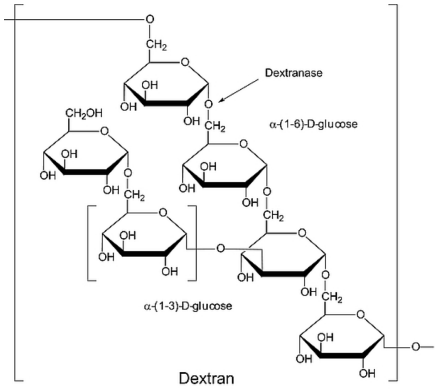	Neutral
Solid lipid nanoparticle	$\sim$ 50	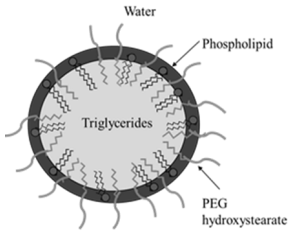	Neutral
Vitamin E liposome	250 - 350	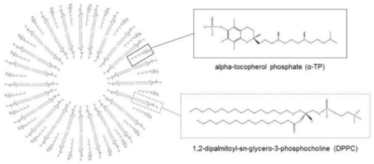	-ve
FluoSpheres polystyrene	100 - 1000		Neutral

Table 2.2: Summary of model drug/probes properties.

Active model/probe	Structure	Hydrophilicity	Analytical method
Minoxidil	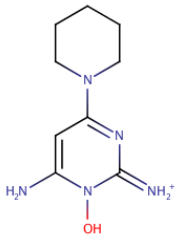	Hydrophobic (pH 7.4)	HPLC-UV
FITC (dextran probe)	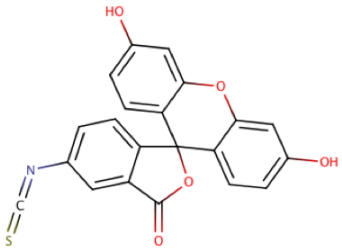	Hydrophobic	Fluorescence spectroscopy
Unknown red dye (polystyrene probe)	patented information	Hydrophobic	Fluorescence spectroscopy
Nile red (SLN & liposome probe)	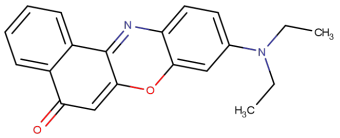	Hydrophobic	Fluorescence spectroscopy

2.2 Materials

Methanol and water both HPLC grade were purchased from Fischer Scientific (Leicestershire, UK). Minoxidil was purchased from Alfa Aesar (Heysham, UK), the stationary phase, a Gemini C18 column (5 μm, 250 mm $\times$ 4.6 mm) was obtained from Phenomenex (Macclesfield, UK), nylon filter papers (0.20 μm) were supplied by Whatman (Kent, UK). FTIC-dextran with average molecular weight of 4 kDa (FD-4), 10 kDa (FD-10), 70 kDa (FD-70) and 150 kDa (FD-150), used without any further purification steps, were supplied by Sigma-Aldrich (Dorset, UK). Nile red was purchased from Sigma-Aldrich (Gillingham, UK). FluoSpheres^{TM} polystyrene microspheres (1.0, 0.5, 0.1 μm), red fluorescent, were purchased from Thermoscientific (Leicestershire, UK). Grade A glass pipettes, grade A volumetric flasks, clear glass HPLC vials and crimpable lids were supplied by Fisher (Loughbrough, UK). Concentrated hydrochloric acid and sodium hydroxide was supplied by Fluka Analytical (Germany). Propylene glycol and glacial acetic acid were purchased from Sigma-Aldrich (Gillingham, UK).

2.3 Methods

2.3.1 High performance liquid chromatography (HPLC)

Quantitative determination of minoxidil was performed using the high performance liquid chromatography (HPLC) system coupled to a flow-through UV detector. The liquid chromatography system consisted of a HP 1090 pump and autosampler (Agilent Technologies UK Ltd., Wokingham, UK). The flow-through UV detector was a HP 1050 Agilent Technologies UK Ltd., Wokingham, UK). Separation was achieved using a Gemini C18 column (5 μm, 250 mm $\times$ 4.6 mm) (Phenomenex, Macclesfield Cheshire, UK), maintained at room temperature. The injection volume was 10 μl and detection wavelength was 281 nm. The mobile phase for minoxidil analysis was a mixture of methanol and water (75:25, v/v) containing 1% (v/v) glacial acetic acid and 0.3% (w/v) docusate sodium (final pH adjusted to 2.5 using hydrochloric acid). As the minoxidil is polar and highly basic, selecting a mobile phase with an

appropriate pH is important. A mixture of diethyl amine or glacial acetic in water was established to be a suitable option that enhanced chromatographic performance (Gaidhane et al., 2011). The mobile phase flow rate through the column was set at 1.0 mL.min^{-1} and the retention time was 7.2 ± 0.5 min. The HPLC system was used to analyse all the minoxidil samples throughout this thesis.

To prove that the HPLC assays was fit for purpose, the linearity, accuracy, precision, limit of detection (LOD) and limit of quantification (LOQ) were determined. The linearity of the assay was measured by plotting the response of known concentrations of the analyte over an increasing concentration range. Regression analysis was used to obtain an equation for linearity and to calculate the correlation coefficient (R^2). The assay accuracy was presented as the percentage recovery of analyte from a series of standard solutions with known analyte concentrations (n $\geq$ 5). The precision of analysis was expressed as the coefficient of variance (CV %) calculated by dividing the standard deviation by the mean response (peak area or absorbance). The lower the CV (%), the greater the precision of the analysis. For intra-day precision, the same series of standards was re-analysed in triplicate and the CV (%) at each of the concentration levels was calculated from the pooled data (n = 18). The inter-day precision was obtained by preparing a fresh series of calibration standards on days 2 and 3 and analysing the two calibration curves. LOD, LOQ and CV % were calculated using (Equation 2.1, 2.2 and 2.3) respectively:

$$CV\ \% = \frac{StandardDeviation}{Average} \times 100 \tag{2.1}$$

$$LOD = y_B + 3S_B \tag{2.2}$$

$$LOQ = y_B + 10S_B \tag{2.3}$$

where S_B was the standard error of the y estimate, and y_B was the intercept from the calibration curve regression line.

The retention time was defined as the time between the sample introduction and maximum point of the peak. Peak asymmetry factor (As) was calculated using (Equation 2.4):

$$A_s = \frac{W_{0.05}}{2d} \tag{2.4}$$

where $W_{0.05}$ = width of the peak at one-twentieth of the peak height, d = distance between the perpendiculars dropped from the peak maximum and the leading edge of the peak at one-twentieth of the peak height.

2.3.2 Chemical stability assessment of minoxidil

The chemical stability of minoxidil was assessed using HPLC. The calibration curve standards were made up on day 1, and compared with the same standards on day 30 using peak area.

2.3.3 Fluorescence Spectroscopy

Both the nanomaterials (nile red and the unknown red fluorescence dye) and the dextran were analysed by detecting fluorescence intensity using a fluorescence spectrometer (Varian Cary Eclipse, Agilent, Cheadle, UK). Full excitation and emission spectra of probes in appropriate solvents (see Table 2.3) were performed and used to identify wavelength of maximal excitation and emission. Wavelengths of the maximums excitation and emission for each of the probes were measured at room temperature, with excitation and emission slit widths of 2.5 nm. Once the excitation and emission maximum were defined, standard solutions in range of 0.02 μg.mL^{-1} to 1 μg.mL^{-1} for nile red (see Table 2.5), 0.02 μg.mL^{-1} to 80 μg.mL^{-1} for red dye in the polystyrene nanoparticles (see Table 2.6) and 0.02 μg.mL^{-1} to 2 μg.mL^{-1} for FITC-dextran (see Table 2.4) were diluted in an appropriate solvent (see Table 2.3). Polystyrene solutions were sonicated in methyl pyrrolidone for 1 h and centrifuged for 10 min to break open the particles, to release the fluorescent dye (Chen et al., 2016). Linear regression was then used to generate calibration curves for

the measurements, i.e., fluorescence intensity vs. concentration. Intra-day and inter-day precision were calculated using the method described previously (Section 2.3.1). LOD and LOQ calculated were determined using Equation 2.2 and 2.3 respectively.

Table 2.3: Appropriate solvent mixture for probes.

	Solvent mixture
Nile red	ethanol: PBS 95:5
red dye	methyl pyrrolidone: PBS 90:10
(FITC)-Dextran	PBS

Table 2.4: Volume of standard solution required for (FITC)-dextran calibration curve.

Theoretical Concentration (μg.mL^{-1})	**Volume of stock solution required (mL)**	**Total volume (mL)**
2	4 (from 20 μg.mL^{-1})	100
1	5 (from 20 μg.mL^{-1})	100
0.5	5 (from 2 μg.mL^{-1})	20
0.1	2 (from 0.5 μg.mL^{-1})	10
0.05	5 (from 1 μg.mL^{-1})	100
0.02	4 (from 0.05 μg.mL^{-1})	10

Table 2.5: Volume of standard solution required for nile red fluorescence calibration curve.

Theoretical Concentration (μg.mL^{-1})	**Volume of stock solution required (mL)**	**Total volume (mL)**
1	5 (from 20 μg.mL^{-1})	100
0.2	1 (from 0.2 μg.mL^{-1})	100
0.1	10 (from 0.2 μg.mL^{-1})	20
0.08	8 (from 0.2 μg.mL^{-1})	20
0.04	4 (from 0.2 μg.mL^{-1})	20
0.02	2 (from 0.04 μg.mL^{-1})	10

Table 2.6: Volume of standard solution required for red dye fluorescence calibration curve.

Theoretical Concentration (μg.mL^{-1})	**Volume of stock solution required (mL)**	**Total volume (mL)**
80	8 (100 μg.mL^{-1})	10
50	5 (100 μg.mL^{-1})	10
20	4 (100 μg.mL^{-1})	20
10	10 (100 μg.mL^{-1})	100
5	10 (10 μg.mL^{-1})	20
2	10 (10 μg.mL^{-1})	50
1	5 (from 20 μg.mL^{-1})	100
0.2	1 (from 0.2 μg.mL^{-1})	100
0.1	10 (from 0.2 μg.mL^{-1})	20
0.04	4 (from 0.2 μg.mL^{-1})	20
0.02	5 (from 0.04 μg.mL^{-1})	10

2.3.4 Fluorescence chemical stability

The chemical stability of the fluorescence probes were assessed at 3 concentrations at 0, 1, 2 and 24 h for nile red and the red dye and 0, 1, 24 and 156 h for (FITC)-dextrans. Samples were stored at room temperature.

2.3.5 Data analysis

All data were expressed as their mean ± standard deviation (SD). The statistical analysis of data was performed using the Statistical Package for Social Sciences software (SPSS version 16.0, SPSS Inc., Chicago, USA) with a significant level of 0.05. The normality (Sapiro-wilk) and homogeneity of variances (Levane's test) of the data were assessed prior to the statistical analysis. As they followed a normal distribution, results were compared using ANOVA (analysis of variance).

2.4 Results

2.4.1 High performance liquid chromatography (HPLC)

System suitability, linearity and sensitivity

The maximum UV absorbance for minoxidil in the mobile phase was 281 nm, which was used as the detection wavelength throughout the study (data not shown). A single peak was eluted in the HPLC chromatogram with a retention time of 7.2 ± 0.5 min (n=30); the peak shape was sharp in all obtained chromatograms with peak symmetry (As) ranging from 0.77 to 1.37 (n=6) over the calibration range. The calibration curves were linear (1-100 μg.mL^{-1}) ($R^2 > 0.999$). A summary of the five calibration curves on a single plot is shown in Figure 2.1. The limit of detection (LOD) and (LOQ) were calculated using Equation 2.3 and 2.4 at 0.13 μg.mL^{-1} and 0.45 μg.mL^{-1} respectively.

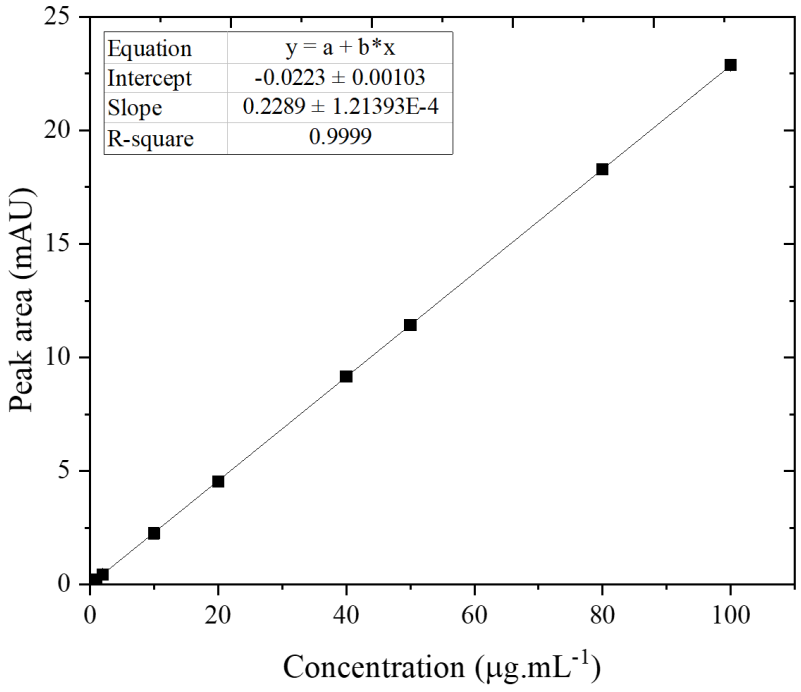

Figure 2.1: Summary of five HPLC minoxidil calibration curves. Each point represents the concentration of minoxidil vs. peak area ± S.D. (the error bars of the standard deviation is too small to be seen (n=3).

There was no significant difference ($P > 0.05$) between the slopes of the 5 HPLC minoxidil calibration curves. The coefficient of variation (CV %) of the peak area gave a measure of analytical method precision. The data was shown to be acceptable with respect to intra-day and inter-day precision, with the coefficient of variation (CV %) ≤ 2 % for the concentration range of 1 to 100 μg.mL^{-1} (see Table 2.7).

Table 2.7: Minoxidil assay variance; Summary of intra-day and inter-day variability. Data represent mean standard deviation, n=18 for intra-day, n=18 for inter-day. CV represents coefficient of variation.

Concentration (μg.mL^{-1})	**CV of the intra-day Peak Area (%)**	**CV of the inter-day Peak Area (%)**
100	0.09	1.10
80	0.15	1.14
50	0.23	1.47
40	0.45	0.76
20	0.91	1.01
10	1.39	1.37
2	1.54	1.87
1	1.95	2.03

2.4.2 Minoxidil chemical stability

It was found that after 30 days the standards showed very little change in terms of peak area, which indicated that minoxidil standards were stable in the mobile phase over 30 days (see Table 2.8 & 2.9). As a result a fresh set of calibration standards was used for a maximum of 30 days during the study.

Table 2.8: Day 30-calibration curve data represent mean ± SD; n=6; CV represents coefficient of variation between day 1 and day 30 (n=6) .

Concentration (μg.mL^{-1})	**Retention Time (min)**	**CV of the intra-day Peak Area (%)**
100	7.6	0.13
80	7.6	0.16
50	7.6	0.32
40	7.6	0.66
20	7.6	1.11
10	7.6	1.76
2	7.6	1.93
1	7.7	2.3

Table 2.9: Stability of minoxidil standards, assessed by the comparison of peak area at day 1 and day 30; temperature below 8°C (n=6)

Concentration (μg.mL^{-1})	**Area (mAU) Day 1**	**Area (mAU) Day 30**	**CV(%) average of Day 1 and Day 30**
100	22.87	23.09	0.11
80	18.28	18.53	0.16
50	11.42	11.56	0.27
40	9.15	9.17	0.55
20	4.52	4.60	1.01
10	2.24	2.33	1.58
2	0.44	0.46	1.74
1	0.22	0.29	2.13

2.4.3 Fluorescence Spectroscopy

Full excitation and emission spectra of florescence probes in their appropriate solutions were generated and used to identify the excitation and emission maxima (see Table 2.10) (n=3).

Table 2.10: Wavelength of maximal excitation λ_{maxex} (nm) and λ_{maxem} (nm) for nile red, polystyrene microspheres and FITC-dextran.

	λ_{maxex} **(nm)**	λ_{maxem} **(nm)**
FITC-Dextran	495	515
Nile red	559	629
FluoSpheres Polystyrene Microspheres	542	612

The (FITC)-dextran calibration curves were linear over the concentration range of 0.02 - 2 μg.mL^{-1} ($R^2 > 0.999$). A summary of the three calibration curves on a single plot is shown in (Figure 2.2). Dextran, interday and intraday variation were lower than 2% (see Table 2.11, 2.12, 2.13 and 2.14). Based on the intraday data the LOD and LOQ for the dextran assays increased in correlation with their molecular weight (see Table 2.15).

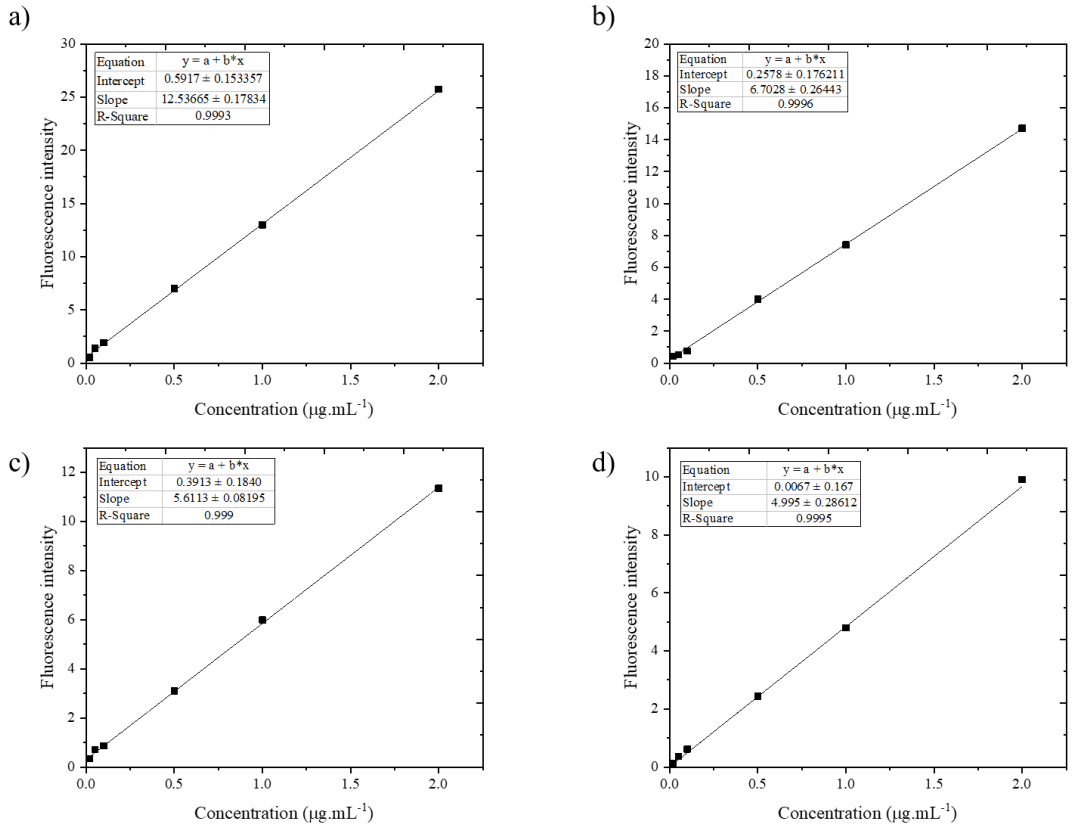

Figure 2.2: Representative calibration curve for a) FD-4, b) FD-10, c) FD-70 and d) FD-150 dextran in PBS using intraday data mean ± SD (n=3, error bars too small to be seen).

Table 2.11: Intra and inter day variation FD-4 as a function of concentration in PBS. Intraday results calculated from measurements made in triplicate at each concentration (n=9). Inter day variation results measured over 3 days (n=9).

Concentration (μg.mL^{-1})	**Intraday CV%**	**Interday CV%**
2	0.11	0.70
1	0.17	0.83
0.5	0.44	1.61
0.1	0.80	4.36
0.05	1.12	6.90
0.02	1.53	8.22

Table 2.12: Intra and inter day variation FD-10 as a function of concentration in PBS. Intraday results calculated from measurements made in triplicate at each concentration (n=9). Inter day variation results measured over 3 days (n=9).

Concentration (μg.mL^{-1})	**Intraday CV%**	**Interday CV%**
2	0.31	0.88
1	0.47	1.09
0.5	0.55	2.71
0.1	0.64	3.03
0.05	1.25	4.03
0.02	1.42	7.02

Table 2.13: Intra and inter day variation FD-70 as a function of concentration in PBS. Intraday results calculated from measurements made in triplicate at each concentration (n=9). Inter day variation results measured over 3 days (n=9).

Concentration (μg.mL^{-1})	**Intraday CV%**	**Interday CV%**
2	0.23	0.84
1	0.37	1.45
0.5	0.63	2.05
0.1	1.07	2.56
0.05	1.34	5.31
0.02	1.40	7.11

Table 2.14: Intra and inter day variation FD-150 as a function of concentration in PBS. Intraday results calculated from measurements made in triplicate at each concentration (n=9). Inter day variation results measured over 3 days (n=9).

Concentration (μg.mL^{-1})	**Intraday CV%**	**Interday CV%**
2	0.16	0.31
1	0.25	0.82
0.5	0.67	1.14
0.1	1.12	2.54
0.05	1.45	4.18
0.02	1.72	6.07

Table 2.15: LOD and LOQ of various dextran molecular weights.

Dextran MW (kDa)	**LOD (μg.mL^{-1})**	**LOQ (μg.mL^{-1})**
4	0.03	0.12
10	0.07	0.26
70	0.09	0.30
150	0.10	0.33

The three nile red calibration curves were linear over the concentration range of 0.02 - 1 μg.mL^{-1} ($R^2 > 0.99$) (Figure 2.3). The intraday and interday precision were $< 2\%$ and $< 8\%$ respectively (see Table 2.7). Based on the intraday data, which was selected because it was more precise, the LOD and LOQ for the nile red assays were 0.003 μg.mL^{-1} and 0.010 μg.mL^{-1} respectively.

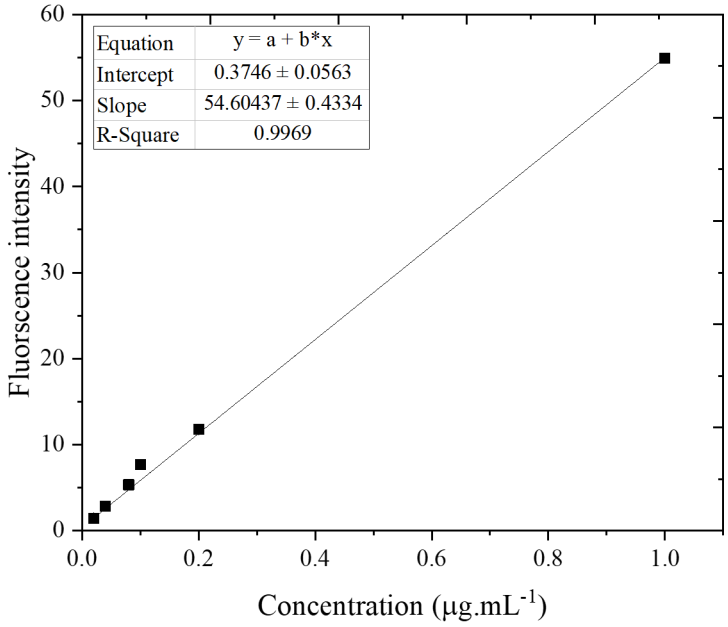

Figure 2.3: A summary of the three data sets generates for the intraday precision for nile red in ethanol: PBS (pH 7.4). Data is the mean ± SD(n=3, error bars too small to be seen).

Table 2.16: Intra and inter day variation in nile red fluorescence as a function of concentration in a mixture of ethanol and PBS. Intraday results calculated from measurements made in triplicate at each concentration (n=9). Inter day variation results measured over 3 days (n=9).

Concentration (μg.mL^{-1})	**Intraday CV%**	**Interday CV%**
1	0.22	0.93
0.2	0.31	1.43
0.1	0.39	1.71
0.08	0.58	2.57
0.04	0.62	2.98
0.02	0.93	3.65

2. Analytical method development

The fluorescence emitted by the solutions of the polystyrene nanoparticles when they were solubilised was used to quantify the particles. The calibration curves were linear over the concentration range of 0.02 - 100 μg.mL^{-1} ($R^2 > 0.999$) (Figure 2.4). The precision of the interday and intraday were $< 2\%$ and $< 10\%$ respectively (see Table 2.17). Based on intraday data the LOD and LOQ for the red fluorescence nanoparticle dye were 0.36 μg.mL^{-1} and 1.20 μg.mL^{-1} respectively.

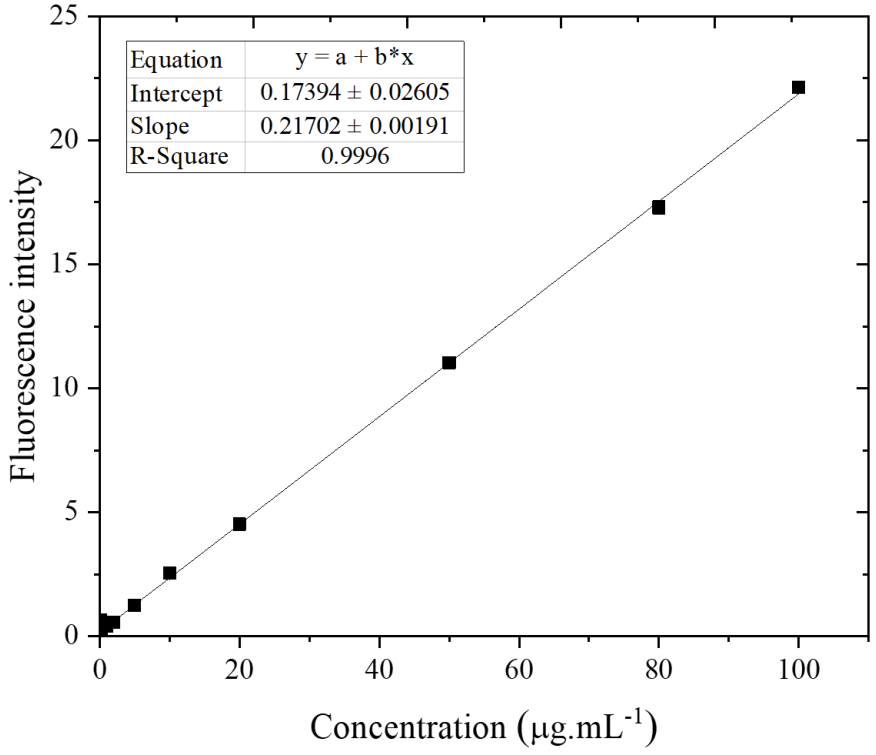

Figure 2.4: Representative calibration curve for red dye fluorescence in (methyl pyrrolidone: PBS) using intraday data mean ± SD (n=3, error bars too small to be seen).

Table 2.17: Intra and inter day variation in polystyrene red dye fluorescence as a function of concentration when dissolved mixture of methyl pyrrolidone: PBS. Intraday results calculated from measurements made in triplicate at each concentration (n=9). Inter day variation results measured over 3 days (n=9).

Concentration (μg.mL^{-1})	**Intraday CV%**	**Interday CV%**
100	0.02	0.86
80	0.14	1.01
50	0.23	1.21
20	0.77	1.43
10	0.84	1.56
5	1.02	1.80
2	1.25	2.13
1	1.57	2.98
0.2	1.89	4.23
0.1	2.07	5.14
0.04	2.17	6.11
0.02	2.34	8.09

2.4.4 Fluorescence stability

The (FITC)-dextrans showed no significant (t-test, $P > 0.05$) sign of degradation for 7 days at room temperature (Figure 2.5). The fluorescence stability of nile red in ethanol: PBS for 24 h was good (no significant change in the intensity) (Figure 2.6). There was no significant (t-test, $P > 0.05$) difference between the fluorescence intensity of nile red, at different time points. Likewise, no significant (t-test, $P > 0.05$) difference observed in the fluorescence intensity of red dye (Figure 2.7).

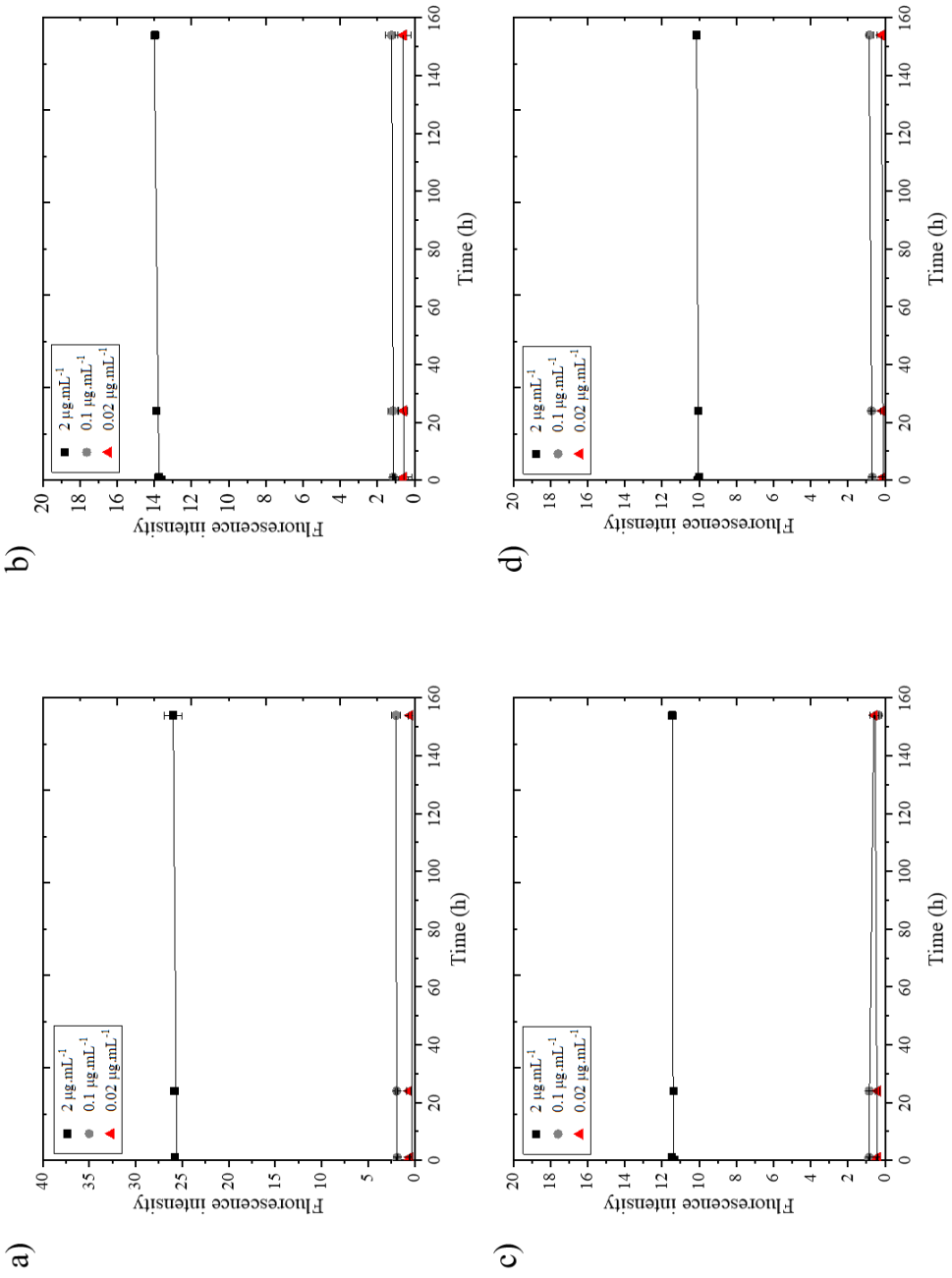

Figure 2.5: Fluorescence stability of a) FD-4, b) FD-10, c) FD-70 and d) FD-150 in different concentrations over 156 h, mean ± SD (n=3, error bars too small to be seen). samples were stored at room temperature.

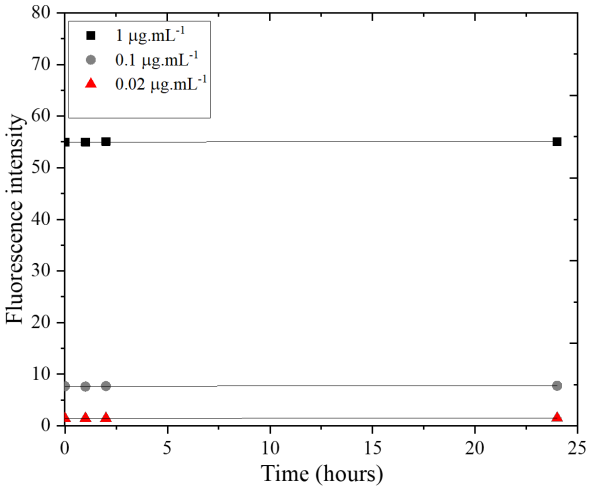

Figure 2.6: Fluorescence stability of nile red in different concentrations over 24 h, mean ± SD (n=3, error bars too small to be seen).

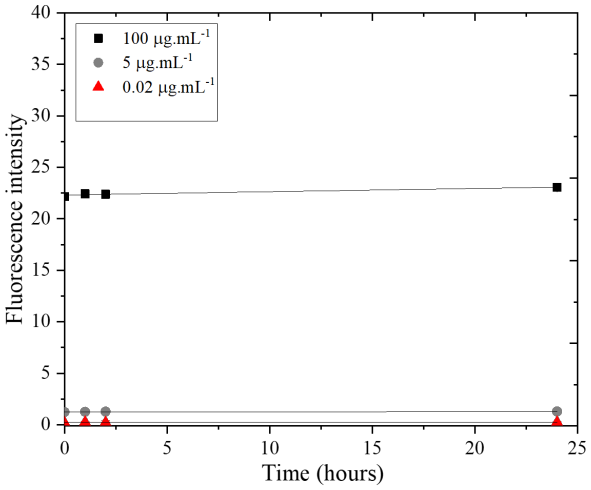

Figure 2.7: Fluorescence stability of red dye in different concentrations over 24 h, mean ± SD (n=3, error bars too small to be seen).

2.5 Discussion

Minoxidil, known chemically as 2, 4-diamino-6-piperidinopyrimidine 3-oxide, is used as anti-alopecia agent. It is an ionisable compound with pKa of 4.6. In the HPLC assay employed in this work it showed a well resolved peak with retention time of 7.2 ± 0.5 min. The mean peak symmetry (As) for minoxidil was within the recommended limit reported by ICH as < 2. The standard calibration curves for minoxidil were linear across the calibration range ($R^2 \geq 0.999$). According to ICH analytical assay guidelines, the use of at least a five point calibration curve that represents a linearity greater than 0.99 is required if the analytical method is to be used to calculate the concentration of analyte. The LOD and LOQ values for minoxidil were calculated using intra-day calibration curve, and they were very similar to those previously reported in the literature, 0.11 μg.mL^{-1} and 0.37 μg.mL^{-1} respectively (Padois et al., 2011). Precision was calculated using inter-day and intra-day values. The inter-day and intra-day values were less than 2% for all concentrations, which fulfills the ICH guideline recommendation. The minoxidil HPLC method was deemed 'fit for purpose' in terms of linearity, sensitivity and precision. This verified method was therefore used to in the *in vitro* permeation study of minoxidil in Chapter 3.

The stability of minoxidil in the mobile phase was measured over 30 days at 4° C. Analyte chemical stability should have CV % of less than 2 % when compared to the fresh samples. In this study, minoxidil showed excellent stability for 30 days with a CV less than 2 %. A similar study on the stability of the minoxidil (stored at 4°C for 2 weeks) indicated no significant changes (< 2 %) relative to day 1 samples (Rudrapal et al., 2016). The HPLC method used in this work was not shown to be a stability-indicating assay i.e., able to detect any minoxidil potential breakdown compounds. Gaidhane et al. (2011) reported a HPLC stability-indicating method for detection of minoxidil and its related compounds including 6-chloropyrimidine-2,4-diamine 3-oxide, 6-chloropyrimidine-2,4-diamine and 6-(piperidin-1-yl)pyrimidine-2,4-diamine (desoxyminoxidil) (Gaidhane et al., 2011). A stability-indicating assay was not

employed in this work because minoxidil chemical stability was not perceived to be a problem in the typical skin permeation timescales.

To quantify the amount of dextran and nanoparticles in future experiments, fluorescence assays were developed for their quantification. A linear relationship between the intensity of fluorescence markers and their concentrations were obtained. Variation in data was measured quantitatively by the coefficient of variation (CV), which should be less than 2 % in order to be accepted for pharmaceutical analyses. Intra-day data value was below this limit for (FITC)-dextran, nile red and unknown red dye. However, at certain analyte concentrations inter-day variation exceeded this value for all tested compounds. This high inter-day variability was subsequently controlled by using a fresh calibration curve in all subsequent permeation experiments. The LOD and LOQ for four different molecular weights (FITC)-dextran were in the range of 0.03-0.1 μg.mL^{-1} and 0.1-0.3 μg.mL^{-1}, respectively. The LOD and LOQ for nile red calculated were 0.003 and 0.010, respectively. LOD and LOQ for red dye were 0.36 μg.mL^{-1} and 1.20 μg.mL^{-1}, respectively. The assays were deemed to 'fit for purpose' for the skin permeation experiments conducted in subsequent chapters.

The probes showed no significant ($P > 0.05$) sign of chemical instability as over time there was no loss in fluorescence intensity. This was important for subsequent *in vitro* and *ex vivo* studies. The chemical stability of the nanoparticles and macromolecules (FITC-dextran) were studied by monitoring the presence of the fluorescent probes. Fluorescence bleaching caused by chemical instability could result in a false estimation of probe penetration and distribution in the skin (Snipstad et al., 2017). In addition, the probes stability was an important factor in permeation studies, which was considered during the selection of probes. A prior study investigated the stability of the thiocarbamoyl binding between the FITC and the dextran molecule in biological systems. This study concluded that the carbamoyl-dextran linkage was highly stable both *in vitro* and *in vivo* conditions and (FITC)-dextran could be used as a tracer (Schröder et al., 1976). Nile red was selected as a nanoparticle probe because of its hydrophobic nature (Küchler

et al., 2009), thus its high affinity for the lipid nanoparticle core (Jose and Burgess, 2006; Greenspan et al., 1985). It is known for its use as a lipid dye for various applications such as localisation of nanoparticles Leroux et al. (1994); Gessner et al. (2001), liposomes (Ogiso et al., 2001) and other lipid microspheres carriers (Ogiso et al., 1996). These investigations on tracking nanoparticles have shown a negligible nile red leakage. The commercial polystyrene particles were filled with an unknown hydrophobic red dye that was represented to be highly stable, however, its exact identity was proprietary. It is important to note that, a probe leakage assay was beyond the aims of this chapter and it has been discussed in Chapter 5.

The aim of this PhD project was to investigate the enhancement of percutaneous drug penetration using hypobaric pressure. The model compounds (see Table 2.18) described in this chapter were used to study the percutaneous drug delivery under hypobaric pressure and thus it was important to develop a 'fit for purpose' methods for quantification of each compound.

Table 2.18: Summary of all analytes used.

Analyte	**Model**	**Analytical method**	**Chemical stability day(s)**
Minoxidil	small MW	HPLC	30
FITC (dextran)	macromolecule	fluorescence	7
Nile red (SLN & liposomes)	nanoparticle probe	fluorescence	1
Unknown red dye polystyrene)	nanoparticle probe	fluorescence	1

2.6 Conclusion

The developed reversed-phase high performance liquid chromatography (RP-HPLC) method was deemed 'fit for purpose' for the quantification of minoxidil. The method precision was deemed to be acceptable, with an intra-day and inter-day variation of < 2 %. The calibration curve had an excellent linearity ($R^2 > 0.999$) throughout the experiment. Minoxidil showed good stability for 30 days. The 'fit for purpose' HPLC analytical method for minoxidil was found to be a quick and reliable. This method will be used to quantify the amount of minoxidil in *in vitro* and *ex vivo* permeation through artificial and porcine membranes in Chapter 3. The fluorescence assays for dextran, nile red and the red dye were found to be suitable in terms of sensitivity, precision and linearity. FITC showed a good stability for 7 days. Nile red and the red dye showed good chemical stability for up to 24 h. These 'fit for purpose' fluorescence methods allowed the investigation of dextran and nanoparticles into the skin to allow the investigations of how hypobaric pressure influenced delivery into the skin in Chapter 4 and 5.

3

Modifying the *in vitro* permeation of minoxidil using hypobaric pressure

3.1 Introduction

Only a selection of drugs can enter the skin at therapeutic concentrations by passive diffusion. More specifically, therapeutic drug deposition in the epidermis is challenging due to its barrier function (Elias, 2005; Michaels et al., 1975). The *stratum corneum*, which is the first layer of epidermis, only allows the passive permeation of agents with a moderate lipophilicity and low molecular weight (Log P 0.8-3, $<$ 500 Da) (Bos and Meinardi, 2000; Naik et al., 2000; Barry, 1983). Physical skin manipulation modifies the structure of the skin by changing the *stratum corneum* barrier. Skin manipulation can be achieved using medical devices such as jet injections , lasers, microneedles, iontophoresis patches, ultrasound (Schramm and Mitragotri, 2002; Gomez et al., 2008; Tuan-Mahmood et al., 2013; Rawat et al., 2008; Polat et al., 2011) and recently hypobaric pressure (Inacio et al., 2016). These methods have been shown to enhance the drug permeation through the skin, however, each have their limitations. One of the the newest of these methods, hypobaric pressure has yet to be investigated fully.

The application of hypobaric pressure (0.25 bar) has been shown to increase the permeation of caffeine by 1.8-fold *in vivo* (Treffel et al., 1993), although no

mechanistic insight was provided. Moreover, another study reported that the application of hypobaric pressure (500 mBar) caused a reduction in epidermis thickness and caused blood vessels enlargement in the dermis (Childers et al., 2007). Suction cups, which generate 400-600 mBar hypobaric pressure, were reported to significantly increase transepidermal water loss (Pedersen and Jemec, 2006). Finally, in a more recent study using tetracaine, diclofenac diethylamine and aciclovir, hypobaric pressure was shown to modify the percutaneous penetration of these agents through enlargement of the follicular infundibula, a reduction in corneocyte size and a reduction in skin thickness (Inacio et al., 2016). Further investigations are now required to assess the influence of hypobaric pressure on a wider range of compounds.

The aim of this Chapter was to investigate the influence of hypobaric pressure upon the delivery of minoxidil. Minoxidil (Figure 3.1) was selected as a model drug because it has been shown to pass into the skin via the hair follicle (Messenger and Rundegren, 2004; Grice et al., 2010; Abd et al., 2018) thus theoretically should work well with hypobaric pressure. Although the application of minoxidil locally to the skin is known to stimulate hair growth, the drug's permeation into the skin via the follicular route is relatively poor (Messenger and Rundegren, 2004).

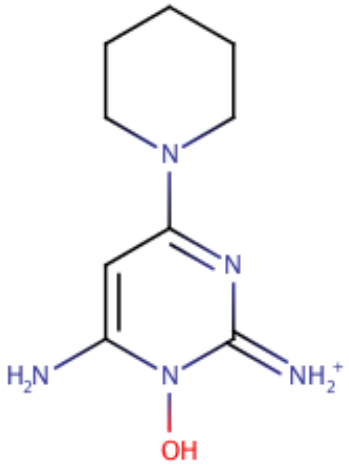

Figure 3.1: Chemical structure of minoxidil.

To perform transport studies in this Chapter, it was necessary to develop an appropriate topical delivery vehicle, therefore the solubility of minoxidil was tested in a series of vehicles to find an appropriate system. Furthermore, the vehicle interactions with the skin was investigated using Orange G (Figure 3.2), a model compound, to investigate skin integrity when the minoxidil delivery vehicle was applied to the tissue.

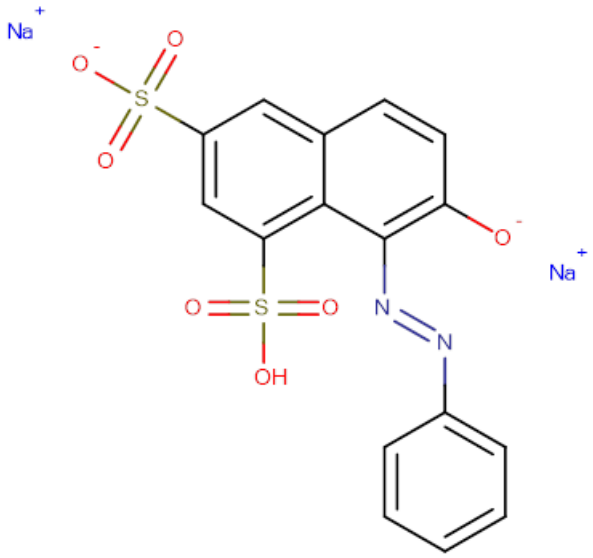

Figure 3.2: Chemical structure of Orange G.

To assess the influence of hypobaric pressure upon the integrity of the membrane, light microscopy was utilised to identify any morphological damages. *In vitro* permeation of minoxidil at atmospheric and hypobaric conditions were assessed using traditional Franz diffusion cells (Franz, 1975) an in-house manufactured hypobaric device. Minoxidil transport through silicone membrane and porcine ear was assessed. The porcine skin was used due to its similarity to human skin in terms of permeability and histological features (Roberts et al., 1991; Dick and Scott, 1992; Fujii et al., 1997; Sato et al., 1991). Moreover, the large follicles on porcine ear are similar to the human intermediate follicles (Meyer, 1996; Meyer and Zschemisch, 2002) and their distribution mimic the hair follicle density on human back and chest (Otberg, Richter, Schaefer, Blume-Peytavi, Sterry and Lademann, 2004), although

it is acceptable that they are not potential sites for administration of minoxidil. The deposition behaviour of minoxidil within the skin layers under atmospheric and hypobaric conditions was assessed to get an idea of the skin distribution of the drug, when the skin was stretched by the application of hypobaric pressure.

3.2 Materials

Methanol and water both HPLC grade were purchased from Fischer Scientific (Leicestershire,UK). Minoxidil (> 98% purity) was purchased from Alfa Aesar (Heysham, UK), stationary phase Gemini C18 column (5 µm, 250 mm × 4.6 mm) was obtained from Phenomenex (Macclesfield, UK), nylon filter papers (0.20 μm) were supplied by Whatman (Kent, UK). Grade A glass pipettes, grade A volumetric flasks, clear glass HPLC vials (2 mL) and crimpable lids were supplied by Fisher (Loughbrough,UK). Orange G dye was from Sigma-Aldrich Ltd (Gillingham, UK). Concentrated hydrochloric acid and sodium hydroxide were supplied by Fluka Analytical (Seelze, Germany). Propylene glycol and glacial acetic acid were purchased from Sigma-Aldrich Ltd (Gillingham, UK). Silicone membranes were purchased from GBUK Healthcare (Selby, UK). O.C.T (optimal cutting temperature) compound was purchased from VWR international (Leuven, Belgium). DPX (distyrene, plasticizer and xylene) mounting medium and xylene were purchased from Fischer Scientific (Leicester, UK). Formalin solution neutral buffered 10% was purchased from Sigma-Aldrich Ltd (Gillingham, UK).

3.3 Methods

3.3.1 Minoxidil vehicle optimisation

The skin permeation rate of a topically applied drug is dependent on the concentration of drug permeation in the applied vehicle. If not enough drug is solubilised in the application vehicle then the donor system will rapidly deplete and skin penetration would be poor. To try and avert this situation in this study the solubility of minoxidil was tested in a series of vehicles in order to search for an appropriate

system to apply the drug to the membranes in the subsequent permeation studies. In order to test the minoxidil solubility a series of minoxidil saturated solutions at different pH values (pH 3-7.4, phosphate buffer saline) was prepared by transferring excess of minoxidil in to a bijou bottle and adding 5 ml of PBS buffer. After adding minoxidil the pH of each sample was measured (using Hanna checker, pH tester) and adjusted using hydrochloric acid if required. Samples were stirred in a water bath at 32°C (to simulate the skin temperature) for 24 h and then at the end of the study centrifuged (1000 rpm, 15 min at 32°C (Maddock and Coller, 1933)) (n=3). Samples were diluted using mobile phase and analysed by using HPLC (Section 2.4.1). The percentage drug ionisation at a particular pH was calculated using the Equation (3.1) and a drug pKa of 4.6 (Moffat et al., 2011).

$$Ionisation\ \% = \frac{10^{\,pKa-pH}}{1+10^{\,pKa-pH}} \times 100 \tag{3.1}$$

where ionisation % was the percentage of minoxidil ionisation in an aqueous solution at different pHs and the pKa was the dissociation constant. pH ranged from 3 to 7.4 in this study. The pKa employed in this study was 4.61 (O'Neil, 2013).

3.3.2 Minoxidil vehicle-skin interactions

The skin is susceptible to mechanical damage, which can impair its barrier function and this must be factored into the design of transport studies. Orange G is a synthetic azo dye used in histology. It is normally available as a disodium salt (Carson et al., 2009). It is a relatively hydrophilic compound, and is larger than minoxidil, with MW of 452.38. It can be useful for transport study as if the membrane is intact, it should not be able to rapidly permeate through the membrane, thus if high concentration of orange G is detected at early time points of a transport study there is a problem with membrane integrity. Orange G was used in this work to investigate skin integrity when the minoxidil delivery vehicle was applied to the tissue in Franz cells. This also served as a training exercise to ensure effective Franz cell use.

Two membrane barriers were employed for the orange G transport studies, silicone membrane (0.12 mm) and porcine ear skin. Fresh white adult porcine ears were obtained from a local butcher. The ears were removed from the carcass after heat treated hair removal. Any damaged ears were discarded. The ears were washed and cleaned with deionised water, the residual water on the skin surface was immediately removed by blotting with tissue, visible hairs were trimmed carefully, and the ears were stored at -20 °C for no longer than 30 days until required (Harrison et al., 1984). On the day of the experiment the skin was defrosted, and the subcutaneous fatty tissue was removed with caution using a scalpel and scissors. The porcine skin was cut into appropriate size, using a cork borer, to fit the Franz diffusion cells.

Previously calibrated Franz diffusion cells (Figure 3.3) (University of Southampton, UK) were used to measure the permeation of orange G across the membranes (silicone, intact and damaged porcine skin). To intentionally damage the skin, samples were pierced using a needle in 5 areas. The Franz cells contained two chambers, a donor and a receiver. The membranes were sealed between the two chambers using parafilm with a 12 mm magnetic flea in the receiver chamber. Sink conditions were maintained throughout the transport assays (drug concentration in the receiver fluid does not exceed 10% of its saturated solubility and less than 10% of the orange G in donor passed into the receiver chamber). The average area available for permeation was 2.1 ± 0.1 cm^2 and the average volume of the receiver compartment was 9.2 ± 0.5 mL. The cells were inverted and filled with the delivery vehicle (PBS: ethanol: propolyn glycol 60:20:20) in the receiver chamber to prevent any solvent gradients. The water bath (Grant Instruments, Cambridge, UK) was set at 37°C to provide a membrane surface temperature of 32°C (skin surface temperature) the difference between 37°C and 32°C is due to heat loss (Maddock and Coller, 1933). The donor and receptor solution were filtered and sonicated before use to reduce air bubbles, which disturb diffusion. The cells were allowed to equilibrate in the water bath for 1 h before the start of the assay. After equilibration, an integrity test was performed by inverting each cell and visually

checking if there is any fluid leakage or receiver fluid back flow. Samples at 0 h were collected prior to the addition of the donor solution. The infinite dose of orange G (1 mL) was applied uniformly to the surface of each membrane and the donor compartment was covered with parafilm to minimise donor phase evaporation.

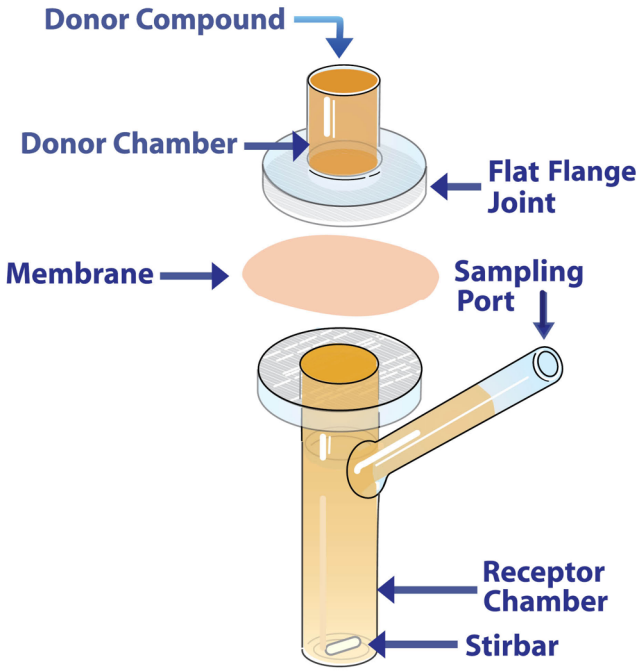

Figure 3.3: Design of a traditional Franz cell (PermeGear, 2018).

At regular time intervals (1, 2, 4, 8 and 24 h) 1 mL aliquots were removed from the receiver chamber and replaced with fresh receiver fluid to keep the liquid volume in the receiver compartment constant. The collection of the samples was conducted by placing the needle of syringe (2 mm outer diameter) between the collection side arm and the body of the receptor compartment (6 flushes). After collection of the sample, the cell was inverted and gently agitated to prevent the formation of bubbles. The collected samples were analysed using a UV-spectoroscopy. Cumulative amounts of drug (μg) penetrating the unit surface of the membrane area (cm^2) was corrected for sample removal and plotted against time (h). A total of 5 replicates of each experiment were performed.

3.3.3 Orange G quantification

The amount of orange G was quantified using (Lambada 5 UV-VIS, Perkin Elmer, Cleveland, USA). The UV absorbance maximum for orange G was 480 nm, which was used as the detection wavelength (data not shown). The assays were verified as 'fit for purpose' by determination of linearity, precision and sensitivity using the methodology described in Section 2.3.1. Linearity was confirmed for concentrations ranging from 1μg.mL^{-1} to 20 μg.mL^{-1} of standard solutions and correlation coefficients were 0.9992 and 0.9997 for orange G in vehicle and PBS respectively. The limit of detection were calculated at 1.5 μg.mL^{-1} and 0.4 μg.mL^{-1} and the limit of quantification were found to be 1.7 μg.mL^{-1} and 1.3 μg.mL^{-1} for vehicle and PBS respectively.

3.3.4 Hypobaric device verification

A traditional Franz cell was attached to an in-house designed aluminum support frame (Figure 3.4) that was able to pressure seal the donor chamber. Hypobaric pressure was produced by extracting air from the sealed system using a syringe and changes were recorded by a manometer (Omni Instruments Ltd., Dundee, UK) (Figure 3.5).

Since the receiver chamber sampling port was not sealed, hypobaric pressure was lost over time. To follow this the pressure was monitored constantly and adjusted to keep it constant during the experiment. The hypobaric pressure application was verified by recording pressure overtime using silicone membrane as a barrier to make sure no major pressure leak occurred during the experiments.

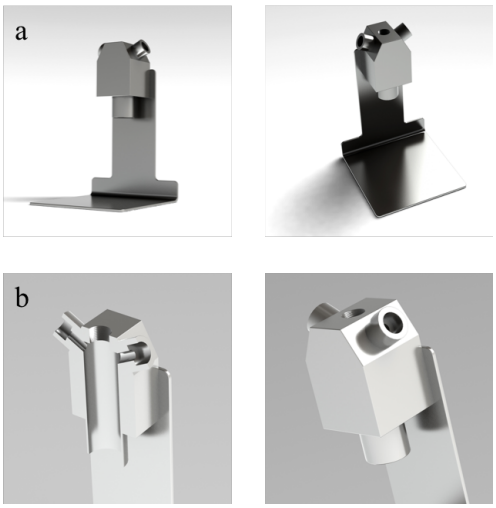

Figure 3.4: Pressure diffusion Franz cell 3 D drawings generated in AutoCad LT software (Autodesk, Farnborough, UK), a) front view, b) hypobaric chamber (Inacio, 2015).

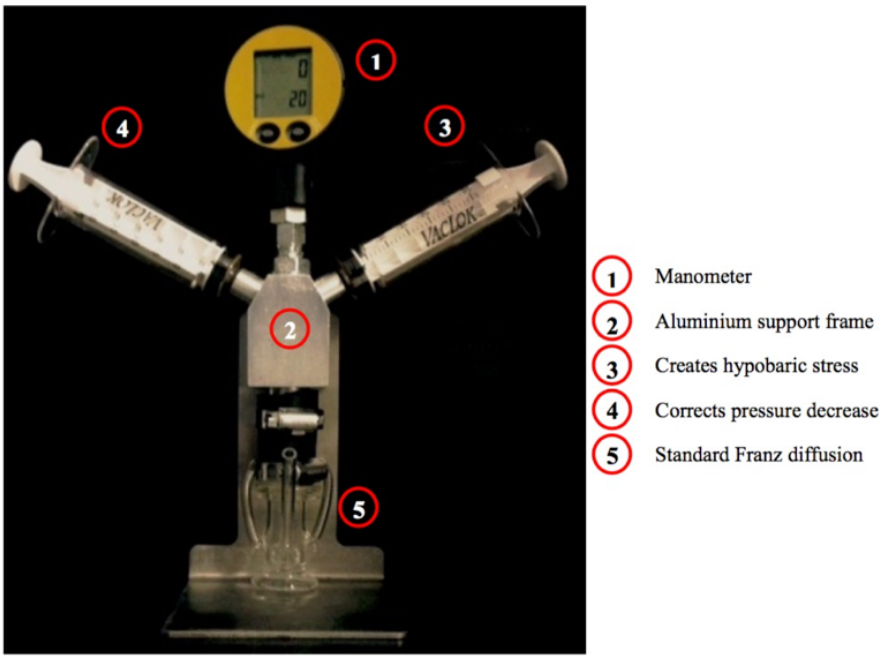

Figure 3.5: In-house developed pressure cell set up. Hypobaric pressure was generated by extracting air using syringes and changes in hypobaric pressure were recorded with a manometer (Inacio, 2015).

3.3.5 *In vitro* minoxidil permeation

For the silicone membrane and porcine minoxidil skin permeation studies the membranes were cut, mounted and sealed with parafilm between two chambers, the receiver chamber filled with the vehicle (PBS: ethanol: propylene glycole, at pH 7.4) as previously described in Section 3.3.2. At regular time intervals (24, 48, 96 and 120 h) and (1, 3, 5 and 24 h) for silicone and porcine membranes respectively, 1 mL of the receiver fluid transferred to a HPLC vial and replaced with fresh fluid. The collected samples were analysed using HPLC previously verified in Section 2.3.1.

Flux was taken from the line of the best fit over at least three-time points with a linearity of ($R^2 \geq 0.98$), which was deemed as the apparent steady state flux (J). Data were expressed as mean ± standard deviation. The permeability coefficient of minoxidil was calculated using Equation (3.2):

$$J = \frac{K_p}{C_v} \tag{3.2}$$

where J (μg.cm^{-2}.h) represented the flux, k_p was the permeability coefficient of the permeant across the membrane and C_v was the concentration of the drug in the vehicle. After sufficient time the graph approaches a straight line and from the slope of the straight line we can calculate the apparent steady state flux, dm/dt Equation (3.3):

$$dm/dt = DC_0/h \tag{3.3}$$

where dm/dt was the flux, also termed J, which was the cumulative mass of drug that penetrated per unit area of the membrane in time t, C_0 was the concentration of drug permeant in the first layer of the membrane and h was the membrane thickness. The lag time of minoxidil, permeation through porcine skin, was determined by the intercept of the steady-state flux with the x axis and it was provided in h. This lag time was used to choose the time point for the subsequent deposition study of minoxidil in the skin.

To design a sound experimental method using hypobaric device a series of transport experiments were performed over a 24 h period using silicone membrane as the controlling barrier. The donor solution consisted of 5% (w/v) minoxidil in vehicle (PBS: ethanol: Propylene glycol) and pH adjusted at 7.4. The hypobaric pressure of 450 ± 50 mBar was applied for the first hour of a 24 h transport study. The collected samples were analysed using the HPLC method that previously verified in Section 2.3.1.

3.3.6 Skin histology studies

Porcine skin samples were exposed to hypobaric pressure (450 ± 50 mBar) for 1 h. Samples were carefully cut into small pieces and fixed with 10% formalin buffer for 24 h at room temprature and then embedded in Tissue-Tek O.C.T as previously described by Hoppert (2006). Cross-section slice of 5 μm thickness were produced using a Bright Model OTF cryostat (Bright Instruments, Huntingdon, UK). Samples were stained using Ellis Hematoxylin and Eosin (H&E) staining protocol (Ellis, 2010). Samples were de-wax using xylene for 10 min and immerse in different concentration of ethanol (100%, 90% and 70%) for 5 min each. Then stained by immersing in hematoxylin solution for 5 min, followed by eosin for 2 min. Samples were washed and immersed in differentiation solution and dehydrated with different volumes of ethanol (70%, 90% and 100%) for 5 min each. The samples were mounted in DPX and covered with cover slips and analysed using Leica DM 200 Led light microscope (Leica Microsystems, Wetzlar, Germany) equipped with a Leica digital camera (Model DFC 295) at a magnification of 5X. Images were processed using Las v4.4 Imaging Software (Leica Microsystems, Wetzlar, Germany).

3.3.7 *Ex vivo* deposition study

Transport studies (donor solution contained a 90% saturated minoxidil solution) were conducted using the method described in Section 3.3.2 under atmospheric pressure (1010 mBar) and hypobaric pressure (450 ± 50 mBar) over 3 h (this time point was selected because minoxidil permeation reached the steady-state).

3. Modifying the in vitro *permeation of minoxidil using hypobaric pressure*

Skin samples were removed and washed with deionised water to clean any residue drug on the skin surface, which did not penetrate into the *stratum corneum*. To measure the skin layer distribution, the *stratum corneum*, epidermis and dermis were separated. The *stratum corneum* was removed using a tape stripping method (22 strips), this was performed by pressing a strip of tape (Scotch 845 book tape, 3M, Bracknell, UK) with a defined surface area slightly larger than the skin onto the skin (25 mm length and 19 mm width), covering with a 300 gram weight for 10 s and stripping slowly with forceps. This method first introduced by Pinkus (1951). The drug on the skin surface was gently collected using two cotton buds followed by two tape stripping as this was considered as formulation residual, which did not penetrate into the *stratum corneum*. The remaining 20 tape strips removed from the samples were put in a glass scintillation vial and methanol was added to extract the drug. After tape stripping process, the viable epidermis was separated from dermis with a scalpel and placed in methanol. All solutions were treated with sonication for 1 h and shaken overnight at ambient temperature. After 24 h the solution was filtered using 0.2 μm syringe filter and analysed for minoxidil content by HPLC previously described in Section 2.3.1.

The effect of hypobaric pressure upon minoxidil permeation ability was represented by an enhancement ratio (ER) according to Equation (3.4):

$$ER = \frac{C_{Hypobaric}}{C_{Atmospheric}} \tag{3.4}$$

where $C_{Hypobaric}$ and $C_{Atmospheric}$ were the amount of minoxidil (μg) per cm^2 of skin under hypobaric and atmospheric pressure conditions respectively.

To assess the extraction recovery efficacy, skin layers were spiked with a known amount of minoxidil. For the *stratum corneum* recovery, 20 pieces of tapes were removed from the skin samples. The viable epidermis was separated from epidermis. All the layers were soaked separately in methanol with a known amount of minoxidil (n=3). The solutions were sonicated for 1 h and shaken overnight at ambient temperature. After 24 h the solutions were filtered (0.2 μm syringe filter) and the

minoxidil content of each was assayed by HPLC (Section 2.3.1). The data were represented as the drug recovery from each skin layer.

Figure 3.6: skin layers were spiked with a known amount of drug in each layer

3.3.8 Statistical analysis

Statistical evaluation was carried out using a statistical package for social sciences software (SPSS version 16.0, SPSS Inc, Chicago, USA). All data were checked in terms of normality (Kolmogorov-Smirnov test) and homogeneity of variances (Levene's test) prior to analysis. Permeation results were analysed using one-way analysis of variance test (i.e. one-way ANOVA). All other data were analysed using either two-way ANOVA or student's t-test. Statistically significant differences were defined when $P < 0.05$. All values were expressed as mean $\pm$ SD. The number of replicates was 3 in all experiments except permeation studies with n=5.

3.4 Results and Discussion

3.4.1 Minoxidil vehicle optimization

The aqueous solubility of minoxidil (Figure 3.7) decreased dramatically as the pH of the aqueous vehicle in which it was dissolved increased. This data suggested that the drug solubility changed in accordance with drug ionisation. The aqueous minoxidil solubility was 87 ± 3.04 mg.mL^{-1} at pH 3 where the minoxidil ionisation was 97.54% (Figure 3.7). At pH 4, both solubility and the ionisation degree dropped to 5.3 ± 0.13 mg.mL^{-1} and 79.92%, respectively, at pH 7.4 the minoxidil solubility decreased to 2.69 ± 0.02 mg.mL^{-1} and the ionisation was 0.15%.

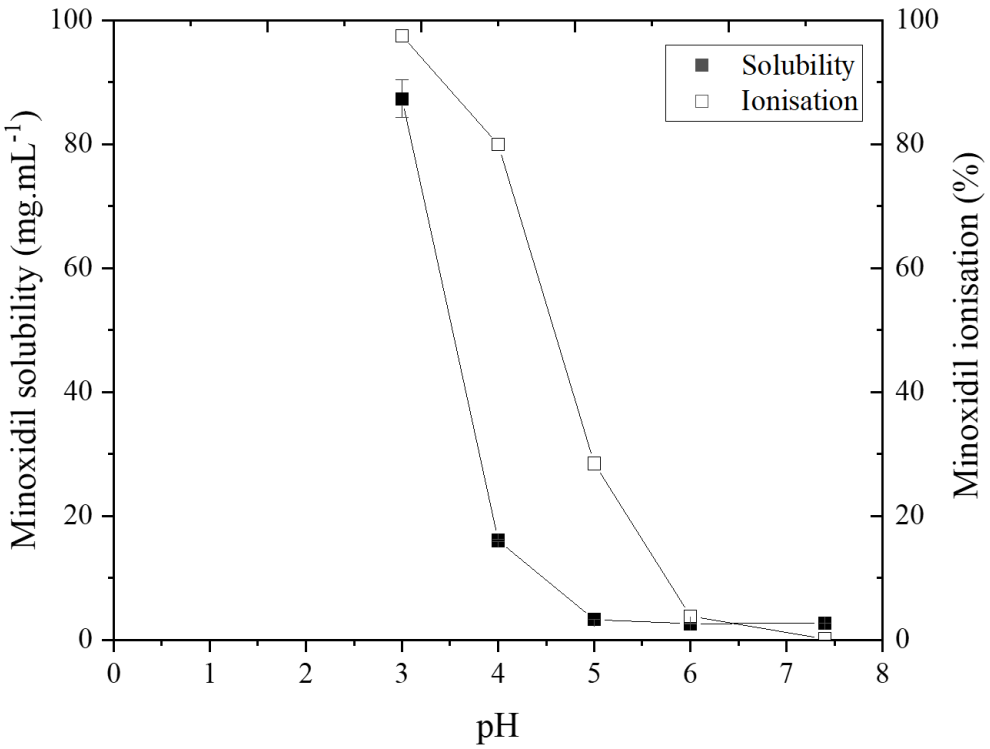

Figure 3.7: The solubility and ionisation percentage of minoxidil in PBS at different pH from 3.0 to 7.4. Data shown is the mean ± standard deviation . Error bars are too small to be seen (n=3).

The solubility of minoxidil in a PBS: ethanol: propylene glycole vehicle was also pH dependent, minoxidil solubility in the vehicle was 108.59 ± 2.72 mg.mL^{-1} at pH 3 where the drug ionisation was 97.54 %. At pH 4, both solubility and the ionisation degree dropped to 42.67 ± 0.89 and the minoxidil ionisation was 79.92 %. At pH 7.4 the solubility decreased to 9.37 ± 2.62 mg.mL^{-1} where the drug ionisation was 0.15% (Figure 3.8). The pKa value of 4.61 was selected followed by the previous study (Zhao et al., 2010).

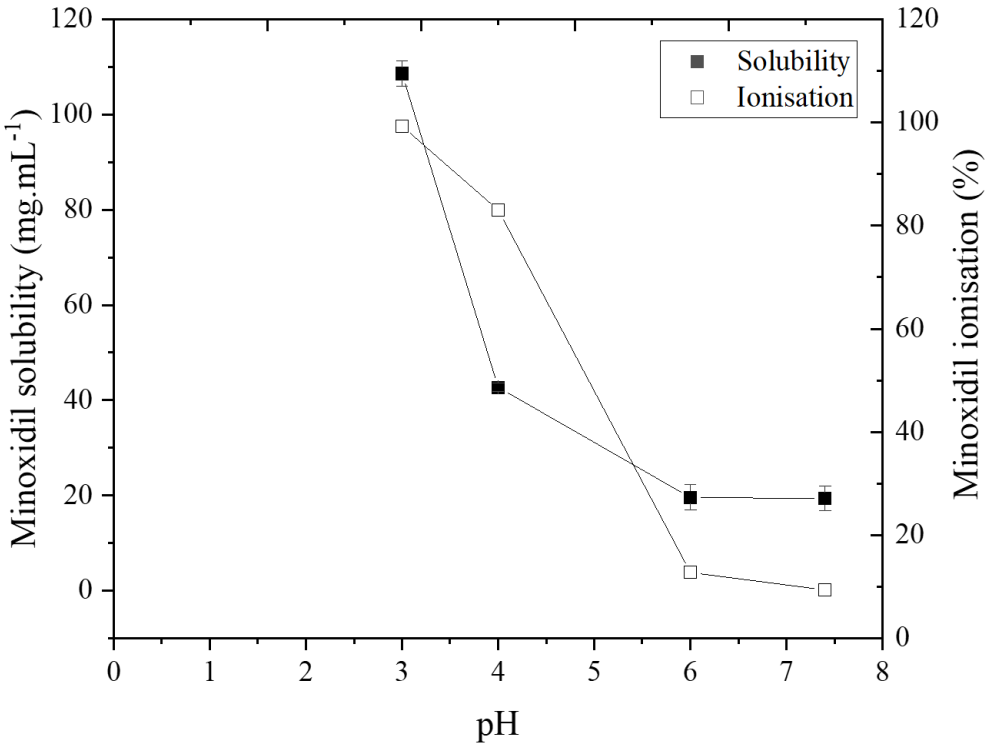

Figure 3.8: The solubility of minoxidil in (PBS: ethanol: propylene glycole) at different pH from 3.0 to 7.4. Data shown is the mean ± standard deviation. Error bars are too small to be seen (n=3).

In a previous published solubility study (Zhao et al., 2010), minoxidil was dissolved in citric acid-phosphate buffer in the pH range from 3 to 7 and the drug solubility followed an identical pattern to the previous data. The solubility of minoxidil was significantly ($P < 0.05$) higher in the vehicle at all pH values compared

to water. The addition of ethanol/propylene glycole to water resulted in an increase in the solubility of minoxidil, because the solubility of minoxidil in alcohols is significantly greater than in water (Yan et al., 2011). The minoxidil nitrogen is thought to form a bond with alcohols (Schultheiss et al., 2010). Moreover, propylene glycol increases the minoxidil solubility in the formulation (Purnak et al., 2011).

As minoxidil was more soluble in the PBS: ethanol: propylene glycol vehicle this vehicle was taken forward to be employed in the future skin permeation studies. It was anticipated that the rate of skin permeation would be proportional to the drugs saturated solubility (Higuchi, 1960). Therefore, using solvents that allow a a specific thermodynamic activity the vehicle could help conrol the experiments ((Higuchi, 1960; Poulsen et al., 1978)). It should be noted that evaporation of ethanol from the water: ethanol: propylene glycole vehicle could form a minoxidil supersaturated solution and result in an enhancement in percutaneous flux through skin (Chia-Ming et al., 1989).

When attempting to deliver a molecule into the skin a balance is required between donor solubility and skin solubility. If the donor systems solubility is too low then the donor system will deplete rapidly. If the the skin solubility is too low the molecules find it difficult to penetrate through the skin. From the solubility data it was thought that pH of 7.4 would be the most appropriate for the permeation study, because this appeared to allow adequate donor solution solubility whilst retaining the drug in the unionised form, i.e., the form that would have the highest skin solubility. According to the pH-partitioning hypothesis, the degree of ionisation of the drug in the vehicle can effect the drug permeation. For instance, unionised drugs penetrate easier through the *stratum corneum* due to their hydrophobic nature, but ionised agents shown low degree of permeation due to their low affinity to the *stratum corneum* lipids (Shore et al., 1957).

In this work, the minoxidil vehicle was composed of three components ethanol, propylene glycol and PBS. This composition was previously used for minoxidil. Ethanol and propylene glycol rapidly diffuse into the membrane and act as penetration enhancers by different mechanisms (Williams and Barry, 2012). Ethanol could

extract or solubilise sebum to enhance follicular transport. Water in the formulation helps membrane hydration, hence promoting transdermal delivery of different substances. This is important when vehicles contain compounds that dehydrate skin, such as ethanol and propolyn glycol (Grice et al., 2010). Free water in the tissue may alter the solubility of a substances in the *stratum corneum* layer which could enhance the permeation of drugs into the membrane (Cornwell and Barry, 1994).

3.4.2 Effect of minoxidil vehicle on skin integrity

Orange G permeation was observed in the damaged skin samples (60.35 ± 25.52 $\mu g.cm^{-2}$), whereas there was no permeation through intact skin samples (Figure 3.9). Since the orange G dye is a hydrophilic compound, it was expected to have a poor penetration through the porcine *stratum corneum* used in the studies unless there was skin damage. The data suggested that the vehicle did not damage the integrity of porcine skin. Although, modifications to it's structure and/or solubility could not be ruled out.

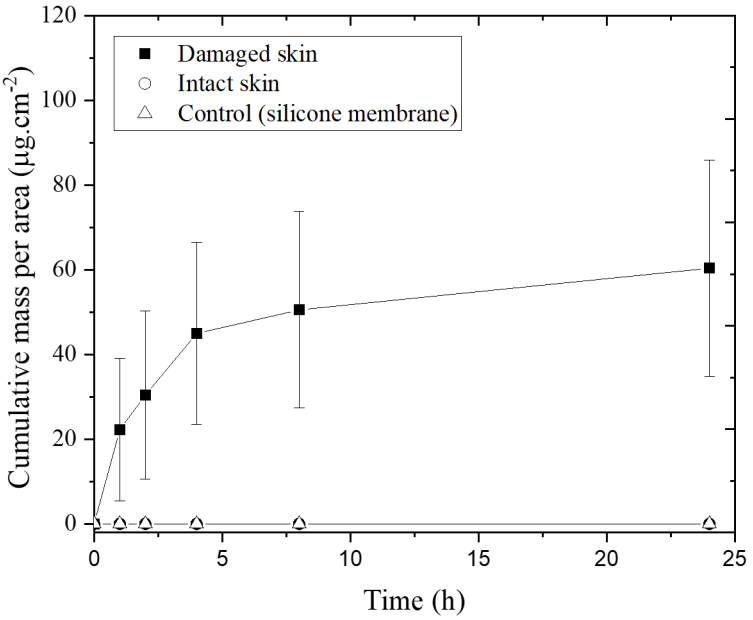

Figure 3.9: Permeation profile of orange G in two conditions, damaged and intact skin membrane. Data shown is the mean ± standard deviation (n=5).

3.4.3 Hypobaric method verification

The in-house hypobaric system was not completely airtight as the Franz cell receiver chamber sampling port was left open and hence, hypobaric pressure was shown to decrease over time (Figure 3.10). When the pressure change was corrected it was stable (455 ± 14.8 mBar over 60 min (n=4)) (Figure 3.11). The 1 h hypobaric pressure application protocol developed herein was used in the transport studies.

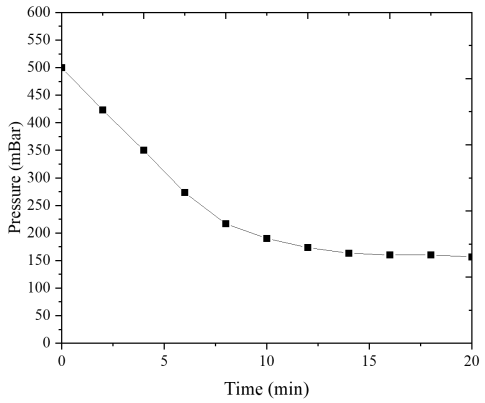

Figure 3.10: Pressure profile of pressure device without adjustment (n=1).

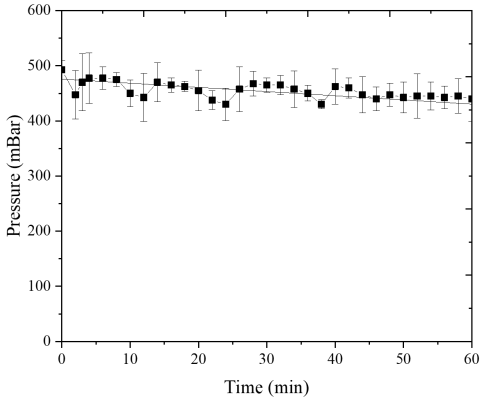

Figure 3.11: Pressure profile of barometric device with adjustment. Data point represents ± standard deviation (n=4).

3.4.4 *In vitro* minoxidil permeation

Permeation through artificial membrane at atmospheric pressure

Three *in vitro* permeation experiments were carried out to investigate the permeation of minoxidil through silicone membrane. The flux of minoxidil increased from 0.13 ± 0.01 μg.cm^{-2}.h^{-1} to 1.13 ± 0.88 μg.cm^{-2}.h^{-1}, respectively over 120 h when the concentration of minoxidil was increased from 2% to 5% (Figure 3.12). Sink conditions were not exceeded through the course of permeation experiment. The silicone membrane restricted the number of drug samples that could be taken from the Franz cell receiver fluid due to the very low concentration of drug, which was close to assay LOD. At each time point the 5% minoxidil concentration delivered significantly (t-test, $P < 0.05$) more drug across the silicone membrane than the 2% concentration although the total quantity of drug in the receiver fluid was less than 0.02% of the applied dose. After 120 h the 5% minoxidil formulation delivered about 4-fold (48.2 ± 11.94 μg.cm^{-2}) more minoxidil compared to the 2% minoxidil formulation (12.97 ± 1.19 μg.cm^{-2}). Regaine® 5% for men (vehicle contains unknown amount of PBS: ethanol: propylene glycol) was analysed as a control, the rate of minoxidil permeation through silicone membrane was 0.81 ± 0.37 μg.cm^{-2}.h^{-1}. The flux over 120 h was not significantly different (t-test, $P < 0.05$) compared to the 5% minoxidil solution that was prepared in the laboratory. A summary of minoxidil permeation can be found in Table 3.1.

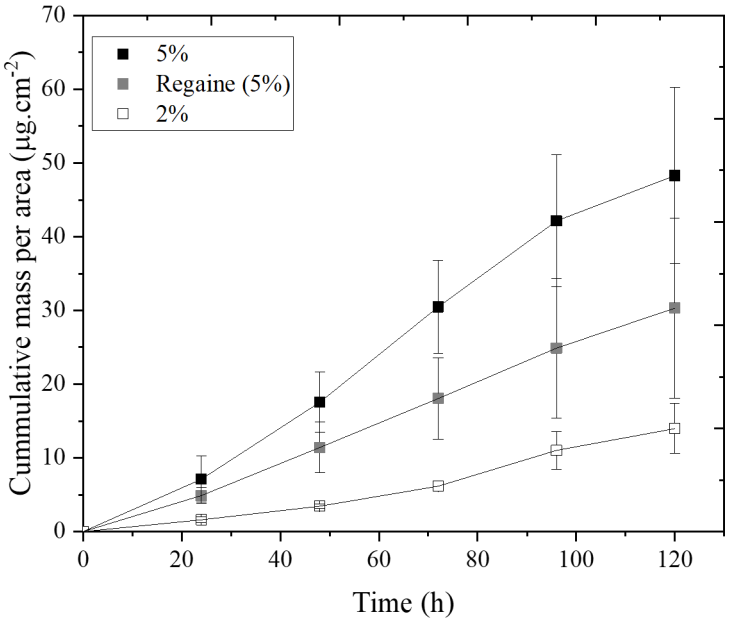

Figure 3.12: Permeation profile of minoxidil across silicone membrane at different concentrations. Data points represent the mean cumulative minoxidil amount over 120 h (n=5 ± SD).

Table 3.1: Permeation of minoxidil through artificial membranes using different dose. (Mean of n=5 ± SD).

Formulation	**Flux** (μ**g.**cm^{-2}**.h**$^{-1}$)	**Cumulative amount**(μ**g.**cm^{-2}) **120 h**
2%(w/v)	0.13 ± 0.0	12.97 ± 1.19
5%(w/v)	1.13 ± 0.88	48.2 ± 11.94
Regaine	0.81 ± 0.44	30.32 ± 12.23

The passive diffusion of minoxidil was influenced by its release from the vehicle and penetration through the membrane. The thermodynamic activity of the agent in the formulation is a major factor controlling the diffusion through the silicone. Theoretically, the flux of minoxidil is proportional to its thermodynamic activity in the vehicle. Moreover, evaporation of the vehicle components could lead to concentrations higher than the agents solubility (Chia-Ming et al., 1989). According to a previous study, there was a significant (t-test, $P < 0.05$) enhancement in the flux

of higher minoxidil concentrations (0.5% to 3%), the flux of minoxidil increased as the concentration increased. Although, at a higher concentration (5% formulation) there was a reduction in the flux rate. The author explained this phenomenon by complete evaporation of ethanol from their formulation (Chia-Ming et al., 1989). However, in our study the flux rate of 5% formulation was higher than the lower concentration formulation, this results suggests that essentially all the ethanol did not evaporate due to the parafilm coverage on the donor chamber.

In the transport studies, the application of hypobaric pressure (450 ± 50 mBar) for 1 h delivered significantly (t-test, $P < 0.05$) more drug across the silicone membrane (Figure 3.13). During 24 h of permeation, samples exposed to hypobaric pressure delivered 4.38 ± 1.07 mg.cm^{-2} of minoxidil across the membrane compared to 0.04 ± 0.01 mg.cm^{-2} permeation of minoxidil with no hypobaric pressure. This was a 109.5-fold increase. The flux was not measured due to not enough points were available in the steady-state.

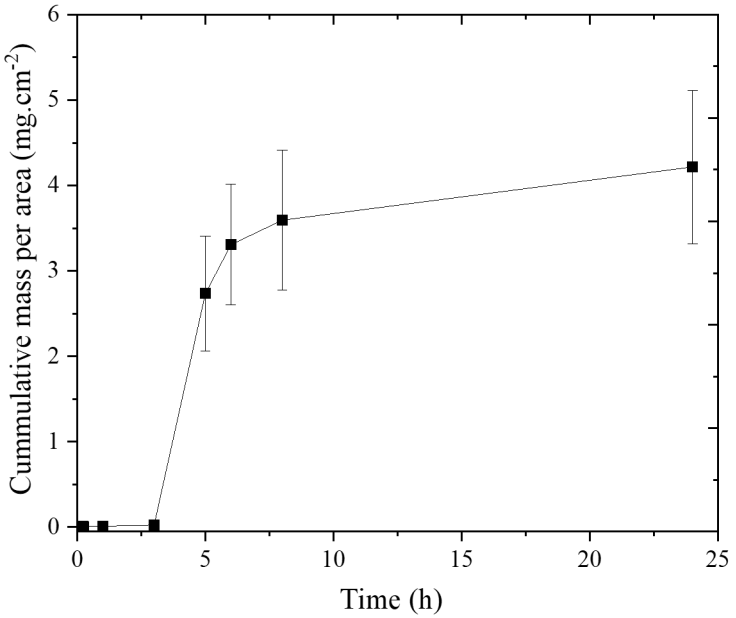

Figure 3.13: Minoxidil permeation profile under atmospheric (1010 mBar) and hypobaric (450 ± 50 mBar) pressure through silicone membrane over 24 h. Each point represents mean ± standard deviation (n=5).

It was suggested by Inacio that the deformation of the membrane caused by the hypobaric pressure could influence the transport of minoxidil through the silicone membrane. This data with minoxidil agrees with the data previously generates with tetracaine, which passed a silicone membrane significantly quicker using hypobaric pressure at 20.2 ± 3.1 μg.cm^{-2}.min^{-1} vs 9.5 ± 1.3 μg.cm^{-2}.min^{-1} at atmospheric pressure (Inacio, 2015). The minoxidil permeation shown a greater enhancement in contrast with tetracaine, wihch might be due to the molecular weight of minoxidil (209.25 g.mol^{-1}) that is slightly smaller than tetracaine (264.39 g.mol^{-1}). Another factor was the partition coefficient (logP) value of minoxidil (1.2), which is lower than tetracaine (2.64). Moreover, tetracaine was shown to aggregate in the solution, this effect did not happen in the minoxidil (aggregation was measured using light scattering, data not shown).

Permeation through porcine skin

By comparing the total minoxidil transport through the membrane in each cell, it can be confirmed that no drug depletion occurred during the experiment, the total quantity of minoxidil in the receiver fluid was less than 0.5% of the applied dose. It was thought that minoxidil was constantly supplied in the permeation experiment and covered the barrier at unity amount, due to the thermodynamic activity of minoxidil in the vehicle as previously discussed in Section 3.4.1. Sink conditions in the receiver fluid was maintained for each cell by measuring the concentration of minoxidil which did not exceed 10% of the saturated solubility (Howes et al., 1996). The lag time was calculated at 3.2 ± 0.5 h as previously described in Section 3.3.5, was used in the *ex vivo* studies for the minoxidil permeation.

The amount of minoxidil that permeated porcine skin was 0.69 ± 0.24 μg.cm^{-2} over 24 h, which was 100-fold higher compared to the silicone membrane study (0.007 ± 0.003 μg.cm^{-2} at 24 h). Since, hair follicles have been reported as the site of action for minoxidil in the literature (Messenger and Rundegren, 2004), it was expected that minoxidil would diffuse more into a barrier containing hair follicles. Silicone is a synthetic membrane that presents as a homogeneous polymer

barrier for agents to permeate through (Ulbricht, 2006). Silicone lacks pores, e.g., hair follicles, thus classical partitioning and diffusion (Higuchi, 1960) are the only processes responsible for the penetration of molecules through the silicon barrier (Pintado-Herrera et al., 2016). Porcine skin by contrast allows agents to diffuse through its barrier via both transcellular and intercellular transport, and through the skin pores (Flaten et al., 2015).

Minoxidil penetration was faster in the porcine skin compared to the silicone membrane, since no drug was detected in the receiver chamber before 24 h in silicone membrane. The follicular routes generally allow the molecules to permeate faster compared to intercellular routes Otberg et al. (2007). It was assumed that the lack of pores in the silicone membrane resulted in a longer process of minoxidil permeation.

Minoxidil lag time during the porcine skin permeation was 3.2 ± 0.5 h (Figure 3.14). A delayed response of 4 h was reported previously for minoxidil from solvent mixture formulations(Abd et al., 2018). The slow uptake of propylene glycol into the membrane and its gradual modification of *stratum corneum* permeability could be one cause of the permeation lag time (Grice et al., 2010). The permeation study found steady-state to facilitate the subsequent skin deposition experiments.

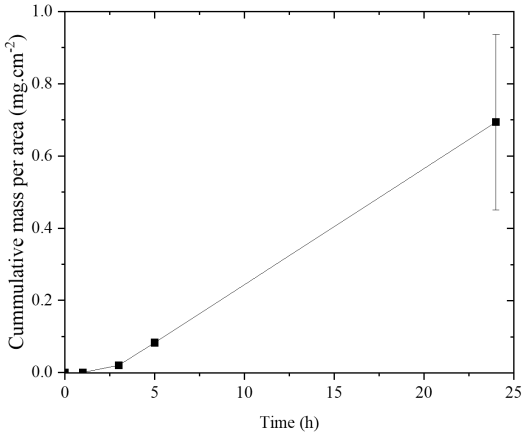

Figure 3.14: Permeation profile of minoxidil across porcine skin. Data points represent the mean cumulative minoxidil amount over 24 h. Data represents ± standard deviation (n=5). Error bar are too small to be seen on some points.

3.4.5 Skin integrity after application of hypobaric pressure

The application of hypobaric pressure (450 ± 50 mBar) to full thickness porcine ear for 1 h resulted in significant (t-test, $P < 0.05$) thinning of the membrane (Figure 3.15). The measured porcine skin thickness was 1.40 ± 0.2 mm, this value decreased to 0.96 ± 0.4 mm after application of hypobaric pressure. Skin thinning after hypobaric pressure has previously been reported in the literature, e.g., between 7 to 17% skin thinning was recorded after suction device application to human skin (Hendriks et al., 2003).

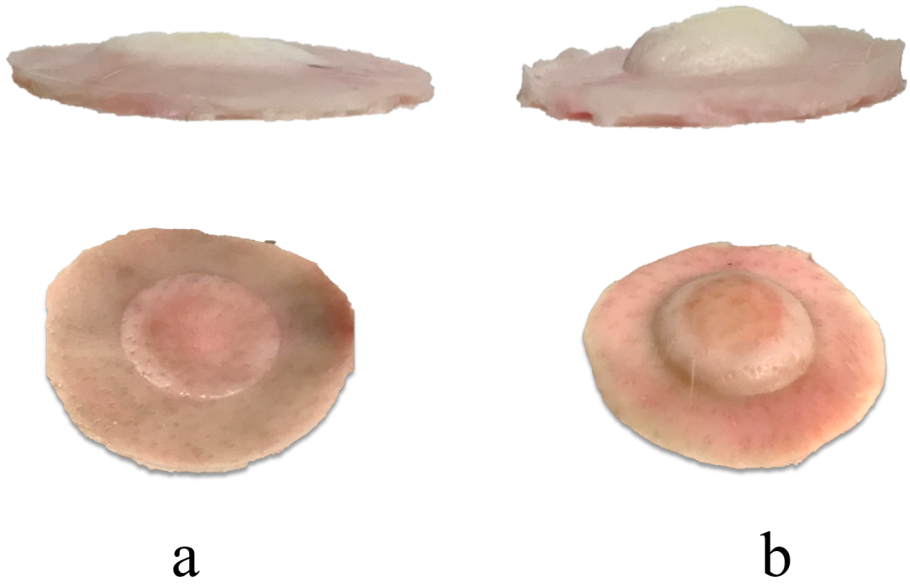

Figure 3.15: Vertical displacement of porcine ear samples after removal from Franz diffusion cell. a) porcine skin at atmospheric pressure (control). b) porcine skin after application of hypobaric pressure for 1 h.

Light microscopy was utilised to study the skin histological changes upon application of hypobaric pressure. These experiments showed that the *stratum corneum* remained intact and connected to the epidermis after exposure to hypobaric pressure (Figure 3.16). No dermal-epidermal detachment was observed in the skin samples to which hypobaric hypobaric pressurehas been applied.

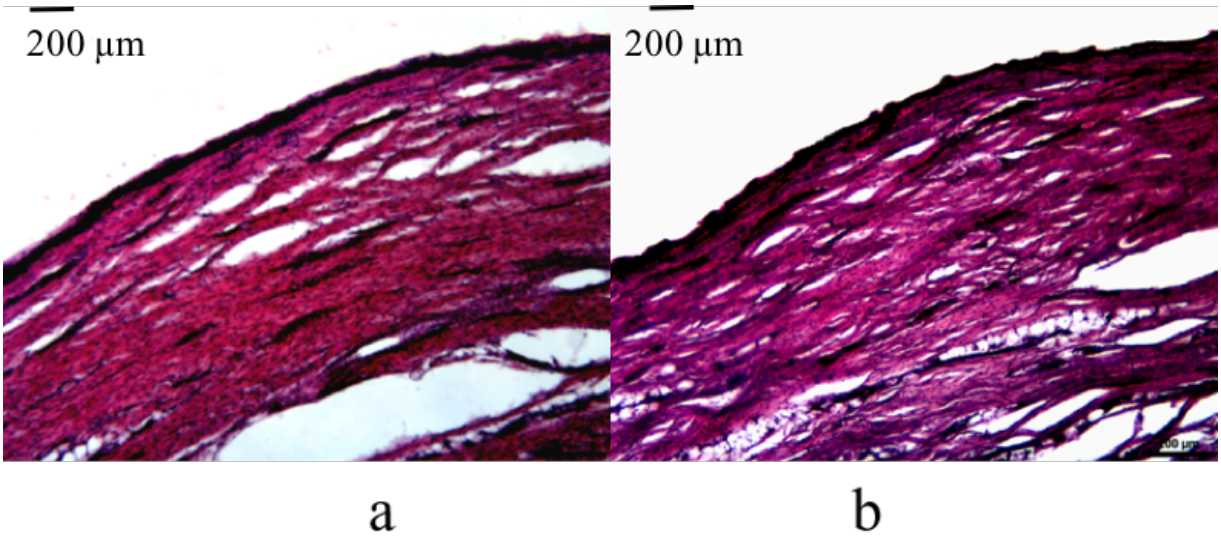

Figure 3.16: Porcine skin histology a) atmospheric pressure (control), and b) after application of hypobaric pressure for 1 h.

3.4.6 *Ex vivo* porcine skin minoxidil deposition study

The amount of minoxidil recovered in all layers during the deposition study was 96.69% ± 3.68. The percentage of minoxidil recovered in each layer were 92.4, 98.7, and 98.8% in *stratum corneum*, epidermis and dermis respectively. As drug recovery was within the 100 ± 15% recovery rate, no correction for recovery in the deposition data was needed (on Specifications for Pharmaceutical Preparations and Organization, 2005).

The hypobaric pressure conditions delivered significantly (t-test, $P < 0.05$) more minoxidil into the skin with an enhancement ratio of 5.6 (Figure 3.17). The effect of hypobaric pressure application on the delivery of minoxidil into the *stratum corneum* was assessed by tape stripping, previously described in Section 3.3.7. The amount of minoxidil recovered from the *stratum corneum* increased by 16.5-fold when hypobaric pressure was applied (Figure 3.17). The minoxidil retained in the epidermis and dermis was enhanced by 5.3 and 5.2-fold respectively (Figure 3.17). The doposition data suggested that hypobaric delivery was found to be effective means to increase minoxidil penetration into the skin.

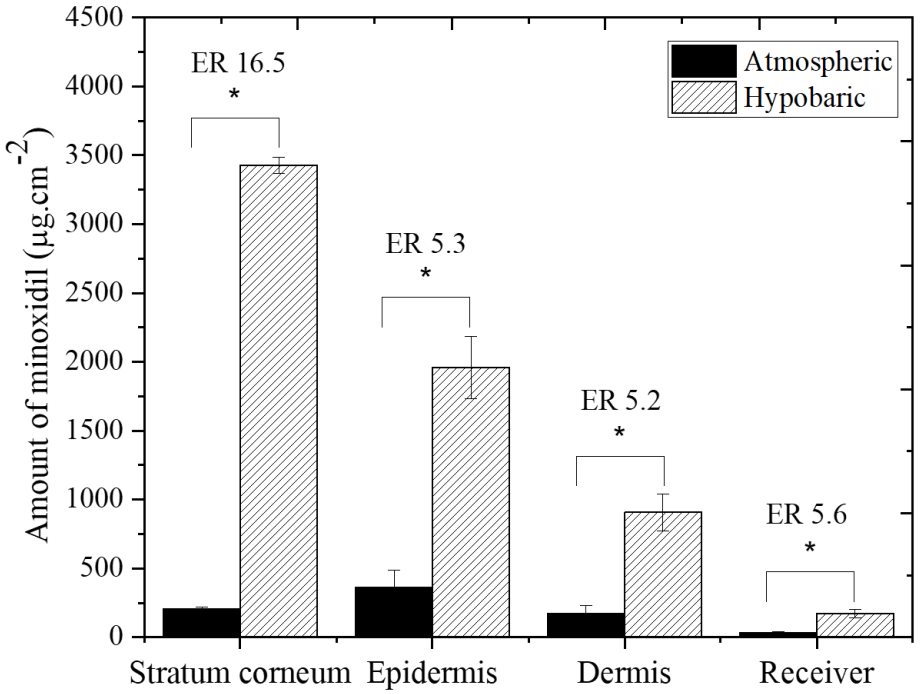

Figure 3.17: *Ex vivo* deposition of minoxidil in porcine skin under atmospheric (1010 mBar) and hypobaric (450 ± 50 mBar) pressure conditions. Data point represent ± standard deviation (n=5) 3h.

Recently, Abd et al. (2018) investigated the enhanced human skin delivery of minoxidil applied in nanoemulsions for the treatment of alopecia. Their eucalyptol nanoemulsions delivered 350 μg.cm^{-2} of minoxidil over 24 h across the skin. In the present study, hypobaric pressure delivered 170 μg.cm^{-2} of minoxidil over just 3 h across the skin (Figure 3.17). However, the amount of minoxidil retained in the skin was 60-fold more in contrast with eucalyptol nanoemulsions study. It was anticipated that the data from porcine skin to be similar to human skin as the hair follicles are similar in size (Patzelt et al., 2011).

Patzelt et al. (2011) reported an enhancement ratio of around 2% for epidermis and dermis for solid lipid nanoparticles versus commercial minoxidil solution, which smaller than the enhancement ratio obtained for epidermis and dermis in the

current study. In another study on targeting and sustaining minoxidil sulphate delivery to hair follicle, a 2-fold enhancement reported when chitosan nanoparticles used (Matos et al., 2015).

According to the obtained data, it was anticipated that the application of hypobaric pressure promoted minoxidil deposition in the *stratum corneum* and deeper skin layers more than the atmospheric pressure. It was hypothesised that hypobaric pressure enhanced minoxidil permeation by either altering the skin structure or through enhancing minoxidil partition into the *stratum corneum*. Skin structure could be modified through enlarging the hair follicles, hence facilitating transappendageal pathway and reducing thickness (Section 3.4.5) through the application of hypobaric pressure. Treffel et al. (1993) suggested that some physiochemical properties of compounds (i.e. solubility) could be influenced by pressure that led into a greater molecule diffusion.

3.5 Conclusion

The application of hypobaric pressure in this Chapter significantly enhanced the permeation of minoxidil through full-thickness porcine skin. Minoxidil was significantly soluble in a water: ethanol: propylene glycol vehicle which was taken forward as the vehicle for transport studies. Minoxidil ionisation increased as the pH decreased therefore, it was most soluble at the lower pH values (i.e. pH 3). This data indicated that minoxidil was more hydrophilic at lower pH. From the solubility data it was thought that a pH of 7.4 would be the most appropriate for the subsequent permeation studies, because this appeared to allow adequate donor solution solubility whilst retaining the drug in the unionised form, i.e., the form that would have the highest skin solubility. Minoxidil membrane transport (over 120 h) was demonstrated to increase by 109.5-fold when 450 ± 50 mBar of hypobaric pressure was applied to the membrane. It was suggested that the deformation of the membrane caused by the suction could influence the transport of minoxidil through the silicone membrane. Two hours after the application of a 1 h dose of hypobaric pressure the minoxidil deposition in the *stratum corneum*, epidermis and dermis was increased by 16.5, 5.3 and 5.2-fold, respectively compared to atmospheric conditions. It was hypothesised that hypobaric pressure significantly ($P < 0.05$) reduced the skin thickness and enlarged the follicular pore size, which resulted in the enhanced permeation. Furthermore, the enhanced minoxidil deposition observed in this study suggests that hypobaric pressure may be a useful percutaneous delivery method for small therapeutic compounds, that diffuse through hair follicles. Consequently, in the next Chapters, two larger model agents (dextran and nanoparticles) were employed to investigate their permeation and delivery pathways modification using hypobaric pressure.

Future work will be required to obtain data on the mechanism in which hypobaric pressure work. These experiments include the FTIR and follicular casting studies, and subsequent *in vivo* studies.

4

The effects of hypobaric pressure on macromolecules delivery into the skin

4.1 Introduction

In the previous Chapter, the skin permeation of the low-molecular weight drug minoxidil was enhanced using the local application of hypobaric pressure to the cutaneous tissue. This Chapter will apply the same technique to the delivery of macromolecules to the skin. Macromolecules have a molecular size in the nano-range, their accumulation in the skin is more difficult compared to low molecular weight agents such as minoxidil due to their slower diffusion (Prausnitz, 1999). As a consequence macromolecules such as proteins and peptides, which are currently used for the treatment of cancer, diabetes and osteoporosis (Kalluri and Banga, 2011) are commonly administrated via the injection, which is not favoured by patients. This is especially true for drugs with a short half-life, which require multiple administrations per day (Kalluri and Banga, 2011).

Macromolecule skin delivery is limited by their permeability through the *stratum corneum*. The *stratum corneum* consists of a highly organised lipophilic layer, which permits only small lipophilic compounds to readily diffuse through it (Choi et al., 2012). Several studies have reported that larger molecules are prone to accumulation on the skin surface because of their inability to penetrate the *stratum*

corneum or concentrated around skin pores such as hair follicles (Lademann et al., 1999; Toll et al., 2004; Trauer et al., 2009; Teichmann et al., 2005). Because the permeation of macromolecules is limited a number of enhancement methods have been proposed for macromolecule delivery into the skin, these include, but not limited to: microneedles, electrophoresis, iontophoresis, sonophoresis and recently hypobaric pressure. McAllister et al. (1999) reported an enhancement of 3 to 4-fold for macromolecules (such as bovine serum albumin and insulin) across human epidermis using microneedels. A previous investigation using rat skin reported the feasibility of transdermal delivery of dextran upto 40 kDa through skin electroporation method (Lombry et al., 2000). Moreover, the iontophoretic delivery of proteins can be successful for molecules with a molecular weight of upto 15 kDa (Kalluri and Banga, 2011). Several studies showed that sonophoresis could enhance the delivery of proteins and peptides such as insulin (5.8 kDa) and heparin (12 kDa) (Luis et al., 2007; Mitragotri and Kost, 2001). Inacio et al. (2016) reported a transdermal delivery enhancement of 2.9 and 19.6-fold for dextran 4 kDa and 10 kDa respectively using hypobaric pressure on rat skin. However, the literature has so far showed limited success with macromolecules $>$ 40 kDa, more specifically biomacromolecules (i.e. therapeutic proteins and antibodies), therefore, new transdermal methods to enhance the delivery of such molecules are still needed.

The application of topical hypobaric pressure to the cutaneous tissue has previously shown to be an effective method to facilitate the delivery of compounds $<$ 10 kDa. However, more work is required to study the behaviour of larger macromolecules under the influence of hypobaric pressure. The aim of this Chapter was to assess the influence of hypobaric pressure on the permeation of macromolecules between 4-150 kDa (see Table 4.1). In this Chapter, fluorescent isothiocyanate (FITC)-dextran with different molecular weights were selected as a model for macromolecule compounds (see Table 4.1). The smaller molecular weight (4 kDa and 10 kDa) dextrans were used for comparison with previous work. *Ex vivo* permeation studies were performed using porcine skin as the barrier in order to investigate the diffusion behaviour of macromolecules with and without the

application of hypobaric pressure. Drug distribution in the skin was investigated using confocal microscope. In order to detect and analyse dextran (see Table 2.1), fluorescein (see Table 2.2) linked to the dextrans was quantified in these studies. It has been reported previously that the fluorescein-dextran linkage was stable in both *in vitro* and *in vivo* studies (Schröder et al., 1976). Porcine skin was selected as a controlling barrier due to its resemblance to human skin in terms of permeability and histological characteristics (Sato et al., 1991; Fujii et al., 1997; Dick and Scott, 1992).

Table 4.1: Physicochemical properties of FITC-Dextrans (FDs) (Sigma-Aldrich).

Property	**Molecular Weight (kDa)**	**Hydrodynamic Radius (nm)**
FD-4	4	1.4
FD-10	10	2.3
FD-70	70	6.0
FD-150	150	8.5

4.2 Materials

FTIC-dextran with average molecular weights of 4 kDa (FD-4), 10 kDa (FD-10), 70 kDa (FD-70) and 150 kDa (FD-150), used without any further purification steps were purchased from Sigma-Aldrich (Dorset, UK). Phosphate buffer saline (PBS) (Dubecco A) tablets were supplied by Oxiod Limited (Hampshire, England). Scotch 845 book tape, 3M, purchased from Scotch (Bracknell, UK). The Tissue-Tek® O.C.T^{TM} compound was purchased from VWR International (Leuven, Belgium). Donkey serum purchased from Sigma-Aldrich (Dorset, UK). Fluoromount-G supplied by Fisher (Loughbrough, UK).

4.3 Methods

4.3.1 Dextran extraction recovery

In order to assess the extraction recovery efficacy of dextran from porcine skin, skin samples were spiked with a known amount of dextran and an extraction process was performed as described previously in Section 3.3.7 using PBS as an extraction fluid. The extraction procedure for FD-4, FD-10, FD-70 and FD-150 from the *stratum corneum*, epidermis, dermis and receptor solution were calculated separately. The dextran content of each was assayed by fluorescence method described in Section 2.3.3. The data were represented as the drug recovery from each skin layer.

4.3.2 Dextran permeation study

Porcine ear hairs were removed using an animal hair clipper, the excess fat adhering to the dermis side was removed carefully using scalpel. Porcine skin was cut into pieces of suitable size and mounted with *stratum corneum* facing the donor compartment of previously calibrated Franz cells. The receptor compartment filled with phosphate buffer saline pH 7.4. The cells were allowed to equilibrate in a water bath (Grant Instruments, Cambridge, UK) at 37°C for 1 h before the start of the study. After equilibration, an integrity test was performed by inverting each cell and visually checking if there was any receiver fluid back flow as previously described in Section 3.3.2. A 1 mL aliquot of each donor solution i.e., an infinite dose (0.6 mg.mL^{-1}) of FD-4, FD-10, FD-70 and FD-150 in phosphate buffer saline at pH 7.4 was applied to the donor compartment, previous studies hence reported infinite doses of dextran applied to the skin (Kijima et al., 2015). Sink condition was controlled as previously described for minoxidil. *Ex vivo* diffusion studies were performed at atmospheric pressure (1010 mBar) and at hypobaric pressure (450 ± 50 mBar). Hypobaric pressure was applied for the first 1 h of a 2 h permeation study as per a published study (Inacio et al., 2016). At the end of the 2 h permeation study, the skin was removed, washed with phosphate buffer saline and blotted dry with cotton buds. The *stratum corneum* of the skin was

removed by tape striping (20 strips until the skin was translucent) using adhesive tape previously described in Section 3.3.7. The extraction of the dextran from the tape strips were performed by immersing the samples in phosphate buffer saline for 24 h. The epidermis and dermis were separated using scalpel and homogenized usign homogenizer (Ultra Turrax, Fisher Scientific, Leicester, Uk). The epidermis and dermis were homogenized in phosphate buffer saline, samples were treated by sonication and shaken in ambient temperature and dextran content was analysed after 24 h employing the dextran fluorescence method described in Section 2.3.3. The effect of hypobaric pressure upon dextran cutaneous delivery was represented by an enhancement ratio (ER) using Equation 3.4.

4.3.3 Confocal Microscopy

At the end of a 2 h dextran permeation study, skin samples were carefully cut in half along the diameter and embedded in Tissue-Tec O.C.T using liquid nitrogen to fix. Cross-section slices of 5 μm thickness were produced using a Bright Model OTF cryostat (Bright Instruments, Huntingdon, UK) as previously described in Section 3.3.5. Sectioning was started from dermis towards the *stratum corneum* in order to avoid dislocation of dextran from the *stratum corneum* surface to the lower layers. Samples were stored in -80°C freezer for 12 h prior to the staining procedure. For staining, samples were immersed in 10% formalin for 15 min to fix sections. Samples washed with phosphate buffer saline and incubated for 15 min in blocking buffer to block free sites in the sample and improve the sensitivity of the assay by eliminating background interference. Samples washed with phosphate buffer saline and DAPI added and left for incubation for 1 h. Skin samples then mounted with mounting medium and covered with glass cover slips. Confocal images were obtained with A1 inverted confocal with spectral detector Nikon (Kingston, United Kingdom) using a low magnification 10× objective. Images were captured in two fluorescence channels to allow the visualisation of the cellular structures stained by DAPI (blue colour) and dextran (green colour) using appropriate filters. Samples without the application of FITC-dextran were also tested as controls, and the autofluorescence of

the skin was negligible, which was adjusted by changing the contrast. Samples with and without the application of dextran were also captured as a control. Images were processed using Image J software (National Institute of Health, Maryland, USA).

4.3.4 Statistical analysis

Statistical evaluation was carried out using a statistical package for social sciences software (SPSS version 16.0, SPSS Inc, Chicago, USA). All data were checked in terms of normality (Kolmogorov-Smirnov test) and homogeneity of variances (Levene's test) prior to analysis. Permeation results were analysed using one-way analysis of variance test (one-way ANOVA). Statistically significant differences were defined when $P < 0.05$. All values were expressed as mean ± SD. The number of replicates was 3 in all experiments except permeation studies (n=5).

4.4 Results and Discussion

4.4.1 Dextran extraction recovery

Extraction recovery for FD-4, FD-10, FD-70 and FD-150, 2 h after incubation with tape strips (*stratum corneum*), epidermis, dermis and receiver fluid were represented in Table 4.2. Dextran extraction was within 100 ± 15 % recovery rate, which is within the acceptable range to use the data without correction for recovery (Health and consumer protection directorate-general, 2006).

Table 4.2: Dextran extraction recovery. Data represents the mean ± standard deviation (n=3).

Dextran MW (kDa)	**Recovery(%)**			
	Stratum corneum	**Epidermis**	**Dermis**	**Receiver**
4	91.6 ± 5.7	98.6 ± 4.8	97.3 ± 5.4	92.7 ± 6.1
10	90.3 ± 5.3	89.1 ± 4.7	92.1 ± 5.9	91.8 ± 7.2
70	93.4 ± 8.5	92.1 ± 3.6	90.4 ± 7.1	88.3 ± 5.4
150	91.8 ± 3.1	85.6 ± 6.1	92.1 ± 3.2	90.7 ± 8.3

4.4.2 Dextran permeation studies

To evaluate the influence of hypobaric pressure on the permeation of macromolecules a transport study of (FITC)-dextran of increasing molecular size (4, 10, 70 and 150 kDa) was performed. The application of local hypobaric pressure modified the skin drug deposition of all of the tested macromolecules. A trend of decreasing permeability across the skin with increasing molecular weights was observed at atmospheric pressure conditions (Figure 4.1). This was consistent with the general relationship between molecular weight and drug transport across a membrane and it suggested the skin was providing a barrier to the transport of the macromolecules (Chopra et al., 2010; Ambati et al., 2000). With the exception of the FD-4, which

was surprisingly high, the amount of dextran that penetrated through the skin into the receiver fluid was negligible under atmospheric pressure. The lowest molecular weight (FD-4) dextran permeated through the membrane significantly ($P < 0.05$) better than the FD-10 (139.9 ± 7.4 μg.cm^{-2} and 5.98 ± 0.27 μg.cm^{-2} respectively), and FD-10 dextran was significantly ($P < 0.05$) better than the FD-70 ($1.4 \pm 0.6\mu$g.cm^{-2}). However, higher molecular weight (FD-70 and FD-150) dextrans penetrates through the skin penetration was found to be equivalent ($P < 0.05$). This has been previously reported for the dextran in the range of 4 kDa to 70 kDa (Fang et al., 2004; Ogiso et al., 1994).

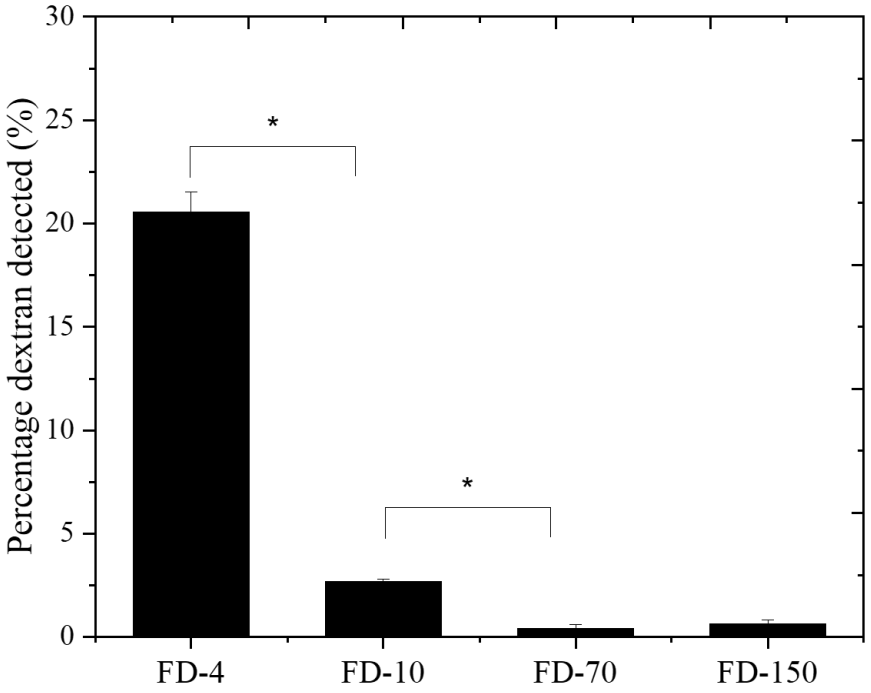

Figure 4.1: *In vitro* permeation of FDs at atmospheric pressure. The data represents the percentage of dextran transfered into the receiver fluid after 2 h transport study. Each point represents mean ± standard deviation (n=3).

The application of hypobaric pressure enhanced the permeation of dextran in most cases, but the effects were specific to the size of dextran, the permeation of dextran into receiver fluid followed the trend 4 kDa > 10 kDa > 70 kDa > 150 kDa (Figure 4.2). This enhancement was thought to be due to the changes in the skin properties caused by hypobaric pressure because previous studies have determined that dextran with various molecular weights were chemically stable during permeation experiments using porcine, mouse and rat skin when similar conditions were applied (Ying-zhe et al., 2009; Fang et al., 2004; Lee et al., 2008; Lombry et al., 2000).

It was not clear why each dextran showed a different enhancement patterns under hypobaric conditions. Hypobaric pressure significantly ($P < 0.05$) enhanced the amount of FD-4 in the *stratum corneum*, epidermis and dermis by 2.9, 2.0 and 1.22 respectively (Figure 4.2a). However, the data showed no permeation enhancement in the receiver fluid when hypobaric pressure was applied. In a previous study using laser to enhance the transdermal dextran delivery, an enhancement of 1.2-fold for FD-4 in porcine skin (Zorec et al., 2017), however, this enhancment could be due to the duration of their study which was 5 h in contrast with the current study which was 2 h. In another study Inacio et al. (2016) reported a 3-fold enhancement in the deposition of FD-4 within dermal tissue when hypobaric pressure applied in rat skin. The different enhancement ratio compared to the current work could have been due to the difference in the membrane characteristics, i.e., thickness or number of follicles. In the same study no enhancement observed in the accumulation of FD-4 in the *stratum corneum*, it was expected that dextran diffused more quickly into the lower layers in rat in contrast with the porcine skin.

The application of hypobaric pressure significantly ($P < 0.05$) enhanced the amount of FD-10 in the epidermis, dermis and across the skin into the receiver fluid by 2.1, 2.6 and 2.3 respectively (Figure 4.2b). Although published works have shown permeation/enhancement in the permeation studies the *stratum corneum* was either damaged or completly removed. For example, Wu et al. (2006) demonstrated that physical pretreatment, such as needle puncture, sandpaper abrasion and tape

stripping can enhance the dextran permeation through the hairless rat skin, enhancement of 10, 20 and 3000-fold respectively. These data showed that the physical penetration enhancers methods work through overcoming the barrier function of the *stratum corneum*. The higher enhancement values in the forementioned study in contrast to the hypobaric pressure method can also be due to the longer period of permeation study, which was 6 h for this experiment.

The application of hypobaric pressure significantly ($P < 0.05$) enhanced the amount of FD-70 in the epidermis and across the skin into the receiver fluid by 1.5 and 8.1 respectively. However, no enhancement was observed in the the *stratum corneum* and dermis layers (Figure 4.2c). The enhancement ratio of FD-70 was significantly ($P < 0.05$) more compare to FD-10 in respect to the receiver fluid. The trends of enhancement ratio in the receiver fluid for FD-4 and FD-10 seemed to suggest that, the hypobaric pressure effects were more pronounced upon the transdermal delivery of the higher molecular weight dextrans. However, the application of hypobaric pressure did not alter the amount of FD-150 within skin layers and across the skin. FD-150 was found to be equivalent ($P < 0.05$) under both hypobaric and atmospheric pressure conditions (Figure 4.2d). This data suggested that hypobaric pressure of 450 ± 50 mBar was only evaluate for molecules with a size less than 150 kDa. In future work hypobaric pressure could be combined with another enhancer method to enhance the permeation of macromolecules with a mass of ≥ 150 kDa.

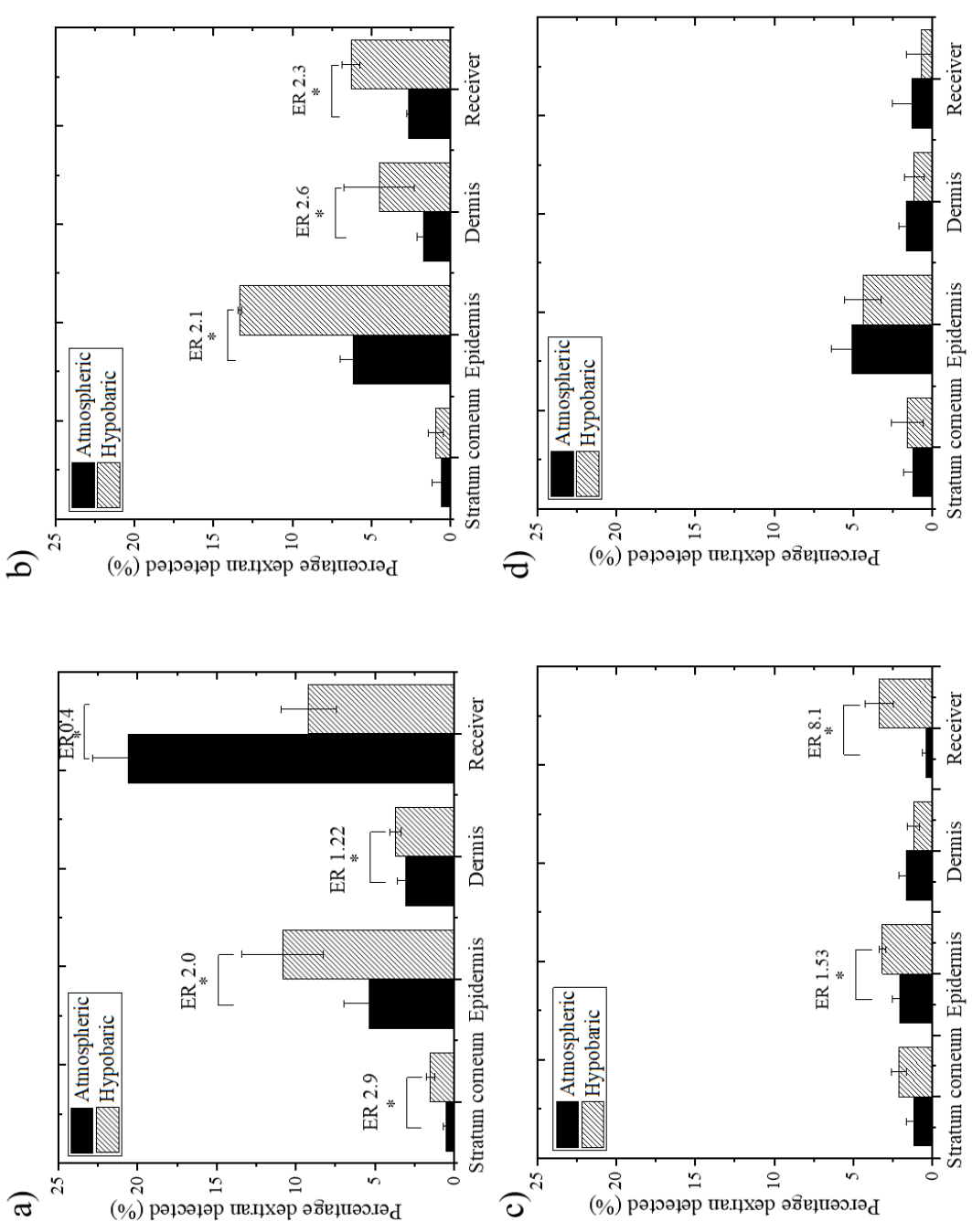

Figure 4.2: Dextran in porcine skin layers after delivery at atmospheric (1010 mBar) and hypobaric (450 ± 50 mBar) pressures. Bars represent mean ± standard deviation (n=3) for both conditions. ER (enhancement ratio) represents the ratio between the % amount of dextran found under hypobaric and atmospheric conditions. a) 4 kDa, b) 10 kDa, c) 70 kDa and d) 150 kDa.

Different molecular weights of dextran (see Table4.3) can mimic the diffusion of different sized macromolecules such as peptides (4 KDa and 10 kDa), cytosines (70 kDa) and antibodies (150 kDa) (Dreher et al., 2006). The obtained data showed that the application of hypobaric pressure can enhance the permeation up-to 70 kDa in size using 1 h application.

Table 4.3: Dextran mass that has penetrated the *stratum corneum* employing hypobaric pressure. $*$ represents no enhancement in hypobaric pressure in contrast with atmospheric pressure. Data represents the mean ± standard deviation (n=3).

Dextran MW (kDa)	**Mass/Area (μg.cm^{-2})**			
	Stratum corneum	**Epidermis**	**Dermis**	**Receiver**
4	4.1 ± 0.5	30.24 ± 7.9	10.43 ± 2.3	*
10	*	29.75 ± 4.9	10.06 ± 1.2	14.05 ± 1.02
70	*	9.5 ± 1.9	*	10.09 ± 3.5
150	*	*	*	*

4.4.3 Dextran skin distribution

The morphology of the skin samples after treatment for 1 h with hypobaric pressure were similar to those treated at atmospheric pressure (Figure 4.4 c and d vs. e and f). The intact *stratum corneum*, or outermost layer of the skin can be seen, followed by the epidermis and dermis. The skin autofluorescence under the experimtal condition was negligible, since no green colour was observed in the control samples. Therefore, the intensity of chromophores, which have similar excitation as dextran, in the skin were too weak to be captured by the confocal microscope (Hanson and Bardeen, 2009).

A thick and intact *stratum corneum* was evident in all samples including those treated with hypobaric pressure. This data suggested that the application of hypobaric pressure did not cause skin damage (Figure 4.4). The tissue samples at

atmospheric pressure showed localised (FTIC)-dextran (FD-4 and FD-70) primarily in the *stratum corneum* and then in epidermal layers (Figure 4.4 c and d). Dexrtran permeation at the tested molecular weights was observed in the lower layers at atmospheric conditions, but the intensity was negligible in contrast with the epidermal layer. Padilla-Martinez et al. (2012) reported previously that fluorescence intensity distribution of dextran in the porcine skin was mainly confined to the surface of the *stratum corneum*.

There was a significant increase in the fluorescence intensity in lower skin layers when samples were exposed to the hypobaric pressure compared to those at atmospheric pressure (Figure 4.4 e and f). The fluorescence intensity was stronger around the perifollicular region (indicated with arrows), which suggested that the dextran permeation enhancement occurred at least in part via the follicular route as reported previously (Todo et al., 2010; Horita et al., 2014). Inacio et al. (2016) suggested that hypobaric pressure enhanced the permeation of dextran through hair follicles. However, in the current work it was evident that dextran also permeated through the skin via intercellular and transcellular pathways, since the green colour, which represented dextran, can be seen in areas without hair follicles. The possible influence of hypobaric pressure on the dextran follicular permeation can be linked to the suction effect. The suction unplugs the hair follicles from corneocytes and sebum that clogges the hair follicles. Lademann et al. (2001) previously showed that some follicles are open, while others are closed for the drug penetration. In another study performed by the same author, mechanical peeling facilitated the drug penetration into the skin through opening the closed follicular routes (Lademann et al., 2008). Moreover, the application of hypobaric pressure cause the skin to stretch, which modifies the follicular structure by increasing the horizontal planar length and reducing its depth. Inacio et al. (2016) reported that horizontal planar length of follicle increased by 78 μm and its depth reduced by 13.9 μm when atmospheric pressure applied.

The distribution of dextran within the skin layers revealed that hypobaric pressure enhanced its permeation not only through follicular routes, but it was

hypothesised that dextran diffusion was through transcellular and/or intercellular routes as well. For example, the treatment with hypobaric pressure could modify the gap junctions. Gap junctions allow the permeation of ions and neutral molecules smaller than 1 kDa (Bennett and Verselis, 1992). It was assumed that the stretching effect of hypobaric pressure enlarged the channel diameter, which resulted in the permeation of higher molecular weight such as 4 kDa (14 Å) and 70 kDa (60 Å). In the epidermal barrier there are also tight junctions, which seal the intercellular spaces. Tight junctions perform vital functions for example, holding cells together and form protective and functional barriers. Tight junctions are highly permeable for molecules up to 4 Å, but almost impermeable for macromolecules (Liang and Weber, 2014). Previous investigation reported the tight junction act as a barrier for fluorescein (0.3 kDa), (FITC)-dextran (3, 4 and 40 kDa) in cultured keratinocytes and a 0.5 kDa tracer in skin (De Benedetto et al., 2011; Mertens et al., 2005; Yuki et al., 2007; Kirschner et al., 2011; Furuse et al., 2002; Kirschner et al., 2010). It was hypothesised that hypobaric pressure caused deformation in the structure of tight junctions through stretching and this could increase dextrans penetration into the skin (Figure 4.3).

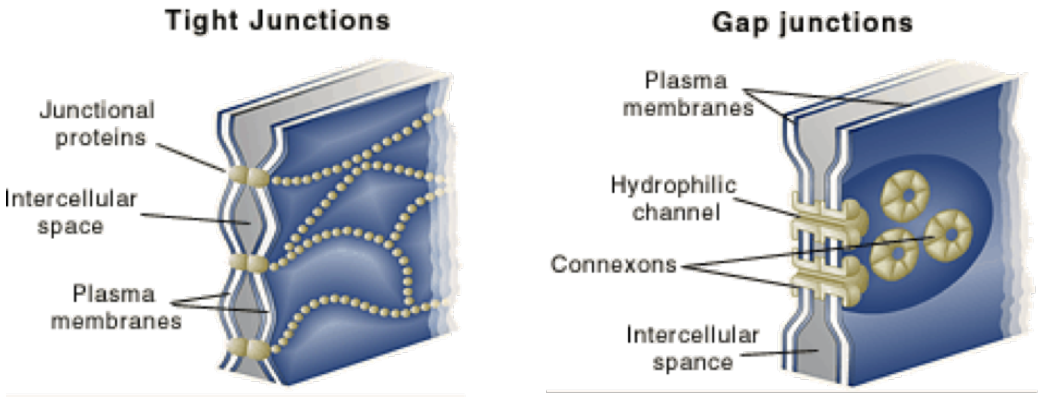

Figure 4.3: Diagram showing the difference between tight junctions and gap junctions (Biology Arizona, 2002).

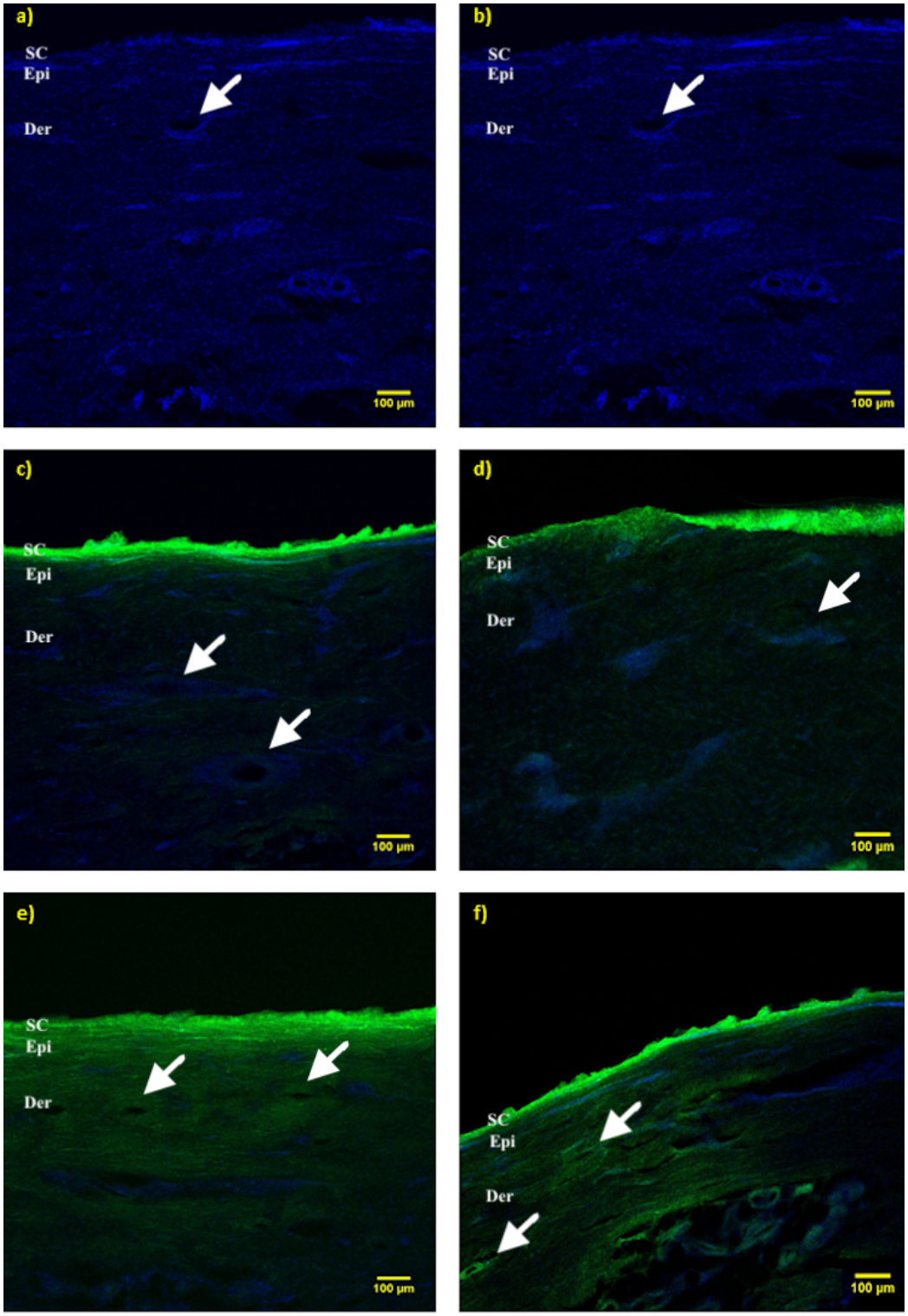

Figure 4.4: Confocal microscopic examination after topical administration of FD-4 and FD-70 dextran under atmospheric conditions (1010 mBar) and hypobaric conditions (450 ± 50 mBar): control samples at atmospheric (a) and (b); topical FD-4 delivery under atmospheric conditions (c) and upon hypobaric pressure (d); topical FD-70 delivery under atmospheric conditions (e) and upon hypobaric pressure (f). Magnification × 10. The arrows indicate the hair follicles.

4.5 Conclusion

To investigate on the permeation of macromoleules through the porcine skin when hypobaric pressure applied different sizes of dextrans were used. Skin permeation of dextran decreased with increasing molecular weight. The data represented a significant ($P < 0.05$) enhancement in the permeation of dextran up-to 70 kDa. It was hypothesised that hypobaric pressure can temporary open up the pores through suction, the effect was reversible since no damage or detachment observed in the skin histology after the treatment. Macromolecules, up to 70 kDa, which been shown to have enormous therapeutic potential in cancer-therapy and other diseases. Skin delivery of these macro-compounds can be done through painless and noninvasive hypobaric method although further *in vivo* investigation are required before proceeding into clinical trials.

In order to widen the scope of molecules that can be used for hypobaric pressure method in the next phase of this project; nanosized particles were used to investigate if hypobaric pressure is a suitable method for a larger size particles.

5

Investigation of hypobaric pressure on nanoparticle penetration into the skin

5.1 Introduction

In the previous Chapters of this thesis hypobaric pressure succeeded in enhancing the percutaneous delivery of a small hydrophobic drug and a series of a larger model hydrophilic compounds. As a consequence, it has been shown to be a useful method to deliver compounds with a size of less than 10 nm. The question then arises, what is this is the cut-off size for delivery enhancement of compounds using hypobaric pressure? Chapter 5 focuses on percutaneous delivery of nanoparticles with a size of $\geq$ 50 nm.

The term "nanoscale" refers to sizes in the range of 1 to 100 nm. However, for the purpose of drug delivery, colloids in the range of 50 – 500 nm are often defined as nanomaterials (Uchechi et al., 2014). Nanotechnology is a field of research, which is spreading rapidly. Scientist are producing nanosized colloids to use in an extraordinary numbers of applications (Keiper, 2003). Therefore, it is not surprising that polymer nanoparticles and solid lipid nanoparticles have been studied as potential carriers for the transdermal drug delivery of molecules such as acyclovir, adapalene , vitmines A and E (Rolland et al., 1993; de Jalon et al., 2001*a*; Wissing and Müller, 2002; Dingler et al., 1999; Jenning et al., 2000).

Nanocarriers can protect chemically unstable compounds, avoid incompatibility between different ingredients in the formulation and facilitates the absorption of compounds by forming a film on the skin surface (Gupta et al., 2013). However, to develop a transdermal delivery system, it is important to investigate the fate of the nanosized drug carrier in the skin. Dye-loaded colloids can be used to measure the accumulation of particles and their distribution within the skin strata.

There have been a number of investigations that have shown that the penetration of topically applied drugs often occurs through the *stratum corneum* via diffusion in the skin lipids around the corneocytes (Bouwstra et al., 2001; Choi et al., 1999; Hadgraft, 2001), but recent studies have also shown that the hair follicles play a significant role in the percutaneous delivery of same molecules (Lauer et al., 1995; Schaefer and Lademann, 2001; Lademann et al., 2001; Ogiso et al., 2002). For example, Feldmann and Maibach revealed an enhancement in absorption rates in skin with higher follicular density (Feldman, 1967). Another study, showed a reduction in percutaneous absorption of appendage-free scarred skin when they compared it to the normal skin (Hueber et al., 1994; Tenjarla et al., 1999). So it is possible that hypobaric pressure could enhance drug delivery by both the intercellular and follicular routes.

The hair follicles have been shown to be an effective reservoir for the topical drugs, which is equivalent to the reservoir of the upper most layer of the skin on several body sites (Otberg, Richter, Schaefer, Blume-Peytavi, Sterry and Lademann, 2004). The highest density of hair follicles is located on the scalp, forehead and calf areas. The reservoir of *stratum corneum* is located in the uppermost 5 μm of the skin (Weigmann et al., 2001), but the reservoir of the hair follicles stretches deep into the tissue (around 2000 μm) from the surface (Toll et al., 2004). The hair follicles are in close contact with the dendritic cells and blood capillaries and this may influence percutaneous transport by this route. In contrast, in the *stratum corneum* the storage of materials is short, because of its high turnover. The reservoir in the hair follicles can be emptied through diffusion into the living cells, or exiting the hair follicles via sebum flow. The storage of substances in

the hair follicles is considered a more long-term reservoir for percutaneous drug delivery (Lademann et al., 1999, 2001).

Size plays an important role in percutaneous delivery; objects greater than 5 nm do not diffuse into the lipid layers in the *stratum corneum*, but they are able to penetrate the infundibula of the hair follicles (Schaefer, 1996). For example, titanium dioxide particle size (100 nm) which, are frequently used in sunscreens, can penetrate the hair follicle, but are not able to diffuse into the living cells (Lademann et al., 1999). Moreover, 100 nm particles are not able to diffuse into the "closed" hair follicles. Closed hair follicles are referred to those follicles that are covered by plug, this barrier can be removed by peeling or cyanoacrylate surface biopsy (Otberg, Richter, Knuttel, Schaefer, Sterry and Lademann, 2004; Otberg, Richter, Jacobi, Blume-Peytavi, Schaefer, Sterry and Lademann, 2004). Toll et al. opened hair follicles and explored the penetration enhancement in the hair follicles using fluorescent dye-labeled microspheres. Particles with a diameter around 750 nm penetrated through the hair follicle (Toll et al., 2004). This prior literature demonstrates that nanoparticles are a promising drug delivery method, but their passage into the skin without barrier alteration is difficult. Therefore, there is need to develop new delivery methods for percutaneous delivery of nano-sized and micro-sized carrier systems.

The aims of this Chapter was to investigate the influence of hypobaric pressure on the percutaneous delivery of nanomaterials. In this Chapter three different types of nanocarriers (solid lipid, liposome and polymer-polystyrene) were investigated, they were chosen because each displayed different surface chemistry, a different surface charge (neutral and negative) and size (50 – 1000 nm). In order to investigate the permeation profile of these nanoparticles, fluorescent dye was encapsulated in them. Nanomaterial permeation profiles under hypobaric (450 $\pm$ 50 mBar) and atmospheric (1010 mBar) conditions were investigated. Confocal microscopy was employed to determine the tissue distribution of the nanocarriers within the full thickness porcine skin.

5.2 Materials

A mixture of medium chain triglycerides (Labrafac® WL 1349) was provided by Gattefossé S.A. (Saint Priest, France). Soybean lecithin (Lipoid S75-3N) was donated by Lipoid Gmbh (Ludwigshafen, Germany), while a mixture of free polyethylene glycol 660 and polyethylene glycol 660 hydroxystearate (Solutol® HS 15) was provided by BASF (Univar, UK). NaCl was purchased from VWR (Leicestershire, UK). FluoSpheres^{TM} polystyrene microspheres (1.0, 0.5, 0.1 μm), red fluorescent, were purchased from (Thermoscientific, UK). 1,2-dipalmitoyl-sn-glycero-3-phosphocholine (DPPC) were purchased from Avanti Polar Lipids (Alabaster, USA). (±)- alpha-tocopherol phosphate disodium salt (α-TP), nile red (technical grade), N.Methyl-2-pyrrolidinon 99.5 % ethanol, acetone were obtained from Sigma-Aldrich (Dorset, UK). HPLC grade water and chloroform were obtained from Fisher Scientific (Leicester, UK). Phosphate buffered saline (Dulbecco A) tablets was supplied by Oxoid Limited (Hampshire, UK). The Tissue-Tek® O.C.T^{TM} compound was purchased from VWR International (Leuven, Belgium). Donkey serum purchased from Sigma-Aldrich (Dorset, UK). Fluoromount-G supplied by Fisher (Loughbrough, UK).

5.3 Methods

5.3.1 Solid lipid nanoparticle fabrication

One of the most commonly used method for production of solid lipid nanoparticle was used in this study, i.e., precipitation from a stable emulsion followed by repeated phase inversion, as previously described by Heurtault et al. (2002). Medium chain triglycerides (4.25 g), phosphatidylcholine (0.4375 g), PEG hydroxystearate (4.25 g) and a 3 % w/v sodium chloride aqueous solution (16.0625 g) were mixed at room temperature and then heated to 85°C at a rate of 4°C per min, with continuous magnetic stirring (Figure 5.1). The mixture was then allowed to cool to 60°C. The temperature of the mixture was cycled between 60°C and 85°C a total of three times. Within this temperature range phase inversion occurred, with an oil-inwater

emulsion being converted to and from a water-in-oil emulsion. Following the final heating cycle, the emulsion was allowed to cool to 72°C, at which point 25 mL of icecold water was added, causing nanoparticles generation. The suspension was stirred for 5 min then made up to a final volume of 50 mL using deionised water. Lipid nanoparticle suspensions were purified of excess excipients and larger particulate matter via centrifugation (Beckman L8-80 ultracentrifuge, Beckman Coulter, Buckinghamshire, UK) at 110,000 g and 25ºC for 1 h. The suspension separated into three distinct layers; an upper gel like layer, a middle lipid nanocapsule suspension layer, and a bottom sediment layer. The purified suspension layer was used for further experimental work.

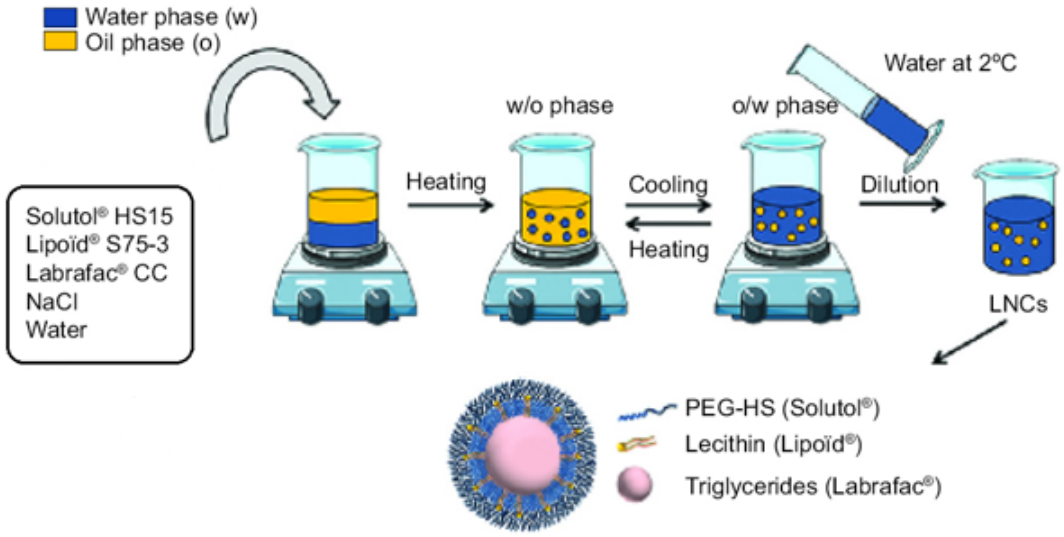

Figure 5.1: : lipid nanocapsule preparation using phase inversion method Heurtault et al. (2002).

5.3.2 SLN size analysis

The size of solid lipid napoparticle was determined by dynamic light scattering with Zetasizer Nano ZS (Malvern Instruments, Worcestershire, UK) at scattering angle of 173°, using water as dispersant (refractive index = 1.33, viscosity = 0.8872 cP at 25°). Mean diameter (Z-average) was reported from intensity-weighted size distribution, which determines particle size distribution based on the diffusion coefficient (D)

of particles undergoing Brownian motion. The Stokes-Einstein equation relates D to the hydrodynamic particle diameter (Equation 5.1):

$$d(H) = \frac{kT}{3\pi\eta D} \tag{5.1}$$

Where d(H) was the hydrodynamic diameter, D was the translational diffusion coefficient, k was Boltzman constant, T was the absolute temperature and η was the viscosity. Each measurement comprised 10-14 runs and was performed in triplicate for each sample. Mean diameters obtained from the size-intensity frequency distributions were reported. Physical stability of particles was assessed based on changes in size, over a 24 h period after preparation.

5.3.3 SLN Zeta potential determination

The zeta potential of the lipid nanoparticles was determined as a function of their electrophoretic mobility using Zetasizer Nano, Malvern Instruments (Worcestershire, UK). This method involved the application of an electric field with fast field reversal to a nanoparticle suspension and the measurement of particle velocity as it moves towards the oppositely charged electrodes, dependent upon the surface charge of the particle coupled with any strongly bound ions (Stern layer) and loosely bound ions (diffuse layer). Samples were analysed following dilution with PBS. Each measurement comprised between 50 to 100 runs and was performed in triplicate at 25°C using a quartz cell.

5.3.4 Dye loading and purification of SLN

Nile red (300 μg) was incorporated into the nanoparticles by addition to the triglyceride phase as a 0.01 % w/v acetonic solution. The acetone was removed by evaporation before continuing with the manufacture protocol. The amount of each probe contained in a) the purified suspension as a whole, b) the lipid nanoparticles only and c) the continuous phase was assayed by appropriate dilution of each compartment with ethanol. The lipid nanoparticles were separated from the continuous phase using Amicon^{TM} ultra 0.5 centrifugal filter devices with ultracel

100 membranes (100 kDa molecular weight cut off) (Millipore, UK). Three 0.5 mL aliquots were removed from the purified lipid nanoparticles suspension and placed in the sample reservoir of the filter devices and centrifuged for 40 min at 14,000 g at ambient temperature (Biofuge Pico centrifuge, Heraeus, Buckinghamshire, UK). During this process any free fluorescent probe in the continuous phase passed through the filter into the receiver chamber, and the nanoparticles were retained on the filter. The lipid nanoparticles were recovered by inverting the filter device into a new receiver chamber and centrifuging for 5 min at 1,000 g prior to dilution in ethanol. The filter was subsequently washed twice with ethanol in order to ensure maximal particle recovery and these washings were combined with the lipid nanoparticles fraction. Fluorescence intensity for all samples was read in triplicate and converted to concentration (μg.mL^{-1}) using the appropriate linear regression equation. The drug content, drug recovery and loading efficiency of the purified lipid nanoparticles suspensions were calculated as follows (Equations 5.2 & 5.3):

$$\text{Drug recovery } \% = \frac{W_{susp}}{W_{input}} \times 100 \tag{5.2}$$

$$\text{Loading efficiency } \% = \frac{W_{lipidnanocapsule}}{W_{susp}} \times 100 \tag{5.3}$$

where W_{susp} was the mass of probe in the nanoparticles suspension, W_{input} was the initial mass of probe added during manufacture $W_{lipidnanocapsule}$ was the mass of probe associated with the nanoparticles. Nile red loaded solid lipid nanoparticles were also assessed for leakage of dye after incubation at 32°C in shaking water bath over 6 h, by quantifying the amount of dye remaining in the solid lipid nanoparticles.

5.3.5 *In vitro* permeation of solid lipid nanoparticles using hypobaric pressure

A permeation study was conducted using porcine skin as previously described in (Section 3.3.3). The study was performed using Franz diffusion cells at atmospheric pressure (1010 mBar) and hypobaric pressure (450 ± 50 mBar) conditions. The receptor compartment filled with PBS. A 1 mL aliquot of SLN suspension (approx.

170 mg.mL^{-1} solid content) was applied to the donor compartment. The skin samples were exposed to hypobaric pressure for 1 h and the experiment was continued for a total of 2 h, the second hour was under atmospheric pressure. At the end of permeation study, the skin layers were separated as previously described in (Section 3.3.8). The dye was extracted by soaking the *stratum corneum* tapes and skin samples in ethanol, and the samples were left overnight in shaking water bath at 37°C, homogenised with a tissue homogeniser (Ultra Turrax, Fisher Scientific, Leiceister, UK) and subsequently sonicated in water bath. The samples were filtered with 0.22 μm membrane filter prior to quantification of dye using fluorescence spectrophotometer (Varian Cary Eclipse, Agilent, Cheadle, UK) as previously described in (Section 2.3.3), to quantify the amount of nile red in separated skin layers.

5.3.6 α-TP liposome fabrication

This Section completed with the assistance of MSc student, Chui Hua Lim. In this study, dipalmitoylphosphatidylcholine (DPPC) and alphatocopherol phosphate (α-TP) were used to fabricate the liposomes. α-TP is the phosphorylated form of the biologically active vitamin E which can self-aggregate in aqueous environment to form bilayer vesicles (Gavin et al., 2017). Liposomes were prepared by solvent evaporation. DPPC and α-TP (total weight of 10 mg) were dissolved in chloroform and the solvent was removed by overnight storage in a vacuum desiccator (Duran, Mainz, Germany). The dry lipid film was hydrated with 0.01 M phosphate buffered saline (PBS) to produce lipid dispersion of 4 mg.mL^{-1} and sonicated in water bath at 40°C for 10 min to produce multilamellar liposomes. Further size reduction and homogenisation of liposomes was achieved using a probe-type sonicator (Soniprep 150, MSE, London UK) at amplitude of 10 μm for 10 min.

5.3.7 α-TP liposome size analysis

The size of the liposome was determined as previously described in (Section 5.3.2). The samples were stored in the fridge at 4°C to avoid chemical degradation of

liposomes, and size was measured at weekly intervals after preparation for four consecutive weeks.

5.3.8 α-TP liposome zeta potential determination

The zeta potential of the liposomes at different concentration of α-TP was analysed with the Zetasizer Nano ZS based on their electrophoretic mobility as previously described is (Section 5.3.3).

5.3.9 Dye loading and purification of α-TP liposome

Nile red was incorporated in liposomes by adding 3 mL of 0.01 % w/v solution in acetone (containing 300 μg nile red) to the lipid mixture prior to solvent evaporation. The unloaded dye was removed by four cycles of centrifugation with Amicon ultra 0.5 centrifugal device. The purified liposomal formulations were assessed for their loading efficiency based on (Equation 5.3) as previously described in (Section 5.3.4).

5.3.10 *In vitro* permeation of α-TP liposome using hypobaric pressure

A permeation study using porcine skin was conducted using the method previously described in (Section 3.3.3). The study was performed using Franz diffusion cells (100 μL of the undiluted liposome formulations containing nile red was applied to the skin, solid content unknown) at both atmospheric pressure (1010 mBar) and hypobaric pressure (450 $\pm$ 50 mBar) conditions, the receiver compartments were filled with PBS and sink condition controlled in all samples. At the end of permeation study, the skin layers were separated as previously described in (Section 3.3.8). The dye was extracted by soaking the tapes and skin samples in ethanol as previously described in (Section 5.3.5). The sample fluorescence intensities were quantified as previously described in (Section 2.3.3).

5.3.11 FluoSphere™

In this study microspheres were used to track and quantify the amount of particles that permeated through the skin layers. Microspheres also known as latex beads are spherical particles in the colloidal size range that are produced from amorphous polymers (i.e. polystyrene). Particles in 3 different size 100, 500 and 1000 nm were purchased from Thermo Fisher scientific. The manufacture fabrication state that the polystyrene particles were swelled in a solvent containing a hydrophobic dye specifically made for the FluoSpheres product. The dye is then able to diffuse into the polystyrene matrix. Then the beads were removed from the solvent and dialysed into an aqueous environment, that reverses the swelling and traps the dye in the polystyrene. The trapped dye is well protected from the external environment. The exact protocol and identity of the hydrophobic dyes are proprietary. Thus these unknown particles are an excellent choice for tracking permeation into the skin because the fluorescent beads shown little to no photobleaching while excited with the intense illumination (ThermoFisher, 2018).

5.3.12 FluoSpheres™ characterisation

The size of the polystyrene nanoparticles were determined as previously described in (Section 5.3.2). The zeta potential of the microspheres particles were analysed with the Zetasizer Nano ZS based on their electrophoretic mobility as previously described in (Section 5.3.3). Release study was determined for 3 h as previously described in (Section 5.3.4). The samples were stored in the fridge at 4°C as per the manufacture's instructions.

5.3.13 *In vitro* permeation of FluoSpheres™ using hypobaric pressure

A permeation study was conducted using porcine skin as previously described (Section 3.3.3). A permeation study used Franz diffusion cells at atmospheric pressure (1010 mBar) and hypobaric pressure (450 ± 50 mBar) conditions, 100 μL (5% solids) of nanoparticles solution was applied to the donor compartment of

each cell, and reciever compartment filled with PBS, sink condition controlled in all samples.

At the end of permeation study, the skin layers were separated as previously described in (Section 3.3.8). The dye was extracted by soaking the tapes and skin samples in 90:10 Methyl pyrrolidone:PBS solution, to dissolve and break open the polystyrene nanoparticles and relieve the fluorescent dye. Samples fluorescence intensity were quantified as previously described in (Section 2.3.3).

5.3.14 Confocal microscopy

At the end of the 2 h skin permeation study, skin samples of 100 nm nanoparticles and 50 nm solid lipid nanoparticles, which represented two different size particles, were carefully cut in half along the diameter and subsequently embedded in Tissue-Tec O.C.T. Cross-section slices of 5 μm thickness were produced using a Bright Model OTF cryostat (Bright Instruments, Huntingdon, UK) as previously described in (Section 3.3.5). Sectioning was started from dermis towards the *stratum corneum* in order to avoid dislocation of dextran from the *stratum corneum* surface to the lower layers. Samples were stored in -80° freezer for 12 h prior to the staining procedure. For staining the samples, first a ring was drawn around the tissue sample using liquid blocker pen. Then samples immersed in 10% formalin for 15 min to fix the sections. Samples washed with phosphate buffer saline and incubated for 15 min in blocking solution (donkey serum). Samples washed with phosphate buffer saline and DAPI added and left for incubation for 1 h. Skin samples then mounted with mounting medium (fluoromount-G) and covered with glass cover slips. Confocal images were obtained with A1 inverted confocal with spectral detector Nikon (Kingston, United Kingdom) using a low magnification 10× objective. Images were captured in two fluorescence channels to allow the visualisation of the cellular structures stained by DAPI (blue colour) and encapsulated dye in the nanoparticles (red colour) using appropriate filters. Samples with and without the application of nanoparticles were also captured as a control. Images were processed using Image J software (National Institute of Health, Maryland, USA).

5.3.15 Data analysis

Statistical evaluation was carried out using a statistical package for social sciences software (SPSS version 16.0, SPSS Inc, Chicago, USA). All data were checked in terms of normality (Kolmogorov-Smirnov test) and homogeneity of variances (Levene's test) prior to analysis. Permeation results were analysed using one-way analysis of variance test (one-way ANOVA). Statistically significant differences were defined when $P < 0.05$. All values were expressed as mean ± SD. The number of replicates was 3 in all experiments except permeation studies (n=5).

5.4 Results and Discussion

5.4.1 Solid lipid nanoparticle characterisation

Suitable characterisation of solid lipid nanoparticles is vital for reproducible manufacture and understanding their skin penetration. For characterisation studies, it was necessary to evaluate the particles size and size distribution and zeta potential. The particle size and zeta potential was analysed using photon correlation spectroscopy, which measured the scattered light produced by the particle movement (Mukherjee et al., 2009). The size data is shown in Figure 5.2.

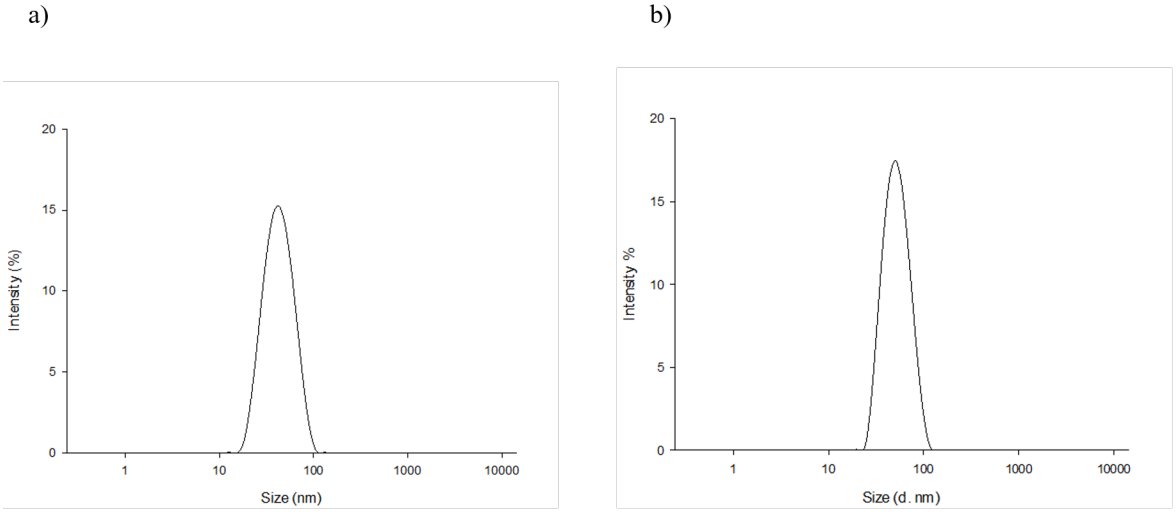

Figure 5.2: Size distribution by intensity of: a) lipid nanoparticle suspension and b) nile-red loaded lipid nanoparticle suspension, measured using zeta nanosizer.

Size analysis of blank particles and nile red-loaded lipid nanoparticles data showed no statistically significant ($P > 0.05$) differences in mean nanparticle size (see Table 5.1). This was in agreement with a previous study of the size analysis of lipid nanoparticles, which showed 45.5 ± 0.7 nm and 45.6 ± 0.2 nm for blank and nile red-loaded lipid nanoparticles respectively (Chana et al., 2015). The zeta potential of the lipid nanoparticle suspensions (see Table 5.1) was neutral in both blank and encapsulated particles. Zeta potential measurements allows predictions of the storage stability of colloidal particles (Müller and Hildebrand, 1996). Normally, particle aggregation is not common for charged particles (high zeta

potential) because of electric repulsion (Müller et al., 2000). In order to evaluate the physical stability of the particles, the change in mean particle size was recorded over 24 h. Data showed that solid lipid nanoparticles were stable for 24 h (Figure 5.3). The stability of particles is an important factor for transport studies, solid lipid nanoparticles were a good candidate for further transport studies. There are some factors that can influence the physical stability of the particles, such as storage temperature (Gao and McClements, 2016), therefore, during the course of experiments particles were fabricated freshly on the day.

Table 5.1: size and zeta potential for unloaded LNP and nile red-loaded lipid nanocapsule. Data represent mean ± SD (n=3).

SLN type	**mean size (nm)**	**Zeta potential (mV)**
Blank	44.82 ± 0.8	-2.49 ± 0.15
Nile red encapsulated	45.3 ± 0.7	-2.74 ± 0.14

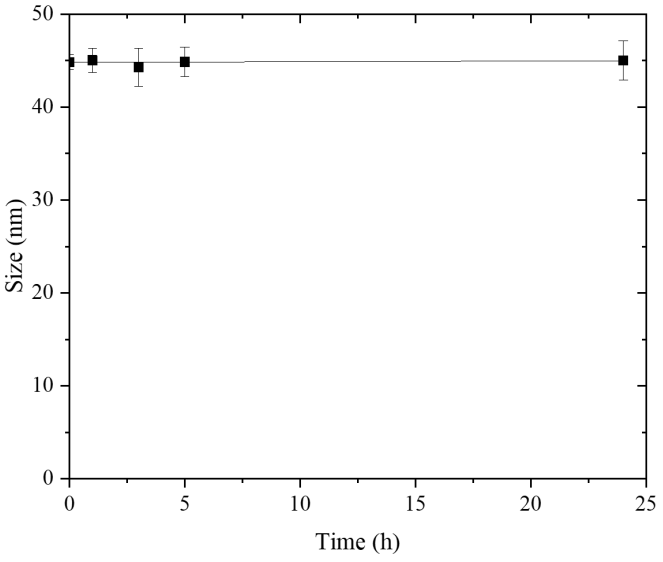

Figure 5.3: Changes in size for solid lipid nanoparticles over 24 h. Each data point represents mean ± standard deviation (n=3).

5.4.2 SLN loading determination

The loading of nile red into the solid lipid nanoparticle suspension was calculated using Equation (5.1 & 5.2). The amount of probe recovered from the purified suspension as a percentage of probe input was high at 92.5 ± 2.03 % of the amount of probe recoverable. The loading efficiency of nile red was 96.7 ± 3.33 %.

In order to investigate whether nile red was stable within the solid lipid particles before the skin permeation study a release study performed after particle purification. The data showed no major leakage for 6 h, all the batches of SLN retained more than 95 ± 4.2 % of nile red (Figure 5.4). In a leakage study performed by Dorraj and Moghimi (2013) less than 2% nile red was released, which correlated with the results in the current work. This results suggest that nile red is encapsulated in solid lipid capsules and did not leak, presumably due to the hydrophobic nature of nile red; its log P is approximately 5 (Greenspan et al., 1985), therefore it is expected to remain in the lipophilic particles. Furthermore, the solid matrix of SLN works as a shield against release of nile red. For example, more than 90% loading efficacy for indomethacin and around 80 % for primidone in similar SLNs (Calvo et al., 1996; Ferranti et al., 1999).

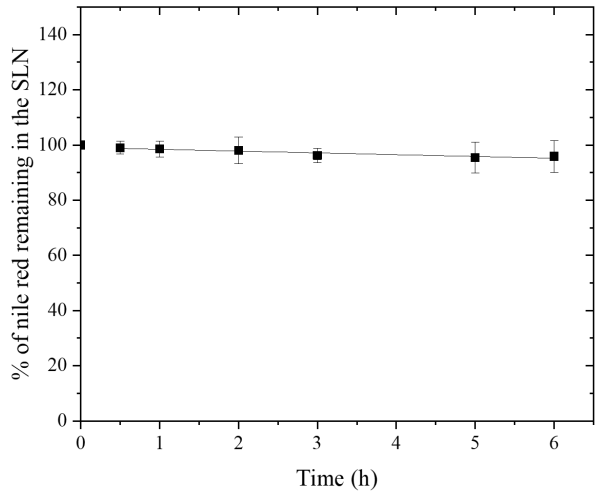

Figure 5.4: Percentage of nile red remaining in solid lipid capsules after incubation at 32°C over 6 h. Each data point represents mean ± standard deviation (n=3).

The data from release study was indicated minimal leakage of nile red within 6 h. It has been reported that the probe association with the particles can influence for epidermal targeting (Santos Maia et al., 2002). The probe stability in the particles is highly important for particle tracking within the skin. previously, a leakage of 1% was reported over the course of 6 h (Chana et al., 2015).

5.4.3 *In vitro* permeation of SLN using hypobaric pressure

Solid lipid nanoparticles (SLN) introduced in 1991 as an alternative carrier delivery system to traditional colloidal carriers. For example, emulsions, liposomes and polymeric microparticles and nanoparticles. Solid lipid nanoparticles contain advantages of the traditional carriers, but evade some of their major disadvantages (Müller et al., 2000).

The use of hypobaric pressure showed an enhancement in the deposition of SLN within the percutaneous skin layers (Figure 5.5). The ability of hypobaric pressure to localise the dye loaded particles within all the skin (layers combined) was found to be significantly greater ($P < 0.05$) when compared to the atmospheric pressure. An enhancement ratio of 1.2, 8.7 and 7.7-fold in *stratum corneum*, epidermis and dermis, respectively was calculated for the hypobaric pressure (Figure 5.6). Previous studies using physical enhancement methods for larger molecules, such as nanoparticles, reported an enhancement of skin permeation. For example, electroporation was reported to enhance the skin permeation of compounds with different lipophilicity and size (less than 10 nm) through generating transient pores during application (Lombry et al., 2000). Or in another study photomechanical waves enhanced the permeability of macrmolecules (8.8 nm dextran and 20 nm latex particles) through *stratum corneum* (Lee et al., 1998).

The increased nanoparticle deposition within the skin layers was thought to be due to a temporary alteration of the skin structure upon the application of hypobaric pressure. The nanoparticle deposition in the skin were further investigated using confocal microscopy. The mass.cm^{-2} of SLN deposited in each layer and also recovery in each conditions summarised in Table 5.2.

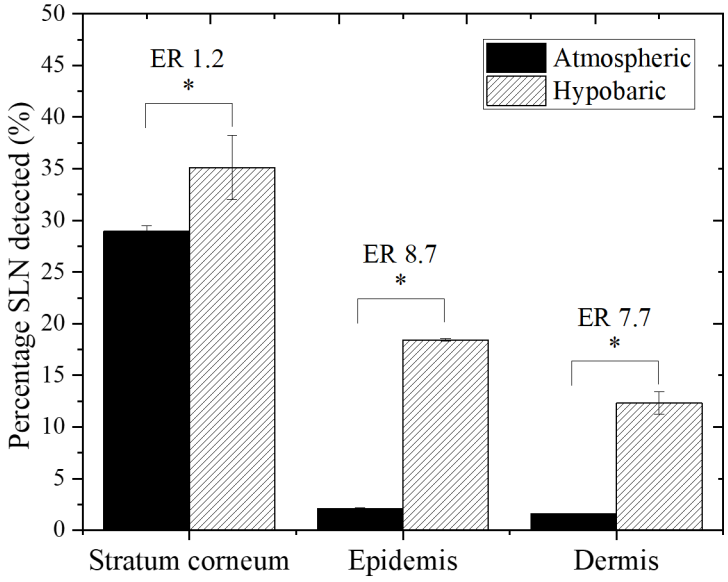

Figure 5.5: *In vitro* profile of SLN deposition in porcine skin layers under atmospheric (1010 mBar) and hypobaric (450 ± 50 mBar) pressure conditions. Each point represents mean ± standard deviation (n=5). * Statistically significant ($P < 0.05$).

Table 5.2: SLN mass per area deposition in porcine skin layers under atmospheric (1010 mBar) and hypobaric (450 ± 50 mBar) pressure conditions, and their recovery %. Each point represents mean ± standard deviation (n=5).

Skin layer	**Atmospheric (μg.cm^{-2})**	**Hypobaric (μg.cm^{-2})**
Stratum corneum	1.55 ± 0.02	1.89 ± 0.15
Epidermis	0.11 ± 0.001	0.99 ± 0.001
Dermis	0.08 ± 0.002	0.66 ± 0.05
Recovery	**95.8 ± 1.8** %	**95.6 ± 4.7** %

Solid lipid nanoparticles have been shown previously to enhance the delivery of sunscreens, vitamins A and E, glucocorticoids triptolide (Santos Maia et al., 2002; Wissing and Müller, 2003*a*, 2002; Jenning et al., 2000; Maia et al., 2000; Dingler et al., 1999; Mei et al., 2003). It was sugessted that the agents skin permeation enhancement was due to the SLN causing an increase in skin hydration as a result of the occlusive film formation on the skin surface by the solid lipid nanoparticle (Mathur et al., 2014). Moreover, it was hypothesised that the suction

mechanism of the hypobaric pressure could influence the follicular pathway size temporary. Since, the nanoparticles main permeation route through the skin is hair follicles (Fang et al., 2014), the hypobaric enhancement of nanoparticles could be explained through follicular alteration. It is possible that SLN released their dye in the skin, which gave false results.

The nature of lipid nanoparticles confers them distinct advantages over conventional carriers (i.e. emulsions, liposomes, and polymer nanoparticle. For example, an excellent tolerability, resulting from the generally recognised as safe status of the excipients employed. Additionally, a better physical stability, protection of combined labile drugs from degradation, cost-effective production method, possibility to control drug release due to the solid nature of the lipid matrix, drug targeting, possibility of scaling-up, and comparatively low cost of excipients (Wissing et al., 2004; Muchow et al., 2008; Venkateswarlu and Manjunath, 2004; Zur Mühlen et al., 1998; Souto et al., 2004; Müller et al., 1997; Wong et al., 2007). Furthermore, their unique characteristics including, reduced size, combined with a large surface area and high drug loading are attractive for a potential development in the enactment of pharmaceuticals, in particular for transdermal delivery (Bhaskar et al., 2009; Joshi and Patravale, 2008).

5.4.4 α-TP Liposome characterisation

In this study, dipalmitoylphosphatidylcholine (DPPC) and alphatocopherol phosphate (α-TP) were used to produce liposomes. According to the previous study, α-TP, the phosphorylated form of the biologically active vitamin E, can self-aggregate in aqueous environment to make bilayer vesicles (Gavin et al., 2017). Pure DPPC liposomes gave a slight positive surface charge (0.5 ± 0.1 mV). α-TP, with a charged phosphate head group, represented a more negatively-charged liposomes with zeta potential of -25.7 ± 0.9 mV at a concentration of 1.8 mM. The liposomes with a mixture of DPPC and α-TP represented an increasingly negative surface charge with increasing amount of α-TP in the formulation (Figure 5.6).

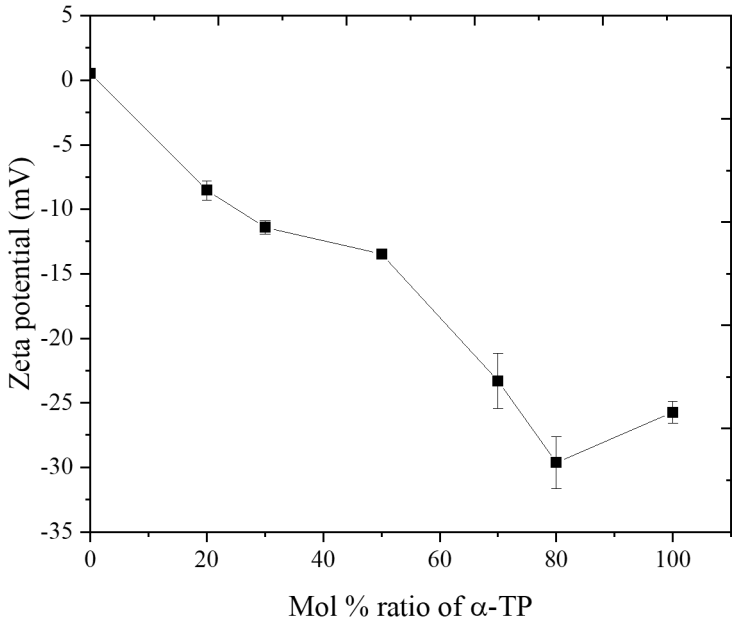

Figure 5.6: Zeta potential of liposomes with increasing mol % ratio of α-TP. Each data point represents mean ± standard deviation (n=3).

The average diameter of liposomes decreased when the amount of α-TP in the mixture increased (see Table 5.3). Size decrease was due to the molecular structure of α-TP that consists of a single hydrophobic tail that results in a formation of smaller unilamellar vesicles (Gavin et al., 2017) compared to the two saturated hydrophobic chain of DPPC. Unilamellar liposomes are spherical, bound by a single bilayer of an amphiphilic lipid or a mixture of such lipids (Pereno et al., 2017). The available charge could have enhanced the curving tendency of liposome bilayer, which could result in a size reduction (Namdeo and Jain, 1999). Polydispersity indexs were low for the mixtures of α-TP-DPPC and this suggested that they were monodispersed and stable (see Table 5.3). The more stable structure commonly is due to a more organised packing of molecules in the bilayer (Quinn, 2012). The incorporation of α-tocopherol has been shown to effect the structure of phospholipid bilayer in a similar way as cholesterol, where it tends to stop reorientation of hydrocarbon chain in ordinary liposomal membrane, making a more rigid bilayer structure (Quinn, 2012).

Table 5.3: Size and zeta potential for unloaded LNP and nile red-loaded lipid nanocapsule. Data represent mean ± SD (n=3).

α-TP:DPPC mol ratio	**Size (nm)**	**Polydispersity index**
0:1 (pure DPPC)	83.2 ± 6.5	0.426 ± 0.073
3:7	65.5 ± 1.0	0.312 ± 0.030
1:1	57.2 ± 1.5	0.351 ± 0.006
7:3	52.9 ± 2.8	0.314 ± 0.056
1:0 (pure α-TP)	114.9 ± 20.4	0.707 ± 0.165

In general, liposomes are thermodynamically unstable, they are likely to aggregate and make larger liposomes (Zhang and Granick, 2006; Yadav et al., 2011). All the liposomes formulations in this study increased in size over 4 weeks post manufacture. Pure DPPC and pure α-TP were demonstrated a growth of 1800% and 200% respectively (Figure 5.7). However, mixed liposomes were more stable is terms of size growth. The most stable liposome appeared to be at mole ratio of 3:7 with a statically insignificant size growth of 7.6% in contrast with the pure liposomes (Figure 5.8). The physical instability of DPPC liposomes can be explained by the absence of surface charge, while α-TP contains a negative surface charge that protects the liposomes form aggregating (Zhang and Granick, 2006; Yadav et al., 2011). Moreover, α-TP is able to protect lipids from autoxidation, that could assist to keep the integrity of phospholipid bilayer and increase liposome's stability (Hunt and Tsang, 1981). These data accord with the lower polydispersity index of α-TP-DPPC liposomes, which indicated a stabilisation influence of the mixed α-TP phospholipid liposomes. In previous studies using α-tocopherol, the stabilisation effect of phosphatidylcholine (PC) (Bac and Kim, 1990; Halks-Miller et al., 1985) and phosphatidylethanolamine (PE) bilayer vesicles were demonstrated (Hiroaki et al., 1994).

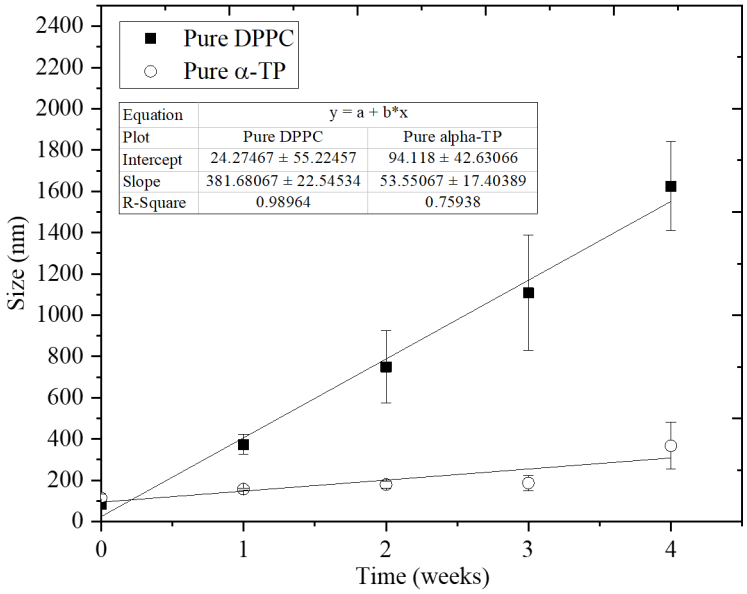

Figure 5.7: Changes in size of pure DPPC and pure α-TP over 4 weeks. Each data point represents mean ± standard deviation (n=3).

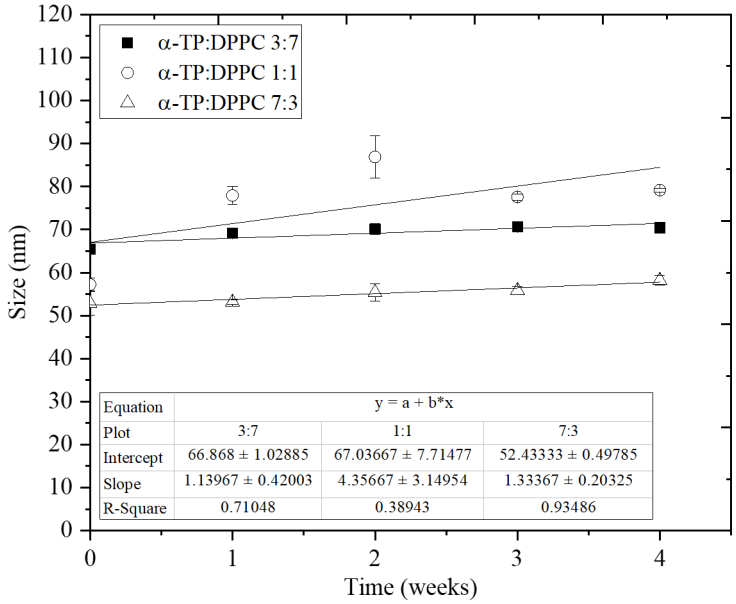

Figure 5.8: Changes in size of DPPC and α-TP mixtures over 4 weeks. Each data point represents mean ± standard deviation (n=3).

5.4.5 α-TP Liposome loading determination

The size of the liposomes increased upon nile red loading (see Table 5.4), presumably due to an alteration in the bilayer structure that produced the liposome. The increased size was particularly evident in the mixtures containing DPPC liposomes, in which the average diameter increased by 7-fold (see Table 5.4). Systems containing a mixture of α-TP and DPPC showed an increase of 4-fold and α-TP showed a size increase of 2-fold compare to the unloaded liposome (see Table 5.4). The mixed liposomes represented a more stable structure, this could result in a more solid membrane structure, as a result they prevent a large amount of nile red to diffuse within their bilayer. The mixture formulations shown a reduced nile red loading efficiency (less than 30%) when compared to the pure liposomes with loading efficiency of 34.3% and 48% for DPPC and α-TP respectively. On the other hand, α-TP was reported to be more flexible (Gavin et al., 2017) to accept higher amount of nile red. The loading efficiency of α-TP liposome was significantly ($P < 0.001$) higher compared to the DPPC-containing liposomes. Overall, loading of nile red resulted in a more negative zeta potential compared to mixtures with less mole ratio of DPPC, which may result in a more stable liposome. However, long-term stability data was not performed to confirm this hypothesis.

Table 5.4: Size, zeta potential and dye loading efficiency for nile red incorporated liposomes. Data represent mean ± standard deviation (n=3).

α-TP:DPPC mol ratio	**Size (nm)**	**Zeta potential (mV)**	**Loading efficiency (%)**
0:1 (pure DPPC)	592.2 ± 79.2	- 17.9 ± 1.0	34.3 ± 2.8
3:7	321.9 ± 20.3	- 32.2 ± 1.1	24.2 ± 2.2
1:1	282.2 ± 7.1	-19.3 ± 0.3	29.2 ± 2.3
7:3	199.9 ± 6.7	- 23.0 ± 1.1	26.9 ± 1.7
1:0 (pure α-TP)	203.0 ± 6.0	- 38.7 ± 3.4	48.0 ± 0.3

To investigate whether nile red was stable in the liposomes a dye release study was performed after liposomes purification. Apart from the pure α-TP and pure DPPC liposomes, all samples retained over 90 ± 5.6 % of nile red in the liposomes for

48 h (Figure 5.9). The amount of nile red retained in α-TP liposomes decreased over time and thus the liposomes are not a good candidates for subsequent hypobaric skin penetration studies. Formulations with no DPPC were shown to increase nile red release, indicating that DPPC and α-TP stabilise each other to reduce the leakage. The formulation with 30% α-TP was showed the least leakage with over 97 $\pm$ 6.7 % of nile red retained in the liposome. This data is similar to a study performed by Halks-Miller et al. that reported formulation with 33% alpha-tocopherol prevented dye leakage more efficiently in egg phosphatidylcholine (PC) liposomes (Halks-Miller et al., 1985). In another study, a lower amount of alpha-tocopherol was reported to work as a stabiliser, for example, 20 mol% alpha-tocopherol in distearoylphosphatidylcholine (DSPC) liposomes successfully retained phenol red inside their structure (Quinn, 2012). In another investigation, 15 mol% alpha-tocopherol prevented the leakage of encapsulated carboxyfluorescein from dimyristoylphosphatidylcholine (DMPC) liposome (Bac and Kim, 1990).

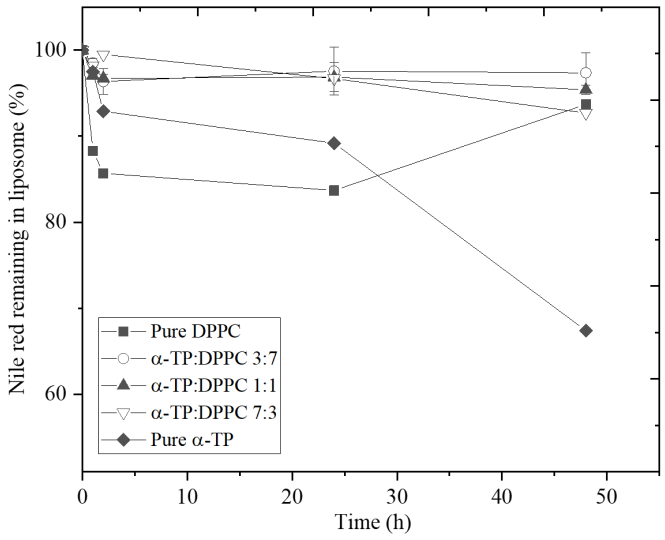

Figure 5.9: Percentage of nile red remaining in liposomes after incubation at 32°C for 1, 2, 24 and 48 h. Data represents mean $\pm$ standard deviation for α-TP:DPPC 1:1 and 3:7 liposomes (n=3) and percentage from n=1 for α-TP:DPPC 7:3, pure DPPC and α-TP liposomes.

Previous investigations have suggested that presence of alpha-tocopherol or its derivative result in a more permeable liposomes (Cushley and Forrest, 1977; Srivastava et al., 1983). However in this study, the dye retained in the liposomes of α-TP:DPPC mol ratio 1:1 and 7:3 was comparable to those of mol ratio 3:7. Gavin et al. (2017) reported that α-TP liposomes have a higher encapsulation efficiency for lipophilic agents in contrast with hydrophilic agents. Therefore, it was expected that nile red (lipid-soluble dye) remained in the liposome. It makes nile red a suitable candidate for skin permeation studies unlike hydrophilic drugs that are less likely to remain in the liposomes. The liposomes with α-TP:DPPC mol ratio of 3:7 and 1:1 systems were used in the skin permeation studies, due to more favoured characteristic.

5.4.6 *In vitro* permeation of α-TP Liposome using hypobaric pressure

The application of hypobaric pressure appeared to enhance the skin deposition profile of each liposome formulation in a different way with an overall recovery of 89.7 $\pm$ 1.3 % and 94.8 $\pm$ 1.4 % for α-TP:DPPC 3:7 and α-TP:DPPC 1:1 respectively. For example, in α-TP:DPPC 3:7 liposomes produced a significantly ($P < 0.05$) greater amount of nile red in the *stratum corneum* (Figure 5.10) while in α-TP:DPPC 1:1 liposomes the diffusion was deeper with a significantly ($P < 0.05$) higher amount of nile red detected in the epidermis (Figure 5.11). Moreover, in both formulations a significantly ($P < 0.05$) higher amount of nile red recorded in dermis. Enhancement ratio of 2.6 and 28.6 were recorded for α-TP:DPPC 3:7 and α-TP:DPPC 1:1 respectively in dermis layer.

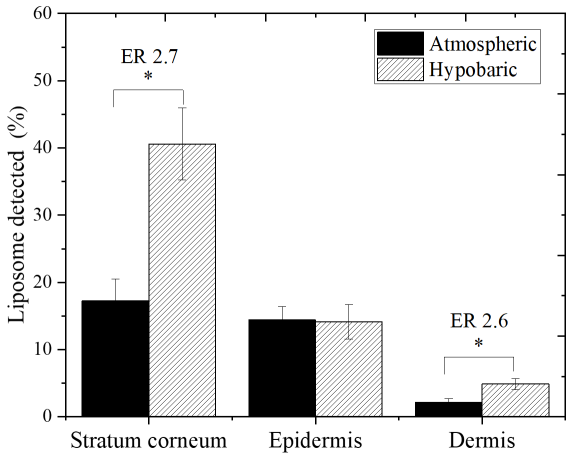

Figure 5.10: Permeation of liposomes with α-TP:DPPC mol ratio of 3:7 into individual skin layer under atmospheric (1010 mBar) and hypobaric pressure (450 ± 50 mBar). Data represents mean ± standard deviation (n=5).

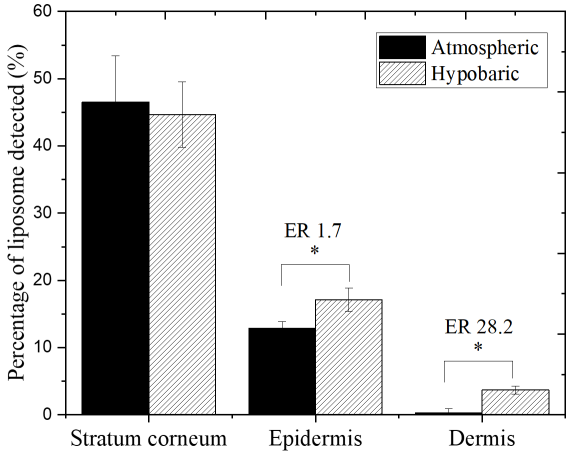

Figure 5.11: Permeation of liposomes with α-TP:DPPC mol ratio of 1:1 into individual skin layer under atmospheric (1010 mBar) and hypobaric pressure (450 ± 50 mBar). Data represents mean ± standard deviation (n=5).

5. Investigation of hypobaric pressure on nanoparticle penetration into the skin

Overall skin deposition was similar for liposomes with α-TP:DPPC mole ratio 1:1 (0.26 $\pm$ 0.02 μg.cm^{-2}) in contrast with 3:7 mole ratio (0.23 $\pm$ 0.02 μg.cm^{-2}). According to a previous study, liposome diffusion is dependent on size, surface charge and composition of the membrane (Jung et al., 2006). Since the size of the liposomes in this study were similar, it was expected to have similar overall deposition. However, α-TP:DPPC mole ratio 1:1 shown a higher deposition in the *stratum corneum*, due to the difference in the surface charge (-19.3 $\pm$ 0.3 mV) in contrast with 3:7 mole ratio (-32.2 $\pm$ 1.1). According to previous studies, liposomes with a negative charge are more problematic to permeate into the skin compared to similar positively charged liposomes due to the skin negatively-charges characteristics (Jung et al., 2006; Manosroi et al., 2004). However, hypobaric pressure enhanced the overall permeation of the liposomes regardless of their surface charge. The enhancement could be due to the enlargement of the skin gaps (e.g., pores, follicular pathway and sweat glands) that improved the permeation of liposomes through the skin. Another factor that influences the liposome permeation through the skin is membrane composition, phospholipid and α-TP with molecular structure similar to surfactants are known to enhance skin penetration (Roberts et al., 2017). Therefore, liposomes with a higher amount of α-TP, regardless of an external enhancer, were expected to have a more flexible structure that can squeeze into the skin pores more easily.

Liposomes are spherical lipid vesicles that enclose an aqueous core (Bangham et al., 1965). These lipid particles are often made of phospholipids with or without cholesterol, which may be organised in one or more bilayers. Hydrophilic activities can be encapsulated in the aqueous area and lipophilic activities in the lipid bilayer area (Fendler and Romero, 1977). The most popular methods for producing liposomes are mechanical agitation, conventional hydration, sonication, reverse-phase evaporation and dehydration-rehydration (Sharata and Katz, 1996).

5.4.7 FluoSpheres^{TM} characterisation

In this study, photon correlation spectroscopy was used to evaluate the size and surface charge of particles as previously described in (Section 5.3.2). Data obtained from light scattering device for size and zeta potential analysis represented in Table 5.5. The size of the polystyrene particles were similar as it was reported by their the manufacture of the product. The zeta potential values were neutral for the polystyrene particles as it was expected. In order to evaluate the physical stability of the particles, the change in mean particle size was recorded over 3 h. Data demonstrated that polystyrene nanoparticles were stable for 3 h (Figure 5.12). A dye release study was performed for 3 h. Data showed no major dye leakage for polystyrene nanoparticles over 3 h, over 98 ± 0.5 % of the dye remained within the particles for 3 h (Figure 5.13).

In previous literature, FluoSphere polystyrene particles were reported to be physically stable, and did not allow dye leaching upon application to human skin. They accumulated in the follicle duct with no leakage of the encapsulated probe (Rancan et al., 2009). Therefore, the amount of dye was assumed to be equal to the amount of polystyrene particles deposited within the skin layers.

Table 5.5: Size and zeta potential for FluoSpheres polystyrene particles. Data represent mean ± SD (n=3).

FluoSpheres polystyrene name	**mean size (nm)**	**Zeta potential (mV)**
PS_{100}	103.1 ± 0.58	0.14 ± 0.47
PS_{500}	484.2 ± 5.42	0.34 ± 0.21
PS_{1000}	1037 ± 4.73	0.08 ± 0.49

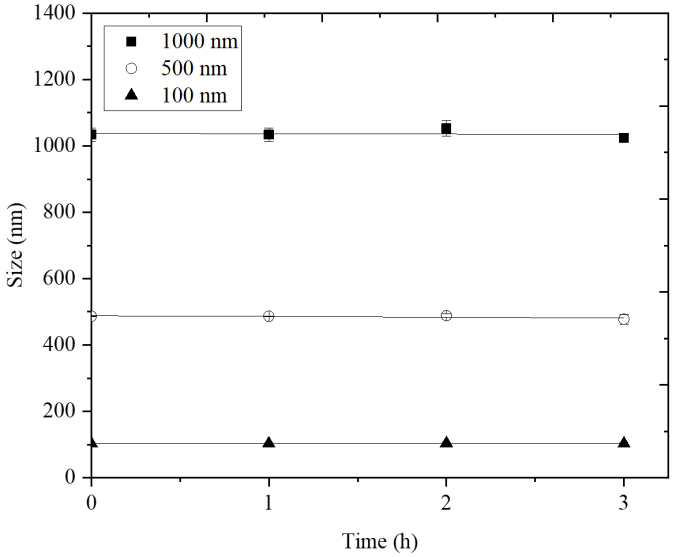

Figure 5.12: Changes in size for polystyrene nanoparticles over 3 h. Each data point represents mean ± standard deviation (n=3).

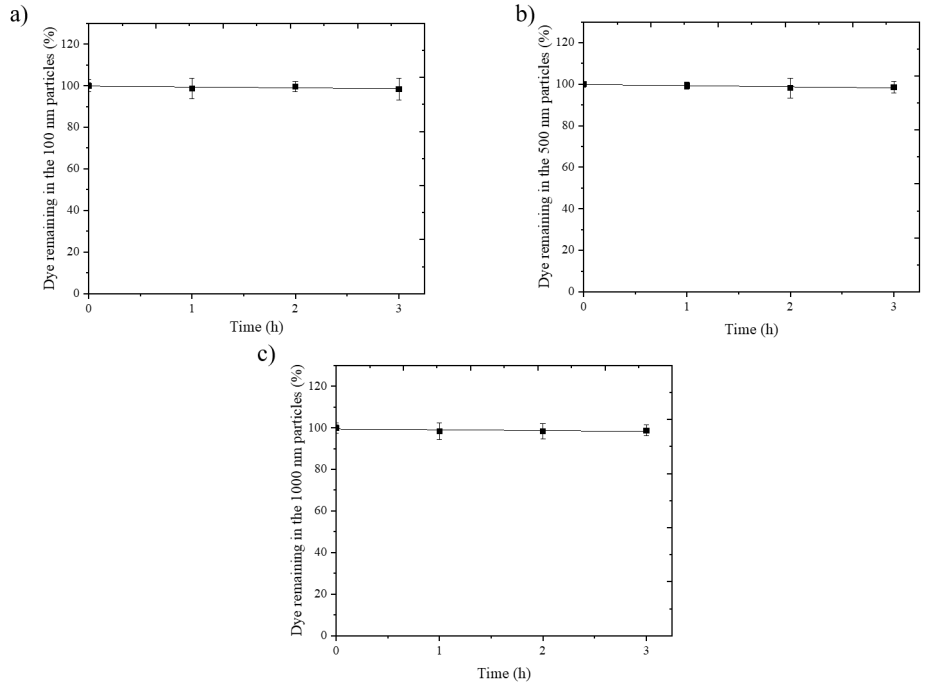

Figure 5.13: Percentage of dye remaining in polystyrene particles after incubation at 32°C over 3 h. a) 100 nm, b) 500 nm and c) 1000 nm. Each data point represents mean ± standard deviation (n=3)

5.4.8 *In vitro* permeation of FluoSpheres particles using hypobaric pressure

The permeation of the polystyrene nanoparticles was size dependent (Figure 5.14). The size of particles has been reported to have a major influence on their follicular targeting (Toll et al., 2004). Previous studies suggested that the ability of the particles to diffuse the skin appendages was in directly related to particles size, when using different size of fluorescent polystyrene microspheres in suspension (Schaefer and Lademann, 2001; Rolland et al., 1993). Particles greater than 10 μm were not able to permeate through the *stratum corneum*. Particles in the range of 9 to 10 μm were accumulated around the opening of the hair follicles without any further permeation. Particles around 7 μm were often observed deep in the follicular rout but hardly penetrate the *stratum corneum*. Rolland et al. (1993) reported, particles smaller than 3 μm were able to permeate into the skin appendages as well as superficial layer of the *stratum corneum*, but not in the viable epidermis, hence the smaller particles used in this study were expected to enter the skin.

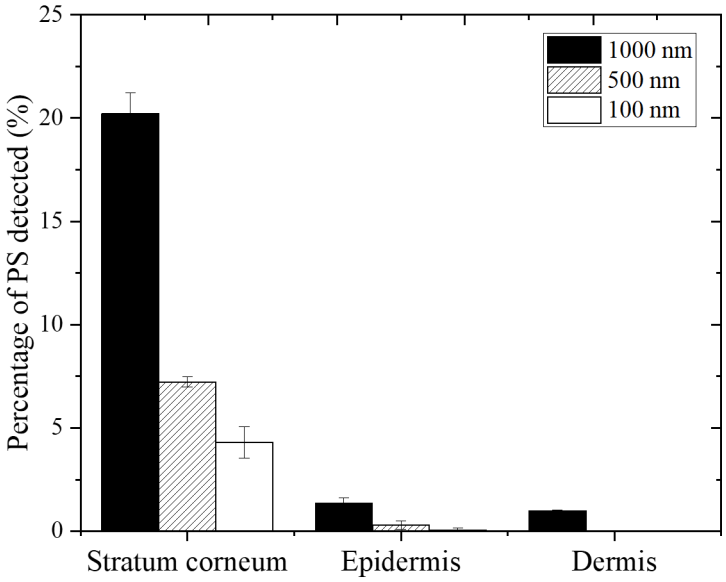

Figure 5.14: Percentage of polystyrene nanoparticles in different size. Data represents mean ± standard deviation (n=5).

Overall hypobaric pressure enhanced the accumulation of particles in the *stratum corneum* (Figure 5.15). Moreover, an enhancement ratio of 2.7 was recorded only in epidermis of particles with the highest size. There was little to no penetration of polystyrene observed in the dermis layer for particles greater than 100 nm. Warheit et al. (2007) reported previously that particles greater than 100 nm can not diffuse through the intact skin barrier into the dermal compartment. The percentage recorded was 59.9 ± 1.5, 79.5 ± 2.8 and 80.7 ± 3.3 respectively for 100, 500 and 1000 particles. Additionally, particles greater in size tend to aggregate more than smaller particles. It has been reported previously by Inacio (2015) that hypobaric pressure was more favourable when agents were aggregating. Therefore, it was expected to observe permeation enhancement at larger particles in lower layers (i.e. 1000 nm). Additionally, particles greater in size tend to aggregate more than smaller particles. It has been reported previously by Inacio (2015) that hypobaric pressure was more favourable when agents were aggregating. Therefore, it was expected to observe permeation enhancement at larger particles in lower layers (i.e. 1000 nm).

Enhancement ratio of 1.3, 2.7 and 0.7 observed in SC layer for 100, 500 and 1000 nm PS (Figure 5.15) when hypobaric pressure applied. Previously, using physical enhancer such as massage increased the permeation of particles (McElnay et al., 1993; Genina et al., 2002). Toll et al. (2004) reported that massage enhance the permeation of microspheres into the hair follicle, due to the dislocation of the follicular cast (a plug), in the follicular infundibulum/orifice resulted from the mechanical massage. It was hypothesised that polystyrene particles permeation enhancement after application of hypobaric pressure was due to the skin pore enlargement, skin thinning and the suction resulted in a smoother surface for particle to permeate (Inacio et al., 2016).

Drug encapsulation, using polymeric material, is a useful pharmaceutical method for modifying the physicochemical characteristics of the encapsulated molecule which can result in an enhancement in the percutaneous delivery of problematic substances (Naik et al., 2004). There are limited number of skin transport studies on biodegradable, polymer microparticles (Rolland et al., 1993; de Jalon et al., 2001*a*)

and solid lipid nanoparticles (Wissing and Müller, 2002; Jenning et al., 2000). For example, PLGA-microparticles were used as a vehicle for skin delivery of acyclovir, dapalene, vitamins A and E (De Jalon et al., 2001*b*). However, the mechanism(s) of interaction between these novel drug carriers and the skin is still unclear and further investigations are required to identify the transport routes within the membrane.

In order to provide more information regarding mechanism of hypobaric pressure on skin permeation enhancement, samples were investigated under confocal microscope. To investigate the agents passage through the skin under hypobaric pressure.

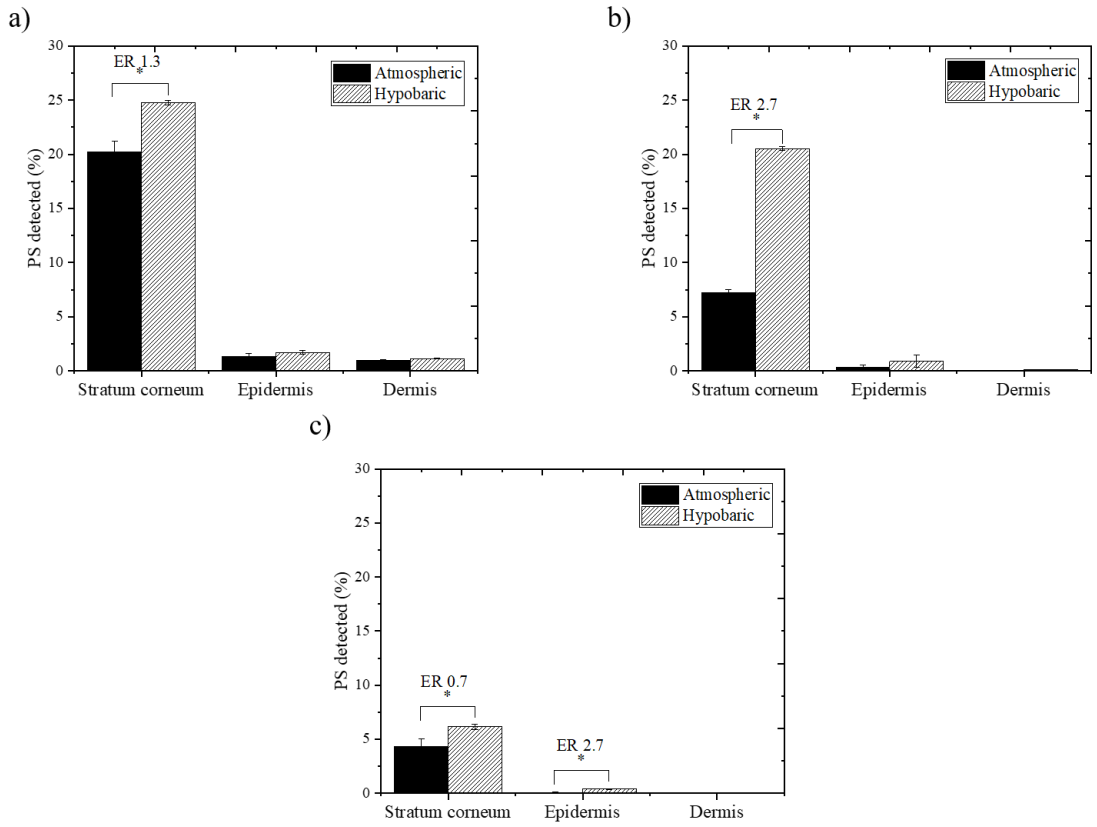

Figure 5.15: Permeation of polystyrene particles into individual skin layer under atmospheric (1010 mBar) and hypobaric pressure (450 ± 50 mBar). a) 100 nm, b) 500 nm and c) 1000 nm. Data represents mean ± standard deviation (n=5).

5.4.9 Nanoparticle skin distribution

In order to investigate the effect of hypobaric pressure upon nanoparticle delivery, cryostat sections of skin at atmospheric and hypobaric pressures were visualised by confocal microscope (Section 4.3.3). In order to visualise the cellular structures of the skin DAPI was used (blue colour). FluoSpheres microspheres particles (100 nm) and solid lipid nanoparticles (approx. 50 nm) were used in this study to visually investigate the skin distribution of the materials after delivery (Figure 5.16). The confocal microscopic studies shown that the distribution of polystyrene particles were limited to the surface of the skin and the hair follicles due to their greater particle size (100 nm). However, solid lipid nanoparticles demonstrated higher distribution within the lower layers due to their smaller particle size. There was a significant increase in the fluorescence intensity in lower skin layers when the samples exposed to hypobaric pressure (450 $\pm$ 50 mBar) compared to those at atmospheric pressure (Figure 5.16 c and f). The penetration enhancement of tested nanoparticles was in line with the previous investigations, in which a significant enhancement in the penetration of 3.5 nm ullerene amino acid-derivatised peptide nanoparticles through the flexing of porcine skin (Rouse et al., 2007). The increased intensity was observed around hair follicles for both particles, it was believed that the furrows between the corneocyte islands provide a space for nanoparticles accumulation within the skin. Therefore, the particles transportation to the deeper layers were facilitated, where the lipophilic compounds such as encapsulated nile red can release into the lipid matrix and move even further into the membrane (Naik et al., 2004).

Particles penetrate the skin through two main routes: intercellular route, in which they diffuse through the lipid channels between the corneocytes into the deeper skin layers, and through the appendage route such as hair follicles and sweat glands. Both pathways are reported to have significant influence on nanoparticle skin deposition (Lademann et al., 2007; Toll et al., 2004; Alvarez-Román, Naik, Kalia, Guy and Fessi, 2004; Alvarez-Román, Naik, Kalia, Fessi and Guy, 2004). Particles size plays an important role in their penetration (Figure 5.16). Previous studies reported that FITC- dextran particles of various sizes (< 4 μm) were

studied with and without mechanical stress. They have indicated a size cut-off of 1 μm for particle permeation under mechanical stress (Tinkle et al., 2003). Kohli and Alpar (2004) suggested that particles up to 500 nm penetrated the barrier when mechanical stress applied.

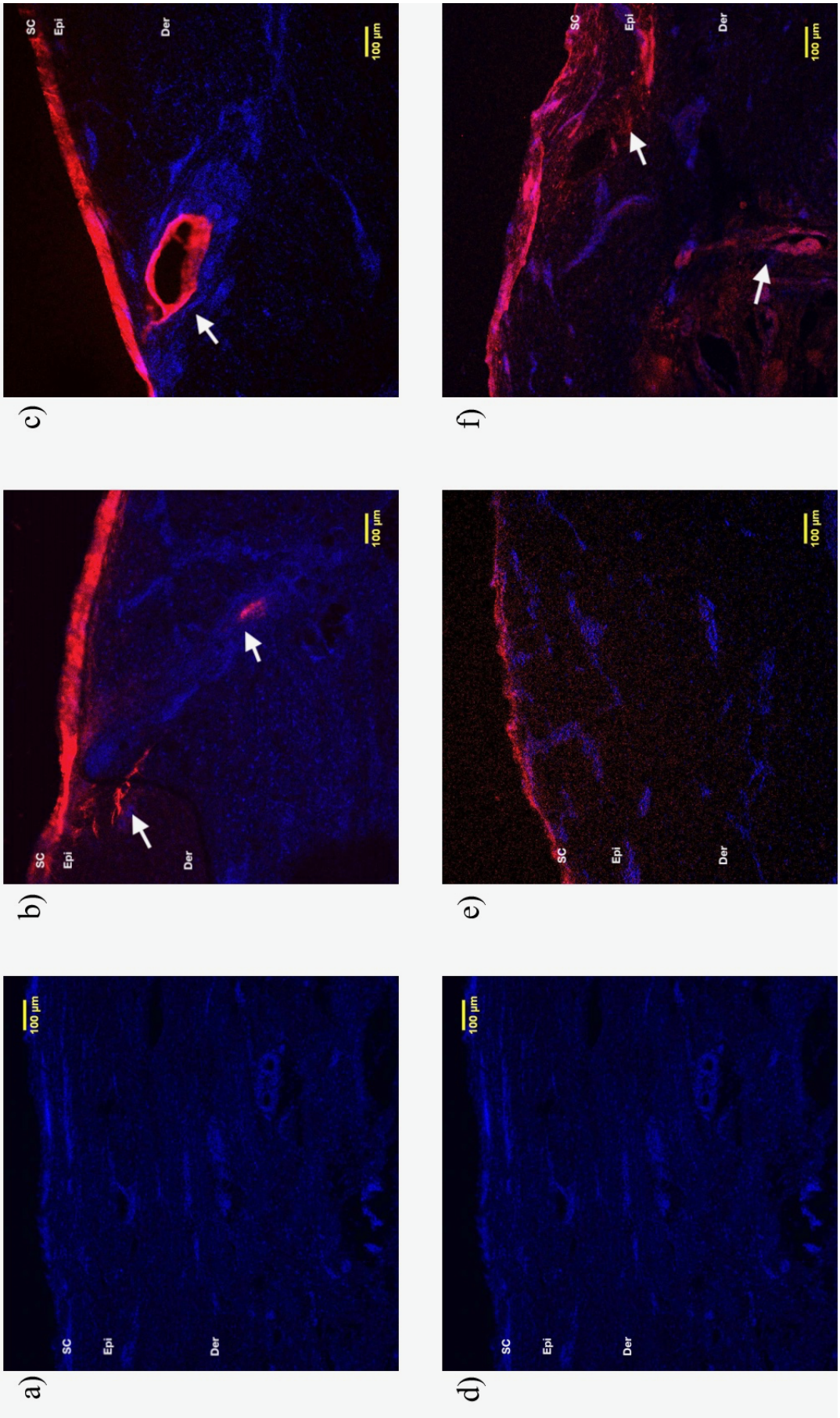

Figure 5.16: Confocal microscopic examination after topical administration of polystyrene and solid lipid nanopartciles under atmospheric (1010 mBar) and hypobaric (450 ± 50) pressure conditions: a) & d) control, b) polystyrene at atmospheric pressure, c) polystyrene at hypobaric pressure, e) solid lipid at atmospheric pressure and f) solid lipid at hypobaric pressure.

5. Investigation of hypobaric pressure on nanoparticle penetration into the skin

At present, the exact mechanisms through which hypobaric pressure enhances nanoparticle penetration is unknown. However, it was hypothesised that the force through the suction applied to the skin during application of hypobaric pressure caused modifications in the morphology and lipid structure of the epidermis upper layers. A temporary enlargement in the size of the intercellular spaces during pressure application could account for the enhancement in the penetration seen in the samples stretched for 1 h using hypobaric pressure. Moreover, further investigation of nanoparticles safety assessment and the effect of mechanical suction on the nanoparticle interactions with the biological environment were required. Table 5.6 summarises the enhancement of all the particles that were employed in this Chapter. Hypobaric pressure enhanced particle permeation in different ways, smaller size particles were appeared to diffuse more in the lower layers although it was important to take the permeation time into account. The permeation experiment was 2 h, this time point was sufficient for small particles to transfer further down into the epidermis and dermis. However, it was assumed that larger particles permeation were slower hence, their permeation enhancement appeared to be less than smaller particles. The surface charge and particle structure also influenced their permeation, the highest dermis permeation enhancement was observed in negatively charged liposome with a flexible structure (LP 1:1).

Table 5.6: Summary of nanoparticles permeation enhancement. sc: stratum corneum, epi: epidermis and der: dermis

Particle	**Size (nm)**	**Enhancement**
SLN	50	1.2, 8.7, 7.7-fold (sc, epi and der)
$LP_{1:1}$	280	1.7, 28.2-fold (epi and der)
$LP_{3:7}$	320	2.7, 2.6-fold (sc and der)
PS_{100}	100	1.3-fold (sc)
PS_{500}	500	2.7-fold (sc)
PS_{1000}	1000	0.7, 2.7-fold (sc and epi)

5.5 Conclusion

This Chapter investigated the effect of hypobaric pressure upon the skin permeation of nanoparticles. In general hypobaric pressure enhanced the penetration of nanopartciles through the *stratum corneum*. The highest penetration amount for all layers was reported for solid lipid nanoparticle, due to their small size and hydrophobic surface. However, negatively charged α-TP liposomes showed the highest amount of dermis penetration, due to their flexible structure. Since liposomes with a higher amount of α-TP were expected to have a more flexible structure they may squeeze into the skin pores more easily. The permeation of nanoparticles was size dependent, specially in the lower layers. The bigger particles were trapped within the *stratum corneum* and smaller particles transported into lower layers. The application of hypobaric pressure caused a transient enlargement of pores such as hair follicles and sweet glands. Moreover, it was hypothesised that the vertical and lateral gaps between corneocytes in the *stratum corneum* that limit the penetration of larger molecules were influenced by skin stretching as a result of hypobaric application. For intense, hypobaric pressure could be a suitable candidate for delivery of vaccine as previously investigated using microneedles (Quinn et al., 2014). In conclusion, these results could help to develop a nanoparticles delivery method, although future works are required specially in understanding the exact mechanism in which nanoparticles diffuse into the intact skin under the influence of hypobaric pressure.

6
General discussion

Skin delivery offers many advantages compared to conventional routes of drug administration such as oral and parenteral delivery (Guy and Hadgraft, 2003; Prausnitz et al., 2004). For example, avoiding the first-pass metabolism, the use of a drug reservoir that can be removed from the body, and providing a convenient and pain-less way of offering controlled release of a drug during a 24 h interval from a single application (Joshi and Raje, 2002; Roberts et al., 2002). That said, the barrier properties of the *stratum corneum* remains a problematic issue for many drugs to be delivered via the skin (Barry, 1983). Only drugs with specific physicochemical properties can diffuse into the skin. Ideal properties include moderate lipophilicity and a small molecular weight (Naik et al., 2000).

Hydrophilic compounds, carriers, e.g., nanoparticles, and larger molecules e.g., peptides and proteins are the most difficult agents to deliver into the skin (Prausnitz and Langer, 2008). Several physical and chemical enhancer methods have been successfully used to deliver some of the compounds into the cutaneous tissue, but these approaches still require optimisation (Prausnitz and Langer, 2008; Arora et al., 2008) and face difficulties in offering a safe and cost-effective system for skin delivery. Furthermore, some of these techniques require a health-care professional to use the device on the patients, which causes dissatisfaction. The application of hypobaric pressure is one strategy. Although hypobaric pressure is an effective and

cheap method to enhance agent delivery into the skin, the range of agents it can deliver is unknown.

The exposure of human body to hypobaric pressure is not uncommon. For instance, pressure fluctuations of passengers is common on commercial flights hypobaric pressure of approx. 850 mBar vs. (atmospheric pressure of 1010 mBar). However, the pressure of aircraft-cabins does not drop below 750 mBar (Muhm et al., 2007). Physiological alterations in blood flow and respiration during pressure fluctuations have been studied under hypobaric conditions, but the consequences of these alterations on the permeability of the skin is not well documented.

A number of previous studies have investigated how the application of local pressure (either hypobaric or hyperbaric) can influence the skin properties. For example, the application of hypobaric pressure (0.25 bar) has been shown to increase the permeation of caffeine by 1.8-fold (Treffel et al., 1993). Another study reported that the application of hypobaric pressure (500 mBar) caused a reduction in epidermis thickness and blood vessel enlargement in the dermis layer (Childers et al., 2007). Furthermore, suction cups, which generate 400-600 mBar hypobaric pressure, have been reported to significantly increase transepidermal water loss (Pedersen and Jemec, 2006). In a more recent study using tetracaine, diclofenac diethylamine and aciclovir, hypobaric pressure was shown to modify the percutaneous penetration of these agents through enlargement of the follicular infundibula, reduction in corneocyte, and reduction in skin thickness (Inacio, 2015). Nevertheless, the use of hypobaric pressure to deliver drug to the skin is still in its infancy and requires further study.

This thesis was focused on the use of hypobaric pressure to enhance the skin delivery of compounds that are particularly problematic to deliver into the tissue. The investigation used model compounds, including minoxidil (small molecular weight), dextran (macromolecular model) and finally nanoparticles (carrier system). To study the effect of hypobaric pressure on these three model agents in Chapter 2, analytical methods were required to track their entry into the skin. Although, several methods have higher sensitivity, HPLC-UV detection of minoxidil was considered

the most appropriate technique because it is relatively inexpensive, rapid and very practical compared to alternative methods. (FITC)-dextran quantification has previously been reported using fluorescence spectroscopy (Lee et al., 2008; Fujiwara et al., 2005; Ohkuma et al., 1982). Fluorescence spectroscopy is inexpensive and the most commonly used analytical method for the detection of dextran. The quantification of nanoparticles is normally achieved via a probe encapsulated in the nanoparticles core. Detection and quantification of the probe was achieved in this work using fluorescence spectroscopy, which has been previously shown to be sufficiently sensitive. In conclusion, in Chapter 2, three analytical methods were developed and shown to be ''fit for the purpose' and sensitive enough for measuring the compounds throughout this thesis.

In Chapter 3 of the thesis, the application of hypobaric pressure was used with minoxidil. Minoxidil was found to have a good solubility in a water: ethanol: propylene glycol vehicle, which was taken forward as a vehicle for subsequent transport studies. Minoxidil ionisation increased as the pH decreased thus, it was most soluble at the lower pH values (i.e. pH 3). From the solubility data it was thought that a pH of 7.4 would be the most appropriate for the permeation study, because this appeared to allow adequate donor solution solubility whilst retaining the drug in the unionised form, i.e., the form that would have the highest skin permeation. Minoxidil silicone membrane transport (over 120 h) was demonstrated to increase 109.5-fold when 450 $\pm$ 50 mBar hypobaric pressure was applied to the membrane. It was suggested that the deformation of the membrane caused by the suction could influence the transport of minoxidil through the silicone membrane. Two hours after the application of a 1 h dose of hypobaric pressure the minoxidil deposition in the stratum corneum, epidermis and dermis was increased by 16.5, 5.3 and 5.2-fold, respectively compared to atmospheric conditions (Figure 6.1). It was hypothesised that hypobaric pressure significantly ($P < 0.05$) reduced the skin thickness and enlarged the follicular pore size, which resulted in the enhanced permeation. Furthermore, the enhanced minoxidil deposition observed in this study suggested that hypobaric pressure may be a useful percutaneous delivery method for

small therapeutic compounds that naturally prefer to diffuse through hair follicles. No experimental data was obtained to understand the mechanics of skin permeation, but it could be the opening up the pores and skin thinning. Further investigation is required to establish the exact mechanism of minoxidil permeation through the skin and how hypobaric pressure influenced this. Although, preliminary IR-mapping studies were conducted results were inconclusive due to weak minoxidil signals. As the focus of this work was to assess a range of molecules, the time did not allow to do further investigation into how minoxidil permeation increased. Further work is required to refine the use of hypobaric pressure. For example, measure the exact amount of minoxidil delivered into the follicular space, this could be achieved through follicular casting (Gelfuso et al., 2013). This crucial factor must be considered before a prototypical device can be conceived.

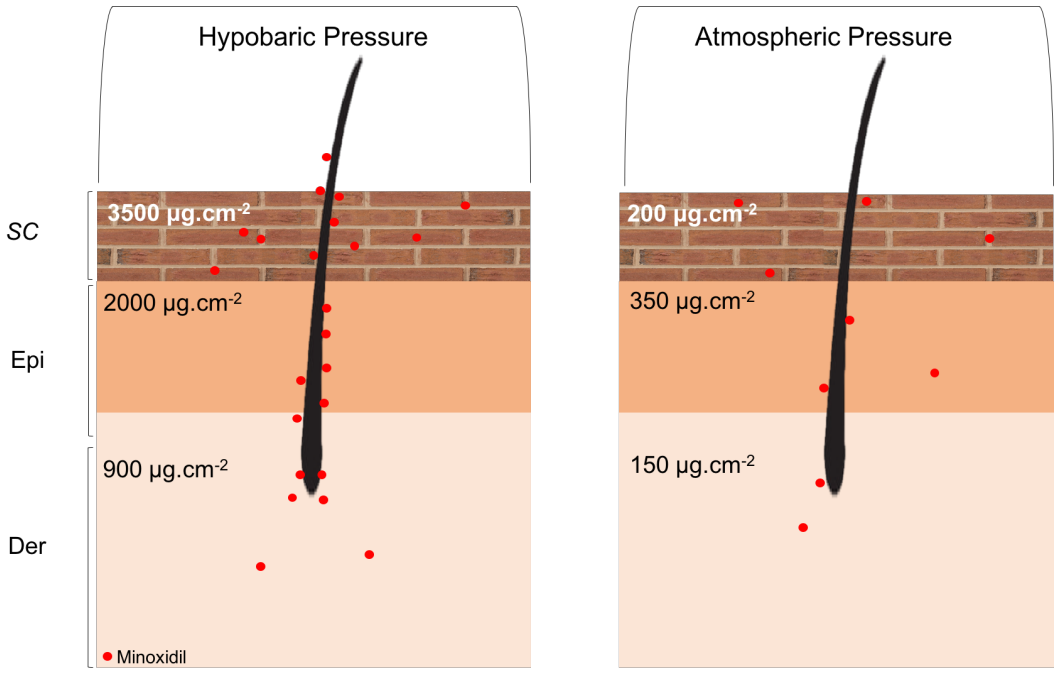

Figure 6.1: Diagram representing the effect of topical hypobaric pressure upon minoxidil skin delivery.

In Chapter 4, a series of FITC-dextrans increasing in molecular weight (4 kDa, 10 kDa, 70 kDa and 150 kDa) were used as model macromolecules because these molecules allowed both the quantification of skin permeation and the visualisation

of skin deposition using fluorescence microscopy. The data showed that dextran skin permeation size-dependent. Furthermore, the data showed a significant ($P < 0.05$) enhancement in the permeation of dextran up-to 70 kDa (Figure 6.2). It is hypothesised that hypobaric pressure can temporarily stretch and open up the pores in the epidermis through suction, which is a reversible alteration since no damage or detachment was observed in the skin histology after the treatment. This data suggested that molecules up to 70 kDa, can be delivered through the skin using the painless and non-invasive hypobaric method. The delivery of larger molecules such as peptides, antigens and proteins through the skin is an attractive approach for the treatment and prevention of certain diseases such as diabetes and cancer (Glenn et al., 2000). To regulate the glycaemic level in the diabetes patients, multiple subcutaneous injections of peptides required in a day, which can be inconvenient for the patients (Shivanand et al., 2010). For example, parathyroid hormone, which a size of 9.4 (kDa) requires 40 μg (non-transdermal) for the treatment of osteoporosis, which is greater compared to the transdermal permeation of similar size dextran (10 kDa) recorded in this study (approx. 30 ± 1.02 μg). However, by increasing the application of hypobaric pressure on the skin and extending the duration of transport study, it could be possible to enhance the therapeutic level. However, further investigations are required prior to proceeding to clinical trials.

Further investigations are required to solve the limitations of the data. For example, enhanced permeation was recorded only for dextran not other macromolecules. Moreover, dextran stability requires further investigations as stability only investigated in the vehicle not in the skin. This can be result in an early detachment of FITC from dextran.

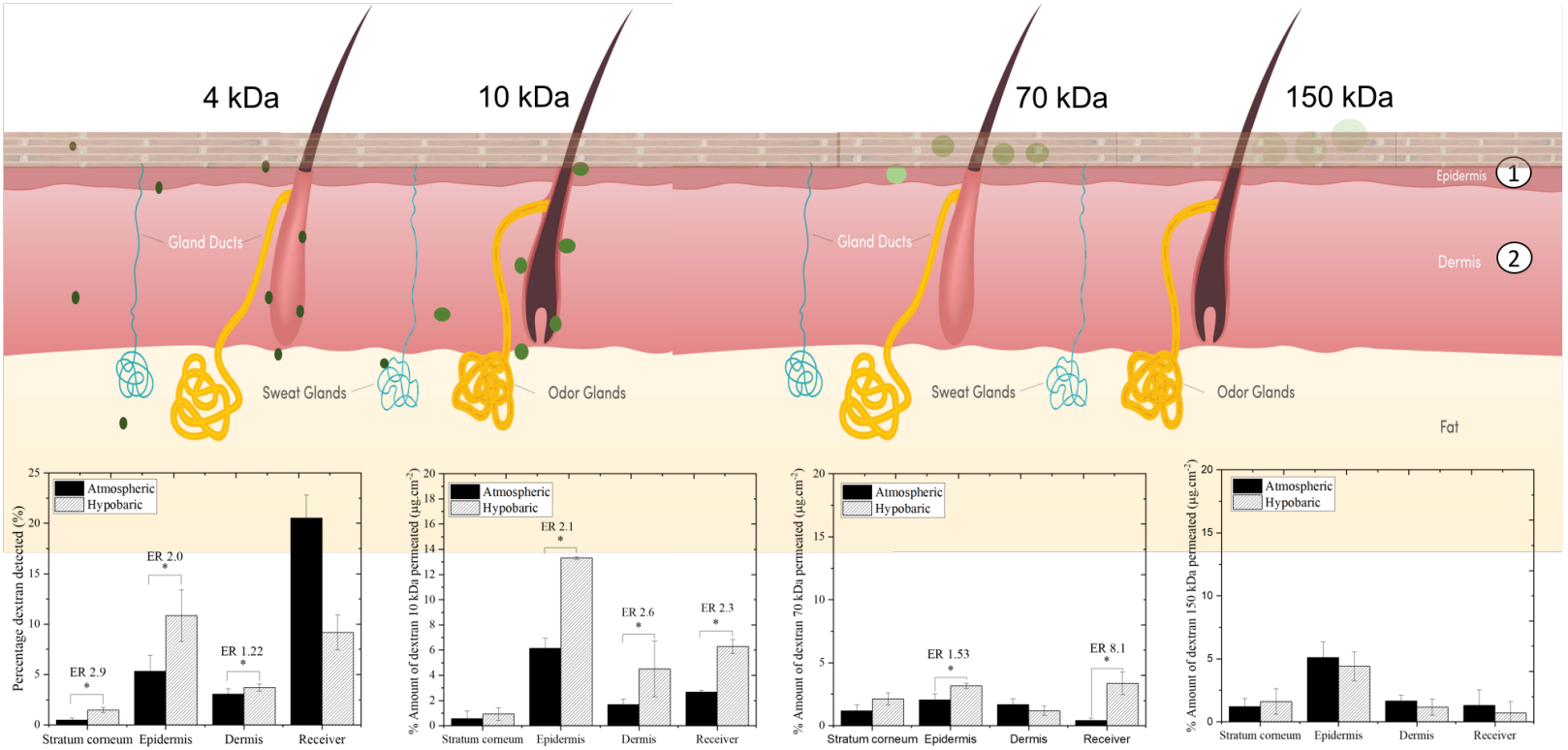

Figure 6.2: Diagram representing the influence of hypobaric pressure in permeation of different size dextran through the skin. 1) Epidermis and 2) dermis.

Vaccine delivery through the skin has gained much attention in the recent years, since it shows potential in the targeting of the skin antigen-presenting cells that could produce an immune response at lower doses in contrast with the deeper injections (Prausnitz and Langer, 2008; Mittal et al., 2013, 2015; Baleeiro et al., 2013). Nanoparticles are a suitable vehicle for the skin delivery of vaccines through the follicular routes, as they could accumulate and diffuse deeper into the hair follicles in contrasts with the traditional formulations (Lademann et al., 2015). Since the application of hypobaric pressure has shown to enhance the permeation of compounds via the hair follicles, such a method could be used to facilitate the transdermal delivery of vaccines.

In Chapter 5, it was found that hypobaric pressure significantly enhanced the penetration of nanoparticles through the *stratum corneum* (Figure 6.3). The highest penetration amount for all layers was reported for the solid lipid nanoparticles, probably due to their small size. However, the negatively charged α-TP liposomes showed the highest amount of dermis penetration, perhaps due to their flexible structure. Liposomes with a higher amount of α-TP, had a more flexible structure, permitting them to squeeze into the skin pores more easily. The permeation of nanoparticles into the skin was size dependent, specially in the lower layers. The bigger particles were trapped within the *stratum corneum* and smaller particles transported into lower layers through follicles. The application of hypobaric pressure caused a transient enlargement of pores, such as hair follicles and sweet glands. Moreover, it was hypothesised that the vertical and lateral gaps between corneocytes in the *stratum corneum* that limit the penetration of larger molecules were influenced by skin stretching as a result of hypobaric application. In conclusion, these results could help to develop a nanoparticle carriers delivery as a method for vaccines, although further work is required specially in understanding the exact mechanism in which nanoparticles diffuse into the intact skin under the influence of hypobaric pressure. Several investigations have shown that nanoparticle could facilitate the transdermal drug delivery (Hansen and Lehr, 2012; Kohli and Alpar, 2004; Lawson et al., 2007).

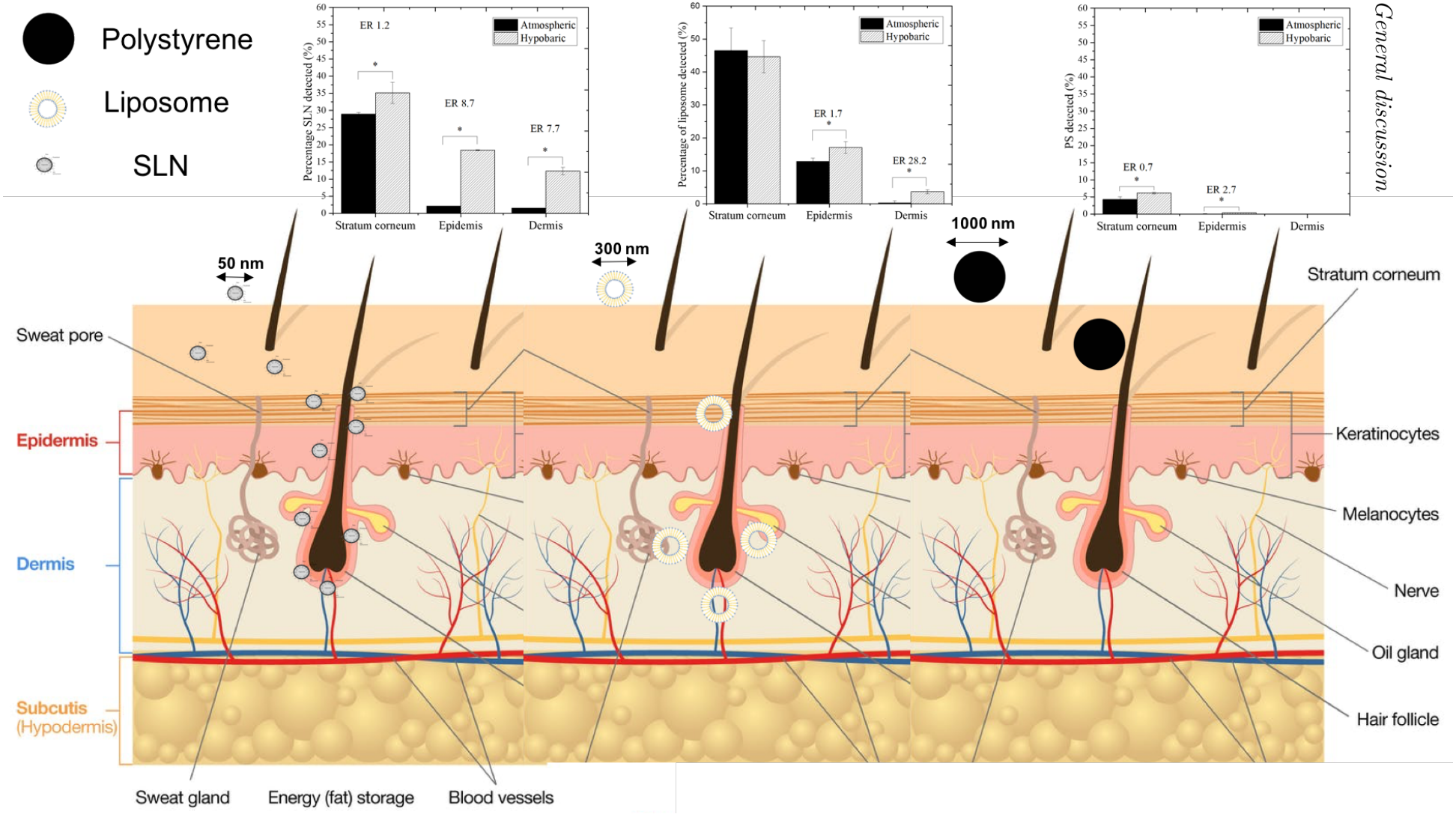

Figure 6.3: Diagram representing the influence of hypobaric pressure in permeation of different size nano-size compounds through the skin.

This thesis focused on the potential of using hypobaric pressure as a novel method to enhance the skin delivery of compounds. It was shown that hypobaric pressure significantly enhanced the delivery of different size molecules into and through the skin. The finding from this study could help to develop a safe and cost-effective suction device that could potentially be applied by patients in sensitive areas (e.g., scalp) for the treatment of a skin disorder in form of pressure induced transdermal patch. Moreover, this device could be used for the delivery of larger compounds (e.g., vaccines) through the skin.

6.1 Future work

In this section avenues for future work are highlighted; several different investigations and experiments are set forth. Broadly, further work will likely involve a deeper analysis of the employed methods.

In Chapter 3 of this thesis, the application of hypobaric pressure was used with minoxidil. Deeper insight into the mechanisms of permeation enhancement of minoxidil would be worth further investigation. For example, using a follicular casting technique to quantify follicular delivery of minoxidil (Grice et al., 2010). Additionally, FTIR analysis of the skin can be a useful method to investigate the interaction between the drug and skin components such as lipid and keratin (Kasliwal et al., 2008). Mura et al. used FTIR imaging technique to evaluate the effective penetration of minoxidil within the skin layer (Mura et al., 2013); similar experiments could investigate the influence of hypobaric pressure on minoxidil topical delivery.

In Chapter 4, a series of FITC-dextrans, increasing in molecular weight (4 kDa, 10 kDa, 70 kDa and 150 kDa), were used as model macromolecules. With regards to the results for dextran permeation, dextran stability could expect to improve by further investigations, as the stability was only investigated in the vehicle and not in the skin. This could result in an early detachment of FITC from dextran. Furthermore, the size range of dextrans employed in this study was similar to certain sizes of vaccines such as 14 kDa (O'Toole and Clyne, 2001), 70 kDa (Bucher et al., 1976) to 100 kDa (Clapp et al., 2011). Additionally, larger maromolecules

of size range similar to DNA plasmid vaccines (Pan et al., 1999) were investigated in Chapter 5. Obviously, the use of other types of macromolecules could enhance the data since the hypobaric pressure might have different influences on them. Different approaches in this direction can be derived from techniques described in the literature, such as (Wei et al., 2018; Hsu and Mitragotri, 2011).

In Chapter 5, it was found that hypobaric pressure significantly enhanced the penetration of nanoparticles through the *stratum corneum*. Since nanoparticles can be tailored for non-invasive application (e.g., hypobaric pressure) and prolonged delivery of the vaccines, it is important to investigate the vaccine delivery using hypobaric pressure. In the future, development of nanovaccines will require new delivery methods.

References

Abd, E., Benson, H. A., Roberts, M. S. and Grice, J. E. (2018), 'Minoxidil skin delivery from nanoemulsion formulations containing eucalyptol or oleic acid: Enhanced diffusivity and follicular targeting', *Pharmaceutics* **10**(1), 19.

Aharon, D., Weitman, H. and Ehrenberg, B. (2011), 'The effect of liposomes' surface electric potential on the uptake of hematoporphyrin', *Biochimica et Biophysica Acta (BBA)-Biomembranes* **1808**(8), 2031–2035.

Ahmadi, F., Gholivand, M. and Yawari, E. (2012), 'Introduce of minoxidil as a very selective ligand for ultra trace detection of copper ion by adsorptive stripping voltammetric method', *Analytical and Bioanalytical Electrochemistry* **4**(4), 431–446.

Akrill, P., Cocker, J. and Dixon, S. (2002), 'Dermal exposure to aqueous solutions of n-methyl pyrrolidone', *Toxicology Letters* **134**(1-3), 265–269.

Alexander, A., Dwivedi, S., Giri, T. K., Saraf, S., Saraf, S., Tripathi, D. K. et al. (2012), 'Approaches for breaking the barriers of drug permeation through transdermal drug delivery', *Journal of Controlled Release* **164**(1), 26–40.

Allen, T. M. and Cullis, P. R. (2004), 'Drug delivery systems: entering the mainstream', *Science* **303**(5665), 1818–1822.

Alvarez-Román, R., Naik, A., Kalia, Y., Fessi, H. and Guy, R. H. (2004), 'Visualization of skin penetration using confocal laser scanning microscopy', *European Journal of Pharmaceutics and Biopharmaceutics* **58**(2), 301–316.

Alvarez-Román, R., Naik, A., Kalia, Y., Guy, R. H. and Fessi, H. (2004), 'Skin penetration and distribution of polymeric nanoparticles', *Journal of Controlled Release* **99**(1), 53–62.

Ambati, J., Canakis, C. S., Miller, J. W., Gragoudas, E. S., Edwards, A., Weissgold, D. J., Kim, I., Delori, F. C. and Adamis, A. P. (2000), 'Diffusion of high molecular weight compounds through sclera', *Investigative Ophthalmology & Visual science* **41**(5), 1181–1185.

Andrade, F., Videira, M., Ferreira, D. and Sarmento, B. (2011), 'Nanocarriers for pulmonary administration of peptides and therapeutic proteins', *Nanomedicine* **6**(1), 123–141.

Anissimov, Y. G. and Roberts, M. S. (2009), 'Diffusion modelling of percutaneous absorption kinetics: 4. effects of a slow equilibration process within stratum corneum on absorption and desorption kinetics', *Journal of Pharmaceutical Sciences* **98**(2), 772–781.

Anselmo, A. C. and Mitragotri, S. (2014), 'An overview of clinical and commercial impact of drug delivery systems', *Journal of Controlled Release* **190**, 15–28.

Arora, A., Prausnitz, M. R. and Mitragotri, S. (2008), 'Micro-scale devices for transdermal drug delivery', *International Journal of Pharmaceutics* **364**(2), 227–236.

Augustijns, P. and Brewster, M. E. (2007), *Solvent systems and their selection in pharmaceutics and biopharmaceutics*, Springer.

Aungst, B. J., Blake, J. A. and Hussain, M. A. (1990), 'Contributions of drug solubilization, partitioning, barrier disruption, and solvent permeation to the enhancement of skin permeation of various compounds with fatty acids and amines', *Pharmaceutical Research* **7**(7), 712–718.

Bac, S.-J. and Kim, N.-H. (1990), 'A study of stabilization effect of α-tocopherol incorporated into liposomal phospholipid membrane', *Archives of Pharmacal Research* **13**(1), 64–68.

Baleeiro, R. B., Wiesmüller, K.-H., Reiter, Y., Baude, B., Dähne, L., Patzelt, A., Lademann, J., Barbuto, J. A. and Walden, P. (2013), 'Topical vaccination with functionalized particles targeting dendritic cells', *Journal of Investigative Dermatology* **133**(8), 1933–1941.

Bangham, A., Standish, M. and Weissmann, G. (1965), 'The action of steroids and streptolysin s on the permeability of phospholipid structures to cations', *Journal of Molecular Biology* **13**(1), 253–IN28.

Baroli, B., Ennas, M. G., Loffredo, F., Isola, M., Pinna, R. and López-Quintela, M. A. (2007), 'Penetration of metallic nanoparticles in human full-thickness skin', *Journal of Investigative Dermatology* **127**(7), 1701–1712.

Barry, B. (1991), 'Lipid-protein-partitioning theory of skin penetration enhancement', *Journal of Controlled Release* **15**(3), 237–248.

Barry, B. (2002), 'Drug delivery routes in skin: a novel approach', *Advanced Drug Delivery Reviews* **54**, S31–S40.

Barry, B. W. (1983), 'Dermatological formulations', *Percutaneous Absorptions* pp. 127–233.

Barry, B. W. (1987), 'Mode of action of penetration enhancers in human skin', *Journal of Controlled Release* **6**(1), 85–97.

Barry, B. W. (2001), 'Novel mechanisms and devices to enable successful transdermal drug delivery', *European Journal of Pharmaceutical Sciences* **14**(2), 101–114.

Barry, B. W. (2004), 'Breaching the skin's barrier to drugs', *Nature Biotechnology* **22**(2), 165.

Batisse, D., Bazin, R., Baldeweck, T., Querleux, B. and Lévêque, J.-L. (2002), 'Influence of age on the wrinkling capacities of skin', *Skin Research and Technology* **8**(3), 148–154.

Beatty, J. (1995), 'The evolutionary contingency thesis', *Concepts, Theories, and Rationality in the Biological Sciences* pp. 45–81.

Benaouda, F., Brown, M., Martin, G. and Jones, S. (2012), 'Triggered in situ drug supersaturation and hydrophilic matrix self-assembly', *Pharmaceutical Research* **29**(12), 3434–3442.

Bennett, M. and Verselis, V. (1992), *Biophysics of gap junctions*, Elsevier.

Benson, H. A. (2012), 'Skin structure, function, and permeation', *Topical and Transdermal Drug Delivery: Principles and Practice; Benson, HA, Watkinson, AC, Eds* .

Benson, H. A. and Namjoshi, S. (2008), 'Proteins and peptides: strategies for delivery to and across the skin', *Journal of Pharmaceutical Sciences* **97**(9), 3591–3610.

Benson, H. A. and Watkinson, A. C. (2012), *Topical and transdermal drug delivery: principles and practice*, John Wiley & Sons.

Bensouilah, J. and Buck, P. (2006), *Aromadermatology: aromatherapy in the treatment and care of common skin conditions*, Radcliffe Publishing.

Bhaskar, K., Mohan, C. K., Lingam, M., Mohan, S. J., Venkateswarlu, V., Rao, Y. M., Bhaskar, K., Anbu, J. and Ravichandran, V. (2009), 'Development of sln and nlc enriched hydrogels for transdermal delivery of nitrendipine: in vitro and in vivo characteristics', *Drug Development and Industrial Pharmacy* **35**(1), 98–113.

Bhatt, V. D., Soman, R. S., Miller, M. A. and Kasting, G. B. (2008), 'Permeation of tecnazene through human skin in vitro as assessed by hs-spme and gc-ms', *Environmental Science & Technology* **42**(17), 6587–6592.

Bolognia, J. L., Jorizzo, J. L. and Schaffer, J. V. (2012), *Dermatology: 2-Volume Set: Expert Consult Premium Edition-Enhanced Online Features and Print, 3e (Bolognia, Dermatology)*, Saunders, Philadelphia.

Bos, J. D. and Meinardi, M. M. (2000), 'The 500 dalton rule for the skin penetration of chemical compounds and drugs', *Experimental Dermatology: Viewpoint* **9**(3), 165–169.

Bouwstra, J. A., Honeywell-Nguyen, P. L., Gooris, G. S. and Ponec, M. (2003), 'Structure of the skin barrier and its modulation by vesicular formulations', *Progress in Lipid Research* **42**(1), 1–36.

Bouwstra, J. A. and Ponec, M. (2006), 'The skin barrier in healthy and diseased state', *Biochimica et Biophysica Acta (BBA)-Biomembranes* **1758**(12), 2080–2095.

Bouwstra, J. A., Thewalt, J., Gooris, G. S. and Kitson, N. (1997), 'A model membrane approach to the epidermal permeability barrier: an x-ray diffraction study', *Biochemistry* **36**(25), 7717–7725.

Bouwstra, J., Pilgram, G., Gooris, G., Koerten, H. and Ponec, M. (2001), 'New aspects of the skin barrier organization', *Skin Pharmacology and Physiology* **14**(Suppl. 1), 52–62.

Brain, K. R., Walters, K. A. and Watkinson, A. C. (1998), 'Investigation of skin permeation in vitro', *Drugs and the Pharmaceutical Sciences* **91**, 161–187.

Brambilla, D., Luciani, P. and Leroux, J.-C. (2014), 'Breakthrough discoveries in drug delivery technologies: the next 30 years', *Journal of Controlled Release* **190**, 9–14.

Bronaugh, R. L. and Maibach, H. I. (1989), *Percutaneous absorption: mechanisms–methodology–drug delivery*, Marcel Dekker Inc.

Bronaugh, R. L. and Maibach, H. I. (2005), *Percutaneous absorption: drugs, cosmetics, mechanisms, methods*, CRC Press.

Brooke, I., Cocker, J., Delic, J., Payne, M., Jones, K., Gregg, N. and Dyne, D. (1998), 'Dermal uptake of solvents from the vapour phase; an experimental study in humans', *The Annals of Occupational Hygiene* **42**(8), 531–540.

Brown, M. B., Martin, G. P., Jones, S. A. and Akomeah, F. K. (2006), 'Dermal and transdermal drug delivery systems: current and future prospects', *Drug Delivery* **13**(3), 175–187.

Bucher, D., Li, S., Kehoe, J. and Kilbourne, E. (1976), 'Chromatographic isolation of the hemagglutinin polypeptides from influenza virus vaccine and determination of their amino-terminal sequences', *Proceedings of the National Academy of Sciences* **73**(1), 238–242.

Bunjes, H. and Koch, M. H. (2005), 'Saturated phospholipids promote crystallization but slow down polymorphic transitions in triglyceride nanoparticles', *Journal of Controlled Release* **107**(2), 229–243.

Burkoth, T. L., Bellhouse, B. J., Hewson, G., Longridge, D. J., Muddle, A. G. and Sarphie, D. F. (1999), 'Transdermal and transmucosal powdered drug delivery', *Critical Reviews™ in Therapeutic Drug Carrier Systems* **16**(4).

Buzea, C., Pacheco, I. I. and Robbie, K. (2007), 'Nanomaterials and nanoparticles: sources and toxicity', *Biointerphases* **2**(4), MR17–MR71.

Calvo, P., Vila-Jato, J. L. and Alonso, M. J. (1996), 'Comparative in vitro evaluation of several colloidal systems, nanoparticles, nanocapsules, and nanoemulsions, as ocular drug carriers', *Journal of Pharmaceutical Sciences* **85**(5), 530–536.

Carrum, G., Abernethy, D. R., Sadhukhan, M. and Wright III, C. E. (1986), 'Minoxidil analysis in human plasma using high-performance liquid chromatography with electrochemical detection: application to pharmacokinetic studies', *Journal of Chromatography B: Biomedical Sciences and Applications* **381**, 127–135.

Carson, F. L., Hladik, C., Carson, F. L. and Hladik, C. (2009), *Histotechnology : a self-instructional text*, 3rd ed edn, [Chicago] : ASCP Press.

Cartier, R., Kaufner, L., Paulke, B., Wüstneck, R., Pietschmann, S., Michel, R., Bruhn, H. and Pison, U. (2007), 'Latex nanoparticles for multimodal imaging and detection in vivo', *Nanotechnology* **18**(19), 195102.

Cevc, G. (1997), 'Drug delivery across the skin', *Expert Opinion on Investigational Drugs* **6**(12), 1887–1937.

Chana, J., Forbes, B. and Jones, S. A. (2015), 'Triggered-release nanocapsules for drug delivery to the lungs', *Nanomedicine: Nanotechnology, Biology and Medicine* **11**(1), 89–97.

Chen, H., Woods, A., Forbes, B. and Jones, S. (2016), 'Controlled drug release from lung-targeted nanocarriers via chemically mediated shell permeabilisation', *International Journal of Pharmaceutics* **511**(2), 1033–1041.

Chia-Ming, C., Flynn, G. L., Weiner, N. D. and Szpunar, G. J. (1989), 'Bioavailability assessment of topical delivery systems: Effect of vehicle evaporation upon in vitro delivery of minoxidil from solution formulations', *International Journal of Pharmaceutics* **55**(2-3), 229–236.

Chien, Y. W., Chien, T.-y., Bagdon, R. E., Huang, Y. C. and Bierman, R. H. (1989), 'Transdermal dual-controlled delivery of contraceptive drugs: formulation development, in vitro and in vivo evaluations, and clinical performance', *Pharmaceutical Research* **6**(12), 1000–1010.

Childers, M. A., Franco, W., Nelson, J. S. and Aguilar, G. (2007), 'Laser surgery of port wine stains using local vacuum pressure: changes in skin morphology and optical properties (part i)', *Lasers in Surgery and Medicine: The Official Journal of the American Society for Laser Medicine and Surgery* **39**(2), 108–117.

Choi, E. H., Lee, S. H., Ahn, S. K. and Hwang, S. M. (1999), 'The pretreatment effect of chemical skin penetration enhancers in transdermal drug delivery using iontophoresis', *Skin Pharmacology and Physiology* **12**(6), 326–335.

Choi, W. I., Lee, J. H., Kim, J.-Y., Kim, J.-C., Kim, Y. H. and Tae, G. (2012), 'Efficient skin permeation of soluble proteins via flexible and functional nanocarrier', *Journal of Controlled Release* **157**(2), 272–278.

Chopra, P., Hao, J. and Li, S. K. (2010), 'Iontophoretic transport of charged macromolecules across human sclera', *International Journal of Pharmaceutics* **388**(1-2), 107–113.

Clapp, T., Siebert, P., Chen, D. and Braun, L. J. (2011), 'Vaccines with aluminum-containing adjuvants: optimizing vaccine efficacy and thermal stability', *Journal of Pharmaceutical Sciences* **100**(2), 388–401.

Contado, C. (2015), 'Nanomaterials in consumer products: a challenging analytical problem', *Frontiers in Chemistry* **3**, 48.

Corbo, M. (1993), 'Development and validation of in vitro testing methods for semisolid formulations', *Pharmaceutical Technology* **17**, 112.

Cornwell, P. and Barry, B. (1994), 'Sesquiterpene components of volatile oils as skin penetration enhancers for the hydrophilic permeant 5-fluorouracil', *Journal of Pharmacy and Pharmacology* **46**(4), 261–269.

Cross, S. E. and Roberts, M. S. (1993), 'Subcutaneous absorption kinetics and local tissue distribution of interferon and other solutes', *Journal of Pharmacy and Pharmacology* **45**(7), 606–609.

Cross, S. and Roberts, M. (2004), 'Physical enhancement of transdermal drug application: is delivery technology keeping up with pharmaceutical development?', *Current Drug Delivery* **1**(1), 81–92.

Cua, A. B., Wilhelm, K.-P. and Maibach, H. (1990), 'Frictional properties of human skin: relation to age, sex and anatomical region, stratum corneum hydration and transepidermal water loss', *British Journal of Dermatology* **123**(4), 473–479.

Cushley, R. J. and Forrest, B. J. (1977), 'Structure and stability of vitamin e–lecithin and phytanic acid–lecithin bilayers studied by 13c and 31p nuclear magnetic resonance', *Canadian Journal of Chemistry* **55**(2), 220–226.

Daniels, R. (2004), Strategies for skin penetration enhancement, *in* 'Skin Care Forum', Vol. 37, pp. 58–65.

Darlenski, R. and Fluhr, J. W. (2012), 'Influence of skin type, race, sex, and anatomic location on epidermal barrier function', *Clinics in Dermatology* **30**(3), 269–273.

De Benedetto, A., Rafaels, N. M., McGirt, L. Y., Ivanov, A. I., Georas, S. N., Cheadle, C., Berger, A. E., Zhang, K., Vidyasagar, S., Yoshida, T. et al. (2011), 'Tight junction defects in patients with atopic dermatitis', *Journal of Allergy and Clinical Immunology* **127**(3), 773–786.

de Jalon, E. G., Blanco-Prieto, M. J., Ygartua, P. and Santoyo, S. (2001*a*), 'Topical application of acyclovir-loaded microparticles: quantification of the drug in porcine skin layers', *Journal of Controlled Release* **75**(1-2), 191–197.

De Jalon, E. G., Blanco-Prieto, M., Ygartua, P. and Santoyo, S. (2001*b*), 'Plga microparticles: possible vehicles for topical drug delivery', *International Journal of Pharmaceutics* **226**(1-2), 181–184.

De Vringer, T. and De Ronde, H. (1995), 'Preparation and structure of a water-in-oil cream containing lipid nanoparticles', *Journal of Pharmaceutical Sciences* **84**(4), 466–472.

Denet, A.-R., Vanbever, R. and Préat, V. (2004), 'Skin electroporation for transdermal and topical delivery', *Advanced Drug Delivery Reviews* **56**(5), 659–674.

Dick, I. P. and Scott, R. C. (1992), 'Pig ear skin as an in-vitro model for human skin permeability', *Journal of Pharmacy and Pharmacology* **44**(8), 640–645.

Dingler, A., Blum, R., Niehus, H., Muller, R. and Gohla, S. (1999), 'Solid lipid nanoparticles (slntm/lipopearlstm) a pharmaceutical and cosmetic carrier for the application of vitamin e in dermal products', *Journal of Microencapsulation* **16**(6), 751–767.

Donnelly, R. F., Singh, T. R. R., Garland, M. J., Migalska, K., Majithiya, R., McCrudden, C. M., Kole, P. L., Mahmood, T. M. T., McCarthy, H. O. and Woolfson, A. D. (2012), 'Hydrogel-forming microneedle arrays for enhanced transdermal drug delivery', *Advanced Functional Materials* **22**(23), 4879–4890.

Donnelly, R. F., Singh, T. R. R., Morrow, D. I. and Woolfson, A. D. (2012), *Microneedle-Mediated Transdermal and Intradermal Drug Delivery*, John Wiley & Sons.

Dorraj, G. and Moghimi, H. R. (2013), 'Preparation and characterization of thermoresponsive in-situ forming poloxamer hydrogel for controlled release of nile red-loaded solid lipid nanoparticles', *Iranian Journal of Pharmaceutical Sciences* **9**(4), 39–50.

Dreher, M. R., Liu, W., Michelich, C. R., Dewhirst, M. W., Yuan, F. and Chilkoti, A. (2006), 'Tumor vascular permeability, accumulation, and penetration of macromolecular drug carriers', *Journal of the National Cancer Institute* **98**(5), 335–344.

Elias, P. M. (2005), 'Stratum corneum defensive functions: an integrated view', *Journal of General Internal Medicine* **20**(5), 183–200.

Ellis, R. (2010), 'Hematoxylin and eosin (h&e) staining protocol', `http://www.ihcworld.com/_protocols/special_stains/h&e_ellis.htm`. Online; accessed August 10, 2018.

Eshuis, A., Leendertse, H. and Thoenes, D. (1991), 'Surfactant-free emulsion polymerization of styrene using crosslinked seed particles', *Colloid and Polymer Science* **269**(11), 1086–1089.

Fang, C.-L., Aljuffali, I. A., Li, Y.-C. and Fang, J.-Y. (2014), 'Delivery and targeting of nanoparticles into hair follicles', *Therapeutic Delivery* **5**(9), 991–1006.

Fang, J.-Y., Lee, W.-R., Shen, S.-C., Wang, H.-Y., Fang, C.-L. and Hu, C.-H. (2004), 'Transdermal delivery of macromolecules by erbium: Yag laser', *Journal of Controlled Release* **100**(1), 75–85.

Feldman, R. J. (1967), 'Regional variation in percutaneous penetration of 14c cortisol in man', *Archives of Dermatology* **48**, 181–183.

Fendler, J. H. and Romero, A. (1977), 'Liposomes as drug carriers', *Life Sciences* **20**(7), 1109–1120.

Feng, S., Zhu, L., Huang, Z., Wang, H., Li, H., Zhou, H., Lu, L., Wang, Y., Liu, Z. and Liu, L. (2017), 'Controlled release of optimized electroporation enhances the transdermal efficiency of sinomenine hydrochloride for treating arthritis in vitro and in clinic', *Drug Design, Development and Therapy* **11**, 1737.

Fernandes, R., Smyth, N. R., Muskens, O. L., Nitti, S., Heuer-Jungemann, A., Ardern-Jones, M. R. and Kanaras, A. G. (2015), 'Interactions of skin with gold nanoparticles of different surface charge, shape, and functionality', *Small* **11**(6), 713–721.

Ferranti, V., Marchais, H., Chabenat, C., Orecchioni, A. and Lafont, O. (1999), 'Primidone-loaded poly-ε-caprolactone nanocapsules: incorporation efficiency and in vitro release profiles', *International Journal of Pharmaceutics* **193**(1), 107–111.

Fick, A. (1855), 'Ueber difusion', *Annalen Der Physik* .

Finnin, B., Walters, K. A. and Franz, T. J. (2011), 'In vitro skin permeation methodology', *Topical and Transdermal Drug Delivery: Principles and Practice* pp. 85–108.

Flaten, G. E., Palac, Z., Engesland, A., Filipović-Grčić, J., Vanić, Ž. and Škalko-Basnet, N. (2015), 'In vitro skin models as a tool in optimization of drug formulation', *European Journal of Pharmaceutical Sciences* **75**, 10–24.

Franz, T. J. (1975), 'Percutaneous absorption. on the relevance of in vitro data', *Journal of Investigative Dermatology* **64**(3), 190–195.

Franz, T. J. (1978), 'The finite dose technique as a valid in vitro model for the study of percutaneous absorption in man.', *Current Problems in Dermatology* **7**, 58–68.

Fujii, M., Yamanouchi, S., Hori, N., Iwanaga, N., Kawaguchi, N. and Matsumoto, M. (1997), 'Evaluation of yucatan micropig skin for use as an in vitro model for skin permeation study', *Biological and Pharmaceutical Bulletin* **20**(3), 249–254.

Fujiwara, A., Hinokitani, T., Goto, K. and Arai, T. (2005), 'Partial ablation of porcine stratum corneum by argon-fluoride excimer laser to enhance transdermal drug permeability', *Lasers in Medical Science* **19**(4), 210–217.

Furuse, M., Hata, M., Furuse, K., Yoshida, Y., Haratake, A., Sugitani, Y., Noda, T., Kubo, A. and Tsukita, S. (2002), 'Claudin-based tight junctions are crucial for the mammalian epidermal barrier: a lesson from claudin-1–deficient mice', *Journal of Cell Biology* **156**(6), 1099–1111.

Gaidhane, H. K., Bidada, J. P., Bhusari, A. S., Navkhare, M. S., Diwanka, G. P. and Tiwari, A. H. (2011), 'Development and validation of stability indicating hplc method for the estimation of minoxidil and related substance in topical formulation', *Journal of Pharmacy Research* **4**(12), 4481–4484.

Gao, S. and McClements, D. J. (2016), 'Formation and stability of solid lipid nanoparticles fabricated using phase inversion temperature method', *Colloids and Surfaces A: Physicochemical and Engineering Aspects* **499**, 79–87.

Gasco, M. (1997), 'Solid lipid nanospheres from warm micro-emulsions: Improvements in sln production for more efficient drug delivery', *Pharmaceutical Technology Europe* **9**, 52–58.

Gavin, P. D., El-Tamimy, M., Keah, H. H. and Boyd, B. J. (2017), 'Tocopheryl phosphate mixture (tpm) as a novel lipid-based transdermal drug delivery carrier:

formulation and evaluation', *Drug Delivery and Translational Research* **7**(1), 53–65.

Gelfuso, G. M., Gratieri, T., Delgado-Charro, M. B., Guy, R. H. and Lopez, R. F. V. (2013), 'Iontophoresis-targeted, follicular delivery of minoxidil sulfate for the treatment of alopecia', *Journal of Pharmaceutical Sciences* **102**(5), 1488–1494.

Gelfuso, G. M., Gratieri, T., Simao, P. S., de Freitas, L. A. P. and Lopez, R. F. V. (2011), 'Chitosan microparticles for sustaining the topical delivery of minoxidil sulphate', *Journal of Microencapsulation* **28**(7), 650–658.

Genina, E. A., Bashkatov, A. N., Sinichkin, Y. P., Kochubey, V. I., Lakodina, N. A., Altshuler, G. B. and Tuchin, V. V. (2002), 'In vitro and in vivo study of dye diffusion into the human skin and hair follicles', *Journal of Biomedical Optics* **7**(3), 471.

Gessner, A., Olbrich, C., Schröder, W., Kayser, O. and Müller, R. (2001), 'The role of plasma proteins in brain targeting: species dependent protein adsorption patterns on brain-specific lipid drug conjugate (ldc) nanoparticles', *International Journal of Pharmaceutics* **214**(1-2), 87–91.

Gill, Harvinder S. Andrews, S. N. (2017), *Microdermabrasion for Enhanced Drug Delivery*, Springer Berlin Heidelberg.

Giusti, F., Martella, A., Bertoni, L. and Seidenari, S. (2001), 'Skin barrier, hydration, and ph of the skin of infants under 2 years of age', *Pediatric Dermatology* **18**(2), 93–96.

Glenn, G. M., Taylor, D. N., Li, X., Frankel, S., Montemarano, A. and Alving, C. R. (2000), 'Transcutaneous immunization: a human vaccine delivery strategy using a patch', *Nature Medicine* **6**(12), 1403.

Godin, B. and Touitou, E. (2007), 'Transdermal skin delivery: predictions for humans from in vivo, ex vivo and animal models', *Advanced Drug Delivery Reviews* **59**(11), 1152–1161.

Golden, M. H. and Zoutendam, P. H. (1987), 'The determination of minoxidil in human serum by high-performance liquid chromatography with amperometric detection', *Journal of Pharmaceutical and Biomedical Analysis* **5**(6), 543–551.

Gomez, C., Costela, A., García-Moreno, I., Llanes, F., Teijón, J. M. and Blanco, D. (2008), 'Laser treatments on skin enhancing and controlling transdermal delivery of 5-fluorouracil', *Lasers in Surgery and Medicine: The Official Journal of the American Society for Laser Medicine and Surgery* **40**(1), 6–12.

Gonzalez, V. D., Gugliotta, L. M. and Meira, G. R. (2008), 'Latex of immunodiagnosis for detecting the chagas disease. i. synthesis of the base carboxylated latex', *Journal of Materials Science: Materials in Medicine* **19**(2), 777–788.

Grandjean, P. (1990), *Skin penetration: hazardous chemicals at work*, CRC Press.

Greene, R. S., Downing, D. T., Pochi, P. E. and Strauss, J. S. (1970), 'Anatomical variation in the amount and composition of human skin surface lipid', *Journal of Investigative Dermatology* **54**(3), 240–7.

Greenspan, P. and Fowler, S. D. (1985), 'Spectrofluorometric studies of the lipid probe, nile red.', *Journal of Lipid Research* **26**(7), 781–789.

Greenspan, P., Mayer, E. P. and Fowler, S. D. (1985), 'Nile red: a selective fluorescent stain for intracellular lipid droplets.', *The Journal of cell biology* **100**(3), 965–973.

Grice, J. E., Ciotti, S., Weiner, N., Lockwood, P., Cross, S. E. and Roberts, M. S. (2010), 'Relative uptake of minoxidil into appendages and stratum corneum and permeation through human skin in vitro', *Journal of Pharmaceutical Sciences* **99**(2), 712–718.

Grice, J. E., Prow, T. W., Kendall, M. A. and Roberts, M. S. (2012), 'Electrical and physical methods of skin penetration enhancement'.

Grimnes, S. (1984), 'Pathways of ionic flow through human skin in vivo.', *Acta Derm. Venereol* **64**(2), 93–98.

Gul, M. O., Jones, S. A., Dailey, L. A., Nacer, H., Ma, Y., Sadouki, F., Hider, R., Araman, A. and Forbes, B. (2009), 'A poly (vinyl alcohol) nanoparticle platform for kinetic studies of inhaled particles', *Inhalation Toxicology* **21**(7), 631–640.

Gupta, S., Bansal, R., Gupta, S., Jindal, N. and Jindal, A. (2013), 'Nanocarriers and nanoparticles for skin care and dermatological treatments', *Indian Dermatology Online Journal* **4**(4), 267.

Gutberlet, T. and Katsaras, J. (2001), *Lipid Bilayers: Structure and Interactions*, Springer Science & Business Media.

Guy, R. H. and Hadgraft, J. (1988), 'Physicochemical aspects of percutaneous penetration and its enhancement', *Pharmaceutical Research* **5**(12), 753–758.

Guy, R. H. and Hadgraft, J. (2003), *Transdermal Drug Delivery*, M. Dekker New York.

Guy, R. H., Hadgraft, J. and Bucks, D. A. (1987), 'Transdermal drug delivery and cutaneous metabolism', *Xenobiotica* **17**(3), 325–343.

Guy, R. H., Kalia, Y. N., Delgado-Charro, M. B., Merino, V., Lopez, A. and Marro, D. (2000), 'Iontophoresis: electrorepulsion and electroosmosis', *Journal of Controlled Release* **64**(1-3), 129–132.

Hadgraft, J. (1999), 'Passive enhancement strategies in topical and transdermal drug delivery', *International Journal of Pharmaceutics* **184**(1), 1–6.

Hadgraft, J. (2001), 'Modulation of the barrier function of the skin', *Skin Pharmacology and Physiology* **14**(Suppl. 1), 72–81.

Hadgraft, J. (2004), 'Skin deep', *European Journal of Pharmaceutics and Biopharmaceutics* **58**(2), 291–299.

Hadgraft, J., Beutner, D. and Wolff, H. M. (1993), 'In vivo-in vitro comparisons in the transdermal delivery of nitroglycerin', *International Journal of Pharmaceutics* **89**(1), R1–R4.

Hadgraft, J. and Lane, M. E. (2016), 'Advanced topical formulations (atf)', *International Journal of Pharmaceutics* **514**(1), 52–57.

Halks-Miller, M., Guo, L. S. and Hamilton, R. L. (1985), 'Tocopherol-phospholipid liposomes: maximum content and stability to serum proteins', *Lipids* **20**(3), 195–200.

Han, T. and Das, D. B. (2015), 'Potential of combined ultrasound and microneedles for enhanced transdermal drug permeation: a review', *European Journal of Pharmaceutics and Biopharmaceutics* **89**, 312–328.

Hansen, S. and Lehr, C.-M. (2012), 'Nanoparticles for transcutaneous vaccination', *Microbial Biotechnology* **5**(2), 156–167.

Hanson, K. M. and Bardeen, C. J. (2009), 'Application of nonlinear optical microscopy for imaging skin', *Photochemistry and Photobiology* **85**(1), 33–44.

Harrison, S., Barry, B. and Dugard, P. (1984), 'Effects of freezing on human skin permeability', *Journal of Pharmacy and Pharmacology* **36**(4), 261–262.

Health and consumer protection directorate-general (2006), 'Basic criteria for in vitro assessment of dermal absorption of cosmetic ingredients', *European Commission SCCP/0970/06* .

Hendriks, F., Brokken, D. v., Van Eemeren, J., Oomens, C., Baaijens, F. and Horsten, J. (2003), 'A numerical-experimental method to characterize the non-linear mechanical behaviour of human skin', *Skin Research and Technology* **9**(3), 274–283.

Heurtault, B., Saulnier, P., Pech, B., Proust, J.-E. and Benoit, J.-P. (2002), 'A novel phase inversion-based process for the preparation of lipid nanocarriers', *Pharmaceutical Research* **19**(6), 875–880.

Higuchi, T. (1960), 'Physical chemical analysis of percutaneous absorption process from creams and ointments', *Journal of the Society of Cosmetic Chemists* **11**, 85–97.

Higuchi, T. (1961), 'Rate of release of medicaments from ointment bases containing drugs in suspension', *Journal of Pharmaceutical Sciences* **50**(10), 874–875.

Higuchi, W. I. (1962), 'Analysis of data on the medicament release from ointments', *Journal of Pharmaceutical Sciences* **51**(8), 802–804.

Hikima, T., Yamada, K., Kimura, T., Maibach, H. I. and Tojo, K. (2002), 'Comparison of skin distribution of hydrolytic activity for bioconversion of β-estradiol 17-acetate between man and several animals in vitro', *European Journal of Pharmaceutics and Biopharmaceutics* **54**(2), 155–160.

Hiroaki, J., Eri, K. and Koichiro, H. (1994), 'ph-sensitive liposomes composed of tocopherol hemisuccinate and of phosphatidylethanolamine including tocopherol hemisuccinate', *Biochimica et Biophysica Acta (BBA)-Lipids and Lipid Metabolism* **1213**(3), 343–348.

Hogan, D. J. and Maibach, H. I. (1990), 'Adverse dermatologic reactions to transdermal drug delivery systems', *Journal of the American Academy of Dermatology* **22**(5), 811–814.

Holmgaard, R. and Nielsen, J. B. (2009), *Dermal absorption of pesticides: evaluation of variability and prevention*, Danish Environmental Protection Agency.

Hoppert, M. (2006), *Microscopic techniques in biotechnology*, John Wiley & Sons.

Horita, D., Yoshimoto, M., Todo, H. and Sugibayashi, K. (2014), 'Analysis of hair follicle penetration of lidocaine and fluorescein isothiocyanate-dextran 4 kda using hair follicle-plugging method', *Drug Development and Industrial Pharmacy* **40**(3), 345–351.

Howes, D., Guy, R., Hadgraft, J., Heylings, J., Hoeck, U., Kemper, F., Maibach, H., Marty, J., Merk, H. and Parra, J. (1996), 'Methods for assessing percutaneous absorption: the report and recommendations of ecvam workshop 13', *Alternatives to Laboratory Animals: ATLA* .

Hsieh, D. S. (1994), *Drug permeation enhancement-theory and applications*, Taylor & Francis.

Hsu, T. and Mitragotri, S. (2011), 'Delivery of sirna and other macromolecules into skin and cells using a peptide enhancer', *Proceedings of the National Academy of Sciences* **108**(38), 15816–15821.

Huang, X., Tanojo, H., Lenn, J., Deng, C. H. and Krochmal, L. (2005), 'A novel foam vehicle for delivery of topical corticosteroids', *Journal of the American Academy of Dermatology* **53**(1), S26–S38.

Hueber, F., Besnard, M., Schaefer, H. and Wepierre, J. (1994), 'Percutaneous absorption of estradiol and progesterone in normal and appendage-free skin of the hairless rat: lack of importance of nutritional blood flow', *Skin Pharmacology and Physiology* **7**(5), 245–256.

Hunt, C. A. and Tsang, S. (1981), 'α-tocopherol retards autoxidation and prolongs the shelf-life of liposomes', *International Journal of Pharmaceutics* **8**(2), 101–110.

Inacio, R. (2015), An investigation into the influence of local barometric stress upon xenobiotic percutaneous penetration, PhD thesis, King's College London.

Inacio, R., Poland, S., Cai, X., Cleary, S., Ameer-Beg, S., Keeble, J. and Jones, S. (2016), 'The application of local hypobaric pressure—a novel means to enhance macromolecule entry into the skin', *Journal of Controlled Release* **226**, 66–76.

Israelachvili, J. (1985), 'Physics of amphiphiles: micelles, vesicles and microemulsions', *Proceedings of the International School of Physics ÔEnrico FermiÕ (SocietaItaliana di Fisica), North-Holland, Amsterdam* p. 24.

Ita, K. (2014), 'Transdermal drug delivery: progress and challenges', *Journal of Drug Delivery Science and Technology* **24**(3), 245–250.

Jenning, V., Gysler, A., Schäfer-Korting, M. and Gohla, S. H. (2000), 'Vitamin a loaded solid lipid nanoparticles for topical use: occlusive properties and drug targeting to the upper skin', *European Journal of Pharmaceutics and Biopharmaceutics* **49**(3), 211–218.

Jones, S. A., Reid, M. L. and Brown, M. B. (2009), 'Determining degree of saturation after application of transiently supersaturated metered dose aerosols for topical delivery of corticosteroids', *Journal of Pharmaceutical Sciences* **98**(2), 543–554.

Jose, J. and Burgess, K. (2006), 'Syntheses and properties of water-soluble nile red derivatives', *The Journal of Organic Chemistry* **71**(20), 7835–7839.

Joshi, A. and Raje, J. (2002), 'Sonicated transdermal drug transport', *Journal of Controlled Release* **83**(1), 13–22.

Joshi, M. and Patravale, V. (2008), 'Nanostructured lipid carrier (nlc) based gel of celecoxib', *International Journal of Pharmaceutics* **346**(1-2), 124–132.

Jung, S., Otberg, N., Thiede, G., Richter, H., Sterry, W., Panzner, S. and Lademann, J. (2006), 'Innovative liposomes as a transfollicular drug delivery system: penetration into porcine hair follicles', *Journal of Investigative Dermatology* **126**(8), 1728–1732.

Kakabakos, S. E., Livanlou, E., Evangelatos, G. and Ithakissios, D. (1990), 'Immobilization of immunoglobulins onto surface-treated and untreated polystyrene beads for radioimmunoassays.', *Clinical Chemistry* **36**(3), 492–496.

Kalluri, H. and Banga, A. K. (2011), 'Transdermal delivery of proteins', *Aaps Pharmscitech* **12**(1), 431–441.

Kao, J., Hall, J. and Helman, G. (1988), 'In vitro percutaneous absorption in mouse skin: influence of skin appendages', *Toxicology and Applied Pharmacology* **94**(1), 93–103.

Kasliwal, N., Derle, D., Negi, J. and Gohil, J. (2008), 'Effect of permeation enhancers on the release and permeation kinetics of meloxicam gel formulations through rat skin', *Asian Journal of Pharmaceutical Sciences* **3**(5), 193–199.

Kattou, P., Lian, G., Glavin, S., Sorrell, I. and Chen, T. (2017), 'Development of a two-dimensional model for predicting transdermal permeation with the follicular pathway: Demonstration with a caffeine study', *Pharmaceutical Research* **34**(10), 2036–2048.

Kawasaki, E. S. and Player, A. (2005), 'Nanotechnology, nanomedicine, and the development of new, effective therapies for cancer', *Nanomedicine: Nanotechnology, Biology and Medicine* **1**(2), 101–109.

Keiper, A. (2003), 'The nanotechnology revolution', *The New Atlantis* **120**(2), 17–34.

Kermode, M. (2004), 'Unsafe injections in low-income country health settings: need for injection safety promotion to prevent the spread of blood-borne viruses', *Health Promotion International* **19**(1), 95–103.

Kessler, R. (2011), 'Engineered nanoparticles in consumer products: understanding a new ingredient', *Environmental Health Perspectives* **119**(3), A120.

Kezic, S. (2008), 'Methods for measuring in-vivo percutaneous absorption in humans', *Human & Experimental Toxicology* **27**(4), 289–295.

Kijima, S., Masaki, R., R Kadhum, W., Todo, H., Hatanaka, T. and Sugibayashi, K. (2015), 'Potential of imaging analysis in establishing skin concentration-distance profiles for topically applied fitc-dextran 4 kda', *ADMET and DMPK* **2**(4), 221–234.

Kim, Y.-C., Park, J.-H. and Prausnitz, M. R. (2012), 'Microneedles for drug and vaccine delivery', *Advanced Drug Delivery Reviews* **64**(14), 1547–1568.

Kirschner, N., Haftek, M., Niessen, C. M., Behne, M. J., Furuse, M., Moll, I. and Brandner, J. M. (2011), 'Cd44 regulates tight-junction assembly and barrier function', *Journal of Investigative Dermatology* **131**(4), 932–943.

Kirschner, N., Houdek, P., Fromm, M., Moll, I. and Brandner, J. M. (2010), 'Tight junctions form a barrier in human epidermis', *European Journal of Cell Biology* **89**(11), 839–842.

Koch, R. and Hanasono, M. M. (2001), 'Microdermabrasion.', *Facial Plastic Surgery Clinics of North America* **9**(3), 377–382.

Kohli, A. and Alpar, H. (2004), 'Potential use of nanoparticles for transcutaneous vaccine delivery: effect of particle size and charge', *International Journal of Pharmaceutics* **275**(1-2), 13–17.

Kornick, C. A., Santiago-Palma, J., Moryl, N., Payne, R. and Obbens, E. A. (2003), 'Benefit-risk assessment of transdermal fentanyl for the treatment of chronic pain', *Drug Safety* **26**(13), 951–973.

Kreilgaard, M. (2002), 'Assessment of cutaneous drug delivery using microdialysis', *Advanced Drug Delivery Reviews* **54**, S99–S121.

Kreuter, J. (2014), 'Drug delivery to the central nervous system by polymeric nanoparticles: what do we know?', *Advanced Drug Delivery Reviews* **71**, 2–14.

Küchler, S., Radowski, M. R., Blaschke, T., Dathe, M., Plendl, J., Haag, R., Schäfer-Korting, M. and Kramer, K. D. (2009), 'Nanoparticles for skin penetration enhancement–a comparison of a dendritic core-multishell-nanotransporter and solid lipid nanoparticles', *European Journal of Pharmaceutics and Biopharmaceutics* **71**(2), 243–250.

Lademann, J., Knorr, F., Richter, H., Blume-Peytavi, U., Vogt, A., Antoniou, C., Sterry, W. and Patzelt, A. (2008), 'Hair follicles–an efficient storage and penetration pathway for topically applied substances', *Skin Pharmacology and Physiology* **21**(3), 150–155.

Lademann, J., Knorr, F., Richter, H., Jung, S., Meinke, M., Rühl, E., Alexiev, U., Calderón, M. and Patzelt, A. (2015), 'Hair follicles as a target structure for nanoparticles', *Journal of Innovative Optical Health Sciences* **8**(04), 1530004.

Lademann, J., Otberg, N., Richter, H., Weigmann, H.-J., Lindemann, U., Schaefer, H. and Sterry, W. (2001), 'Investigation of follicular penetration of topically applied substances', *Skin Pharmacology and Physiology* **14**(Suppl. 1), 17–22.

Lademann, J., Richter, H., Teichmann, A., Otberg, N., Blume-Peytavi, U., Luengo, J., Weiss, B., Schaefer, U. F., Lehr, C.-M., Wepf, R. et al. (2007), 'Nanoparticles–an efficient carrier for drug delivery into the hair follicles', *European Journal of Pharmaceutics and Biopharmaceutics* **66**(2), 159–164.

Lademann, J., Weigmann, H.-J., Rickmeyer, C., Barthelmes, H., Schaefer, H., Mueller, G. and Sterry, W. (1999), 'Penetration of titanium dioxide microparticles in a sunscreen formulation into the horny layer and the follicular orifice', *Skin Pharmacology and Physiology* **12**(5), 247–256.

Lampe, M. A., Burlingame, A., Whitney, J., Williams, M. L., Brown, B. E., Roitman, E. and Elias, P. M. (1983), 'Human stratum corneum lipids: characterization and regional variations.', *Journal of Lipid Research* **24**(2), 120–130.

Lane, M. E., Santos, P., Watkinson, A. C. and Hadgraft, J. (2012), 'Passive skin permeation enhancement', *Topical and Transdermal Drug Delivery. Wiley, Hoboken* pp. 23–42.

Larraneta, E., Lutton, R. E., Woolfson, A. D. and Donnelly, R. F. (2016), 'Microneedle arrays as transdermal and intradermal drug delivery systems: materials science, manufacture and commercial development', *Materials Science and Engineering: R: Reports* **104**, 1–32.

Lasic, D. (1995), 'Application of liposomes ii handbook of biological physics i eds. r. lipowsky, e. sackmann'.

Lauer, A. C., Lieb, L. M., Ramachandran, C., Flynn, G. L. and Weiner, N. D. (1995), 'Transfollicular drug delivery', *Pharmaceutical Research* **12**(2), 179–186.

Lawson, L., Freytag, L. and Clements, J. (2007), 'Use of nanocarriers for transdermal vaccine delivery', *Clinical Pharmacology & Therapeutics* **82**(6), 641–643.

Lee, S., McAuliffe, D. J., Flotte, T. J., Kollias, N. and Doukas, A. G. (1998), 'Photomechanical transcutaneous delivery of macromolecules1', *Journal of Investigative Dermatology* **111**(6), 925–929.

Lee, W.-R., Pan, T.-L., Wang, P.-W., Zhuo, R.-Z., Huang, C.-M. and Fang, J.-Y. (2008), 'Erbium: Yag laser enhances transdermal peptide delivery and skin vaccination', *Journal of Controlled Release* **128**(3), 200–208.

Leroux, J.-C., Gravel, P., Balant, L., Volet, B., Anner, B. M., Allémann, E., Doelker, E. and Gurny, R. (1994), 'Internalization of poly (d, l-1actic acid) nanoparticles by isolated human leukocytes and analysis of plasma proteins adsorbed onto the particles', *Journal of Biomedical Materials Research* **28**(4), 471–481.

Li, L., Lishko, V. and Hoffman, R. M. (1993), 'Liposome targeting of high molecular weight dna to the hair follicles of histocultured skin: a model for gene therapy of the hair growth processes', *In Vitro Cellular & Developmental Biology-Animal* **29**(4), 258–260.

Liang, G. H. and Weber, C. R. (2014), 'Molecular aspects of tight junction barrier function', *Current Opinion in Pharmacology* **19**, 84–89.

Lin, S.-Y., Capek, I., Hsu, T.-J. and Chern, C.-S. (1999), 'On the emulsion polymerization of styrene in the presence of a nonionic emulsifier', *Journal of Polymer Science Part A: Polymer Chemistry* **37**(23), 4422–4431.

Liu, P., Higuchi, W. I., Song, W.-q., Kurihara-Bergstrom, T. and Good, W. R. (1991), 'Quantitative evaluation of ethanol effects on diffusion and metabolism of β-estradiol in hairless mouse skin', *Pharmaceutical Research* **8**(7), 865–872.

Liu, S., Jin, M.-n., Quan, Y.-s., Kamiyama, F., Katsumi, H., Sakane, T. and Yamamoto, A. (2012), 'The development and characteristics of novel microneedle arrays fabricated from hyaluronic acid, and their application in the transdermal delivery of insulin', *Journal of Controlled Release* **161**(3), 933–941.

Lombardo, D., Calandra, P., Barreca, D., Magazù, S. and Kiselev, M. (2016), 'Soft interaction in liposome nanocarriers for therapeutic drug delivery', *Nanomaterials* **6**(7), 125.

Lombardo, D., Kiselev, M. A., Magazù, S. and Calandra, P. (2015), 'Amphiphiles self-assembly: basic concepts and future perspectives of supramolecular approaches', *Advances in Condensed Matter Physics* **2015**.

Lombry, C., Dujardin, N. and Préat, V. (2000), 'Transdermal delivery of macromolecules using skin electroporation', *Pharmaceutical Research* **17**(1), 32–37.

Lu, M., Zhou, J., Wang, L., Zhao, W., Lu, Y., Zhang, L. and Liu, Y. (2010), 'Design and preparation of cross-linked polystyrene nanoparticles for elastomer reinforcement', *Journal of Nanomaterials* **2010**, 7.

Luis, J., Park, E. J., Meyer Jr, R. J. and Smith, N. B. (2007), 'Rectangular cymbal arrays for improved ultrasonic transdermal insulin delivery', *The Journal of the Acoustical Society of America* **122**(4), 2022–2030.

Madara, J. L. (1998), 'Regulation of the movement of solutes across tight junctions', *Annual Review of Physiology* **60**(1), 143–159.

Maddock, W. G. and Coller, F. A. (1933), 'The role of the extremities in the dissipation of heat', *American Journal of Physiology-Legacy Content* **106**(3), 589–596.

Madison, K. C. (2003), 'Barrier function of the skin:"la raison d'etre" of the epidermis', *Journal of Investigative Dermatology* **121**(2), 231–241.

Maia, C. S., Mehnert, W. and Schäfer-Korting, M. (2000), 'Solid lipid nanoparticles as drug carriers for topical glucocorticoids', *International Journal of Pharmaceutics* **196**(2), 165–167.

Manosroi, A., Kongkaneramit, L. and Manosroi, J. (2004), 'Stability and transdermal absorption of topical amphotericin b liposome formulations', *International Journal of Pharmaceutics* **270**(1-2), 279–286.

Mathur, V., Satrawala, Y. and Rajput, M. S. (2014), 'Physical and chemical penetration enhancers in transdermal drug delivery system', *Asian Journal of Pharmaceutics (AJP): Free full text articles from Asian J Pharm* **4**(3).

Matos, B. N., Reis, T. A., Gratieri, T. and Gelfuso, G. M. (2015), 'Chitosan nanoparticles for targeting and sustaining minoxidil sulphate delivery to hair follicles', *International Journal of Biological Macromolecules* **75**, 225–229.

McAllister, D. V., Kaushik, S., Patel, P., Mayberry, J., Allen, M. and Prausnitz, M. (1999), Microneedles for transdermal delivery of macromolecules, *in* '[Engineering in Medicine and Biology, 1999. 21st Annual Conference and the 1999 Annual Fall Meetring of the Biomedical Engineering Society] BMES/EMBS Conference, 1999. Proceedings of the First Joint', Vol. 2, IEEE, pp. 836–vol.

McCrudden, M. T., Singh, T. R. R., Migalska, K. and Donnelly, R. F. (2013), 'Strategies for enhanced peptide and protein delivery', *Therapeutic Delivery* **4**(5), 593–614.

McElnay, J. C., Benson, H. A., Harland, R. and Hadgraft, J. (1993), 'Phonophoresis of methyl nicotinate: a preliminary study to elucidate the mechanism of action', *Pharmaceutical Research* **10**(12), 1726–1731.

Mehnert, W. and Mäder, K. (2012), 'Solid lipid nanoparticles: production, characterization and applications', *Advanced Drug Delivery Reviews* **64**, 83–101.

Mei, Z., Chen, H., Weng, T., Yang, Y. and Yang, X. (2003), 'Solid lipid nanoparticle and microemulsion for topical delivery of triptolide', *European Journal of Pharmaceutics and Biopharmaceutics* **56**(2), 189–196.

Menon, G. K. (2002), 'New insights into skin structure: scratching the surface', *Advanced Drug Delivery Reviews* **54**, S3–S17.

Mertens, A. E., Rygiel, T. P., Olivo, C., van der Kammen, R. and Collard, J. G. (2005), 'The rac activator tiam1 controls tight junction biogenesis in keratinocytes

through binding to and activation of the par polarity complex', *Journal of Cell Biology* **170**(7), 1029–1037.

Messenger, A. and Rundegren, J. (2004), 'Minoxidil: mechanisms of action on hair growth', *British Journal of Dermatology* **150**(2), 186–194.

Meyer, W. (1996), 'Comments on the suitability of swine skin as a biological model for human skin', *Der Hautarzt; Zeitschrift fur Dermatologie, Venerologie, und verwandte Gebiete* **47**(3), 178–182.

Meyer, W. and Zschemisch, N. (2002), 'Die hautschichten am ohr des hausschweins', *Mit Besonderer Berücksichtigung der Nutzung des Ohrintegu-ments in der Humandermatologischen forschung. Berl Münch Tierärztl Wschr* **115**, 401–6.

Michaels, A., Chandrasekaran, S. and Shaw, J. (1975), 'Drug permeation through human skin: theory and in vitro experimental measurement', *AIChE Journal* **21**(5), 985–996.

Mitragotri, S. and Kost, J. (2001), 'Transdermal delivery of heparin and low-molecular weight heparin using low-frequency ultrasound', *Pharmaceutical Research* **18**(8), 1151–1156.

Mittal, A., Raber, A. S., Schaefer, U. F., Weissmann, S., Ebensen, T., Schulze, K., Guzmán, C. A., Lehr, C.-M. and Hansen, S. (2013), 'Non-invasive delivery of nanoparticles to hair follicles: a perspective for transcutaneous immunization', *Vaccine* **31**(34), 3442–3451.

Mittal, A., Schulze, K., Ebensen, T., Weißmann, S., Hansen, S., Lehr, C. M. and Guzmán, C. A. (2015), 'Efficient nanoparticle-mediated needle-free transcutaneous vaccination via hair follicles requires adjuvantation', *Nanomedicine: Nanotechnology, Biology and Medicine* **11**(1), 147–154.

Moffat, A. C., Osselton, M. D., Widdop, B. and Watts, J. (2011), *Clarke's analysis of drugs and poisons*, Pharmaceutical Press London.

Moghimi, S. M., Hunter, A. C. and Murray, J. C. (2001), 'Long-circulating and target-specific nanoparticles: theory to practice', *Pharmacological Reviews* **53**(2), 283–318.

Montagna, W. (2012), *The structure and function of skin*, Elsevier.

Monteiro-Riviere, N. A. (2010), *Structure and function of skin*, CRC Press.

Morgan, C., Renwick, A. and Friedmann, P. (2003), 'The role of stratum corneum and dermal microvascular perfusion in penetration and tissue levels of water-soluble drugs investigated by microdialysis', *British Journal of Dermatology* **148**(3), 434–443.

Morgan, T. M., O'Sullivan, H. M., Reed, B. L. and Finnin, B. C. (1998), 'Transdermal delivery of estradiol in postmenopausal women with a novel topical aerosol', *Journal of Pharmaceutical Sciences* **87**(10), 1226–1228.

Muchow, M., Maincent, P. and Müller, R. H. (2008), 'Lipid nanoparticles with a solid matrix (sln®, nlc®, ldc®) for oral drug delivery', *Drug Development and Industrial Pharmacy* **34**(12), 1394–1405.

Muhm, J. M., Rock, P. B., McMullin, D. L., Jones, S. P., Lu, I., Eilers, K. D., Space, D. R. and McMullen, A. (2007), 'Effect of aircraft-cabin altitude on passenger discomfort', *New England Journal of Medicine* **357**(1), 18–27.

Mukherjee, S., Ray, S. and Thakur, R. (2009), 'Solid lipid nanoparticles: a modern formulation approach in drug delivery system', *Indian Journal of Pharmaceutical Sciences* **71**(4), 349.

Müller, R. and Dingler, A. (1998), 'The next generation after the liposomes: solid lipid nanoparticles (sln, lipopearls) as dermal carrier in cosmetics', *Eurocosmetics* **7**(8), 19–26.

Müller, R. H. and Hildebrand, G. E. (1996), 'Zetapotential und partikelladung in der laborpraxis(einführung in die theorie praktische messdurchführung dateninterpretation)', *Paperback APV* .

Müller, R. H., Mäder, K. and Gohla, S. (2000), 'Solid lipid nanoparticles (sln) for controlled drug delivery–a review of the state of the art', *European Journal of Pharmaceutics and Biopharmaceutics* **50**(1), 161–177.

Müller, R. H., Radtke, M. and Wissing, S. A. (2002), 'Solid lipid nanoparticles (sln) and nanostructured lipid carriers (nlc) in cosmetic and dermatological preparations', *Advanced Drug Delivery Reviews* **54**, S131–S155.

Müller, R. H., Rühl, D., Runge, S., Schulze-Forster, K. and Mehnert, W. (1997), 'Cytotoxicity of solid lipid nanoparticles as a function of the lipid matrix and the surfactant', *Pharmaceutical Research* **14**(4), 458–462.

Mura, S., Manconi, M., Fadda, A. M., Sala, M. C., Perricci, J., Pini, E. and Sinico, C. (2013), 'Penetration enhancer-containing vesicles (pevs) as carriers for cutaneous delivery of minoxidil: in vitro evaluation of drug permeation by infrared spectroscopy', *Pharmaceutical Development and Technology* **18**(6), 1339–1345.

Naik, A., Kalia, Y. N. and Guy, R. H. (2000), 'Transdermal drug delivery: overcoming the skin's barrier function', *Pharmaceutical Science & Technology Today* **3**(9), 318–326.

Naik, A., Kalia, Y. N., Guy, R. H., Fessi, H. et al. (2004), 'Enhancement of topical delivery from biodegradable nanoparticles', *Pharmaceutical Research* **21**(10), 1818–1825.

Namdeo, A. and Jain, N. (1999), 'Niosomal delivery of 5-fluorouracil', *Journal of Microencapsulation* **16**(6), 731–740.

Nordstrom, K. M., Labows, J. N., McGinley, K. J. and Leyden, J. J. (1986), 'Characterization of wax esters, triglycerides, and free fatty acids of follicular casts', *Journal of Investigative Dermatology* **86**(6), 700–705.

Norlen, L. (2008), *The physical structure of the skin barrier*, Informa Healthcare USA, Inc. New York, NY.

Obata, Y., Tajima, S. and Takeoka, S. (2010), 'Evaluation of ph-responsive liposomes containing amino acid-based zwitterionic lipids for improving intracellular drug delivery in vitro and in vivo', *Journal of Controlled Release* **142**(2), 267–276.

OECD (2004), *Guidance Document for the Conduct of Skin Absorption Studies*. **URL:** *https://www.oecd-ilibrary.org/content/publication/9789264078796-en*

Ogiso, T., Niinaka, N. and Iwaki, M. (1996), 'Mechanism for enhancement effect of lipid disperse system on percutaneous absorption', *Journal of Pharmaceutical Sciences* **85**(1), 57–64.

Ogiso, T., Paku, T., Iwaki, M. and Tanino, T. (1994), 'Mechanism of the enhancement effect of n-octyl-β-d-thioglucoside on the transdermal penetration of fluorescein isothiocyanate-labeled dextrans and the molecular weight dependence of water-soluble penetrants through stripped skin', *Journal of Pharmaceutical Sciences* **83**(12), 1676–1681.

Ogiso, T., Shiraki, T., Okajima, K., Tanino, T., Iwaki, M. and Wada, T. (2002), 'Transfollicular drug delivery: penetration of drugs through human scalp skin and comparison of penetration between scalp and abdominal skins in vitro', *Journal of Drug Targeting* **10**(5), 369–378.

Ogiso, T., Yamaguchi, T., Iwaki, M., Tanino, T. and Miyake, Y. (2001), 'Effect of positively and negatively charged liposomes on skin permeation of drugs', *Journal of Drug Targeting* **9**(1), 49–59.

Ohkuma, S., Moriyama, Y. and Takano, T. (1982), 'Identification and characterization of a proton pump on lysosomes by fluorescein-isothiocyanate-dextran fluorescence', *Proceedings of the National Academy of Sciences* **79**(9), 2758–2762.

on Specifications for Pharmaceutical Preparations, W. E. C. and Organization, W. H. (2005), *WHO Expert Committee on Specifications for Pharmaceutical Preparations: Thirty-ninth Report*, World Health Organization.

O'Neil, M. J. (2013), *The Merck index: an encyclopedia of chemicals, drugs, and biologicals*, RSC Publishing.

Ongpipattanakul, B., Burnette, R. R., Potts, R. O. and Francoeur, M. L. (1991), 'Evidence that oleic acid exists in a separate phase within stratum corneum lipids', *Pharmaceutical Research* **8**(3), 350–354.

Otberg, N., Richter, H., Jacobi, U., Blume-Peytavi, U., Schaefer, H., Sterry, W. and Lademann, J. (2004), 'In vivo method to assess active and inactive hair follicles: B3. 1', *Journal der Deutschen Dermatologischen Gesellschaft* **2**(6), 501.

Otberg, N., Richter, H., Knuttel, A., Schaefer, H., Sterry, W. and Lademann, J. (2004), 'Laser spectroscopic methods for the characterization of open and closed follicles', *Laser Physics Letters* **1**(1), 46–49.

Otberg, N., Richter, H., Schaefer, H., Blume-Peytavi, U., Sterry, W. and Lademann, J. (2004), 'Variations of hair follicle size and distribution in different body sites', *Journal of Investigative Dermatology* **122**(1), 14–19.

Otberg, N., Teichmann, A., Rasuljev, U., Sinkgraven, R., Sterry, W. and Lademann, J. (2007), 'Follicular penetration of topically applied caffeine via a shampoo formulation', *Skin Pharmacology and Physiology* **20**(4), 195–198.

O'Toole, P. W. and Clyne, M. (2001), Cell envelope, *in* 'Helicobacter pylori: Physiology and Genetics', ASM Press.

Padilla-Martinez, J. P., Banks, D., Ramirez-San-Juan, J. C., Ramos-Garcia, R., Sun, F. and Aguilar, G. (2012), 'Towards the enhancement of transdermal drug delivery through thermocavitation', *Photonics & Lasers in Medicine* **1**(3), 183–193.

Padois, K., Cantiéni, C., Bertholle, V., Bardel, C., Pirot, F. and Falson, F. (2011), 'Solid lipid nanoparticles suspension versus commercial solutions for dermal delivery of minoxidil', *International Journal of Pharmaceutics* **416**(1), 300–304.

Pan, W., Ravot, E., Tolle, R., Frank, R., Mosbach, R., Türbachova, I. and Bujard, H. (1999), 'Vaccine candidate msp-1 from plasmodium falciparum: a redesigned 4917 bp polynucleotide enables synthesis and isolation of full-length protein from escherichia coli and mammalian cells', *Nucleic Acids Research* **27**(4), 1094–1103.

Patzelt, A., Richter, H., Knorr, F., Schäfer, U., Lehr, C.-M., Dähne, L., Sterry, W. and Lademann, J. (2011), 'Selective follicular targeting by modification of the particle sizes', *Journal of Controlled Release* **150**(1), 45–48.

Paudel, K. S., Milewski, M., Swadley, C. L., Brogden, N. K., Ghosh, P. and Stinchcomb, A. L. (2010), 'Challenges and opportunities in dermal/transdermal delivery', *Therapeutic Delivery* **1**(1), 109–131.

Pavliv, L., Freebern, K., Wilke, T., Chin-Chih, C., Shetty, B. and Tyle, P. (1994), 'Topical formulation development of a novel thymidylate synthase inhibitor for the treatment of psoriasis', *International Journal of Pharmaceutics* **105**(3), 227–233.

Pedersen, L. and Jemec, G. B. (2006), 'Mechanical properties and barrier function of healthy human skin', *Acta Dermato-Venereologica* **86**(4), 308–311.

Pellett, M., Castellano, S., Hadgraft, J. and Davis, A. (1997), 'The penetration of supersaturated solutions of piroxicam across silicone membranes and human skin in vitro', *Journal of Controlled Release* **46**(3), 205–214.

Pereno, V., Carugo, D., Bau, L., Sezgin, E., Bernardino de la Serna, J., Eggeling, C. and Stride, E. (2017), 'Electroformation of giant unilamellar vesicles on stainless steel electrodes', *ACS omega* **2**(3), 994–1002.

PermeGear (2018), 'Franz cells', `http://permegear.com/franz-cells/`. Online; accessed August 10, 2018.

Pfaffen, V. and Ortiz, P. I. (2006), 'Electrochemical determination of minoxidil in different pharmaceutical formulations by flow injection analysis', *Analytical Sciences* **22**(1), 91–94.

Pinkus, H. (1951), 'Examination of the epidermis by the strip method of removing horny layers: I. observations on thickness of the horny layer, and on mitotic activity after stripping', *Journal of Investigative Dermatology* **16**(6), 383–386.

Pintado-Herrera, M. G., Lara-Martín, P. A., González-Mazo, E. and Allan, I. J. (2016), 'Determination of silicone rubber and low-density polyethylene diffusion and polymer/water partition coefficients for emerging contaminants', *Environmental Toxicology and Chemistry* **35**(9), 2162–2172.

Pirogov, A. V., Chernova, M. V., Dar'ya, S. N. and Shpigun, O. A. (2003), 'Sulfonated and sulfoacylated poly (styrene–divinylbenzene) copolymers as packing materials for cation chromatography', *Analytical and Bioanalytical Chemistry* **376**(5), 745–752.

Polat, B. E., Hart, D., Langer, R. and Blankschtein, D. (2011), 'Ultrasound-mediated transdermal drug delivery: mechanisms, scope, and emerging trends', *Journal of Controlled Release* **152**(3), 330–348.

Potts, R. O. and Francoeur, M. L. (1991), 'The influence of stratum corneum morphology on water permeability', *Journal of Investigative Dermatology* **96**(4), 495–499.

Poulsen, B., Chowhan, Z., Pritchard, R. and Katz, M. (1978), The use of mixtures of topical corticosteroids as a mechanism for improving total drug bioavailability: a preliminary report, *in* 'Skin-Drug Application and Evaluation of Environmental Hazards', Vol. 7, Karger Publishers, pp. 107–120.

Prausnitz, M. R. (1999), 'A practical assessment of transdermal drug delivery by skin electroporation', *Advanced Drug Delivery Reviews* **35**(1), 61–76.

Prausnitz, M. R. (2004), 'Microneedles for transdermal drug delivery', *Advanced Drug Delivery Reviews* **56**(5), 581–587.

Prausnitz, M. R. and Langer, R. (2008), 'Transdermal drug delivery', *Nature Biotechnology* **26**(11), 1261.

Prausnitz, M. R., Mitragotri, S. and Langer, R. (2004), 'Current status and future potential of transdermal drug delivery', *Nature Reviews Drug Discovery* **3**(2), 115.

Purnak, T., Senel, E. and Sahin, C. (2011), 'Liquid formulation of minoxidil versus its foam formulation', *Indian Journal of Dermatology* **56**(4), 462.

Quinn, H. L., Kearney, M.-C., Courtenay, A. J., McCrudden, M. T. and Donnelly, R. F. (2014), 'The role of microneedles for drug and vaccine delivery', *Expert Opinion on Drug Delivery* **11**(11), 1769–1780.

Quinn, P. J. (2012), 'The effect of tocopherol on the structure and permeability of phosphatidylcholine liposomes', *Journal of Controlled Release* **160**(2), 158–163.

Radomska-Galant, I. and Basinska, T. (2003), 'Poly (styrene/α-tert-butoxy-ω-vinylbenzylpolyglycidol) microspheres for immunodiagnostics. principle of a novel latex test based on combined electrophoretic mobility and particle aggregation measurements', *Biomacromolecules* **4**(6), 1848–1855.

Rancan, F., Papakostas, D., Hadam, S., Hackbarth, S., Delair, T., Primard, C., Verrier, B., Sterry, W., Blume-Peytavi, U. and Vogt, A. (2009), 'Investigation of polylactic acid (pla) nanoparticles as drug delivery systems for local dermatotherapy', *Pharmaceutical Research* **26**(8), 2027–2036.

Rao, J. P. and Geckeler, K. E. (2011), 'Polymer nanoparticles: preparation techniques and size-control parameters', *Progress in Polymer Science* **36**(7), 887–913.

Rawat, S., Vengurlekar, S., Rakesh, B., Jain, S. and Srikarti, G. (2008), 'Transdermal delivery by iontophoresis', *Indian Journal of Pharmaceutical Sciences* **70**(1), 5.

Reese, C. E. and Asher, S. A. (2002), 'Emulsifier-free emulsion polymerization produces highly charged, monodisperse particles for near infrared photonic crystals', *Journal of Colloid and Interface Science* **248**(1), 41–46.

Riviere, J. E. and Monteiro-Riviere, N. A. (2005), *Dermal absorption models in toxicology and pharmacology*, CRC Press.

Riviere, J., Sage, B. and Williams, P. (1991), 'Effects of vasoactive drugs on transdermal lidocaine iontophoresis', *Journal of Pharmaceutical Sciences* **80**(7), 615–620.

Roberts, M., Dong, G., Zheng, P. and Murphy, G. F. (1991), 'Hairless micropig skin. a novel model for studies of cutaneous biology.', *The American Journal of Pathology* **138**(3), 687.

Roberts, M., Mohammed, Y., Pastore, M., Namjoshi, S., Yousef, S., Alinaghi, A., Haridass, I., Abd, E., Leite-Silva, V., Benson, H. et al. (2017), 'Topical and cutaneous delivery using nanosystems', *Journal of Controlled Release* **247**, 86–105.

Roberts, M. S. and Cross, S. E. (1999), 'A physiological pharmacokinetic model for solute disposition in tissues below a topical application site', *Pharmaceutical Research* **16**(9), 1392–1398.

Roberts, M. S., Cross, S. E. and Pellett, M. A. (2002), 'Skin transport', *Drugs and The Pharmaceutical Sciences* **119**, 89–196.

Rolland, A., Wagner, N., Chatelus, A., Shroot, B. and Schaefer, H. (1993), 'Site-specific drug delivery to pilosebaceous structures using polymeric microspheres', *Pharmaceutical Research* **10**(12), 1738–1744.

Romero, E. L. and Morilla, M. J. (2013), 'Highly deformable and highly fluid vesicles as potential drug delivery systems: theoretical and practical considerations', *International Journal of Nanomedicine* **8**, 3171.

Roskos, K. V., Maibach, H. I. and Guy, R. H. (1989), 'The effect of aging on percutaneous absorption in man', *Journal of Pharmacokinetics and Biopharmaceutics* **17**(6), 617–630.

Rouse, J. G., Yang, J., Ryman-Rasmussen, J. P., Barron, A. R. and Monteiro-Riviere, N. A. (2007), 'Effects of mechanical flexion on the penetration of fullerene amino acid-derivatized peptide nanoparticles through skin', *Nano Letters* **7**(1), 155–160.

Roy, S. D. and Flynn, G. L. (1989), 'Transdermal delivery of narcotic analgesics: comparative permeabilities of narcotic analgesics through human cadaver skin', *Pharmaceutical Research* **6**(10), 825–832.

Rudrapal, M., Kiran, B. S., Sridhar, N. and Raghavendra, M. (2016), 'development and validation of rp-hplc method for simultaneous estimation of minoxidil and aminexil in topical formulation', *Asian Journal of Chemistry* **28**(1), 157.

Rytting, E., Nguyen, J., Wang, X. and Kissel, T. (2008), 'Biodegradable polymeric nanocarriers for pulmonary drug delivery', *Expert Opinion on Drug Delivery* **5**(6), 629–639.

Sackmann, E. (1995), 'Physical basis of self-organization and function of membranes: physics of vesicles', *Handbook of Biological Physics* **1**, 213–304.

Santos Maia, C., Mehnert, W., Schaller, M., Korting, H., Gysler, A., Haberland, A. and Schäfer-Korting, M. (2002), 'Drug targeting by solid lipid nanoparticles for dermal use', *Journal of Drug Targeting* **10**(6), 489–495.

Sato, K., Sugibayashi, K. and Morimoto, Y. (1991), 'Species differences in percutaneous absorption of nicorandil', *Journal of Pharmaceutical Sciences* **80**(2), 104–107.

Schaefer, H. and Lademann, J. (2001), 'The role of follicular penetration', *Skin Pharmacology and Physiology* **14**(Suppl. 1), 23–27.

Schaefer, H.; Redelmeier, T. E. (1996), *Principles of Percutaneous Absorption*, Karger: Basel, Switzerland.

Schaefer, H., Watts, F., Brod, J. and Illel, B. (1990), 'Follicular penetration', *Prediction of Percutaneous Penetration. Methods, Measurements, Modelling* **163**, 732.

Schäfer-Korting, M., Mehnert, W. and Korting, H.-C. (2007), 'Lipid nanoparticles for improved topical application of drugs for skin diseases', *Advanced Drug Delivery Reviews* **59**(6), 427–443.

Scheuplein, R. J. (1965), 'Mechanism of percutaneous adsorption: I. routes of penetration and the influence of solubility', *Journal of Investigative Dermatology* **45**(5), 334–346.

Scheuplein, R. J. (1967), 'Mechanism of percutaneous absorption: Ii. transient diffusion and the relative importance of various routes of skin penetration', *Journal of Investigative Dermatology* **48**(1), 79–88.

Scheuplein, R. J. and Blank, I. H. (1971), 'Permeability of the skin', *Physiological Reviews* **51**(4), 702–747.

Schnetz, E. and Fartasch, M. (2001), 'Microdialysis for the evaluation of penetration through the human skin barrier—a promising tool for future research?', *European Journal of Pharmaceutical Sciences* **12**(3), 165–174.

Schoellhammer, C. M., Blankschtein, D. and Langer, R. (2014), 'Skin permeabilization for transdermal drug delivery: recent advances and future prospects', *Expert Opinion on Drug Delivery* **11**(3), 393–407.

Schramm, J. and Mitragotri, S. (2002), 'Transdermal drug delivery by jet injectors: energetics of jet formation and penetration', *Pharmaceutical Research* **19**(11), 1673–1679.

Schreier, H. and Bouwstra, J. (1994), 'Liposomes and niosomes as topical drug carriers: dermal and transdermal drug delivery', *Journal of Controlled Release* **30**(1), 1–15.

Schröder, U., Arfors, K.-E. and Tangen, O. (1976), 'Stability of fluorescein labeled dextrans in vivo and in vitro', *Microvascular Research* **11**(1), 33–39.

Schultheiss, N., Lorimer, K., Wolfe, S. and Desper, J. (2010), 'Attempted construction of minoxidil: carboxylic acid cocrystals; 7 salts and 1 cocrystal resulted', *CrystEngComm* **12**(3), 742–749.

Schwarz, C., Mehnert, W., Lucks, J. and Müller, R. (1994), 'Solid lipid nanoparticles (sln) for controlled drug delivery. i. production, characterization and sterilization', *Journal of Controlled Release* **30**(1), 83–96.

Sharata, H. H. and Katz, K. H. (1996), 'Liposomes', *International Journal of Dermatology* **35**(11), 761–769.

Shivanand, P., Patel, J. and Patel, K. (2010), 'Various emerging technologies in insulin delivery system', *International Journal of Pharmaceutical Sciences Review and Research* **2**(1), 14–16.

Shore, P. A., Brodie, B. B. and Hogben, C. A. M. (1957), 'The gastric secretion of drugs: a ph partition hypothesis', *Journal of Pharmacology and Experimental Therapeutics* **119**(3), 361–369.

Siddiqui, O., Roberts, M. and Polack, A. (1989), 'Percutaneous absorption of steroids: relative contributions of epidermal penetration and dermal clearance', *Journal of Pharmacokinetics and Biopharmaceutics* **17**(4), 405–424.

Siddiraju, S. and Sahithi, M. (2015), 'Stability indicating rp-hplc method development and validation for the simultaneous determination of aminexil and minoxidil in pharmaceutical dosage form', *Annales Pharmaceutiques Francaises* **73**(2), 114–122.

Siekmann, B. and Westesen, K. (1996), 'Investigations on solid lipid nanoparticles prepared by precipitation in o/w emulsions', *European Journal of Pharmaceutics and Biopharmaceutics* **42**(2), 104–109.

Singh, P. and Roberts, M. S. (1994), 'Effects of vasoconstriction on dermal pharmacokinetics and local tissue distribution of compounds', *Journal of Pharmaceutical Sciences* **83**(6), 783–791.

Singh, R. and Lillard Jr, J. W. (2009), 'Nanoparticle-based targeted drug delivery', *Experimental and Molecular Pathology* **86**(3), 215–223.

Sjöström, B., Westesen, K. and Bergenståhl, B. (1993), 'Preparation of submicron drug particles in lecithin-stabilized o/w emulsions: Ii. characterization of cholesteryl acetate particles', *International Journal of Pharmaceutics* **94**(1-3), 89–101.

Škalko, N., Čajkovac, M. and Jalšenjak, I. (1992), 'Liposomes with clindamycin hydrochloride in the therapy of acne vulgaris', *International Journal of Pharmaceutics* **85**(1-3), 97–101.

Sloan, K. B. (1992), *Prodrugs: Tropical and ocular drug delivery. Drug and the Pharmaceutical Sciences*, New York: Marcel Dekker Inc.

Smith, N. B. (2007), 'Perspectives on transdermal ultrasound mediated drug delivery', *International Journal of Nanomedicine* **2**(4), 585.

Snipstad, S., Hak, S., Baghirov, H., Sulheim, E., Mørch, Ý., Lélu, S., von Haartman, E., Bäck, M., Nilsson, K. P. R., Klymchenko, A. S. et al. (2017), 'Labeling nanoparticles: Dye leakage and altered cellular uptake', *Cytometry Part A* **91**(8), 760–766.

Souto, E., Wissing, S., Barbosa, C. and Müller, R. (2004), 'Development of a controlled release formulation based on sln and nlc for topical clotrimazole delivery', *International Journal of Pharmaceutics* **278**(1), 71–77.

Spencer, J. M. (2005), 'Microdermabrasion', *American Journal of Clinical Dermatology* **6**(2), 89–92.

Srivastava, S., Phadke, R. S., Govil, G. and Rao, C. (1983), 'Fluidity, permeability and antioxidant behaviour of model membranes incorporated with α-tocopherol and vitamin e acetate', *Biochimica et Biophysica Acta (BBA)-Biomembranes* **734**(2), 353–362.

Steinsträsser, I. and Merkle, H. P. (1995), 'Dermal metabolism of topically applied drugs: pathways and models reconsidered', *Pharmaceutica Acta Helvetiae* **70**(1), 3–24.

Suhonen, T. M., Bouwstra, J. A. and Urtti, A. (1999), 'Chemical enhancement of percutaneous absorption in relation to stratum corneum structural alterations', *Journal of Controlled Release* **59**(2), 149–161.

Suzuki, M. (1987), 'Protective effect of fine-particle titanium dioxide on uvb-induced dna damage in hairless mouse skin', *Photodermatol.* **4**, 209–211.

Tanner, T. and Marks, R. (2008), 'Delivering drugs by the transdermal route: review and comment', *Skin Research and Technology* **14**(3), 249–260.

Teichmann, A., Jacobi, U., Ossadnik, M., Richter, H., Koch, S., Sterry, W. and Lademann, J. (2005), 'Differential stripping: determination of the amount of topically applied substances penetrated into the hair follicles', *Journal of General Internal Medicine* **20**(5), 264–269.

Tenjarla, S. N., Kasina, R., Puranajoti, P., Omar, M. S. and Harris, W. T. (1999), 'Synthesis and evaluation of n-acetylprolinate esters—novel skin penetration enhancers', *International Journal of Pharmaceutics* **192**(2), 147–158.

ThermoFisher (2018), 'Fluospheres polystyrene microspheres, red fluorescent (580/605), for tracer studies', `https://www.thermofisher.com/order/catalog/product/F13083`. Online; accessed August 26, 2018.

Tinkle, S. S., Antonini, J. M., Rich, B. A., Roberts, J. R., Salmen, R., DePree, K. and Adkins, E. J. (2003), 'Skin as a route of exposure and sensitization in chronic beryllium disease.', *Environmental Health Perspectives* **111**(9), 1202.

Todo, H., Kimura, E., Yasuno, H., Tokudome, Y., Hashimoto, F., Ikarashi, Y. and Sugibayashi, K. (2010), 'Permeation pathway of macromolecules and nanospheres through skin', *Biological and Pharmaceutical Bulletin* **33**(8), 1394–1399.

Toll, R., Jacobi, U., Richter, H., Lademann, J., Schaefer, H. and Blume-Peytavi, U. (2004), 'Penetration profile of microspheres in follicular targeting of terminal hair follicles', *Journal of Investigative Dermatology* **123**(1), 168–176.

Trauer, S., Patzelt, A., Otberg, N., Knorr, F., Rozycki, C., Balizs, G., Büttemeyer, R., Linscheid, M., Liebsch, M. and Lademann, J. (2009), 'Permeation of topically applied caffeine through human skin–a comparison of in vivo and in vitro data', *British Journal of Clinical Pharmacology* **68**(2), 181–186.

Treffel, P., Humbert, P., Remoussenard, O., Bechtel, Y. and Agache, P. (1993), 'Effect of pressure on in vitro percutaneous absorption of caffeine', *Acta Derm Venereol (Stockh)* **73**, 200–202.

Tuan-Mahmood, T.-M., McCrudden, M. T., Torrisi, B. M., McAlister, E., Garland, M. J., Singh, T. R. R. and Donnelly, R. F. (2013), 'Microneedles for intradermal and transdermal drug delivery', *European Journal of Pharmaceutical Sciences* **50**(5), 623–637.

Tuncel, A. and Piskln, E. (1991), 'Polystyrene latex particles: preparation and properties', *Biomaterials, Artificial Cells and Immobilization Biotechnology* **19**(1), 229–253.

Tupker, R. A., Coenraads, P.-J., Pinnagoda, J. and Nater, J. P. (1989), 'Baseline transepidermal water loss (tewl) as a prediction of susceptibility to sodium lauryl sulphate', *Contact Dermatitis* **20**(4), 265–269.

Twist, J. N. and Zatz, J. L. (1988), 'Membrane–solvent–solute interaction in a model permeation system', *Journal of Pharmaceutical Sciences* **77**(6), 536–540.

Twist, J. and Zatz, J. (1986), 'Influence of solvents on paraben permeation through idealized skin model membranes', *Journal of the Society of Cosmetic Chemists* **37**(6), 429–444.

Uchechi, O., Ogbonna, J. D. and Attama, A. A. (2014), Nanoparticles for dermal and transdermal drug delivery, *in* 'Application of Nanotechnology in Drug Delivery', InTech.

Ulbricht, M. (2006), 'Advanced functional polymer membranes', *Polymer* **47**(7), 2217–2262.

Vairale, A., Sivaswaroop, P. and Bandana, S. (2012), 'Development and validation of stability-indicating hplc method for betamethoasone dipropionate and related substances in topical formulation', *Indian Journal of Pharmaceutical Sciences* **74**(2), 107.

Valiveti, S., Wesley, J. and Lu, G. W. (2008), 'Investigation of drug partition property in artificial sebum', *International Journal of Pharmaceutics* **346**(1-2), 10–16.

van der Maaden, K., Jiskoot, W. and Bouwstra, J. (2012), 'Microneedle technologies for (trans) dermal drug and vaccine delivery', *Journal of Controlled Release* **161**(2), 645–655.

Van der Molen, R., Spies, F., Van't Noordende, J., Boelsma, E., Mommaas, A. and Koerten, H. (1997), 'Tape stripping of human stratum corneum yields cell layers that originate from various depths because of furrows in the skin', *Archives of Dermatological Research* **289**(9), 514–518.

Venkateswarlu, V. and Manjunath, K. (2004), 'Preparation, characterization and in vitro release kinetics of clozapine solid lipid nanoparticles', *Journal of Controlled Release* **95**(3), 627–638.

Vitorino, C., Almeida, J., Gonçalves, L., Almeida, A., Sousa, J. and Pais, A. (2013), 'Co-encapsulating nanostructured lipid carriers for transdermal application: from experimental design to the molecular detail', *Journal of Controlled Release* **167**(3), 301–314.

Waich, K., Sandholzer, M., Mayr, T., Slugovc, C. and Klimant, I. (2010), 'A highly flexible polymerization technique to prepare fluorescent nanospheres for trace ammonia detection', *Journal of nanoparticle research* **12**(4), 1095–1100.

Walters, K. A. (2002*a*), *Dermatological and transdermal formulations*, Taylor & Francis.

Walters, K. A. (2002*b*), 'Dermatological and transdermal formulations', *Taylor & Francis* .

Walters, K. A. and Roberts, M. S. (2002), 'The structure and function of skin', *Drugs and the Pharmaceutical Sciences* **119**, 1–40.

Warheit, D. B., Borm, P. J., Hennes, C. and Lademann, J. (2007), 'Testing strategies to establish the safety of nanomaterials: conclusions of an ecetoc workshop', *Inhalation Toxicology* **19**(8), 631–643.

Watkinson, A. C., Bunge, A. L., Hadgraft, J. and Lane, M. E. (2013), 'Nanoparticles do not penetrate human skin—a theoretical perspective', *Pharmaceutical Research* **30**(8), 1943–1946.

Wei, J. C., Haridass, I. N., Crichton, M. L., Mohammed, Y. H., Meliga, S. C., Sanchez, W. Y., Grice, J. E., Benson, H. A., Roberts, M. S. and Kendall, M. A. (2018), 'Space-and time-resolved investigation on diffusion kinetics of human skin following macromolecule delivery by microneedle arrays', *Scientific Reports* **8**(1), 17759.

Weigmann, H.-J., Lademann, J., Schanzer, S., Lindemann, U., Von Pelchrzim, R., Schaefer, H., Sterry, W. and Shah, V. (2001), 'Correlation of the local distribution of topically applied substances inside the stratum corneum determined by tape-stripping to differences in bioavailability', *Skin Pharmacology and Physiology* **14**(Suppl. 1), 98–102.

Wells, F. V. and Lubowe, I. I. (1964), *Cosmetics and the Skin*, Reinhold Pub. Corp.

Wickett, R. R. and Visscher, M. O. (2006), 'Structure and function of the epidermal barrier', *American Journal of Infection Control* **34**(10), S98–S110.

Williams, A. (2003), *Transdermal and topical drug delivery: from theory to clinical practice*, Pharmaceutical Press London.

Williams, A. and Barry, B. (1992), 'Skin absorption enhancers.', *Critical Reviews in Therapeutic Drug Carrier Systems* **9**(3-4), 305–353.

Williams, A. C. and Barry, B. W. (2012), 'Penetration enhancers', *Advanced Drug Delivery Reviews* **64**, 128–137.

Wissing, S. A. and Müller, R. H. (2003*a*), 'Cosmetic applications for solid lipid nanoparticles (sln)', *International Journal of Pharmaceutics* **254**(1), 65–68.

Wissing, S. A. and Müller, R. H. (2003*b*), 'The influence of solid lipid nanoparticles on skin hydration and viscoelasticity–in vivo study', *European Journal of Pharmaceutics and Biopharmaceutics* **56**(1), 67–72.

Wissing, S., Kayser, O. and Müller, R. (2004), 'Solid lipid nanoparticles for parenteral drug delivery', *Advanced Drug Delivery Reviews* **56**(9), 1257–1272.

Wissing, S. and Müller, R. (2001), 'A novel sunscreen system based on tocopherol acetate incorporated into solid lipid nanoparticles', *International Journal of Cosmetic Science* **23**(4), 233–243.

Wissing, S. and Müller, R. (2002), 'Solid lipid nanoparticles as carrier for sunscreens: in vitro release and in vivo skin penetration', *Journal of Controlled Release* **81**(3), 225–233.

Wong, H. L., Bendayan, R., Rauth, A. M., Li, Y. and Wu, X. Y. (2007), 'Chemotherapy with anticancer drugs encapsulated in solid lipid nanoparticles', *Advanced Drug Delivery Reviews* **59**(6), 491–504.

Woolfson, A., Morrow, D., Morrissey, A., Donnelly, R. and Mccarron, P. (2009), 'Microneedles/delivery device and method. british patent application no 0718996.2', *International Publication No WO2009040548* .

Wu, X.-M., Todo, H. and Sugibayashi, K. (2006), 'Effects of pretreatment of needle puncture and sandpaper abrasion on the in vitro skin permeation of fluorescein isothiocyanate (fitc)-dextran', *International Journal of Pharmaceutics* **316**(1-2), 102–108.

Xiao, L., Takada, H., hui Gan, X. and Miwa, N. (2006), 'The water-soluble fullerene derivative 'radical sponge®' exerts cytoprotective action against uva irradiation but not visible-light-catalyzed cytotoxicity in human skin keratinocytes', *Bioorganic & Medicinal Chemistry Letters* **16**(6), 1590–1595.

Yadav, A., Murthy, M., Shete, A. and Sakhare, S. (2011), 'Stability aspects of liposomes', *Indian Journal Of Pharmaceutical Education And Research* **45**(4), 402–413.

Yan, H., Li, R., Li, Q., Wang, J. and Gong, J. (2011), 'Solubility of minoxidil in methanol, ethanol, 1-propanol, 2-propanol, 1-butanol, and water from (278.15 to 333.15) k', *Journal of Chemical & Engineering Data* **56**(5), 2720–2722.

Yan, K., Todo, H. and Sugibayashi, K. (2010), 'Transdermal drug delivery by in-skin electroporation using a microneedle array', *International Journal of Pharmaceutics* **397**(1-2), 77–83.

Ying-zhe, Li, Y.-z., Quan, Y.-s., Zang, L., Jin, M.-n., Kamiyama, F., Katsumi, H., Tsutsumi, S. and Yamamoto, A. (2009), 'Trypsin as a novel potential absorption enhancer for improving the transdermal delivery of macromolecules', *Journal of Pharmacy and Pharmacology* **61**(8), 1005–1012.

Yuki, T., Haratake, A., Koishikawa, H., Morita, K., Miyachi, Y. and Inoue, S. (2007), 'Tight junction proteins in keratinocytes: localization and contribution to barrier function', *Experimental Dermatology* **16**(4), 324–330.

Zaheer, Z. A., Mirza, S., Moazzam, I. and Sayad, I. W. (2012), 'Uv spectrophotometric determination of minoxidil and its application to the assay in pharmaceutical dosage forms', *Der Pharma Chemica* **4**(1), 568–573.

Zhai, H. and Maibach, H. I. (2001), 'Effects of skin occlusion on percutaneous absorption: an overview', *Skin Pharmacology and Physiology* **14**(1), 1–10.

Zhang, L. and Granick, S. (2006), 'How to stabilize phospholipid liposomes (using nanoparticles)', *Nano Letters* **6**(4), 694–698.

Zhao, Y., Brown, M. B. and Jones, S. A. (2010), 'The effects of particle properties on nanoparticle drug retention and release in dynamic minoxidil foams', *International Journal of Pharmaceutics* **383**(1-2), 277–284.

Zorec, B., Škrabelj, D., Marinček, M., Miklavčič, D. and Pavšelj, N. (2017), 'The effect of pulse duration, power and energy of fractional er: Yag laser for transdermal delivery of differently sized fitc dextrans', *International Journal of Pharmaceutics* **516**(1-2), 204–213.

Zur Mühlen, A., Schwarz, C. and Mehnert, W. (1998), 'Solid lipid nanoparticles (sln) for controlled drug delivery–drug release and release mechanism', *European Journal of Pharmaceutics and Biopharmaceutics* **45**(2), 149–155.